Frequency Scaling of Rain Attenuation on Satellite Links in the Ku/Ka-bands using OLYMPUS Satellite Data

Jeff D. Laster

Thesis submitted to the Faculty of the

Virginia Polytechnic Institute and State University

in partial fulfillment of requirements for the degree of

Master of Science

in

Electrical Engineering

APPROVED:

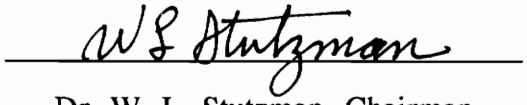

Dr. W. L. Stutzman, Chairman

Dr. T. Pratt

Dr. D. A. deWolf

November 5, 1993

Blacksburg, Virginia

c.2

Frequency Scaling of Attenuation in the Ku/Ka-bands using OLYMPUS Satellite Data

ABSTRACT

Frequency scaling of attenuation is the prediction of attenuation at a desired frequency from attenuation values at a base frequency. The attenuation at the base frequency is often known from prior measurements. Frequency scaling of attenuation is of interest because of the eventual need to exploit higher frequency bands. Most satellite communications traffic now use C-band (4-8 GHz) and Ku-band (12-18 GHz). The next approved, yet largely unused, frequency allocation for domestic use is in the K-band (18-27 GHz) to Ka-band (27-40 GHz). At these higher frequencies, however, earth-space radio links suffer atmospherically induced impairments as frequency increases. In particular, rain causes severe fading. Consequently, satellite systems in these higher bands are very susceptible to outages due to rain-induced fades. Reliable frequency scaling models are needed in system design to estimate the effect of these rain-induced fades.

Between August 1990 and August 1992, V.P.I. & S.U.'s SATCOM Group performed extensive measurements of slant path attenuation using the 12, 20, and 30 GHz beacon signals (in the Ku/Ka-bands) of the European OLYMPUS experimental satellite. The experimental results are used to evaluate the usefulness of scaling models proposed by other researchers, both for instantaneous and statistical purposes. New models are presented for accurate scaling of attenuation within the Ku/Ka-bands.

ACKNOWLEDGEMENTS

The author acknowledges the work of many at Virginia Tech who envisioned this propagation experiment and who worked very hard to make it a success. Dr. Warren Stutzman has proved to be an excellent advisor; I have benefited from his knowledge of the field, his generosity, and his patience. Dr. Tim Pratt and Dr. David deWolf have always given me encouraging words and helpful advice; I am honored that they have served on my thesis committee. Will Remaklus and Bernie Nelson, fellow graduate students, have greatly helped in the processing and generation of the data.

TABLE OF CONTENTS

LIST OF FIGURES

LIST OF TABLES

CHAPTER 1

INTRODUCTION

1.1 The Importance of Frequency Scaling of Attenuation

Frequency scaling of attenuation is of interest because of the need to exploit higher frequency bands. Most of current satellite communications traffic uses C-band (4-8 GHz) [1] at the 6/4 GHz satellite allocation (i.e., 6/4 indicates uplink/downlink frequencies), and there is also traffic in the Ku-band (12-18 GHz) at the 14/12 GHz satellite allocation. The next approved frequency allocation for domestic use is in the K-band (18-27 GHz) and Ka-band (27-40 GHz) at 30/20 GHz; we will refer to 30/20 GHz as Ka-band frequencies.

Ka-band satellite communication is advantageous, not only to gain more spectrum, but also because terrestrial interference is not present in the Ku- to Ka-bands (C-band has shared uses). However, at these higher frequencies, earth-space radio links suffer increasing atmospherically induced impairments as frequency increases. Rain attenuation is the primary impairment since rain attenuation in dB increases approximately as the square of the operating frequency. Consequently, satellite systems are very susceptible to outages due to rain-induced fades. Reliable scaling models are needed in system design to estimate the effects of these rain-induced fades, avoiding the need for expensive experiments.

Frequency scaling of attenuation is the prediction of attenuation at a desired frequency from attenuation values at another frequency. The attenuation at the base frequency is often known from prior measurements. Many scaling models have been developed from theory, empirical data from various propagation experiments, or both.

Frequency scaling of attenuation is examined in detail in this report. The investigation began with a thorough examination of one year of measured data. These results were used to evaluate the accuracy of available scaling models. Because of inadequacies in available models, new models are proposed here to more accurately reflect the measured data.

Frequency scaling of attenuation can be applied to the problem of rain-induced fades by the methods of statistical scaling and instantaneous scaling. **Statistical frequency scaling** is the use of statistics available from prior measurements (at a base frequency) to predict attenuation statistics at a desired frequency. **Instantaneous frequency scaling** is the scaling of base frequency attenuation to predict attenuation at a desired frequency at each sample time (i.e., "instantaneously"). Whether or not statistical frequency scaling results can be used for instantaneous frequency scaling (explained below) is a subject of ongoing research; in fact, in Section 6.1.2, Virginia Tech OLYMPUS results demonstrate that statistical frequency scaling can be used to predict average instantaneous frequency scaling. Statistical frequency scaling facilitates the calculation of link (or power) budgets for new systems (with fixed margin). Traditional system design incorporates margin in a link budget to overcome expected fading. The fade margin value must be accurate because too much margin means a costly over designed system and too little margin results in lower system reliability due to rain outages. Since deep fades occur only for a few hours out of the year, one can tradeoff costs (of higher transmitter power or increased antenna size) with tolerable (or acceptable) levels of outage.

An alternative to the inclusion of power margin all of the time is the use of adaptive fade countermeasures, such as adaptive power control and adaptive coding (trading bit rate for error correction) [2]. One can increase transmit power as needed

to compensate for fading (adjusting the earth station transmitter power is referred to as uplink power control, ULPC). Adaptive schemes allocate resources to overcome fades only as needed (i.e., as long as the fade persisted). **Instantaneous frequency scaling** is important in this application.

Instantaneous scaling of rain attenuation means that attenuation values measured at a base frequency are scaled at each sample instant (0.1 s in the Virginia Tech experiment) for which base frequency data are available to predict attenuation values at another frequency. As an example, instantaneous scaling allows power transmitted to a satellite (i.e., on the uplink) to be increased to compensate for increased path loss, where the path loss is determined by scaling from real time attenuation data obtained at a lower frequency from the satellite to the earth (i.e., on the downlink). This varying of power on the uplink to compensate for path loss is known as uplink power control (ULPC). In addition, the move toward VSAT systems (Very Small Aperture Antennas -- having a diameter less than 1 meter) emphasizes the need for adaptive fade countermeasures, since the simplicity and small size of the VSATs imply low system margins (e.g., margins of 3 dB are proposed). In VSAT data networks, adaptive coding is a promising technique to compensate for fading. Both statistical scaling and instantaneous scaling are discussed in more detail in Chapter 2.

1.2 A Brief History of the OLYMPUS Spacecraft

In July 1989 the European Space Agency, ESA, launched OLYMPUS, an experimental telecommunications satellite. OLYMPUS carried four payloads to facilitate a wide range of applications which included: a 12/20/30 GHz Propagation Payload, a 12/14 GHz Specialized Services Payload, a Direct Broadcast Payload, and a

20/30 GHz Communications Payload [3,4]. The nominal frequencies of the propagation payload - 12, 20, and 30 GHz - are actually 12.5, 19.77, and 29.66 GHz.

The OLYMPUS satellite had a unique history. It left its geostationary orbit on May 29, 1991, and after seventy-six days and a trip around the world, ESA restored the spacecraft to its proper orbit and, in the middle of August 1991, turned the beacons back on. Also, in May 1992, ESA abandoned regular north-south station keeping because of low satellite fuel supply, contributing to diurnal (or daily) fluctuations in satellite signal strength. OLYMPUS ceased operation in August 1993.

1.3 Overview of the Virginia Tech Experiment

Under Jet Propulsion Laboratory sponsorship, the SATCOM Group of Virginia Polytechnic Institute and State University (Blacksburg, Virginia) constructed four earth terminals: one to receive each of the 12.5, 19.77, and 29.66 GHz beacon frequencies of the 12/20/30 GHz Propagation Payload plus a second 20 GHz terminal for short baseline diversity experiments. Between August 1990 and August 1992, the group made continuous measurements of the slant path attenuation for the 12.5, 19.77, and 29.66 GHz beacons. Because of early hardware and software debugging, August 1990 and September 1990 are not included in the overall data set.

The elevation angle for the Blacksburg - OLYMPUS link is 13.93° [5,7]. Since the lowest elevation angle in contiguous United States for utilizing domestic geostationary satellites is about 14°, these measurements represent a lower performance limit case (i.e., worst case) for domestic slant path attenuation [6,7]. This experiment characterizes earth-space propagation across the Ku- and Ka-frequency bands, and it purports to be the most comprehensive earth-space propagation experiment that has

been performed in North America [7]. The Virginia Tech OLYMPUS experiment is documented in a first year report [8] and the second year report [7], and these reports should be referred to for details on the hardware and on the data reduction. The characteristics of the terminals are summarized in Table 1.3-1.

Table 1.3-1

Characteristics of OLYMPUS Receivers at Virginia Tech [7]

Terminal	12	20	30
Frequency (GHz)	12.5	19.77	29.65
Polarization	Y	Switched X,Y (933 Hz)	Y
Switching loss (dB)	------	6	------
EIRP toward Blacksburg (dBW)	9.1	15.7	17.7
Antenna size (m) Beamwidth (deg.)	4.0 0.4	1.5 0.6	1.2 0.5
C/N in 3 Hz BW (dB)	50.3	46.4	44.9

Notes:
Y = Perpendicular to equatorial plane at S/C; 51° from vertical at Blacksburg.
X = Perpendicular to Y

A feature of the Virginia Tech experiment, which is unique in North America when compared to previous experiments (refer to Chapter 4) is the simultaneous reception of satellite signals spanning Ku-band through Ka-band from the same orbital slot. This permits direct frequency scaling in a way that has not been done before [7]. Extensive measurements have been made in the Ku-band (e.g., 12 GHz) and some measurements have been taken spanning the K- to Ka-band (e.g., 20 and 30 GHz), but

very little has been done spanning Ku- to Ka-band (e.g., 12, 20, and 30 GHz simultaneously).

OLYMPUS left its geostationary orbit during the summer of 1991. In order to obtain a full year of data for analysis purposes, June 1992 to August 1992 data are substituted for June 1991 to August 1991 in the one year data set. Thus, the analysis year reported on here consists of January-March 1991, June-August 1992, and September-December 1991. Virginia Tech's procedure for data preprocessing (summarized in Section 2.2) compensates for diurnal (daily) fluctuations in the beacon signals (especially May 1992 when ESA abandoned regular north-south station keeping). Most of the diurnal variations have been removed from the data set.

1.4 References

1. Stutzman, W.L., and Thiele, G.A., Antenna Theory and Design, New York: John Wiley & Sons, 1981, p. 562.
2. Sweeney, D.G., "Adaptive Power Control as a Fade Countermeasure on Satellite Links," Unpublished doctoral dissertation, Report EESATCOM 93-2, Virginia Polytechnic Institute & State University, Department of Electrical Engineering, Blacksburg, VA, January 1993.
3. ESA Communications System Division , "OLYMPUS User's Guide: Executive Summary," Report UG-6-1-S, Issue 3, Noordwijk, the Netherlands: European Space Agency, June 1988.
4. ESA OLYMPUS Earth Station Working Group, "Earth Station Considerations for OLYMPUS Communications Experiments," Issue 2, Noordwijk, the Netherlands: European Space Agency, March 1989.
5. Allnutt R. M., "Total Power Radiometers at 12, 20 and 30 GHz Used in the OLYMPUS Experiment at Virginia Tech," Unpublished master's thesis, Virginia Polytechnic Institute & State University, Blacksburg, VA, 1991.
6. Laster, J.D., "System Design Evaluation of the Co-operative OLYMPUS Data Experiment," Unpublished class paper, Virginia Polytechnic Institute & State University, Blacksburg, VA, December 1991.
7. Stutzman, W.L., *et al.*, "Communications and propagation experiments using the OLYMPUS spacecraft - Analysis of OLYMPUS Propagation Data for the

Period January to May 1991," Report EESATCOM 92-5, Virginia Polytechnic Institute & State University, Department of Electrical Engineering, Blacksburg, VA, JPL Contract No. 958435, November 1991, p. 3.

8. Stutzman, W.L., *et al.*, "Communications and propagation experiments using the OLYMPUS spacecraft - Report on the first year of data collection," Virginia Polytechnic Institute & State University, Department of Electrical Engineering, Blacksburg, VA, JPL Contract No. 958435, October 1991.

CHAPTER 2

PRINCIPLES OF ATTENUATION SCALING

2.1 Sources of Attenuation

Signal attenuation on earth-space links is caused by phenomena such as precipitation absorption and scattering, absorption by atmospheric gases (comprised primarily of oxygen and water vapor), absorption by fog and clouds, and scintillation. The effects of propagation phenomena must be treated separately for accurate evaluation of power budgets on satellite links. With the focus of the experiment on the rain component, attenuation due to absorption by fog and clouds (generally less than 1-2 dB) is small compared to rain attenuation (generally greater than 1-2 dB) and therefore is neglected. Scintillation and attenuation due to atmospheric gaseous absorption (*AGA*), however, must be separated from precipitation.

Other sources of attenuation include system effects such as elevation angle, polarization, diurnal variations, and frequency. Since all three beacon receivers are in the same location, the elevation angle is the same. Fukuchi, Awaka, and Oguchi [10] developed a frequency scaling relation for the prediction of depolarization statistics by calculating the forward scattering amplitudes of the Pruppacher Pitter type raindrops at 33 frequencies from 3 to 40 GHz. However, since rain fading is so severe above 20 GHz, rain fading becomes the limiting factor so that the effects of depolarization tend to be irrelevant above 20 GHz. In addition, Virginia Tech's low elevation angle means that Virginia Tech is too far off of the main beam to get good isolation. For these reasons, the Virginia Tech experiment ignores depolarization effects. The data reduction process in the Virginia Tech experiment removes diurnal, or daily, variations

(discussed in Section 2.1.4) leaving frequency and the characteristics of rain itself as the most significant variables in the Virginia Tech experiment.

2.1.1 Precipitation absorption and scattering

Electromagnetic waves are absorbed and scattered as they travel through particulate water (i.e., precipitation in the form of rain, snow, or hail). Rain absorption increases rapidly with frequency between 10 and 100 GHz and presents a major problem during severe storms. On earth-space radio signals above 5 GHz, the primary cause of fading is rain; consequently, other forms of precipitation such as snow and hail are often ignored.

The scattering component of the total loss is mostly a function of the ratio of the wavelength to the drop diameter. This loss is very small relative to the absorptive component when the wavelength is large relative to the drop diameter. For frequencies below 30 GHz, the scattering loss is small compared to the absorptive loss [1] and can also be ignored.

2.1.1.1 Raindrop Dynamics

The shape of a raindrop is often modeled as an oblate spheroid [1], i.e., a flattened sphere, having its largest dimension oriented approximately horizontally. The cross-section through the axis of symmetry of a raindrop (oriented vertically) is usually modeled as an ellipse with its major axis aligned with the horizontal (and its minor axis aligned with the vertical). The tilt of the minor axis relative to vertical, referred to as the drop canting angle, is a function of wind shear. Large drops are not constant in shape but oscillate in a number of modes which depend on the drop size.

Researchers have proposed several models for drop size distribution (DSD). The commonly used Laws and Parsons DSD [2] yields a skewed normal distribution. The drop size distribution is a function of the rain rate.

For linearly polarized signals, attenuation is greatest for polarizations parallel to the drop major axis (i.e., approximately horizontal). The attenuation of a circularly polarized signal is independent of the drop canting angle and is equal to that of a signal linearly polarized at 45° to the drop major axis (i.e., approximately 45° to the horizontal). For widespread, horizontally stratified rain, the path length, and thus the total attenuation, increases with decreasing path elevation angle. Theoretically, the total attenuation produced by a volume of raindrops can be calculated by summing the losses over all the drops sizes and shapes and by taking into account the drop size and drop shape distributions, the wave polarization state, the elevation angle, and the drop temperature.

A commonly used relationship between attenuation and the rain rate per unit length is the following specific attenuation empirical formula [3]:

$$\alpha = aR^b \qquad \text{[dB/km]} \tag{2.1-1a}$$

where α is the attenuation per kilometer (dB/km), R is the rain rate (mm/h), and a and b are constants which take into account the above factors. Parameters a and b are functions of frequency, polarization angle, and elevation angle; these values are tabulated in CCIR Report 721-2. [4] The attenuation A (in dB) on a link is the integration of α over the path length L (km)

$$A = \int_0^L \alpha dl = \alpha L_e \tag{2.1-1b}$$

where L_e is the effective path length. The values of a and b depend on the drop size distribution. To the degree that the drop size distribution and rain rate distribution are

confidently known, the effects of hydrometeors along a link can be accurately computed. In practice, however, the DSD is dynamic throughout a precipitation event and is difficult to predict. Direct measurements, which are impractical, are required for a full understanding.

2.1.2 Atmospheric Gaseous Attenuation (*AGA*)

Absorption due to gases such as oxygen and water vapor introduces atmospheric gaseous attenuation (*AGA*). A method for determining the attenuation due to atmospheric gases is given by the CCIR relation [20] as follows (this relation assumes a surface air temperature of 15° C) for elevation angle $\theta > 10°$:

$$AGA = \frac{\gamma_o h_o e^{-h_s/h_o} + \gamma_w h_w}{\sin\theta} \qquad (2.1\text{-}2a)$$

where h_s is the height (km) of the terminal above mean sea level and γ_o is the specific attenuation (in dB/km) at the surface terminal (i.e., at height h_s) for dry air where for frequency $f < 57$ GHz

$$\gamma_o = \left[7.19 * 10^{-3} + \frac{6.09}{f^2 + 0.227} + \frac{4.81}{(f-57)^2 + 1.5} \right] f^2 * 10^{-3} \qquad (2.1\text{-}2b)$$

The specific attenuation for water vapor at the surface, γ_w, (dB/km) for $f < 350$ GHz is

$$\gamma_w = \left[0.05 + 0.0021\rho_w + \frac{3.6}{(f-22.2)^2 + 8.5} + \frac{10.6}{(f-183.3)^2 + 9.0} + \frac{8.9}{(f-325.4)^2 + 26.3} \right] f^2 \rho_w 10^{-4} \qquad (2.1\text{-}2c)$$

where ρ_w, is the water vapor density (g/m^3) at the surface. The equivalent height for dry air, h_o, is 6 km for $f < 57$ GHz, and the equivalent height for water vapor, h_w, (km) for $f < 350$ GHz is given by

$$h_w = h_{w_o}\left[1 + \frac{3.0}{(f-22.2)^2+5} + \frac{5.0}{(f-183.3)^2+6} + \frac{2.5}{(f-325.4)^2+4}\right] \quad (2.1\text{-}2d)$$

where h_{w_o} is 1.6 km in clear weather and 2.1 km in rain.

These equations assume a surface air temperature of 15° C. The values tabulated in Table 2.1-1 for Blacksburg, Virginia assume a mean value of $\rho_w = 7.5$ g/m^3, $h_s = 0.649$ km, and $\theta = 13.93^o$. *AGA* at 20 GHz is higher than *AGA* at 30 GHz because of water vapor absorption due to pressure spreading of the 22.3 GHz absorption spectral line of water vapor.

Table 2.1-1

Atmospheric Gaseous Attenuation for 12, 20, and 30 GHz
Calculated from CCIR [20] model for *AGA* (2.1-2)
(h_{w_o} is 1.6 km in clear air and 2.1 km in rain)

Beacon frequency, f	12 GHz	20 GHz	30 GHz
AGA - clear air	0.25 dB	1.01 dB	0.95 dB
AGA - in rain	0.28 dB	1.26 dB	1.12 dB

A gaseous attenuation scaling ratio (*RAG*) can be defined as

$$RAG(f_L, f_U) \equiv \frac{AGA(f_U)}{AGA(f_L)} \quad (2.1\text{-}3)$$

where f_U and f_L are the upper and lower frequencies, respectively. Values for *RAG* for the frequencies under consideration are given in Table 2.1-2

Table 2.1-2

Gaseous Attenuation Ratios for 30/20, 20/12, and 30/12
Calculated by (2.1-3) using CCIR model for *AGA* [20]

Frequency Ratio, f_U / f_L	30/20	20/12	30/12
RAG - clear air	0.94	4.04	3.79
RAG - in rain	0.89	4.50	4.01

AGA is due to absorption by gases such as oxygen and water vapor. Water vapor attenuation is usually less than oxygen attenuation, but around 20 GHz, water vapor attenuation is larger than attenuation due to oxygen because of pressure spreading of the 22.3 GHz absorption spectral line of water vapor. Attenuation due to water vapor is primarily a function of humidity and temperature, which are both likely to change in a storm. If water vapor attenuation is not distinguished from rain attenuation, Sweeney calculates that potential errors as large as 1.68 dB can result in scaling from 20 GHz to 30 GHz in the implementation of uplink power control [5]. Because water vapor attenuation depends on factors which are difficult to quantify during a storm and because the error caused by water vapor attenuation is relatively small, Sweeney, in his study, and Ihara and Furahama [6], in their experiment, ignore this source of error. Because *AGA* is a function of temperature and atmospheric pressure, Sweeney [5] maintains that the change in atmospheric gaseous attenuation (*AGA*) during a storm will be relatively small and can be ignored.

However, it is apparent from Table 2.1-2 and predicted rain attenuation ratio values (see models in Chapter 3) that gaseous attenuation ratios can differ significantly from rain attenuation ratios. Therefore, gaseous attenuation will tend to increase the error in the frequency scaling of attenuation if AGA is not separated from rain attenuation. In the Virginia Tech experiment, attenuation with respect to clear air, ACA (refer to Section 2.2), is derived by subtracting AGA. Consequently, ACA is used in attenuation scaling because it does not include the AGA.

2.1.3 Scintillation

Scintillation is the rapid change in signal strength (that is, both fading and enhancements) caused by refractive index inhomogeneities in the troposphere. These small scale turbulent variations produce distortions of the wave front incident on the receiving antenna. Scintillation is directly analogous to the twinkling of the stars at night. [7] Because the rapid fluctuation in the received signal is caused by refractive index inhomogeneities, attenuation (or fading) due to scintillation is a non-absorptive effect.

Scintillation is greatest on low elevation angle paths operating above 10 GHz (such as the Virginia Tech OLYMPUS experiment), and it tends to increase in summer, under hot and humid conditions. Signal variations are fairly symmetrical about a mean value, except on very low elevation paths where variations tend to become asymmetrical with reductions in signal level being greater than signal enhancements.

Some researchers [8, 9] distinguish between wet scintillations (during rain conditions) and dry scintillations (during clear-sky conditions). However, experimental

results indicate that there is no apparent difference in the scaling properties of wet and dry scintillations [9].

A CCIR [4] relation states that scintillations scale with frequency using a scintillation ratio

$$RS = (f_U / f_L)^{7/12} \tag{2.1-4}$$

for upper and lower frequencies f_U and f_L. Evaluation of the CCIR formula for the OLYMPUS frequencies (see Section 1.2) results in scaling ratios shown in Table 2.1-3.

Table 2.1-3

Scintillation Scaling Ratios (computed from the CCIR model)

Frequency Ratio, f_U / f_L	30/20	20/12	30/12
Scintillation Ratio, *RS*	1.27	1.31	1.66

Because scintillation attenuation ratios are significantly less than rain attenuation ratios, scintillation will tend to increase the error in the frequency scaling of attenuation if scintillation is not separated from rain attenuation. Scintillations of ±3 dB were frequently observed during the OLYMPUS experiment. Consequently, if the receivers for each frequency are not co-located, an error of as much as 6 dB (3 dB -(-3 dB)) can result between the upper frequency attenuation and the lower frequency attenuation. We used a 30-s moving average to remove scintillation from the rain attenuation data (explained in more detail in Section 2.2). Haidara [21] gives a detailed discussion of scintillation in the Virginia Tech OLYMPUS data.

2.1.4 Diurnal variations

A slant path propagation experiment is subject to system and equipment fluctuations, as well as to propagation effects. Some examples of system effects which are detrimental to experimental data are

- Variations in satellite power
- Changes or drifts in the receiver gain
- Water on the antenna (particularly on the feed, but also on the dish),
- Movement of the satellite in its geostationary orbit; the interaction of this motion with the earth terminal antenna pattern leads to diurnal (daily) fluctuations in the received signal.

The Virginia Tech experiment minimized these effects by the removal of diurnal variations in the preprocessing of data.

2.2 Adjusting for Sources of Attenuation

Because some of the attenuation effects vary slowly with time, the absolute reference level of beacon attenuation is difficult to determine. Thus, beacon measurements are relative, and an auxiliary measurement is needed to set a reference level. With over twenty years of experience with satellite beacon, radiometer, and radar measurements, Virginia Tech has developed hardware and data reduction techniques to a sophisticated level. In early experiments (many of which are documented in Chapter 4), beacon signals on chart recording paper or analog plots reconstructed from digital data were examined, and reference levels were set based on "quiet times" before and after propagation events (i.e., the time between events is

assumed equal to "clear air"). This early procedure does not account for clear air absorption. The approach is fairly accurate if events are on the order of hours, but where slow receiver drift and diurnal fluctuations become significant, it is inaccurate over longer periods of time.

A superior approach, used in the Virginia Tech OLYMPUS experiment, employs radiometers operating at frequencies close to the beacon receivers, to provide the auxiliary measurements needed to set an absolute reference level and to remove the diurnal spacecraft-induced fluctuations. The Virginia Tech radiometer design is unique in that it uses the RF chain of the beacon receiver. Radiometers have the advantage of not displaying scintillation behavior observed by beacon receivers. [11]

2.2.1 Radiometer Derived Attenuation (*ARD*)

The Virginia Tech experiment employs total power radiometers [12] to find the absolute reference level of the beacon signals, to remove diurnal fluctuations, and also to predict path attenuation [13]. A radiometer measures noise power, P_N in the predetection bandwidth, B. One of the advantages of the Virginia Tech experiment is the use of calibrated radiometers to determine the absolute beacon level. Stutzman, *et al.*, [13, 15] describe this process in detail. Calibration of the radiometers is of utmost importance for reference level setting, and it is accomplished by irregular hot load/cold load calibrations and regular interval noise diode /reference load calibrations. [14] Calibrations at two known temperature levels are used in preprocessing to convert the receiver output voltage to Radiometric Derived Attenuation (*ARD*).

When properly calibrated, the radiometer measures atmospheric gaseous attenuation (*AGA*) due to water vapor and oxygen in an absolute sense. *ARD* also

contains precipitation (or hydrometeor) effects, principally due to rain. When it is raining, radiometric derived attenuation is primarily due to rain because precipitation absorption dominates gaseous absorption (that is, *ARD* is dominated by precipitation absorption, not gaseous absorption, past a certain attenuation threshold, *AT*). To calculate *AT*, the sky noise temperature is assumed to be 110 K, yielding an *ARD* = AT = 2.17 dB [15]. Above the threshold *AT* (i.e., for *ARD* values smaller than *AT*), *ARD* is assumed to be dominated by *AGA*. Conversely, below the threshold *AT* (i.e., for *ARD* values greater than *AT*), *AGA* is assumed to be overwhelmed by rain attenuation and takes the value of *AT*. Consequently, the attenuation due to gaseous absorption, *AGA*, is given by the following equation [13]:

$$AGA = \begin{cases} ARD & ARD < AT \\ AT & ARD > AT \end{cases} \tag{2.2-1}$$

2.2.2 Attenuation with Respect to Free Space (*AFS*)

The radiometer measurement, though limited in dynamic range, does not contain the diurnal effects and is of the proper absolute attenuation level. For the removal of diurnal variations, a different threshold, *AT'*, is used. The threshold values are obtained from sample data on rainy days where the radiometric attenuation is associated with light rain along the path instead of gaseous absorption. Summing the beacon signal and radiometer measurement results in attenuation with respect to free space and diurnal effects. Assuming that the satellite beacon power is constant, and since free space does not vary with time, the variations in attenuation of this sum are due to diurnal effects. For periods when $AGA \leq AT'$, the diurnal variations are

estimated by sixth-order polynomial interpolation (using one minute samples of a six minute moving average) and form the curve fit signal, *SD*.

Attenuation with Respect to Free Space (*AFS*) is the dB difference between the instantaneous signal, *S*, and the free space reference level (*SFS*). *SFS* is the signal that would be received if the propagation medium were a vacuum. *SFS* is determined by using signal averaging (a moving thirty-second filter in this experiment) to remove scintillation effects (usually due to multipath enhancement or fading) and radiometer data to eliminate atmospheric absorption. The diurnal curve fit signal, *SD*, is assumed to be the free space reference level (*SFS*), and it is used as follows to derive *AFS*

$$AFS = SD - S \tag{2.2-2}$$

where *S* is the received (instantaneous) signal sampled at 10 Hz (used with the most recent six-minute *SD* value). *AFS* includes fading losses due to gaseous absorption, water vapor, clouds, scintillation, and rain. Though normally positive, it can be negative in clear weather when the signal enhancement exceeds the losses due to gases and water vapor. [15]

2.2.3 Attenuation with Respect to Clear Air (*ACA*)

Attenuation with Respect to Clear Air (*ACA*) is the dB difference between the instantaneous signal, *S*, and the clear air reference level (*SCA*).

$$ACA = S - SCA \tag{2.2-3}$$

SCA is the signal that would be received if the propagation medium were clear air. *SCA* includes scintillation, rain, and cloud effects but excludes gaseous absorption.

ACA follows directly from *AFS* by removing gaseous attenuation (*AGA*) and is also written as,

$$ACA = AFS - AGA \quad (2.2\text{-}4)$$

This definition of *ACA* is directly applicable to most satellite system design and is used for carrier level in the carrier-to-noise ratio, *C/N*, which assumes clear air conditions; in many satellite system designs, gaseous absorption losses are included in the power budget as a loss. The procedure described in Section 2.2.2 and in this section is accurate to within 0.2 dB for *ACA* and *AFS*. [13] ESA developed a similar bias removal method as part of the processing and analysis program DAPPER [16]. Vogel, *et al.*, [17] also presents a diurnal correction method.

2.2.4 *ARD*, *AFS*, and *ACA*

Data sets of attenuation with a common time base on different channels for *ARD*, *AFS*, and *ACA* are denoted for each combination of frequencies as shown in Table 2.2-1. The combinations have a common time base; that is, data points are only included in a data set if the frequencies (or channels) of interest each have valid measured data at that sample instant. Data sets of attenuation at the individual frequencies of 12, 20, and 30 GHz are also generated.

Table 2.2-1

Common Time Bases

Time Base Designation	Frequency Combination
C1	12 & 20 GHz
C2	12 & 30 GHz
C3	20 & 30 GHz
C4	12, 20, & 30 GHz

ARD, *AFS*, and *ACA* are often plotted as a percentage of time exceeded [15] (refer to Chapter 5). This type of plot allows the outage time to be easily determined; a system outage can be expressed as a system reliability in percent outage time. For example, the yearly *ACA* plot of Figure 5.2-1 (for 20 and 30 GHz) reveals that if a communications system operating at 20 GHz can handle only 26 dB of attenuation with respect to clear air, it will experience outage about 0.01 % of the time (approximately 52 minutes of the year). By way of comparison, public telephone companies usually require less than 20 minutes of outage per year. [18]

2.3 Instantaneous Attenuation Scaling

A unique aspect of the OLYMPUS experiment is the simultaneous reception of satellite signals spanning Ku-band through Ka-band for the same elevation angle. This controlled experiment yields frequency as the only system variable; that is, all potential variables (such as location, elevation angle, and azimuth angle) other than rain variables across the 12, 20, and 30 GHz frequency receivers are constant except frequency. Therefore, any differences in signal strength are due to frequency- and hydrometeor-dependent effects.

As mentioned, data sets of attenuation with a common time base are generated for the different combinations of frequencies. This assures that reliable data exist simultaneously on the frequencies of interest (hence, each channel experiences the same medium conditions), allowing for meaningful comparison and scaling.

Because rain and clear air (gaseous) effects scale differently, Attenuation with Respect to Clear Air (*ACA*) is used in attenuation ratio calculations. Since *ACA* does

not include gaseous attenuation, ACA isolates the rain component of attenuation. Thus, attenuation ratio, RA, is defined as

$$RA(f_L, f_U, t) = \frac{ACA(f_U, t)}{ACA(f_L, t)} \tag{2.3-1}$$

where f_L and f_U are the lower and upper frequencies of interest, respectively, the ACA values are in dB, and t is the sample time. In the Virginia Tech experiment, RA is computed at each instant of time t in 0.1 seconds intervals (10 Hz sample rate). ACA is accurate to within 0.2 dB, and RA typically has a potential error less than 10% but the error can become higher as ACA values become small ($\cong$ 1 dB).

In Virginia Tech's experiment, RA values are computed and archived into bins during the analysis phase of data reduction. ACA values are binned into 1-dB bins which span the following ranges:

$$\begin{aligned} 1\ dB &< ACA(12) < 16\ dB \\ 1\ dB &< ACA(20) < 35\ dB \\ 1\ dB &< ACA(30) < 35\ dB \end{aligned} \tag{2.3-2}$$

The 12 GHz receiver measures fades reliably to 16 dB; beyond 16 dB it loses frequency lock. Since frequency lock on the 20 and 30 receivers is derived from the 12 receiver, wide dynamic range is possible. The 20 and 30 GHz receivers could measure down to their noise floors (approximately 35 dB dynamic range).

Attenuation ratio (RA) is plotted both as a function of percent-time-of-occurrence and as a function of the lower frequency attenuation level . Plots are generated for various time bases (i.e., by event, by month, by year) and over various ranges (i.e., exceeding dB threshold levels and by 1 dB bins). Primary examples are given in Chapter 5 with other plots to be found in Appendix A.

It has been found that the ratio of attenuations at different frequencies is relatively independent of the level of attenuation [4]. Such results support the use of attenuation ratio *RA* as a principal quantity in frequency variation studies. If attenuation scaling is solely dependent on frequency, then *RA* would be a constant. It will be shown, however, that measured *RA* varies (i.e., is not constant) for a given pair of frequencies. Sweeney's work [5] suggests that attenuation scaling by frequency may also be level dependent or at least dependent on the drop size distribution of rain.

The studies of McGuinness, *et al.*, [19] predicted that short-term (i.e., instantaneous) attenuation ratios depend on the type of rain, and they may vary within a storm. As previously indicated, attenuation ratio can be expected to be a function of drop size distribution, as well as frequency. This variation in attenuation ratio is discussed further in Chapter 3.

2.4 Statistical Attenuation Scaling

Statistical attenuation ratio, *RAS*, is generated from separate statistics of attenuation with respect to clear air, *ACAS*, for the frequencies involved. The ratio of attenuation value is formed for the same percentage of time, p ; that is,

$$RAS(f_L, f_U, p) = \frac{ACAS(f_U, p)}{ACAS(f_L, p)} \tag{2.4-1}$$

where f_L and f_U are the lower and upper frequencies of interest, respectively, p is the percentage of time a given attenuation exceeds a threshold value, and *ACAS* values are in dB. For a common time base, values for *ACAS* are determined from the percent-time-of-occurrence plots (time exceedance plots) for *ACA* at the respective frequencies

(refer to Figures 5.2-1, 5.2-2, and 5.2-3). *RAS* is plotted both as a function of percent-time-of-occurrence and as a function of the base (lower) frequency *ACAS* values.

The instantaneous nature of attenuation scaling by frequency is not present in *RAS*. However, Figures 5.4-1 to 5.4-3 demonstrate that if statistically derived attenuation ratio, *RAS*, can be applied to individual rain events (e.g., to instantaneous attenuation ratio, *RA*). If statistical attenuation ratio can be used in place of instantaneous attenuation ratio, it permits the use of more widely available attenuation statistics in the computation of attenuation ratio for system design.

2.5 References

1. R.G. Howell, J.W. Harris, M. Mehler, "Satellite Co-Polar Measurements at BT Laboratories," *BT Tech. J.*, vol. 10, No. 4, pp. 34-51, Oct. 1992.
2. Laws, J.O. and Parsons, D.A., "The relation of raindrop size to intensity," *Trans Amer Geophys Union*, 24, pp. 452-460, 1943.
3. Olsen, R.L., Rogers, D.V., and Hodge, D.B., "The aR^b Relation in the Calculation of Rain Attenuation," *IEEE Transactions on Antennas and Propagation*, Vol. AP-26, No. 2, pp. 318-329, March 1978.
4. CCIR, "Propagation in Non-ionized Media," Recommendations and Reports of the CCIR, Report 721-2, V, 1990.
5. Sweeney, D.G., "Adaptive Power Control as a Fade Countermeasure on Satellite Links," Unpublished doctoral dissertation, Report EESATCOM 93-2, Virginia Polytechnic Institute & State University, Department of Electrical Engineering, Blacksburg, VA, January 1993, p. 62.
6. Ihara, Toshio and Furuhama, Yoji, "Frequency Scaling of Rain Attenuation at Centimeter and Millimeter Waves Using a Path-Averaged Drop Size Distribution," *Radio Science*, vol. 16, No. 6, pp. 1365-1372, Nov/Dec 1981.
7. R.G. Howell, J.W. Harris, M. Mehler, "Satellite Co-Polar Measurements at BT Laboratories," *BT Tech. J.*, vol. 10, No. 4, pp. 34-51, Oct. 1992.
8. Dintelmann, F., Ortgies, G., Rücker, and Jakoby, R., "Results From 12 to 30 GHz German Propagation Experiments Carried out with Radiometers and the

OLYMPUS Satellite," Research Centre, Deutsche Bundespost Telekom, Darmstadt, Germany, 1992, p. 8.

9. Haidara, Fatim, personal conversation, Virginia Polytechnic Institute & State University, Department of Electrical Engineering, Blacksburg, VA, March 1993.
10. H. Fukuchi, J. Awaka, T. Oguchi, "Frequency Scaling of Depolarisation at Centimetre and Millimetre Waves," *Electronics Letters*, pp. 10-11, 3 Jan. 1985.
11. Bryant, D.L., "Low elevation angle 11 GHz beacon measurements at Goonhilly earth station," *BT Technology Journal*, Vol. 10, No. 4, pp. 68-75, October 1992.
12. Allnutt R. M., "Total Power Radiometers at 12, 20 and 30 GHz Used in the OLYMPUS Experiment at Virginia Tech," Unpublished master's thesis, Virginia Polytechnic Institute & State University, Blacksburg, VA, 1991.
13. Stutzman, W.L., Haidara, F., and Remaklus, P.W., "Correction of Satellite Beacon Propagation Data Using Radiometer Measurements," Virginia Polytechnic Institute & State University, Department of Electrical Engineering, Blacksburg, VA, October 1992.
14. Bostian, C.W., "Noise Temperature Measurements," Unpublished class notes, Virginia Polytechnic Institute & State University, Department of Electrical Engineering, Blacksburg, VA, 16th April 1991 (amplified by John Musson, graduate student)
15. Stutzman, W.L., *et al.*, "Communications and propagation experiments using the OLYMPUS spacecraft - Analysis of OLYMPUS Propagation Data for the Period January to May 1991," Report EESATCOM 92-5, Virginia Polytechnic Institute & State University, Department of Electrical Engineering, Blacksburg, VA, JPL Contract No. 958435, November 1991, p. 15.
16. Koller, J., Diermaier, G., and Murr, F., "User's Requirement Document Part I: Data Preprocessing Software," European Space Agency, November 1988.
17. Vogel, W.J., Torrence, G.W., and Allnutt, J.E., "Estimating Satellite Beacon Attenuation from Radiometric Data: Error Statistics Based on Two years of Low Attenuation Angle Measurements at 11.2 GHz," *Proceedings of the International Conference on Antennas and Propagation (York)*, pp. 362-365, April 1991.
18. Engineering Consideration for Microwave Consideration Systems, GTE Lenkurt, 1972.
19. McGuiness, R.G., Holt, A.R., and Evans, B.G., "The dependency on the propagation environment of the frequency scaling of attenuation," *URSI Symp. on Wave Propagation and Remote Sensing*, ESA SP-194, 425-436, 1983 (cited in Upton, S.A.J., Holt, A.R., and Upton, G.J.G., "Some

Aspects of the Analysis of Experimental Data for Short-Term Frequency Scaling," *Int. J. of Sat. Comm.*, vol. 5, pp. 249-260, 1988).

20. CCIR, "Propagation data and prediction methods required for earth-space telecommunication systems," Report 564-4, V, 1990.

21. Haidara, Fatim, "Characterization of Tropospheric Scintillations on Earth-Space Paths in the Ku and Ka Frequency Bands Using the Results from the Virginia Tech OLYMPUS Experiment," Unpublished doctoral dissertation, Report EESATCOM 93-11, Virginia Polytechnic Institute & State University, Department of Electrical Engineering, Blacksburg, VA, May 1993.

CHAPTER 3

MODELS OF ATTENUATION SCALING BY FREQUENCY

Numerous models exist for attenuation scaling by frequency. Both theoretical models (based on derivation from theoretical principles) and empirical models (based on measurements) as well as hybrid models are in use. Models which contain any empirical elements usually employ parameter values determined by comparison with statistical data, and as such, their primary application is in the prediction of statistical behavior. However, as seen in Section 3.3, models primarily intended for statistical scaling (long term) can also be useful in instantaneous scaling (short-term).

3.1 General Discussion of Attenuation

Attenuation on an earth-space link generally depends on system parameters and medium parameters. Attenuation caused by the system results from parameters such as the operating frequency f, elevation angle ε, and tilt angle τ. Attenuation, A, due to the medium can be related to parameters such as effective path length, L_e, (through rain), drop-size distribution, N_o, raindrop cross-section, Q, depolarization loss, q, and refractive indices in the atmosphere, η. Thus,

$$A \equiv A(f, \varepsilon, \tau; L_e, N_o, Q, q, \eta, \ldots) \tag{3.1-1}$$

At the higher frequencies above 12 GHz rain is responsible for most of the attenuation, and so most of the other effects can be ignored. Above a certain level of attenuation (about 1 dB), most variables can be considered clamped except the system parameters

and the rain parameters, leaving attenuation A a function solely of system parameters and rain.

The beacon receivers operating at 12, 20, and 30 GHz in the Blacksburg experiment have the same system parameters. That is, they are closely located (i.e., within a few meters of each other, though not co-located), have the same elevation and azimuth angles to the satellite, and are operating simultaneously. In addition, the antenna beamwidths are similar. Thus, frequency is the only system variable, and frequency dependence of attenuation can be extracted with confidence.

It is noted , though, that the terminal separations of a few meters does lead to some decorrelation of scintillations. In the Virginia Tech experiment, the scintillations are assumed to be averaged out by implementing a 30-s moving average on the data. For 10 Hz sampling rate, a 30-s moving average takes the average of 300 consecutive sample points (at 10 Hz sample rate), resulting in a 30-s averaged attenuation, $A_{30-s\ ave}$ as follows:

$$A_{30-s\ ave}(t_i) = \frac{1}{300} \sum_{j=i-150}^{i+150} A(t_j) \tag{3.1-2}$$

where t_i is the sample time and i is an index.

3.2 Statistical Attenuation Scaling Models

Researchers have proposed many relationships to scale long term attenuation statistics, each with its own applications and limitations [1, 2]. Most of these relations are intended for scaling attenuation statistics (that is, for calculating *RAS*), and not for instantaneous (real time) scaling of attenuation.

3.2.1 Ratio models (Statistical Attenuation Ratio - *RAS*)

The statistical attenuation ratio, *RAS*, also referred to as a scaling ratio, is defined in (2.4-1) as the ratio of statistical attenuation with respect to clear air values, *ACAS*, for a given pair of frequencies at the same percentage time of occurrence, p. Equation (2.4-1) is repeated here for convenience.

$$RAS(f_L, f_U, p) = \frac{ACAS(f_U, p)}{ACAS(f_L, p)} \tag{3.2-1}$$

A ratio model is one where the relationship between upper frequency attenuation and base frequency attenuation (i.e., $A(f_U)$ and $A(f_L)$) can be expressed in a strict ratio form. Ratio models predict scaling ratios such as *RAS*. The following models have been proposed to predict *RAS* behavior.

3.2.1.1 *RAS* Models as a Function of Frequency Alone

Many models for *RAS* include an explicit dependence on frequency. Of course, such a relationship yields a constant value for *RAS* when frequency values are inserted.

3.2.1.1.1 The CCIR model

The statistical scaling ratio given by the CCIR [2] is widely used; it is

$$RAS_{CCIR} = \frac{A(f_U)}{A(f_L)} = \frac{\phi(f_U)}{\phi(f_L)} \qquad \text{where} \quad \phi(f) = \frac{f^{1.72}}{1 + 3 * 10^{-7} f^{3.44}} \tag{3.2-2}$$

where $A(f_U)$ and $A(f_L)$ are attenuations in dB at frequencies f_U and f_L in GHz. This results in the constant scaling ratios shown in Table 3.2-1.

Table 3.2-1

CCIR Attenuation Scaling Ratios - *RAS* (Based on Exact OLYMPUS Frequencies)

Frequency pairs f_U / f_L [GHz/GHz]	30/20	20/12	30/12
RAS_{CCIR}	1.96	2.19	4.28

3.2.1.1.2 Power scaling law

A frequently employed scaling formula is the power law model, RAS_n:

$$RAS_n = \frac{A(f_u)}{A(f_L)} = \left(\frac{f_U}{f_L}\right)^n \tag{3.2-3}$$

Ro (1973) and Drufuca (1974) [3] propose $n=1.72$ for frequencies between 11.2 and 18.7 GHz. A value of $n=2$ is often employed for frequencies above about 20 GHz. Owolabi and Ajayi (1980) (cited in [3]) examined the specific attenuation for a Laws and Parsons drop size distribution, and they found that an $(f_U / f_L)^n$ relation holds over the range 10-20 GHz for $n = 2$. They found a trend of decreasing n with increasing rain rate.

3.2.1.1.3 Method of Battesti

One of the simplest and most direct methods for statistical attenuation scaling by frequency for terrestrial links is proposed by Battesti (1981) [3]. His expressions were

found by examining specific attenuations computed for spatially uniform rain of typical drop size distribution (DSD). He presented the following approximate relations:

$$\frac{A(f_u)}{A(f_L)} = \frac{f_U - 6}{f_L - 6} \qquad \text{for } f_L, f_U \leq 20 \text{ GHz} \tag{3.2-4}$$

$$\frac{A(f_u)}{A(f_L)} = \frac{f_U - 10}{f_L - 10} \qquad \text{for } f_L, f_U \geq 20 \text{ GHz} \tag{3.2-5}$$

If $f_L < 20$ GHz and $f_U > 20$ GHz, then one proceeds first from frequency f_1 to f_x by means of (3.2-4), and then from f_x to f_U by means of (3.2-5). Therefore, setting f_x=20 GHz,

$$\frac{A(f_U)}{A(f_L)} = 1.4\frac{f_U - 10}{f_L - 6} \qquad f_L < 20 \text{ GHz}, \quad f_U > 20 \text{ GHz} \tag{3.2-6}$$

3.2.1.2 *RAS* from Attenuation Models

Other models do not include an explicit dependence on frequency, but stem from attenuation models. These attenuation models yield attenuation values which can form a ratio to predict *RAS* for a given pair of frequencies.

3.2.1.2.1 Attenuation with Respect to Clear Air (*ACA*)

As discussed in Chapter 2, statistical attenuation ratio (*RAS*) is generated from the statistical distributions of measured attenuation with respect to clear air, *ACAS*, of the frequencies to be scaled at the same levels of occurrence. For example, the ratio from (3.2-1) using two of the OLYMPUS frequencies would be

$$RAS(30/20,\ 1\%) = \frac{ACAS(30,\ 1\%)}{ACAS(20,\ 1\%)} \tag{3.2-7}$$

where $RAS(30/20,\ 1\%)$ exceeds its calculated value for only 1 % of the time. Values for $ACAS$ are determined from the percent-time-of-occurrence plots (percentage of time exceeded plots) for ACA at the respective frequencies (refer to Figures 5.4-1 to 5.4-3 for OLYMPUS results). RAS is plotted both as a function of percent-time-of-occurrence and as a function of the base (lower) frequency $ACAS$ values.

A major disadvantage of such a totally empirical model is that it (without other proof) is applicable only to the same frequency pair.

3.2.1.2.2 Method of Inferred Size Distribution (MISD)

One of the problems of attenuation scaling by frequency is that the drop size distribution (DSD) can vary widely, even during a single rain event. Nevertheless, many analytic models exist for DSD. The method of inferred size distribution (MISD) [9] attempts to by-pass this problem by employing the concept of a path-averaged drop size distribution. Attenuation at a desired frequency is derived from the path-averaged drop size distribution which is inferred from rain attenuations measured at several frequencies. The MISD method has been successfully applied to scaling time-sequential data.

The MISD method can be derived as follows. Instantaneous rain attenuation $A_{MISD}(f)$ at frequency f is given by

$$A_{MISD}(f) = c\int_0^L \int_0^{D_m} Q_t(D,f)N(D,z)dDdz \tag{3.2-8}$$

where c is constant, $Q_t(D,f)$ is the total cross section for a spherical raindrop with diameter D, $N(D,z)$ is the drop size distribution at location z, L is the total rain path

length, and D_m is the maximum raindrop diameter. The path-averaged drop size distribution $\overline{N}(D)$ is defined as

$$\overline{N}(D) \equiv \frac{1}{L}\int_0^L N(D,z)dz \tag{3.2-9}$$

so that

$$A_{MISD}(f) = cL\int_0^{D_m} Q_t(D,f)\overline{N}(D)dD \tag{3.2-10}$$

This is the basic equation for MISD. Since $Q_t(D,f)$ is a known function, $\overline{N}(D)$ is determined numerically. Instantaneous values for $\overline{N}(D)$ can be found for instantaneous values of $A_{MISD}(f)$, and in the same way, statistical values of $\overline{N}(D)$ can be defined in every percentage of time for equiprobability values of $A_{MISD}(f)$. Once $\overline{N}(D)$ is determined (by numerical analysis), $A_{MISD}(f)$ at any other frequency can be calculated directly, because $Q_t(D,f)$ is a known function of D and f and because c, L, and D_m are given parameters.

Assuming a trial function of $\overline{N}(D)$:

$$\overline{N}(D) = N_o e^{-\Gamma D} \tag{3.2-11}$$

where N_o and Γ are unknown parameters, $A(f)$ can be written as

$$A_{MISD}(f) = cLN_o h(\Gamma,f) \tag{3.2-12a}$$

where

$$h(\Gamma,f) = \int_0^{D_m} Q_t(D,f)e^{-\Gamma D}dD \tag{3.2-12b}$$

The above equation is calculated numerically for the equiprobability values of rain attenuation at different frequencies. N_o and Γ are then determined in order to minimize the quantity Q defined by

$$Q \equiv \sum_{i=1}^{N}\left\{\left[A_{MISD}(f_i) - cLN_o h(\Gamma,f_i)\right]/\varepsilon_i\right\}^2 \tag{3.2-13}$$

where $\varepsilon_i (i = 1,\cdots,N)$ are measurement errors.

Inferring a path-averaged rain rate is another application of MISD. The rain rate $R(z)$ as a function of position z is related to $N(D,z)$ by

$$R(z) = \int_0^{D_m} \frac{4\pi}{3}\left(\frac{D}{2}\right)^3 v(D)N(D,z)dD \tag{3.2-14}$$

where $v(D)$ is the fall velocity of a raindrop with diameter D from Gunn and Kinzer, (1949) [10]. Path-averaged rain rate is defined as

$$\overline{R} \equiv \frac{1}{L}\int_0^L R(z)dz \tag{3.2-15a}$$

using (3.2-14) in (3.2-15a) given the basic relation between $\overline{R}$ and $\overline{N}(D)$:

$$\overline{R} = \int_0^{D_m} \frac{4\pi}{3}\left(\frac{D}{2}\right)^3 v(D)\overline{N}(D)dD \tag{3.2-15b}$$

Attenuation values derived by the MISD can form a ratio to yield an *RAS* model.

$$RAS_{MISD} = \frac{A_{MISD}(f_U)}{A_{MISD}(f_L)} \tag{3.2-16}$$

3.2.1.2.3 Simple Attenuation Model (SAM)

Stutzman and Dishman [11] developed the simple attenuation model (SAM) for earth-space links by examining the spatial nature of rain and finding an exponential rain rate profile. Stutzman and Yon [12] improved the model by taking into account the non-spherical shape of raindrops. SAM gives attenuation as

$$A_{SAM}(R) = \begin{cases} aR^b L & R \le 10mm/h \\ aR^b \left[\dfrac{1 - \exp\left[-\gamma b \ln(\dfrac{R}{10}) L \cos\varepsilon \right]}{\gamma b \ln\left(\dfrac{R}{10}\right) \cos\varepsilon} \right] & R > 10mm/h \end{cases} \quad (3.2\text{-}17)$$

where A_{SAM} is the attenuation (dB), R is the rain rate (mm/h), L is the path length (km), a and b are coefficients which include DSD, ε is elevation angle, $\gamma = 1/14$, and .

$$L = \frac{H_e - H_o}{\sin\varepsilon} \quad (3.2\text{-}18a)$$

$$H_e = \begin{cases} H_i & R \le 10mm/hr \\ H_i + \log(R/10) & R > 10mm/hr \end{cases} \quad (3.2\text{-}18b)$$

$$H_i = \begin{cases} 4.8 & |\Gamma| \le 30^o \\ 7.8 - 0.1|\Gamma| & |\Gamma| > 30^o \end{cases} \quad (3.2\text{-}18c)$$

where Γ is the latitude of the earth station in degrees.

The empirical constant γ in the model was found by a best fit to 36 data sets from around the world. The a and b coefficients are found from

$$\begin{aligned} a &= \left[a_H + a_V + (a_H - a_V)\cos^2\varepsilon \ \cos 2\tau \right] \\ b &= \left[a_H b_H + a_V b_V + (a_H b_H - a_V b_V)\cos^2\varepsilon \ \cos 2\tau \right] / 2a \end{aligned} \quad (3.2\text{-}19)$$

where a_H, a_V, b_H, and b_V are obtained from available tables [13] and τ is the tilt angle.

Attenuation values derived by SAM can form a ratio to yield an *RAS* model

$$RAS_{SAM} = \frac{A_{SAM}(f_U)}{A_{SAM}(f_L)} \quad (3.2\text{-}16)$$

3.2.2 Non-ratio models

A non-ratio model is one where the relationship between upper frequency attenuation and base frequency attenuation (i.e., $A(f_U)$ and $A(f_L)$) cannot be expressed in a strict ratio form. Ratio models predict ratios such as *RA* and *RAS*. Non-ratio models do not predict *RA* or *RAS* but quantify the relationship between $A(f_U)$ and $A(f_L)$ in other ways.

3.2.2.1 Models for Scaling from One Frequency

3.2.2.1.1 CCIR model

Experimental data indicates that scaling ratio can depend on the level of attenuation at the base frequency [4]. An approximation which accounts for base frequency attenuation is given by Fedi, *et al.* [5, 6]

$$A_2 = 4k_2\left(\frac{A_1}{4k_1}\right)^{\frac{a_2}{a_1}} \tag{3.2-21}$$

where k and a are constants that depend on frequency and drop-size-distribution (DSD) and are tabulated by Fedi and his colleagues [5, 6]. Equation (3.2-21) assumes a constant path length of 4 km. The formula yields good results for frequencies below 60 GHz.

To remove the DSD-dependence inherent in k and a, Boithias [1] proposed a non-ratio empirical expression for a scaling factor which yields attenuation ratio directly as a function of frequency and attenuation as follows:

$$A_2 = A_1\left(\frac{\varphi_2}{\varphi_1}\right)^{1-H(\varphi_1,\varphi_2,A_1)} \tag{3.2-22a}$$

$$\varphi(f) = \frac{f^2}{1+10^{-4}f^2} \tag{3.2-22b}$$

$$H(\varphi_1,\varphi_2,A_1) = 1.12\times 10^{-3}\left(\frac{\varphi_2}{\varphi_1}\right)^{0.5}(\varphi_1 A_1)^{0.55} \tag{3.2-22c}$$

where frequency f is in GHz.

3.2.2.1.2 Method of Kheirallah

The technique of Kheirallah, *et al.*, [7] uses the specific attenuation, α, relation formulated by Olsen, Rogers, and Hodge [8] (discussed in Sections 3.3.2.1 and 3.3.2.2):

$$A = \alpha L_e = aR^b L_e \tag{3.2-23}$$

where α is the specific attenuation (dB/km), R is the rain rate (mm/h), a and b are tabulated parameters dependent on frequency and DSD, L_e (km) is the effective path length through the rain, and represents frequency.

Assuming that the two frequencies under consideration are coincident (looking through the same path, so that R and L_e can be assumed to be the same) the scaling relation is

$$A_2 \approx a_2\left(A_1 / a_1\right)^{b_2/b_1} \tag{3.2-24}$$

3.2.2.1.3 Hodge model

Hodge (1977) [3] assumed that the point rain rate along the propagation path could be expressed as a Gaussian function of position. Therefore, the instantaneous attenuation could be formulated as

$$A = \int_0^L aR(x)^b dx \qquad \text{where } R(x) = R_o e^{-(x/l_o)^2} \tag{3.2-25}$$

R_o is the peak rain rate along the path L. The distance x is measured from the position of maximum rain rate intensity, and $l_o >> L$ is a measure of the cellular rain structure. Under these conditions, the attenuation ratio for frequencies f_1 and f_2 is given by Hodge as follows:

$$\frac{A_2}{A_1} = \frac{k_2}{k_1}\sqrt{\frac{\alpha_1}{\alpha_2}}\left\{\frac{A_1}{k_1}\sqrt{\frac{\alpha_1}{\pi}}\right\}^{\left(\frac{\alpha_2}{\alpha_1}-1\right)} \tag{3.2-26}$$

where α_1, k_1, α_2, and k_2 are parameters associated with frequencies f_1 and f_2, respectively. Note that Hodge's model is not a strict ratio relationship because A_2 / A_1 is a function of A_1.

3.2.2.1.4 Rue model

Misme and Fimbel (1975) [3] presented a method for calculating rain attenuation statistics based on log-normal approximation to the cumulative rain rate distribution. Their model assumed rain to consist of an intense, compact core of constant rain rate surrounded by a much larger area of very light "residual" rain. Rue (1977) [3] simplified the Misme-Fimbel model and produced

$$A_2 = k_2 R_{res}^{\alpha_2} D + k_2 d \left\{ \frac{A_1 - k_1 R_{res}^{\alpha_1} D}{k_1 d} \right\}^{\alpha_2/\alpha_1} \quad (3.2\text{-}27)$$

where d is the diameter of the idealized, cylindrical rain core (assumed to be 3.0 km), R_{res} is the residual rate of 5 mm/h (Rue, 1980), and D is the lesser of 27 km and L - 3.0 km, where L is the path length through rain. The Misme-Fimbel model is most applicable to high rain rates (e.g., rain rates ≥ 20 mm/h).

3.2.2.2 Models for Scaling from Two Frequencies

Most models assume that attenuation at one frequency is being used to scale to attenuation at another frequency. Some evidence exists, however, to support the use of two attenuations at two frequencies to scale to attenuation at a third frequency in order to achieve greater accuracy [14]. Two frequency scaling models generally can be categorized as either linear or nonlinear.

3.2.2.2.1 Linear scaling

A linear scaling model based on attenuation at two different frequencies f_2 and f_1 has the form

$$\hat{A}_3 = \alpha + \beta A_2 + \gamma A_1 \quad (3.2\text{-}28)$$

where $\hat{A}_3$ is the estimate of attenuation at frequency f_3, and A_2, and A_1 are attenuations, usually measured, at frequencies f_2 and f_1. β and γ are the scaling coefficients, and α is the offset.

3.2.2.2.2 Nonlinear scaling

An example of a non-linear two frequency scaling relation is the following technique of Hogg [15]:

$$\hat{A}_3 = a_3 \left(\frac{A_1}{a_1} \right)^{\frac{b_3 - b_2}{b_1 - b_2}} \left(\frac{A_2}{a_2} \right)^{\frac{b_1 - b_3}{b_1 - b_2}} \qquad \text{(dB)} \tag{3.2-29}$$

where a_i, b_i, and c_i are parameters associated with frequency f_i. The following approximations were used to obtain (3.2-29):

$$\left(\frac{L_{e2}}{L_{e1}} \right)^{1 - b_3 b_2} \approx 1 \tag{3.2-30a}$$

$$\left(\frac{L_{e2}}{L_{e1}} \right)^{b_1 b_2 - 1} \approx 1 \tag{3.2-30b}$$

and

$$\left(\frac{L_{e2}}{L_{e1}} \right)^{(b_3 b_2 - 1)(b_1 - b_2)(b_1 - b_3)} \approx 1 \tag{3.2-30c}$$

Hogg assumed implicitly that $L_{e2} \approx L_{e1}$. The effective path length L_e, cancels out implying no frequency dependence. In general, however, L_e is a function of frequency.

Equation (3.2-29) can be expressed in general form as

$$\hat{A}_3 = c\, A_2^a\, A_1^b \qquad \text{(dB)} \tag{3.2-31}$$

3.3 Instantaneous Attenuation Scaling Models

3.3.1 Ratio models (Instantaneous Attenuation Ratio- *RA*)

Instantaneous attenuation ratio, *RA*, is the quotient of attenuation with respect to clear air (*ACA*) at an upper frequency and *ACA* at a base frequency as given in (2.3-1). Virtually no models have been proposed to predict *RA*. Most research has focused on *RAS*, instead of *RA*.

3.3.2 Non-ratio models

3.3.2.1 Hysteresis Effect

Figure 3.3-1 is a plot of measured *ACA* at 30 GHz versus measured *ACA* at 20 GHz for a rain event on the 5th/6th November 1990. Referring to Figure 3.3-1, Sweeney [18] notes that this attenuation plot forms a loop. It underestimates the CCIR relation of (3.2-2) (a straight line in this example) prior to reaching an attenuation maximum and then closely follows the CCIR relation after reaching the attenuation maximum. The straight lines labeled MP DSD and J-T DSD correspond to attenuation predicted using (3.2-23) where the drop sized distribution (DSD) is assumed to be Marshall-Palmer (MP) and Joss-"thunderstorm" (J-T), respectively. None of the various ratio relations between attenuations previously examined explain the hysteresis effect in scaling ratio that has been observed during some events [4, 16, 17].

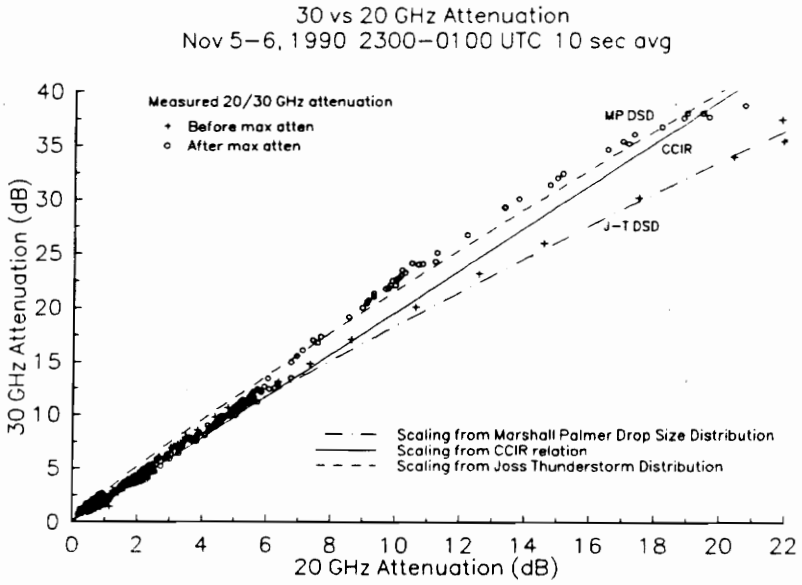

Figure 3.3-1 ACA30 vs. ACA20 plotted with various scaling relations, 5th/6th Nov. 1990

Sweeney, Pratt, and Bostian [4] attribute this hysteresis behavior to changes in the drop size distribution (DSD) during an event. Thunderstorm rain tends to have more large drops than a uniform (stratiform) rain with the same rain rate (in the Virginia Tech experiment, rain rate is found from a tipping bucket rain gauge which records the time between tips). Sweeney [18] calculated the specific attenuation using $\alpha = aR^b$ of (3.2-23), where α is the specific attenuation (dB/km), R is the rain rate (mm/h), and a and b are parameters tabulated by Olsen, Rogers, and Hodge [8]. Sweeney found that the coefficients a and b for the "Thunderstorm" drop size distribution of Joss , J-T, [19] (describing heavy thunderstorm rain) produced a curve in Figure 3.3-1 which fit well with the leading portion of the event (prior to attenuation maximum) while coefficients a and b for the Marshall-Palmer, MP, drop size distribution (describing uniform rain) produced a curve which fit well with the trailing portion of the event. At lower base frequency attenuation levels (in this example, for ACA20 $<$ 6 dB), both distributions predict scaling ratios very close to that of the CCIR relation of (3.2-2). In addition, the hysteresis effect was not observed for less intense events (such as widespread stratiform rain where the peak attenuation does not exceed 4 dB at 20 GHz).

Because, drop size distribution varies greatly from event to event, specific attenuation (often obtained from radar reflectivity measurements) exhibits wide variation. Battan [20] lists sixty-nine different relationships developed from radar measurements by researchers from around the world from 1947 to 1970.

A varying scaling ratio complicates the use of a simple scaling relation to drive a fade countermeasure. However, because the effect does not appear at lower attenuations, a simple scaling relation might be successfully implemented at lower levels. Since most proposed fade countermeasures only compensate for about 10 dB of

uplink fade at 30 GHz (corresponding to a 6 dB fade at 20 GHz), a simple attenuation controller could be implemented for ULPC if the dynamic range of attenuation at 30 GHz is limited to approximately 10 dB [18].

This hysteresis effect is important to attenuation scaling because it means that attenuation does not scale simply by a constant value. Other factors beside frequency (such as DSD) affect attenuation.

3.3.2.2 Possible Models

As with ratio instantaneous scaling, virtually no non-ratio models have been proposed to quantify the instantaneous relationship between upper frequency attenuation and base frequency attenuation. In Section 6.3 non-ratio Virginia Tech models are proposed to quantify this instantaneous relationship to predict upper frequency attenuation from base frequency attenuation. These are empirical models based on Virginia Tech's OLYMPUS data.

3.4 Elevation Angle Scaling of Attenuation

Since statistics exist from previous experiments with other satellites (see Chapter 4), one can scale attenuation at one frequency and elevation angle to attenuation at the same frequency but differing elevation angle. For example, the Virginia Tech OLYMPUS results can be compared with the Virginia Tech SIRIO satellite measurements (same frequencies; different elevation angles).

For elevation angle $\theta > 10°$, total attenuation A is given by [21]

$$A = \frac{F(f)}{\sin\theta} \tag{3.5-1}$$

where $F(f)$ is a lengthy function of frequency only. For a fixed frequency, it follows from (3.5-1) that attenuation scales with elevation angle as

$$\frac{A(\theta_2)}{A(\theta_1)} = \frac{\sin\theta_1}{\sin\theta_2} \tag{3.5-2}$$

Coupled with the frequency scaling techniques in this report, attenuation data at one frequency and elevation angle can be scaled to a different frequency and elevation angle.

For example, since the Blacksburg/OLYMPUS link has a low elevation angle of 14°, the elevation angle scaling model of (3.5-1) allows the direct application of Blackburg measured data at other elevation angles operating at the same frequencies.

3.5 References

1. Boithias, Lucien, "Similitue en frequence pour l'affaiblissement par la pluie," *Ann. Telecommun.*, 44, No. 3-4, 1986, pp.186-191 (cited in Sweeney, D.G., "Adaptive Power Control as a Fade Countermeasure on Satellite Links," Unpublished doctoral dissertation, Report EESATCOM 93-2, Virginia Polytechnic Institute & State University, Department of Electrical Engineering, Blacksburg, VA, January 1993, p. 53).
2. "Attenuation by Hydrometeors, in Precipitation, and Other Atmospheric Particles," CCIR Report 721-3, *Propagation in Non-Ionized Media*, Vol. 5, ITU, Geneva, 1990.
3. Cited in Segal, B., "Rain Attenuation Statistics for Terrestrial Microwave Links in Canada," Communications Research Centre Report No. 1351-E, Ottawa, Canada, January 1982, p. 14.

4. Sweeney, D.G., Pratt, T., and Bostian, C.W., "Hysteresis Effects in Instantaneous Frequency Scaling of Attenuation on 20 and 30 GHz Satellite Links," *Electronic Letters*, 2nd January 1992, Vol. 28, No. 1.
5. Fedi, F., "A simple procedure for frequency scaling of rain attenuation," Fondazione Ugo Bordoni, Report 1B1680.
6. Barbaliscia, F., Fedi, F., Maggiori, D., and Migliorini, P., "Frequency scaling of rain induced attenuation at 11, 18, and 30 GHz, *Ann. des Télécomm.*, Vol. 35, **11-12**, 1980, pp. 450-455.
7. Kheirallah, H.N., Knight, J.P., Olsen, R.L., McCormick, K.S., and Segal, B., "Frequency dependence of effective path length in prediction of rain attenuation statistics," *Electronic Letters*, 1980, **16**, pp. 448-450.
8. Olsen, R.L., Rodgers, D.V., and Hodge, D.B., "The aR^b Relation in the Calculation of Rain Attenuation," *IEEE Transactions on Antennas and Propagation*, Vol. AP-26, No. 2, March 1978, pp. 318-329.
9. Ihara, Toshio and Furuhama, Yoji, "Frequency Scaling of Rain Attenuation at Centimeter and Millimeter Waves Using a Path-Averaged Drop Size Distribution," *Radio Science*, vol. 16, No. 6, pp. 1365-1372, Nov/Dec 1981.
10. Gunn, K.L.S. and Kinzer, G.D., "The terminal velocity of fall for water droplets in stagnant air," *J. Meterol., 16,* 1949, p.243.
11. Stutzman, W.L. and Dishman, W.K., "A simple model for the estimation of rain-induced attenuation along earth-space paths at millimeter wavelengths," *Radio Science*, vol. 17, pp. 1465-1476, Nov/Dec 1982.
12. Stutzman, W.L. and Yon, K.M., "A simple rain attenuation model for earth-space radio links operating at 10-35 GHz," *Radio Science*, vol. 21, pp. 65-72, Jan/Feb 1986.
13. Stutzman, W.L., "Signal Power Calculation Procedures for Communication Systems," Unpublished class notes, Virginia Polytechnic Institute & State University, Department of Electrical Engineering, Blacksburg, VA, September 1991, p. 14.
14. Kheirallah, H.N., and Olsen, R.L., "Comparison on one- and two-frequency techniques of frequency scaling of rain attenuation statistics," *Electronic Letters*. Vol. 18, No. 2, 21, January 1982, pp. 51-53.
15. Hogg, D.C., "Intensity and extent of rain on earth-space paths," *Nature*, 1973, **243**,pp. 337-338.
16. Ortgies, G., Rucker, F., and Dintelmann, F., "Some Aspects of Attenuation Frequency Scaling," *Proceedings of the URSI Commission F Symposium of Microwave Propagation*, London, Ontario, Canada, June 1991, p.450.
17. Dintelmann, F., Ortgies, G., Rücker, and Jakoby, R., "Results From 12 to 30 GHz German Propagation Experiments Carried out with Radiometers and the OLYMPUS Satellite," Research Centre, Deutsche Bundespost Telekom, Darmstadt, Germany, 1992.

18. Sweeney, D.G., "Adaptive Power Control as a Fade Countermeasure on Satellite Links," Unpublished doctoral dissertation, Report EESATCOM 93-2, Virginia Polytechnic Institute & State University, Department of Electrical Engineering, Blacksburg, VA, January 1993.
19. Joss, J., Thams, J.C., and Waldvogel, A., "The variation of raindrop size distributions at Locarno," *Proceedings of the International Conference on Cloud Physics*, 1968, pp. 369-373.
20. Battan, L.J., Radar Observation of the Atmosphere, The University of Chicago Press, Chicago, 1973, pp. 90-92 (cited in Sweeney, D.G., "Adaptive Power Control as a Fade Countermeasure on Satellite Links," Unpublished doctoral dissertation, Report EESATCOM 93-2, Virginia Polytechnic Institute & State University, Department of Electrical Engineering, Blacksburg, VA, January 1993, p. 57).
21. CCIR, "Propagation in Non-ionized Media," Recommendations and Reports of the CCIR, Report 721-3, V, 1990.

CHAPTER 4

A REVIEW OF PRIOR SLANT PATH EXPERIMENTS

Several experiments have been performed in the Ku/Ka bands, but most data are near 12 GHz. This chapter summarizes some of the work which precedes OLYMPUS and the Virginia Tech experiment. European OLYMPUS research results are included in as much as they are available. The Ku/Ka-band experiments described are summarized in Table 4.1-1 on the following page.

4.1 Japanese Experiments

4.1.1 CS (SAKURA) satellite test

The 30/20 GHz Japanese CS satellite was launched in December 1977 by the Japanese Ministry of Post and Telecommunications in association with Nippon Telegraph and Telephone Public Corporation (NTT) [1]. This test satellite notably carried the first 30/20 GHz transponders. Kosaka [2] scaled the downlink attenuation by a factor of two in order to obtain an estimate for uplink attenuation. The actual scaling value derived from measurements (equivalent to *RA*) varied from two, but Kosaka reported no significant numerical measure of error. The test program ended in 1985.

Table 4.1-1

Overview of Various Ku/Ka-Band Experiments

Country	Satellite or path	Frequency (GHz)	Elev. angle	Researchers	Comments
Japan	CS	20 & 30	48°	Kosaka [2]	*RA* = 2 w/ variation
"	CS & BSE	12, 14, 20, 30	48°, 37°	Kozu [3]	Disagree w/MP DSD
"	terrestrial path	11.5, 34.5, 81.8	--	Ihara [5]	Validation of MISD
Britain	ATS 6	20 & 30	22.7°	Upton [7]	Variation in *RA*
"	OTS	11.6, 11.8, 14.5	29.9°	Upton [7]	Discuss data aver.
"	INTELSAT V	11.2, 11.5, 14.3	8.3-11.8°	Howell [6]	Wide variation in *RA*
"	OLYMPUS	12, 20, 30	27.5°	BT Labs [9]	Wide variation in *RA*
"	INTELSAT	11.198	3.3°	Bryant [11]	Quantifying scint.
U.S.A.	ATS 6	20 & 30	not given	Altshuler [13]	Quant. varied *RA*
"	INTELSAT V	11.2, 11.5, 14.3	38.1°	COMSAT [14]	ULPC study
	INTELSAT V	11.198	5.8°	Vogel [36]	Attenuation statistics
"	OLYMPUS	12, 20, 30	13.9°	Stutzman [32]	*RAS* & *RA* correlate
Germany	OLYMPUS	12, 20, 30	27°	Ortgies [19]	Hysteresis effect
Italy	SIRIO	11.6 & 17.8	not given	Paraboni [22]	$n=2$ power law
Canada	terrestrial path	11-17	--	Butler [25]	Variation in *RA*
"	terrestrial path	11-30	--	Segal [26]	Validate Hodge
India	terrestrial path	11, 18, & 22.2	--	Raina [27]	Agree w/ square-law
Australia	INTELSAT	11.6, 19.5, 28.5	63°	J. Cook U. [28]	Corr. w/ Boithias

4.1.2 CS and BSE experiment

Kozu, Fukuchi, and Nakamara [3] measured attenuation at 12, 14, 20, and 30 GHz from the Communication Satellite (CS) and the Broadcasting Satellite for Experimental Purposes (BSE) for ten rainfall events from 1979 to 1981. They measured drop size distribution (DSD) by use of a disdrometer and found disagreement with theoretical predictions based on the Marshall and Palmer. They also found that attenuation ratio (*RA*) varies widely from event to event. They set the reference level by using clear sky data before and after an event, thereby ignoring gaseous attenuation. They also maintain that drop size distribution measured on the ground is useful in improving the accuracy of frequency scaling [4].

4.1.3 Radio Research Laboratories

Ihara and Furuhama [5] examined the applicability of rain attenuation scaling models to cumulative distributions of rain attenuations at 81.8, 34.5, and 11.5 GHz measured in the same horizontal propagation path of 1.3 km for 1 year. They applied the method of an inferred size distribution (MISD) which employs the concept of a path-averaged raindrop size distribution. They concluded that MISD yields good results.

4.2 British Experiments

4.2.1 British Telecom (BT) Laboratories

British Telecom (BT) Laboratories, Martlesham Heath, near Ipswich, carried out four major satellite slant-path propagation measurement programs between 1975 and 1991. The BT Laboratories measurement complex is described in a published paper [6]. BT Labs sample all satellite data at a 2 Hz rate, and utilized radiometer measurements to reference measured attenuation data to a vacuum, thus producing *AFS*.

4.2.1.1 ATS-6

Measurements of the linearly polarized 20 and 30 GHz beacons of the NASA ATS-6 satellite were taken between 4 August 1975 and 9 July 1976. The path elevation was 22.7°. Though signal levels were continuously monitored, only attenuation during propagation events was included in the data base; this reduced data base comprises 20 events totaling about 24 hours.

4.2.1.2 OTS

Data from the European Space Agency's Orbital Test Satellite (OTS) were collected from 21 June 1978 to 31 December 1981, with a path elevation of 29.9°, at frequencies of 11.6, 11.8, and 14.5 GHz. One hundred twenty-nine events comprise the OTS data base, totaling about 89 hours.

Upton, Holt, and Upton [7] analyzed over one hundred hours of half-second sampled event data from the British Telecom data base for the OTS and AT-6 satellites and calculated *RA*. They concluded that *RA* is particularly vulnerable to system effects and noise and that appreciable variation occurs in the mean value of the short-term (instantaneous) ratio from event to event. Tables are given quantifying the maximum, minimum, and mean attenuation and standard deviation for various events. They also examined scaling results at different threshold values (i.e., where the attenuation at the lower frequency exceeds a threshold dB level -- say 1 dB or 2 dB). They found that attenuation ratio rarely differs once an attenuation level of 3 dB has been reached (that is, it remains fairly constant for attenuations above 3 dB).

Because of unexplained random variations and because of considerable round-off errors, Upton, Holt, and Upton maintain that a least squares analysis of upper frequency attenuation versus lower frequency attenuation is not suitable for short time periods (on the order of a few minutes). They recommend minimizing the sum of the squares of the distances between the observed points and the fitted regression line, working in a direction orthogonal to the fitted line (and not parallel to an axis). They also found considerable differences in ratios obtained using different minimization procedures. Their results suggest that one needs to take block averages of 10 minute or longer intervals before the choice of block size becomes negligible. This presents a problem because, in taking 10 minute moving averages, the fine structure of the storm is lost. Though they conclude that the least-squares fitting method is unsatisfactory for short time periods, they adopt the method of least squares for entire events. For short-term scaling, they recommend a moving average of 30 s to 1 minute to smooth out the rapid fluctuations caused by scintillations and then the formation of "instantaneous" ratios based on each average sample (similarly, in the Virginia Tech experiment, a

thirty-second moving average is applied to 10 Hz data). Upton, Holt, and Upton state that such smoothing does not change attenuation ratio.

Another experimenter, Thirwell, in his comprehensive review of analysis and prediction methods for long-term ratios (i.e., statistical scaling), includes a discussion on mean event ratios for the BT data sets [8].

4.2.1.3 INTELSAT-V

BT Labs conducted a four-year experiment commencing 1 July 1983, at 11.2, 11.5, and 14.3 GHz with INTELSAT-V. The slant path elevation angle ranged from 8.3° to 11.8°. The measured data was combined with the data from ATS-6, OTS, and OLYMPUS into a composite data base. In evaluating the data, Howell, Harris, and Mehler [9] observed a wide variation in the instantaneous ratio about the mean value in all the measurements.

4.2.1.4 OLYMPUS

BT Labs conducted measurements of OLYMPUS beacons, beginning 1 November 1989, at an elevation angle of 27.5°. Results are tabulated in Table 4.3-1. BT Labs found a wide variation in the instantaneous ratio about a mean value in all the measurements, both in the short term (over a few minutes) and over the long term (from event to event), attributed to the variation in drop size distributions within and between rainstorms. Nevertheless, they concluded that their results generally agreed with the scaling models proposed in CCIR Report 564-3 [10] (refer to Section 3.1.1.1).

Table 4.3-1

Attenuation Scaling Ratios Measured by BT Labs using OLYMPUS

	Attenuation Ratio Frequencies		
Data Set	30/20	20/12	30/12
All Data	1.8	2.5	4.3
At 0.001% outage	2.0	3.1	6.5

4.2.2 Goonhilly experiment

The Goonhilly earth station, in the extreme southwest of England, investigated slant-path propagation effects for an elevation angle of 3.3° in the 11 GHz satellite band from the INTELSAT satellite. Bryant [11] found that scintillation becomes much more pronounced as

- elevation angle is reduced (more troposphere along the path)
- frequency is increased
- antenna diameter is reduced (antenna beamwidth broadens to take in more multipath signals and interference)

4.3 U.S. Experiments

4.3.1 ATS 6

Ippolito (1972 and 1975) [29,30] obtained data at 20 and 30 GHz in North Carolina from the ATS 6, and Fang and Harris (1979) [31] also made measurements from the ATS 6 in Maryland. In summarizing these results, Altshuler and Telford [13]

infer from Henry's work [12] that the 30/13 ratio ranges from 3 to 8 and that the attenuation ratios of Ippolito are widely scattered over a range of approximately 1 to 5, while the data measurements of Fang and Harris showed ratios with much less scatter.

4.3.2 INTELSAT

4.3.2.1 COMSAT Measurements

COMSAT conducted experiments with Uplink Power Control (ULPC) during the winter of 1986/1987 and during the late summer of 1987 in Maryland at 14/11 GHz on the INTELSAT-V (F-3) satellite [14]. Their elevation angle to the satellite was 38.1°. COMSAT also employed a second 11.2 GHz downlink. COMSAT used a statistical attenuation ratio of 1.5 (derived from techniques published by Olsen, Rogers, and Hodge [15, 16]), which is slightly less than the theoretical *RAS* derived from a square law relation ($n = 2$) using 11 GHz as the base frequency:

$$RAS = \left(\frac{f_U}{f_L}\right)^2 = \left(\frac{14\ \text{GHz}}{11\ \text{GHz}}\right)^2 = 1.62 \qquad (4.3\text{-}1)$$

Employing the second 11.2 GHz downlink frequency yields a value much closer to 1.5,

$$RAS = \left(\frac{f_U}{f_L}\right)^2 = \left(\frac{14\ \text{GHz}}{11.2\ \text{GHz}}\right)^2 = 1.56 \qquad (4.3\text{-}2)$$

COMSAT's loop-back system for ULPC (described in detail by Sweeney [1]), could compensate for fades on the 14 GHz signal up to about 7.5 dB. Though they used an *RAS* equal to 1.5, COMSAT concluded that the scale factor for average rain was approximately 1.65, yet stated that this difference in scaling contributed insignificant

error over the 7.5 dB control range. COMSAT also found that gaseous attenuation (*AGA*) scaled by a factor of 1.5 (refer to Section 2.1.2), that is,

$$\frac{AGA(14\ \text{GHz})}{AGA(11.2\ \text{GHz})} = 1.5 \tag{4.3-3}$$

4.3.2.2 COMSAT Data Compared to Va Tech OLYMPUS Data

COMSAT set the clear sky reference level using the previous day's base line level. Though they improved their algorithm over time [14], they still assumed that at Ku-band frequencies, cloud and water vapor attenuation effects were small enough to ignore, especially since fades only occur for a small percentage of the year. COMSAT assumed that changes in the reference clear sky level will occur much more slowly than propagation induced changes. COMSAT does not extract attenuation with respect to clear air (*ACA*). Virginia Tech does not assume the gaseous attenuation (*AGA*) is negligible. Virginia Tech determines cloud and water vapor attenuation (*AGA*) from radiometer measurements, and removes *AGA* from *AFS* leaving *ACA*.

Like Virginia Tech, COMSAT separates the rain fade from the attenuation due to scintillation, *SA*, (COMSAT used a 20-s moving average filter, whereas Virginia Tech used a 30-s filter). Sweeney [1] shows (with a plotted example) that scintillation is the difference between the received signal attenuation and a 30-s moving average of the signal attenuation. Using a square law relation (power law relation with $n = 2$), COMSAT scaled the downlink attenuation, $A_{down_{rain}}$, to the uplink rain attenuation, $A_{up_{rain}}$ as

$$A_{up_{rain}} = A_{down_{rain}} \left(\frac{f_{up}}{f_{down}} \right)^2 \quad (dB) \tag{4.3-4}$$

Similarly, COMSAT used the classical power law relation with $n = 7/12$ [14] to scale scintillations by

$$S_{up} = S_{down}\left(\frac{f_{up}}{f_{down}}\right)^{\frac{7}{12}} \quad (dB) \tag{4.3-5}$$

For ULPC applications, it may be necessary to include all fading mechanisms. Scaled uplink attenuation due to rain and the scaled uplink scintillations produces the estimated uplink attenuation, $\hat{A}_{up}$:

$$\hat{A}_{up} = A_{up_{rain}} + S_{up} \quad (\text{dB}) \tag{4.3-6}$$

where (4.3-4) and (4.3-5) are used to find $A_{up_{rain}}$ and S_{up}. COMSAT utilized this ULPC to obtain a control accuracy better than ± 2 dB.

4.3.2.3 Measurement Program at the University of Texas

Vogel and Torrence [36] of the Unversity of Texas at Austin performed extensive measurements using 11.58 GHz beacon signals on INTELSAT V-F10 and INTELSAT VI-F2 from June 1988 through May 1991. The elevation angle was very low at 5.8°. Because attenuation measurements were made on only one frequency, there is little application to frequency scaling of attenuation. However, attenuation models (discussed in Section 3.2.1.2) can be validated by the Texas attenuation data. Reliable attenuation models could be useful in statistical attenuation scaling (e.g., *RAS*) from attenuation models.

4.4 German Experiments

Dintelmann, *et al.* [17], reported on data collected from 1 May 1990 to 30 April 1991 from the 12, 20, and 30 GHz beacons of OLYMPUS with an elevation angle of 27°. They separated out rain, cloud, and gaseous attenuation (though they admit that the distinction between cloud and rain attenuation is sometimes ambiguous). Radiometers were employed to reference the beacon signals, which were sampled at 80 Hz. Attenuation was observed to increase with frequency f, for a fixed level of availability (percentage of time), from Ku-band (12-18 GHz) to Ka-band (27-40 GHz), proportional to a $f^{1.8}$ law. Dintelmann, *et al.* found that CCIR procedures (see Section 3.1.1.1) overestimate rain attenuation for time exceedance percentages greater than 0.01%, explaining that CCIR predictions represent only rain attenuation and not gaseous and cloud attenuations; they also found that depolarization is significantly underestimated by CCIR predictions [18]. They conclude that margins of 3 dB are sufficient if availabilities of 97-99% are acceptable.

Ortgies, *et al.*, [19] found that instantaneous frequency scaling of attenuation (*RA*) exhibits a hysteresis effect, which they attributed to variations of the drop size distribution and the effective path length through rain, as well as antenna effects [20]. They maintain that hysteresis effect begins much sooner than that observed by Sweeney, *et al.* [21]

4.5 Italian Experiments

4.5.1 SIRIO

Matricciani and Paraboni [22] performed measurements using the Italian satellite SIRIO beacons signals at 11.6 and 17.8 GHz. They set their reference level by assuming clear air before and after an event, thus eliminating gaseous attenuation. This is an approximation to attenuation with respect to clear air (*ACA*). A total time base of about 108 hours (38 rain events) was analyzed. The data were sampled at 10 Hz and "averaged over intervals of 0.8 second to smooth out fluctuations induced by the spin velocity of the satellite" [22]. They also found that the average attenuation ratio decreased as attenuation increased.

In another similar propagation experiment, Carassa, Mauri, and Paraboni [37] acquired data from SIRIO at 11.6 and 17.8 GHz over a five year period (1978-1982). Data collection using the downlink (11.6 GHz) was almost continuous, while the uplink (17.8 GHz) averaged about 75% uptime over the five years. They state that experimental results for attenuation statistics disagreed with CCIR predictions found in CCIR Doc. 564-2 [10]. They also found an extremely high year to year variability. Frequency scaling at equiprobable values of attenuation was found to change very little over the five-year period, with an average scaling ratio of 2.1, consistent with the Drufuca relation [23] (i.e., a power law relation with $n = 1.72$)

$$\frac{A_2}{A_1} = \left(\frac{f_2}{f_1}\right)^{1.72} = \left(\frac{17.8}{11.6}\right)^{1.72} = 2.1 \qquad (4.5\text{-}1)$$

This relation is very similar to a CCIR relation in CCIR Doc. 564-2. Mauri and Paraboni [24] also report that a long-term (statistical) probability distribution can be fitted well by a power law formula up to a 9 dB attenuation level.

4.5.2 OLYMPUS

Dossi, *et al.*, [35] performed measurements on OLYMPUS at a 1 Hz sampling frequency. They reported an *RA* scaling factor of 1.86 for the 30/20 frequency pair. This results is based on a total of 13 rain events.

4.6 Canadian Experiments

4.6.1 Butler experiment

Butler [25] conducted a terrestrial microwave propagation experiment near Ottawa, Canada in 1979 on two 16 km paths in the 11-17 GHz range. He found that attenuation for vertical polarization is only about 79% (in dB) of that of horizontal polarization across the 11-17 GHz range. He also observed variations in attenuation ratio during rain events (i.e., attenuation ratio *RA* is not constant).

4.6.2 Communications Research Centre

Segal [26] compiled data for the Communications Research Centre of Ottawa, Canada based on measurements over 20 to 80 km terrestrial links. For frequencies between 11 and 30 GHz, he found that power-law scaling (3.2-3) produced good

approximations to the measured data which had an average value of $n=1.98$, with a range between 1.87 to 2.17. He noted that Hodge's formula (3.2-26) is a close approximation to the power law expression, being fitted by curves having an average value of $n=1.88$. Calculations based on the data confirmed the accuracy of the two-frequency scaling model of Hogg.

4.7 Indian Experiment

Raina and Uppal of the National Physical Laboratory, New Delhi, India, conducted measurements at frequencies of 11, 18, and 22.2 GHz between June 1978 and August 1979 [27]. They found *RAS* values of 2.2 for 18/11 and 2.8 for 22.2/11. These values fall short of those predicted by a square law relation (frequency squared values are 2.7 for 18/11 and 4.1 for 22.2/11). Their findings agree with Oguchi's work [33] and with values predicted by CCIR formulas [34].

4.8 Australian Experiment

James Cook University of North Queensland, Australia, made measurements from INTELSAT at 7.5, 11.6, 19.5, and 28.5 GHz at an elevation angle of 63° during the tropical wet season from November 1987 to March 1988 (with rain rates up to 350 mm/h) [28]. They employed a 1.8 m antenna Dicke switched radiometers and sampled at a rate of 1 Hz. Their results show reasonable correlation with the CCIR model of Boithias (see Section 3.2.2.1.1) as long as the difference between scaling frequencies is not excessive.

4.10 References

1. Sweeney, D.G., "Adaptive Power Control as a Fade Countermeasure on Satellite Links," Unpublished doctoral dissertation, Report EESATCOM 93-2, Virginia Polytechnic Institute & State University, Department of Electrical Engineering, Blacksburg, VA, January 1993.
2. Kosaka, K., Suzuki, Y., and Nishiyama, I., "Japan's CS (Sakura) Communications Satellite Experiments. Part VI-E: Communications Experiments: Experiments on Measures Against Rain Attenuation," *IEEE Transactions on Aerospace and Electronics Systems*, Vol. AES-22, May 1986, pp. 302-309.
3. Toshiaki Kozu, Jun Awaka, Hajime Fukuchi, Kenji Nakamura, "Rain Attenuation Ratios on 30/20- and 14/12-GHz Satellite-to-Earth Paths," *Radio Science*, vol. 23, No. 3, May/June 1988, pp. 409-418.
4. Kozu, T., "Proposed Amendment to CCIR Report 564-3 -- Rain Attenuation Ratios on 30/20 and 14/12 GHz Earth-Space Paths: Measurement and Analysis with Disdrometer Data," CCIR IWP 5/2, July 1987.
5. Ihara, Toshio and Furuhama, Yoji, "Frequency Scaling of Rain Attenuation at Centimeter and Millimeter Waves Using a Path-Averaged Drop Size Distribution," *Radio Science*, vol. 16, No. 6, pp. 1365-1372, Nov/Dec 1981.
6. Howell, R.G., Stucky, R.L., and Harris, J.W., "The BT Laboratories slant-path measurement complex," *BT Technology Journal*, 10, No. 4, October 1992.
7. Upton, S.A.J., Holt, A.R., and Upton, G.J.G., "Some Aspects of the Analysis of Experimental Data for Short-Term Frequency Scaling," *Int. J. of Sat. Comm.*, vol. 5, pp. 249-260, 1988.
8. Thirwell, J., "Frequency scaling of slant path attenuation," *British Telecom (BT) Technology. Journal*, **2**,(2), 1984, pp. 62-73.
9. Howell, R.G., Harris, J.W., and Mehler, M., "Satellite Co-polar Measurements at BT Laboratories," *BT Technology Journal*, Vol. 10, No. 4, October 1992.
10. CCIR, "Propagation in Non-ionized Media," Recommendations and Reports of the CCIR, Report 564-3, V, 1990.
11. Bryant, D.L., "Low elevation angle 11 GHz beacon measurements at Goonhilly earth station," *BT Technology Journal*, Vol. 10, No. 4, October 1992, pp. 68-75.
12. Henry, P., "Measurement and frequency extrapolation of microwave attenuation statistics on the earth-space path of 13, 19, and 30 GHz," *IEEE Trans. Antennas Propagat.*, AP-23(2), pp. 271-274, 1975.

13. Altshuler, E.E. and Telford, L.E., "Frequency dependence of slant path rain attenuation at 15 and 35 GHz," *Radio Science*, Volume 15, Number 4, pp. 781-796, July-August 1980.
14. Dissanayake, Asoka and Chaim Zaks, "Up-link Power Control Developments at COMSAT Laboratories," COMSAT Technical Note, STD/92-005, February 1992 (cited in Sweeney, D.G., "Adaptive Power Control as a Fade Countermeasure on Satellite Links," Unpublished doctoral dissertation, Report EESATCOM 93-2, Virginia Polytechnic Institute & State University, Department of Electrical Engineering, Blacksburg, VA, January 1993, p. 38).
15. Olsen, R.L., Rogers, D.V., and Hodge, D.B., "The aR^b Relation in the Calculation of Rain Attenuation," *IEEE Transactions on Antennas and Propagation*, Vol. AP-26, 1978, pp. 318-329.
16. Hodge, D.B., "Frequency Scaling of Rain Attenuation," *IEEE Transactions on Antennas and Propagation*, Vol. AP-25, 1977, pp. 446-447.
17. Dintelmann, F., Ortgies, G., Rücker, and Jakoby, R., "Results From 12 to 30 GHz German Propagation Experiments Carried out with Radiometers and the OLYMPUS Satellite," Research Centre, Deutsche Bundespost Telekom, Darmstadt, Germany, 1992.
18. CCIR, "Propagation data and prediction methods required for earth-space telecommunication systems," Report 564-4, Reports of the CCIR, Annex to Vol. 5, Geneva, 1990.
19. Ortgies, G., Rücker, F., and Dintelmann, F., "Some aspects of attenuation frequency scaling," *North American Radio Science Meeting and Internat IEEE/AP-S, Symposium*, London, Canada, 1991.
20. Ortgies, G. Rücker, F., Dintelmann, F., and Jakoby, R., "Effect-specific analysis of propagation parameters," *Proc. of the 16th NASA Propagation Experimenters Meeting (NAPEX XVI) and ACTS Propagation Studies Miniworkshop*, Houston, USA, 1992, pp. 143-154.
21. Sweeney, D.G., Pratt, T., and Bostian, C.W., "Hysteresis Effects in Instantaneous Frequency Scaling of Attenuation on 20 and 30 GHz Satellite Links," *Electronic Letters*, 2nd January 1992, Vol. 28, No. 1.
22. Matricciani, E. and Paraboni, A.,"Instantaneous Frequency Scaling of Rain Attenuation at 11.6-17.8 GHz with SIRIO Data," *IEEE Trans. on Ant. & Prop.*, vol. AP-33, No. 3, pp. 335-337, March 1985.
23. Drufuca, G., "Rain attenuation statistics for frequencies above 10 GHz from raingauge observations," *Journal de Recherches Atmospheriques*, vol. VIII, n. 1-2, pp. 39-411, 1974.
24. Mauri, M. and Paraboni, A., "Attenuation Statistics at 11.6 GHz From Satellite SIRIO After Three Years' Activity in Italy," *Electronic Letters*, vol. 17, pp. 440-441, 25 June 1981.

25. Butler, R.S., "Frequency and Polarisation Scaling of Microwave Attenuation During Rainfall," *Electronics Letters*, vol. 21, No. 19, pp. 826-827, 12 Sept. 1985.
26. Segal, B., "Rain Attenuation Statistics for Terrestrial Microwave Links in Canada," Communications Research Centre Report No. 1351-E, Ottawa, Canada, January 1982, p. 15.
27. M.K. Raina, G.S. Uppal, "Frequency Dependence of Rain Attenuation Measurements at Microwave Frequencies," *IEEE Trans. on Ant. & Prop.*, vol. AP-32, No. 2, pp. 185-187, Feb. 1984.
28. B.J. Bowthorpe, G.H. Allen, C.J. Kikkert, J.E. Allnutt, P.L. Arlett, "Frequency Scaling of Slant-Path Attenuation in Tropical Regions," *Int. J. of Sat. Comm.*, vol. 8, 1990, pp. 223-228.
29. Ippolito, L.J., "Eath-satellite propagation above 10 GHz," *NASA /GSFC Doc. X-751-72-208*, 8-1-8-27, 1972.
30. Ippolito, L.J., "Millimeter wave propagation and communications experiments at 20 and 30 GHz, *IEEE Trans. Aerospace Electron. Syst., AES-11(6)*, 1975, pp. 1067-1082.
31. Fang, D.J., and J.M. Harris, "Precipitation attenuation studies based on measurements of ATS-6 20/30 GHz beacon signals at Clarksburg, MD," *IEEE Trans. on Ant. & Prop., AP-27*(1), 1979, pp. 1-11.
32. Stutzman, W.L., *et al.*, "Communications and propagation experiments using the OLYMPUS spacecraft - Analysis of OLYMPUS Propagation Data for the Period January to May 1991," Report EESATCOM 92-5, Virginia Polytechnic Institute & State University, Department of Electrical Engineering, Blacksburg, VA, JPL Contract No. 958435, November 1991.
33. Oguchi, T. and Hosoya, Y., "Scattering properties of oblate rain drops and cross-polarisation of radiowaves due to rain (Part-II); Calculations at Microwave and Millimetre wave region," *J. Radio Res. Labs.* (Tokyo), vol. 21, no. 105, pp. 191-259, 1974.
34. Attenuation and scattering by precipitation and other atmospheric particles, DOC 5/1026-E CCIR XIVth Plenary Assembly, Kyoto, 1978.
35. Dossi, L., Mauri, M., Matricciani, E., and Giovannoni, M., "A Dual-Band Frequency Diversity Experiment with OLYMPUS," *Proceedings of International OLYMPUS Utilisation Conference, Seville, Spain*, April 1993.
36. Vogel, W. & Torrence, G., "INTEL-540B: Three years of Low Elevation Angle, Ku Band Satellite Beacon and Radiometer Measurement Results for Austin, Texas," Electrical Engineering Research Laboratory, University of Texas at Austin, 25 September, 1991.
37. Carassa, F., Mauri, M., and Paraboni, A., "Attenuation statistics in Itlay as measured by th eSIRIO satellite during its five years lifetime," *IEEE Trans. Antennas Propagation.*, vol. AP-32, pp. 1251-1255, Nov. 1984.

CHAPTER 5

OLYMPUS EXPERIMENT RESULTS

One year of fully processed data has been generated to facilitate meaningful analysis of the propagation effects. Because OLYMPUS left its orbit for the summer of 1991, approximately three months of data are missing from the 1991 calendar year. In the Virginia Tech experiment, the data from the summer of 1992 was substituted for the missing data in 1991. The "analysis year", also denoted "One Year (91/92)", is made up from the months of January 1991 to May 1991, June 1992 to August 1992, and September 1991 to December 1991.

5.1 Precipitation Data

Since the Virginia Tech experiment quantified the behavior of 12, 20, and 30 GHz signals through precipitation, it is appropriate to include the precipitation statistics for the year. Two rain gauges were located within a few feet of the receivers. The data acquisition system (DAS) monitored the gauges 10 times every second (at 10 Hz) to see if the tipping buckets had tipped; each tip was given a time label. Rain rate, R, is calculated by the relation

$$R = 914.4 / (t_i - t_{i-1}) \qquad \text{[mm/h]} \tag{5.1-1}$$

where t_i and t_{i-1} are the times in s for consecutive tips. Figure 5.1-1 shows the measured rain rate at Blacksburg, Virginia, for the analysis year for the percentage of time exceeding the abscissa value. Table 5.1-1 tabulates the rain accumulation at Virginia Tech's tracking station and as well as other local measurements (taken at the Virginia Tech's Horticulture Farm, about 7 km south of the Tracking Station) and the

average accumulations for Blacksburg (for the period 1892 to 1930 from the U.S. Department of Commerce Weather Bureau Climatic Summary). Figure 5.1-2 shows the absolute worst month compiled from the highest rain rates in any given month. Individual monthly plots for rain rate are included in Appendix A.1.

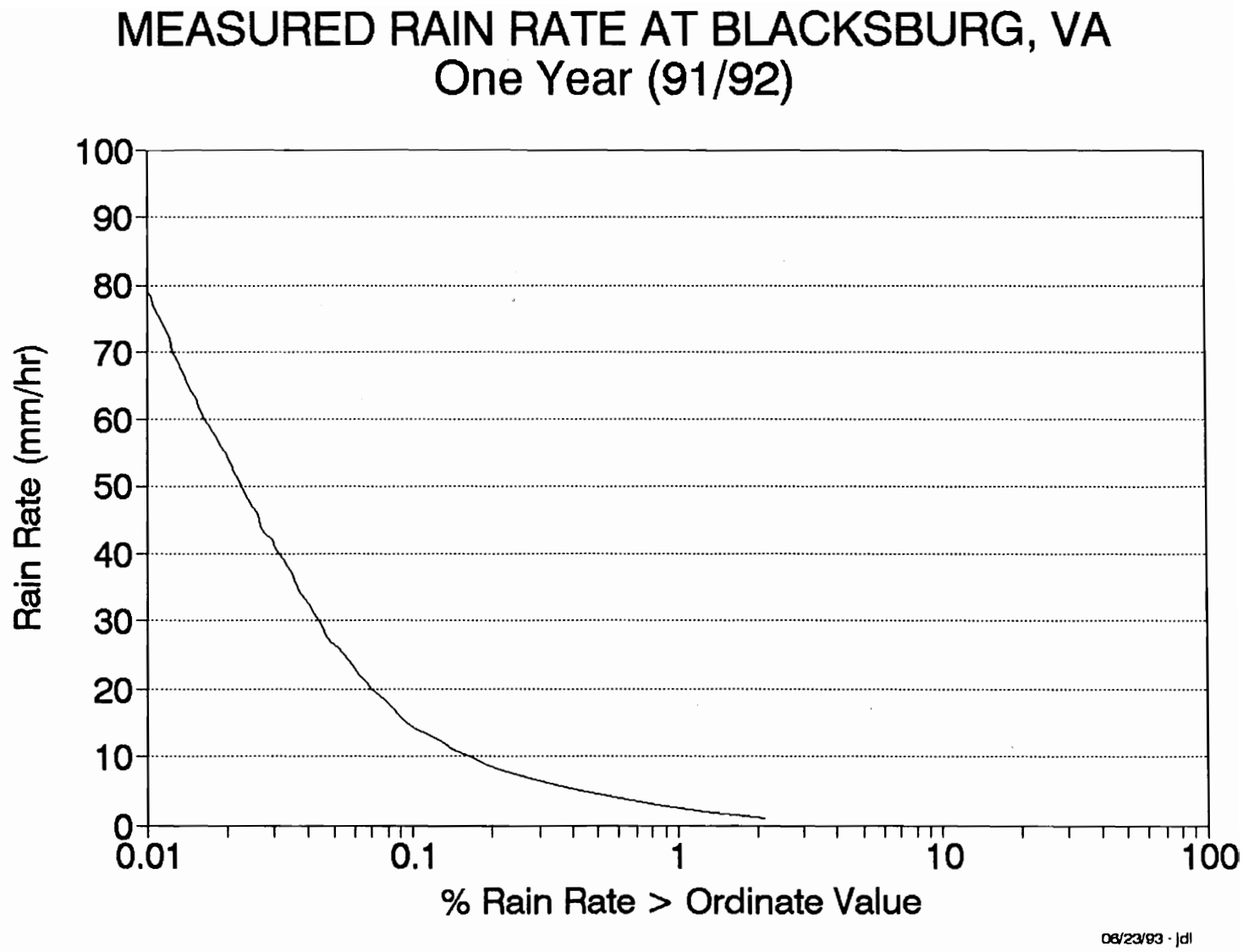

Figure 5.1-1 Measured rain rate at Blacksburg, VA - One Year (91/92)

Olympus Experiment

Table 5.1-1

Rain Accumulation at Blacksburg, VA - One Year (91/92)

Virginia Tech

Month	Tracking Station	Horticulture Farm	Blacksburg Normals
January 1991	1.95 "	2.96 "	3.21 "
February 1991	2.03 "	2.15 "	3.17 "
March 1991	5.52 "	5.86 "	3.52 "
April 1991	2.48 "	2.78 "	3.07 "
May 1991	4.73 "	4.66 "	3.68 "
June 1992	4.94 "	6.20 "	4.32 "
July 1992	9.35 "	9.35 "	5.03 "
August 1992	3.38 "	5.10 "	3.92 "
September 1991	0.53 "	0.49 "	3.16 "
October 1991	0.26 "	0.26 "	3.00 "
November 1991	3.24 "	2.99 "	2.30 "
December 1991	3.66 "	5.50 "	3.16 "
TOTALS	42.07	48.30	41.54

06/23/93 - JDL

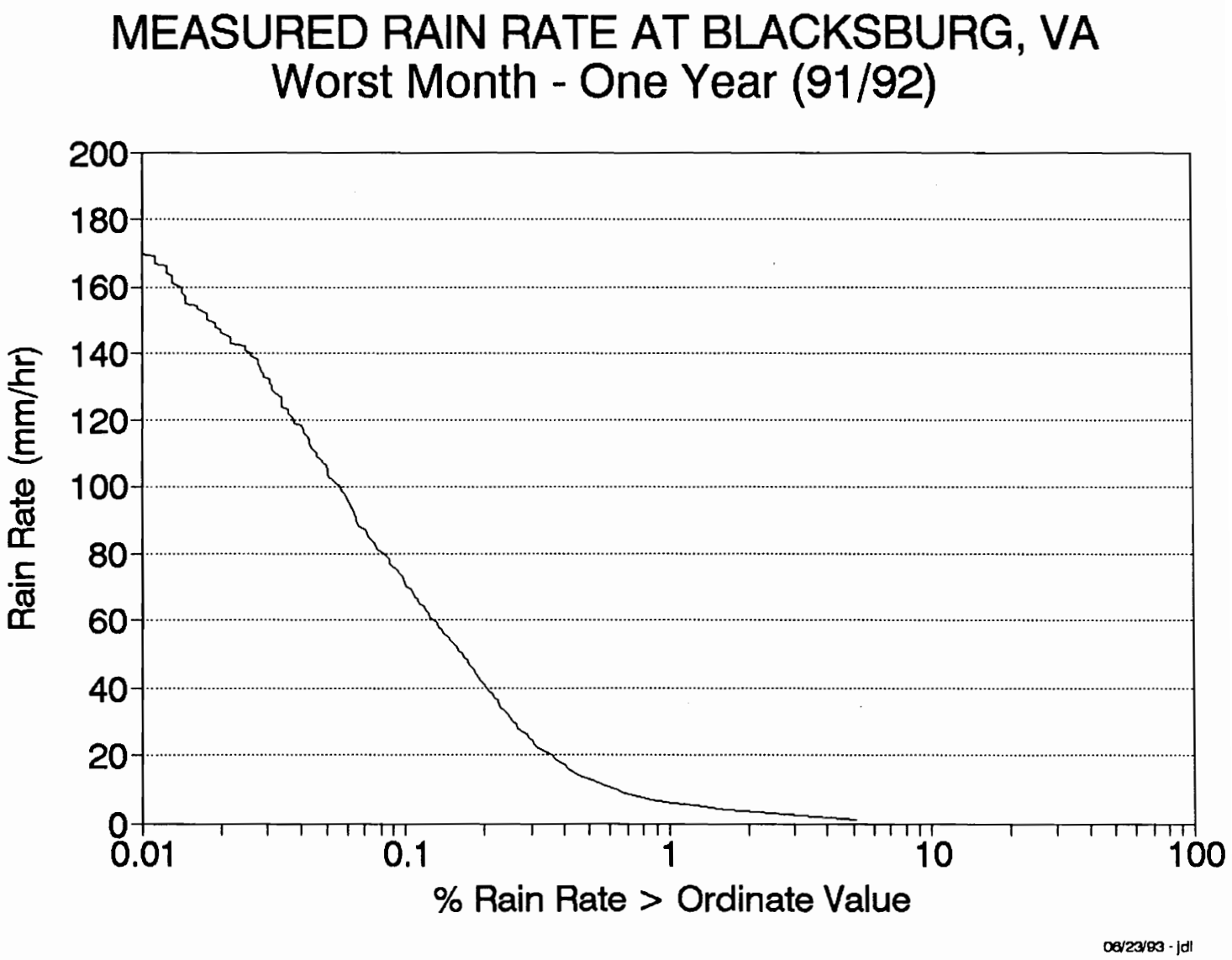

Figure 5.1-2 Measured rain rate at Blacksburg, VA, worst month - One Year (91/92)

5.2 Statistics of Attenuation with Respect to Clear Air (*ACA*)

Since statistical attenuation ratio (*RAS*) is based on the statistics of *ACA* (*ACAS*), it is appropriate to show the time exceedance plots for *ACA*, which give values for *ACAS*. Figures 5.2-1 to 5.2-3 show the percentage of time in the experiment year that *ACA* exceeds some specified value for the pairs of frequencies under consideration (30/20, 20/12, and 30/12, respectively). *ACA* values must be available for both frequencies at the same sample times to calculate *RAS*; in other words, there must be a common time base for the attenuations at both frequencies. The common time base is total "up-time". The common time bases (in percentage of the month and of the year) for each month and for the experiment year for each pair of frequencies are given in Table 5.2-1. Consequently, Figures 5.2-1 to 5.2-3 for the experiment year are each based on a common time base. *ACA* values of 12, 20, and 30 GHz for their common time base (i.e., where data is present on all three frequencies) are plotted in Figure 5.2-4. A common time base permits direct evaluation of *RAS*. Table 5.2-1 includes Attenuation with Respect to Free Space (*AFS*) because *AFS* has the same time base as *ACA*. The value of *ACAS* for a particular frequency is the statistical *ACA* value exceeded for a given percentage of time. As an example, statistical attenuation values are tabulated in Table 5.2-2 for common time base of 12, 20, and 30 GHz for *AFS*, *ARD*, and *ACA*. *ACA* values in Table 5.2-2 correspond to plotted values in Figure 5.2-4. Individual monthly plots for *ACA* vs. % Time Exceeded are given in Appendix A.2.

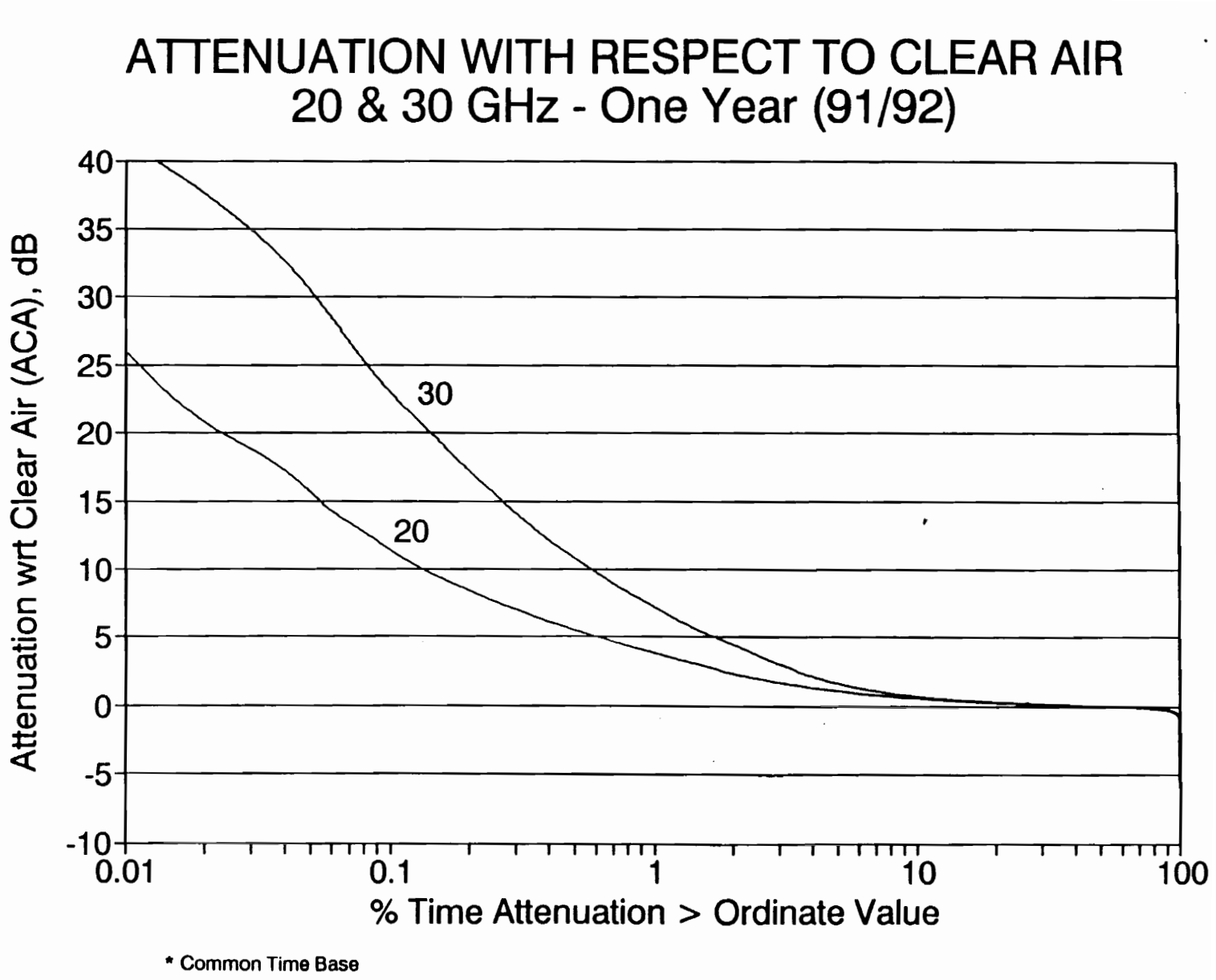

Figure 5.2-1 Attenuation with Respect to Clear Air, 20 & 30 GHz - One Year (91/92)

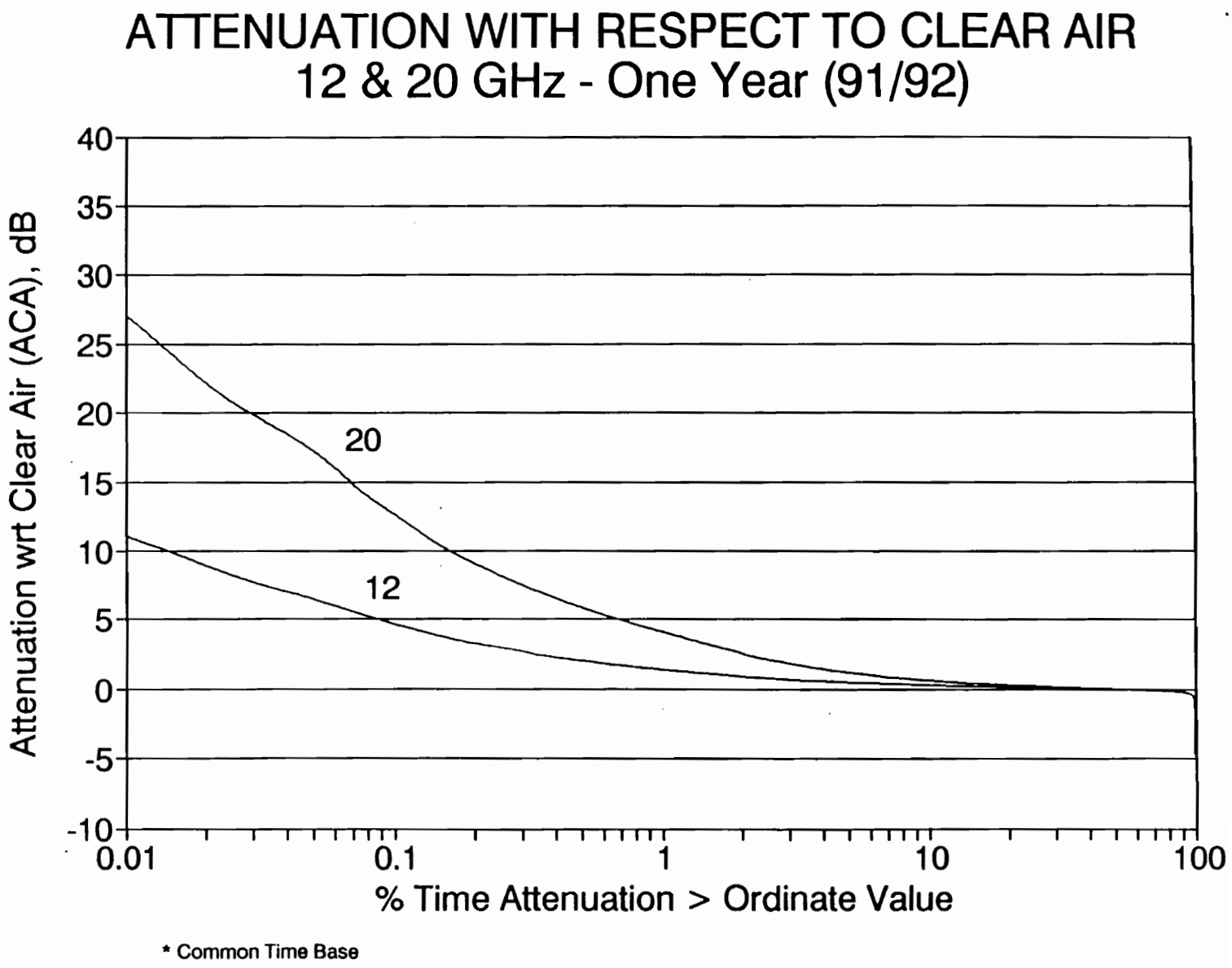

Figure 5.2-2 Attenuation with Respect to Clear Air, 12 & 20 GHz - One Year (91/92)

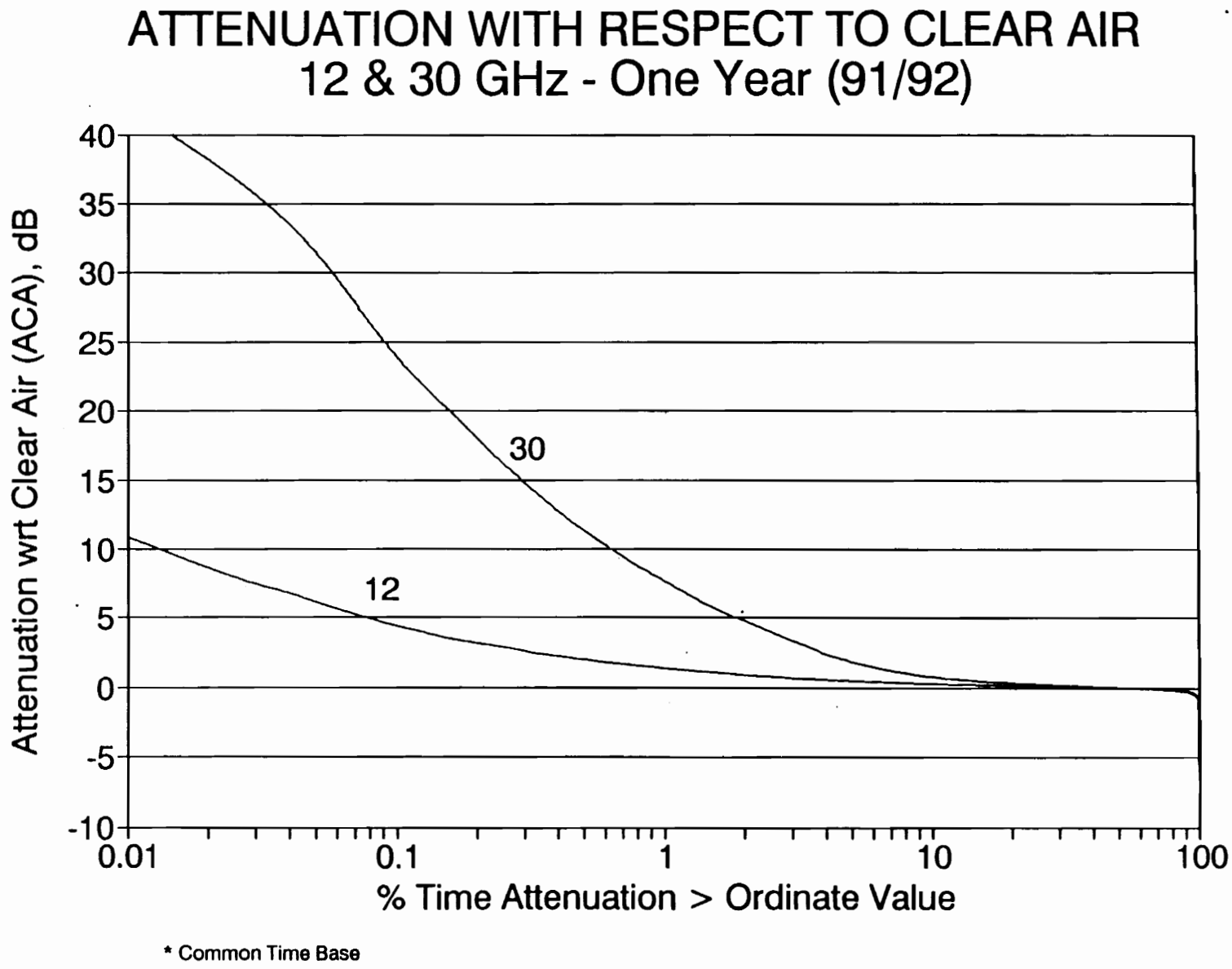

Figure 5.2-3 Attenuation with Respect to Clear Air, 12 & 30 GHz - One Year (91/92)

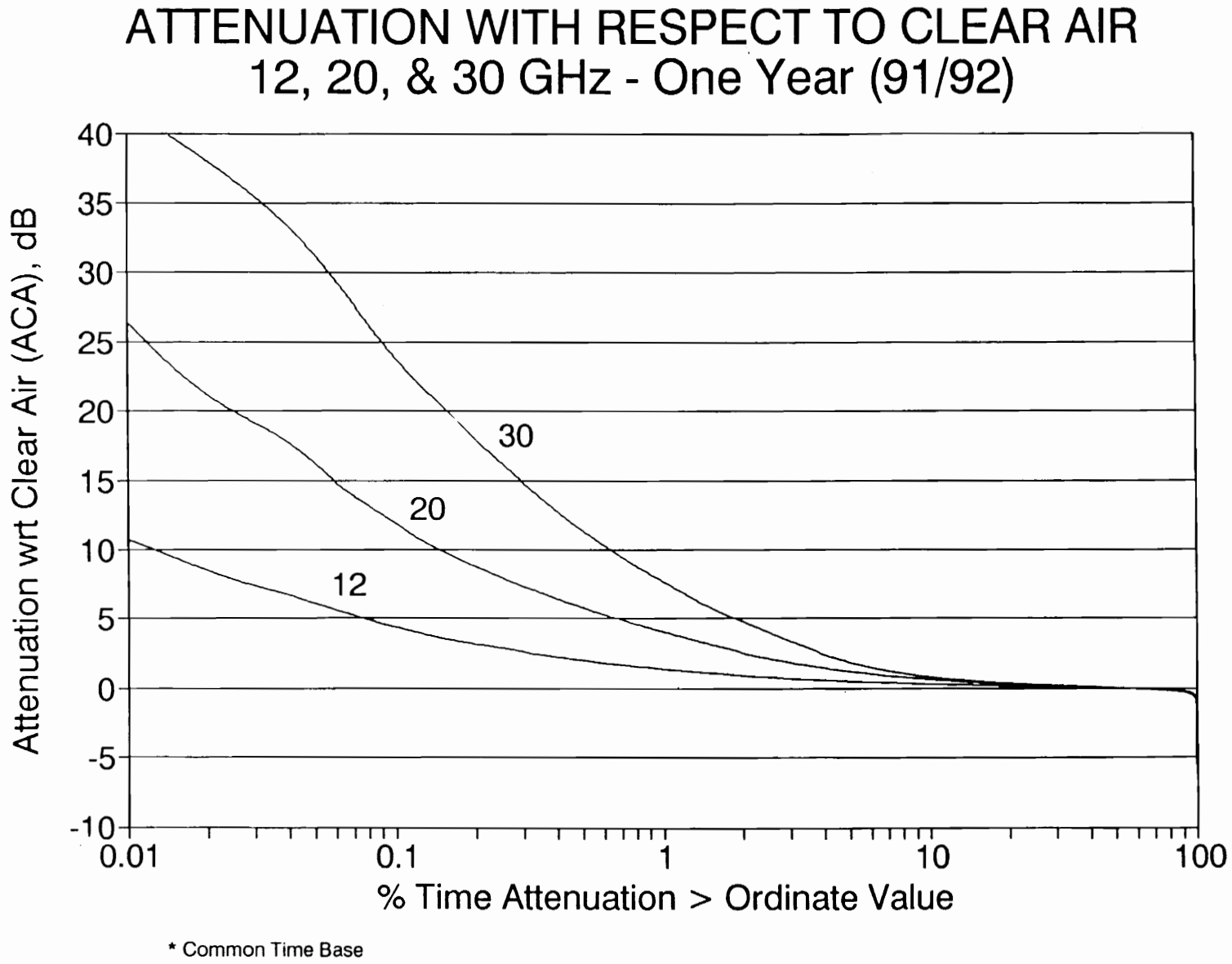

Figure 5.2-4 Attenuation with Respect to Clear Air, 12, 20, & 30 GHz - One Year (91/92)

Table 5.2-1
Percentage of Valid Data by Month for the Analysis Year

Quantity		Percentage of Month												
		Jan 91	Feb 91	Mar 91	Apr 91	May 91	Jun 92	Jul 92	Aug 92	Sep 91	Oct 91	Nov 91	Dec 91	Year 91/92
Paired Beacons AFS and ACA	20/12	76.5	85.0	84.6	79.1	82.9	95.0	99.2	94.6	75.1	73.4	67.8	80.8	82.7
	30/12	76.0	85.1	84.3	77.0	82.9	95.0	99.0	94.4	74.5	73.5	67.8	80.7	82.4
	30/20	95.2	99.4	95.8	90.9	87.3	97.2	99.7	99.8	74.5	74.6	73.8	98.9	90.4
Tripled Beacon AFS and ACA	30/20/12	76.0	84.9	84.2	76.7	82.9	95.0	99.0	94.4	74.4	73.4	67.7	80.7	82.3

Table 5.2-2

Attenuation Statistics for 12, 20, & 30 GHz (Common Time Base)

Percent Time Exceeded	AFS			ARD			ACA		
	12	20	30	12	20	30	12	20	30
50.000	0.68	1.58	1.42	0.70	1.55	1.41	0.01	0.04	0.04
30.000	0.85	2.03	1.89	0.81	1.97	1.82	0.10	0.17	0.20
20.000	0.96	2.31	2.23	0.86	2.23	2.08	0.17	0.31	0.36
10.000	1.17	2.77	2.80	0.98	2.59	2.62	0.31	0.65	0.82
5.000	1.42	3.37	4.04	1.19	3.08	3.61	0.51	1.22	1.88
3.000	1.67	4.05	5.50	1.41	3.68	4.69	0.71	1.88	3.33
2.000	1.91	4.70	6.93	1.65	4.22	5.78	0.94	2.54	4.76
1.000	2.42	6.21	9.8.	2.08	5.33	7.83	1.41	4.04	7.69
0.500	3.04	7.93	13.55	2.50	6.46	10.29	2.03	5.76	11.38
0.300	3.61	9.47	16.99	2.79	7.32	12.16	2.59	7.31	14.82
0.200	4.12	10.90	20.08	3.08	8.21	13.85	3.11	8.73	17.90
0.100	5.39	14.11	26.05	3.63	9.86	16.57	4.37	11.93	23.87
0.050	7.10	18.37	33.47	4.26	11.92	19.13	6.08	16.21	31.29
0.030	8.38	21.28	37.66	4.75	13.66	21.13	7.37	19.12	35.50
0.020	9.50	23.31		5.12	15.39	22.60	8.48	21.15	38.06
0.010	11.74	28.60		6.09	18.08	25.83	10.72	26.43	
0.005	13.92	33.55		7.47	20.72	28.39	12.90	31.37	
0.003	14.96	36.44		10.18	22.84	31.32	13.94	34.27	
0.002	15.67	38.56		18.05	24.39	31.39	14.65	36.39	
0.001	17.16				27.33		16.14		

5.3 Instantaneous Scaling (Attenuation Ratio)

Attenuation ratio, *RA*, given by (2.3-1) is the quotient of the measured *ACA* value at the higher frequency (e.g., 30 GHz) divided by the measured *ACA* value at the lower frequency (e.g., 20 GHz) evaluated at each sample time ("instantaneously"; 0.1 s in the Virginia Tech experiment). Each *RA* value is assumed to represent the whole 0.1 second sample interval. The *RA* values are averaged with a 30-s moving average given in (3.2-1). The occurrences of these *RA* values are binned in increments of 0.05 for each binned 1-dB increments of the base frequency attenuation (e.g., for the 30/20 ratio, in any given month there might be 100 occurrences of *RA* values between 1.95 and 2.00 when ACA20 is between 3 and 4 dB). In this section, statistics of *RA* are generated based on the binned *RA* values.

5.3.1 *RA* vs. % time exceeded for One Year (91/92)

These binned occurrences are summed and plotted as a cumulative distribution; that is, *RA* is plotted as a function of the percentage of time (in the month or year) that *RA* exceeds some specific value. Final plots for the analysis year show the percentage of time in the year that attenuation ratio exceeds some specific value of *RA*. Figures 5.3-1, 5.3-2, and 5.3-3 give the ratios of 30/20, 20/12, and 30/12.

The attenuation ratios in Figures 5.3-1 through 5.3-3 represent the data set where the attenuation of the base frequency exceeds 1 dB. The 1 dB threshold assures rejection of most signal impairments caused by atmospheric effects other than precipitation. In this type of plot, all data are pooled regardless of base frequency

attenuation level (as long as $A(f_L) > 1$ dB). Refer to Appendix A.3.3 for example plots (i.e., for January 1991) of *RA* vs. % Time Exceeded for other attenuation threshold levels. The percentages of the months and the experiment year that the base frequency attenuation exceeds 1 dB (e.g., ACA20 > 1 dB for 30/20) are tabulated in Table 5.3-1. For example, ACA20 exceeds 1 dB for 1.23 % (specifically, 1.2292%) of the year (1.23% times 90.4% from Table 3.2-1 yields about 95 hours) for the 30/20 *RA* statistics.

Table 5.3-1

Percentage of Time that the Base Frequency Attenuation Exceeds 1 dB

RA Frequencies	30/20	20/12	30/12
Time Period	Percentage of Time		
January 1991	0.45	0.35	0.35
February 1991	0.50	0.45	0.50
March 1991	2.35	2.35	2.35
April 1991	0.88	0.88	0.91
May 1991	1.85	1.85	1.85
June 1992	1.82	1.82	1.80
July 1992	1.16	1.16	1.15
August 1992	1.41	1.41	1.41
September 1991	0.21	0.21	0.21
October 1991	0.02	0.02	0.02
November 1991	0.65	0.65	0.65
December 1991	3.32	3.32	3.32
Year 1991/92	1.23	1.23	1.23

Attenuation ratio can also be plotted as a function of the ranges of base frequency attenuation values (e.g., 1 dB < ACA20 < 2 dB for 30/20) to examine attenuation variation with the severity of rain fading. This type of plot becomes important as receiver saturation becomes more significant (see Section 5.3.3). Plotted

examples of *RA* vs. % Time Exceeded for ranges of base frequency attenuation values are given in Appendix A.3.4.

Note that the distribution of attenuation ratio in Figures 5.3-1, 5.3-2, and 5.3-3, though varying across a fairly tight range, can be approximated by a constant for each of the three ratios. This is especially true for the 30/20 GHz ratio, which approximates a constant value of 2. A tight range for attenuation ratio value indicates potential application to adaptive control. The 50% value is the median *RA*, RA_{med}, value for the experiment year. *RA* exceed (or are less than) RA_{med} for 50% of the time that the base attenuation exceeds 1 dB (as tabulated in Table 5.3-1 for the months and experiment year). RA_{med} values are given in Table 5.3-2 for the frequency pairs. Occurrence extremes (i.e., below about 5% and above about 95% of the time) yield relatively large and small attenuation ratios for very small amounts of time (that is, the *RA* values are unlikely; i.e., occur with low probability). Plots of *RA* vs. % Time Exceeded for the months in the year are also included in Appendix A.3.1.

Table 5.3-2

RA_{med}, for One Year of Olympus Data (for $ACA(f_L) > 1\text{dB}$)

Model/Data	30/20	20/12	30/12
VaTech RA_{med}	1.93	2.86	5.56

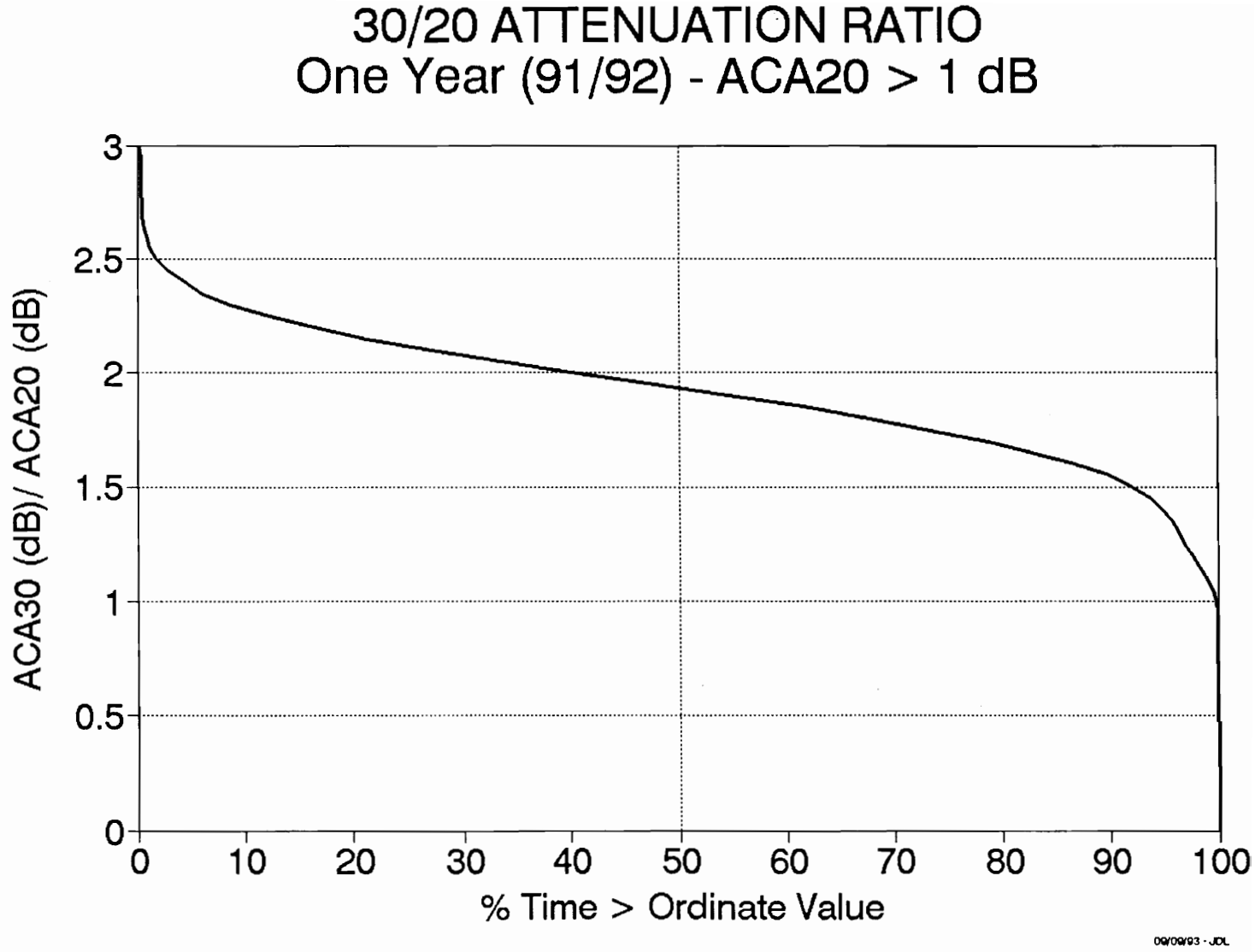

Figure 5.3-1 30/20 *RA* vs. % Time - One Year (91/92) - ACA(20) > 1 dB

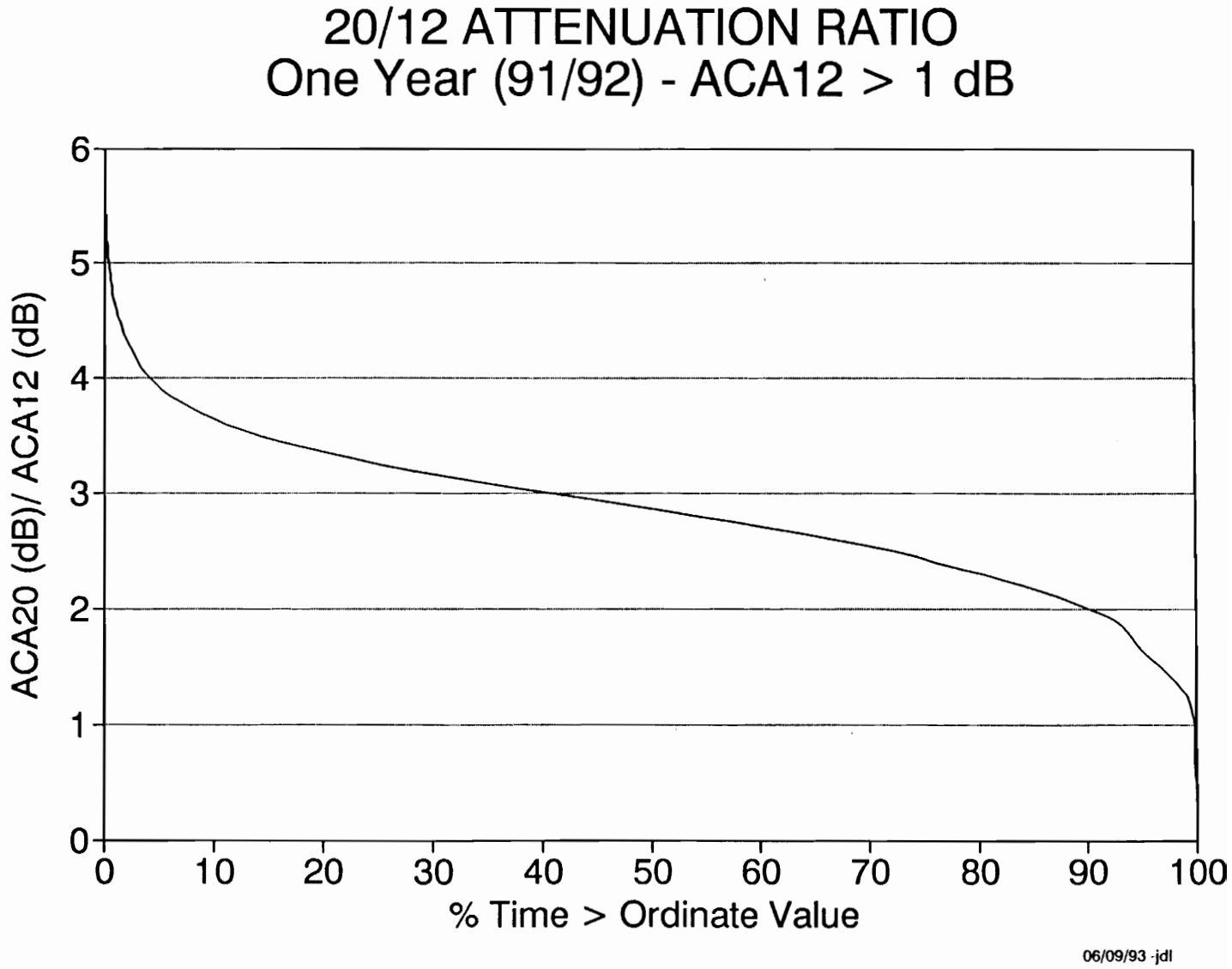

Figure 5.3-2 20/12 *RA* vs. % Time - One Year (91/92) - ACA(12) > 1 dB

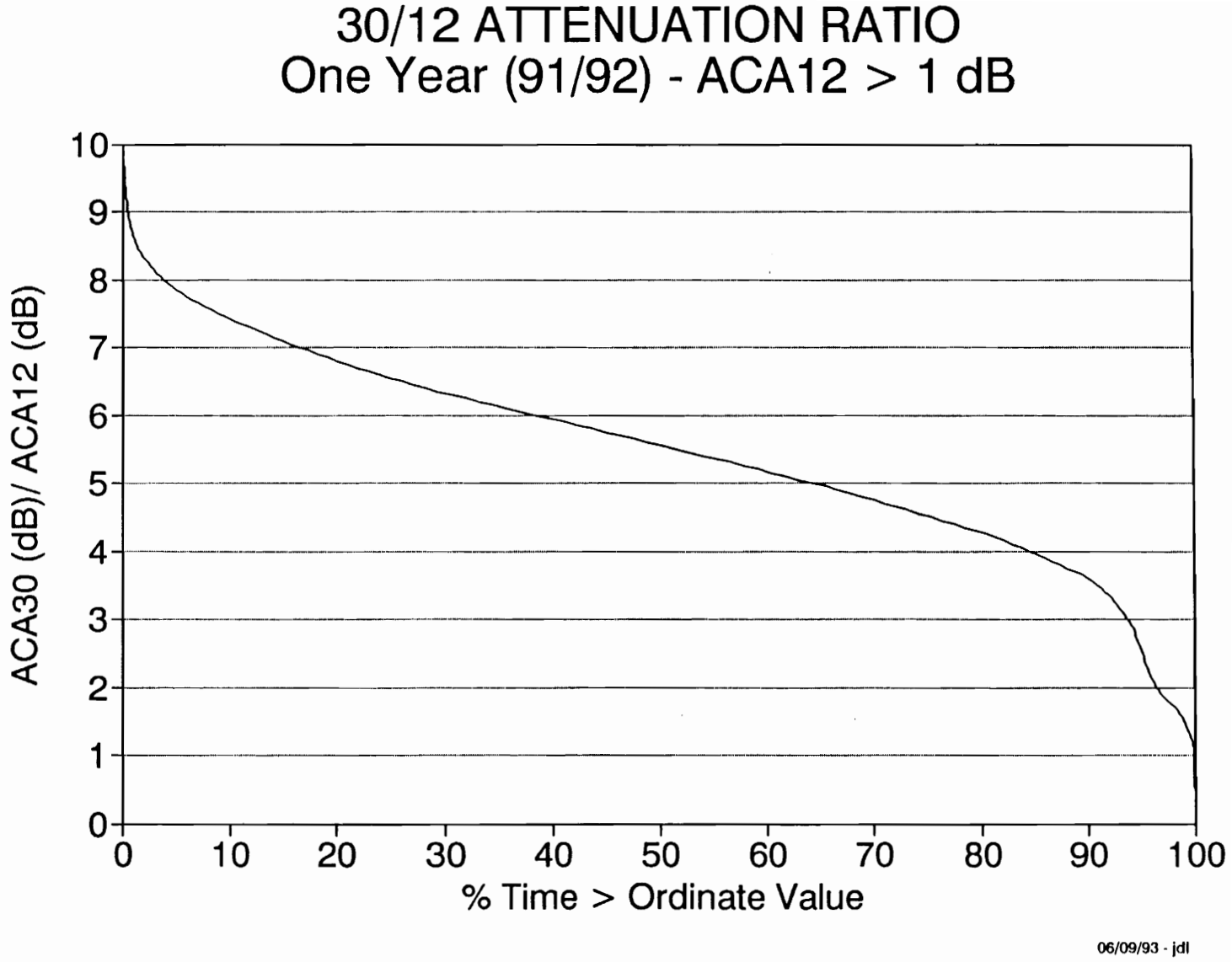

Figure 5.3-3 30/12 *RA* vs. % Time - One Year (91/92) - ACA(12) > 1 dB

5.3.2 *RA* vs. base attenuation for the Analysis Year

In Section 5.3.1, all *RA* data were pooled regardless of attenuation level. The binned *RA* values can also be plotted as a function of the base frequency attenuation for a constant percentage of time exceeded. Yearly plots where attenuation ratio exceeds a specific value for 1%, 10%, 50%, 90% and 99% of the time are given in Figures 5.3-4, 5.3-5, and 5.3-6 for the frequency ratios under consideration (30/20, 20/12, and 30/12) The percentage of time exceeded is for each range of base frequency attenuation values (e.g., 1-2 dB, 2-3 dB, 3-4 dB, etc.). For example, for the 20/12 attenuation ratio data in Figure 5.3-5, when attenuation at 12 GHz is between 6 and 7 dB, attenuation ratio is equal to or less than 2.9 for 90 % of the time that the 12 GHz attenuation is between 6 and 7 dB. Plotting *RA* as a function of base frequency attenuation reveals the dependence *RA* on fade level.

The total time base is different than that of the plots of *RA* versus percentage of time exceeded. As an example, the total time base for 30/20 plot of Figure 5.3-4 is the amount of time that ACA20 exceeds 1 dB (about 1.23% of the year from Table 5.3-1 times the percentage of the year represented by 30/20 which is 90.4% from Table 5.2-1). The 99% level of occurrence is based on this portion of the year. The 50% level of occurrence of *RA*, RA_{med_i}, is the median of *RA* for each *i*th 1-dB bin on the base frequency attenuation Plots for the individual months are included in Appendix A.3.2.

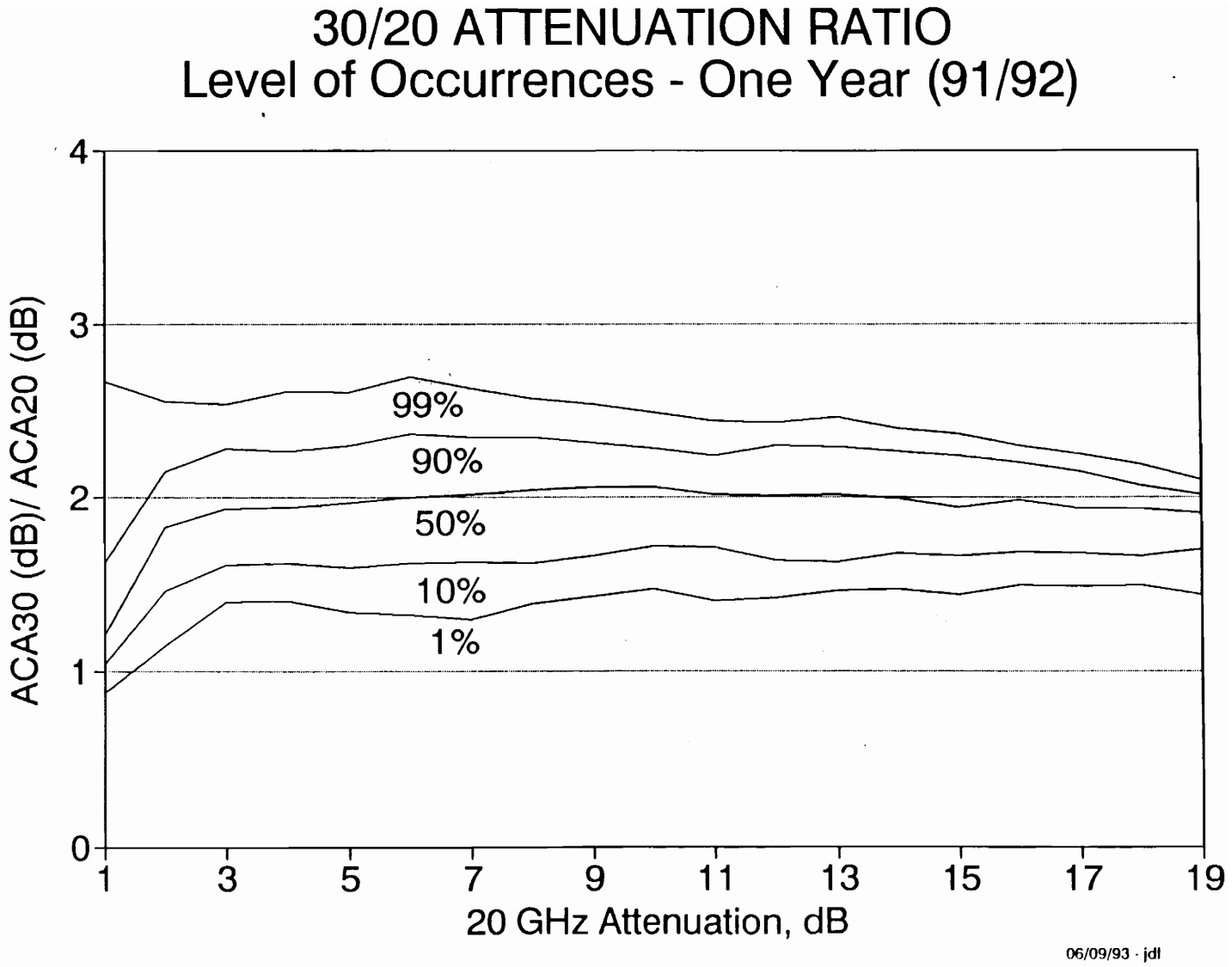

Figure 5.3-4 30/20 *RA* vs. ACA20, Level of Occurrences - One Year (91/92)

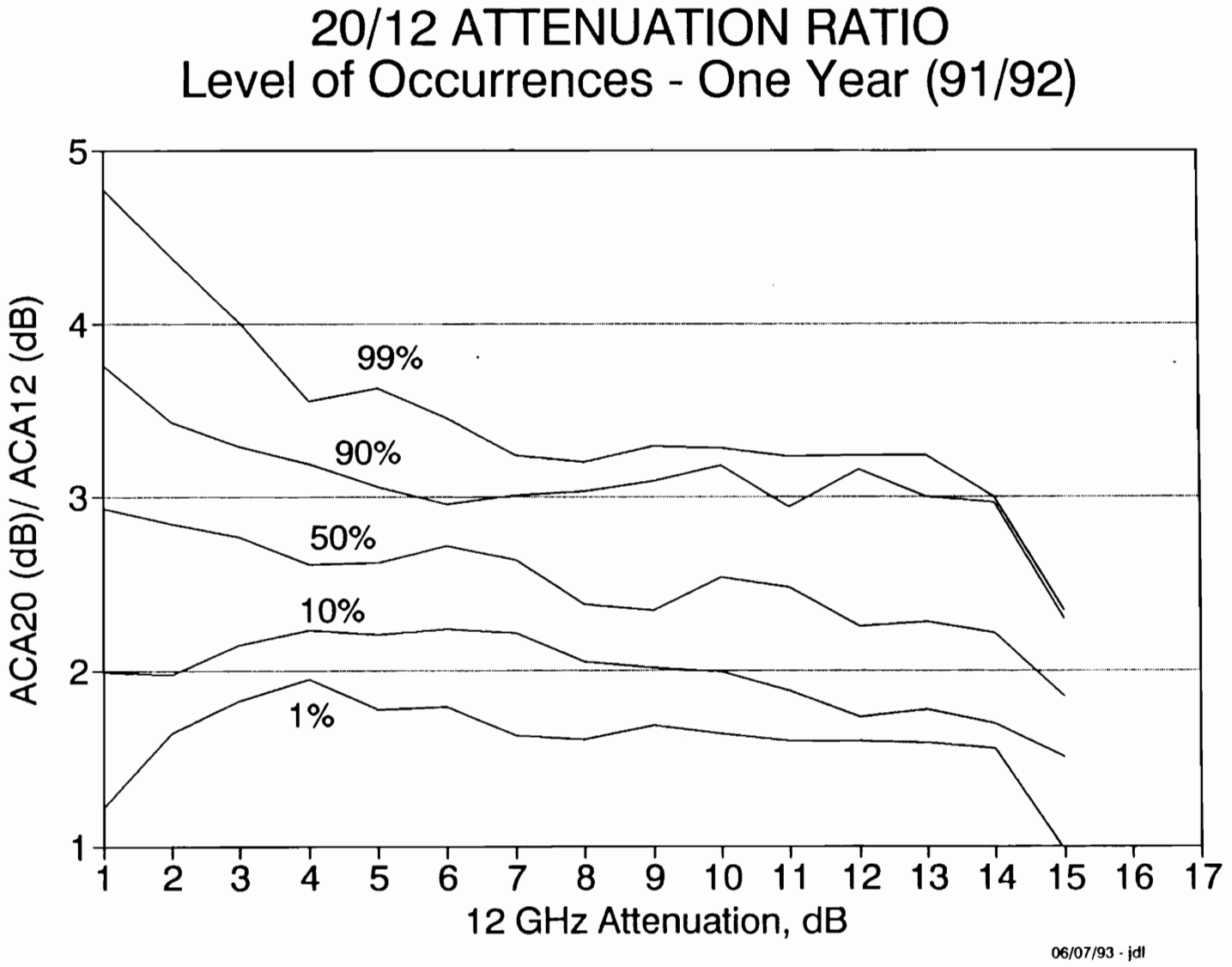

Figure 5.3-5 20/12 *RA* vs. ACA12, Level of Occurrences - One Year (91/92)

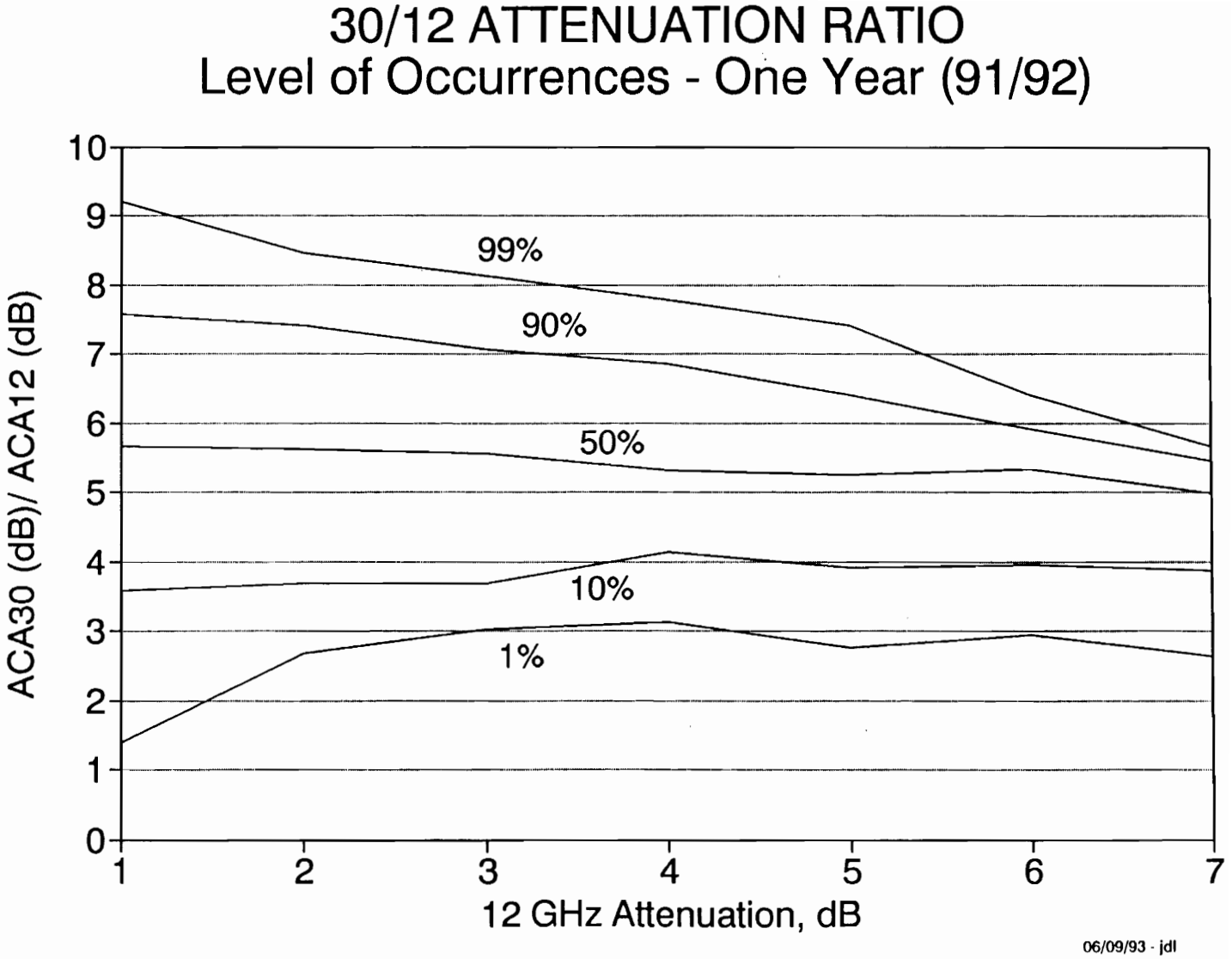

Figure 5.3-6 30/12 *RA* vs. ACA12, Level of Occurrences - One Year (91/92)

A linear regression was performed on the 50% level of occurrence at each 1 dB base attenuation level for $ACA(f_U)$ versus $ACA(f_L)$ for the experiment year. The slope of the line gives an attenuation ratio for the year averaged over the attenuation levels. This can be contrasted with Figures 5.3-1, 5.3-2, and 5.3-3 which pool all data without regard to attenuation level. This removes the heavy bias of the much more frequently occurring low attenuation levels. RA_{ave} is defined as the slope of the line given by linear regression. RA_{ave} is the average of the medians for 1-dB binned values of base frequency attenuation. Linear regressions are shown for the ratios 30/20, 20/12 and 30/12 in Figures 5.3-7, 5.3-8 and 5.3-9. The slopes and standard deviation of error are given in Table 5.3-3.

Table 5.3-3

RA_{ave} at 30/20, 20/12, & 30/12 - One Year (91/92)

f_U / f_L	30/20	20/12	30/12
Slope, RA_{ave}	2.01	2.52	5.43
Std. Dev. of Error	0.34	0.90	0.44

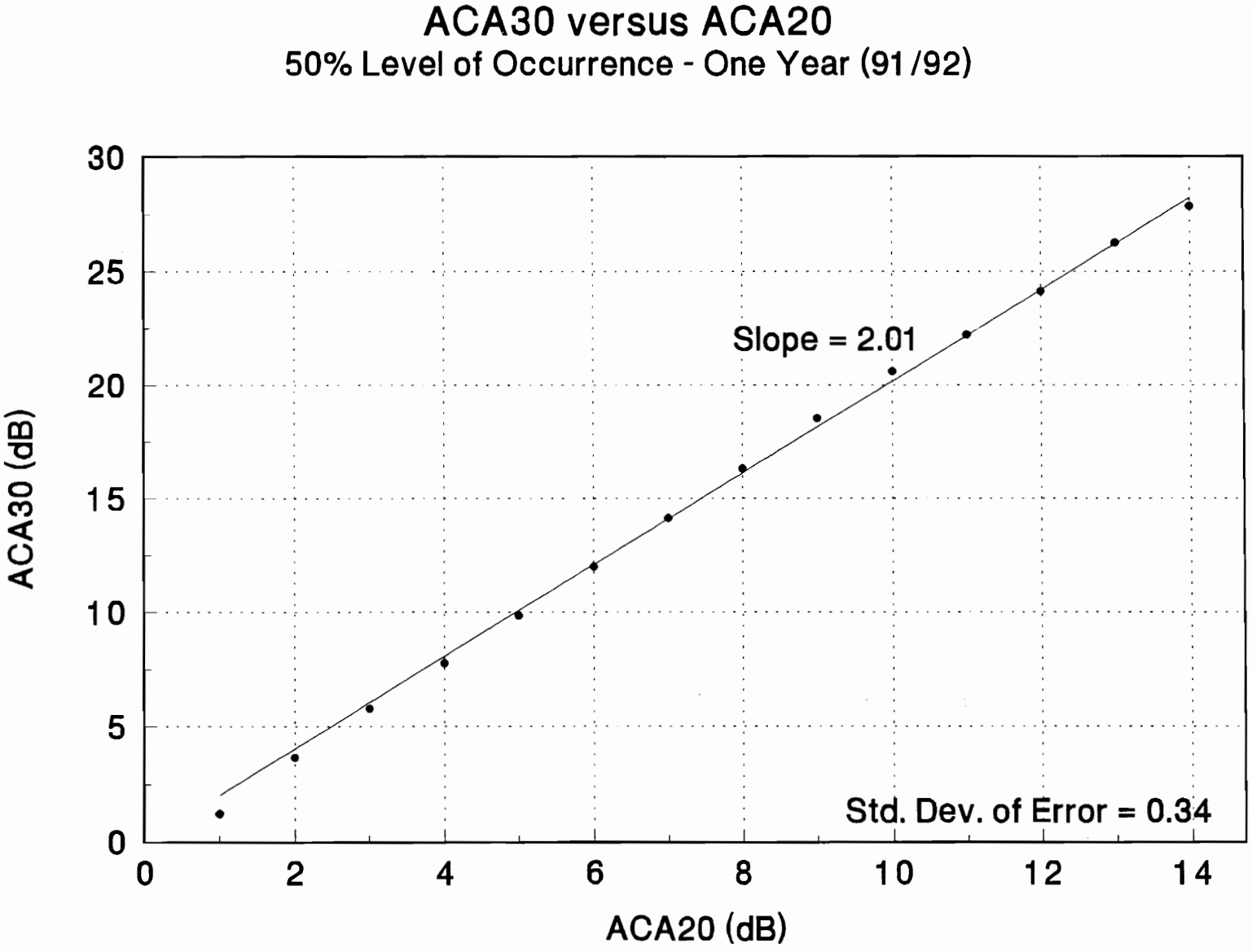

Figure 5.3-7 ACA30 vs. ACA20, 50% Level of Occurrence - One Year (91/92)

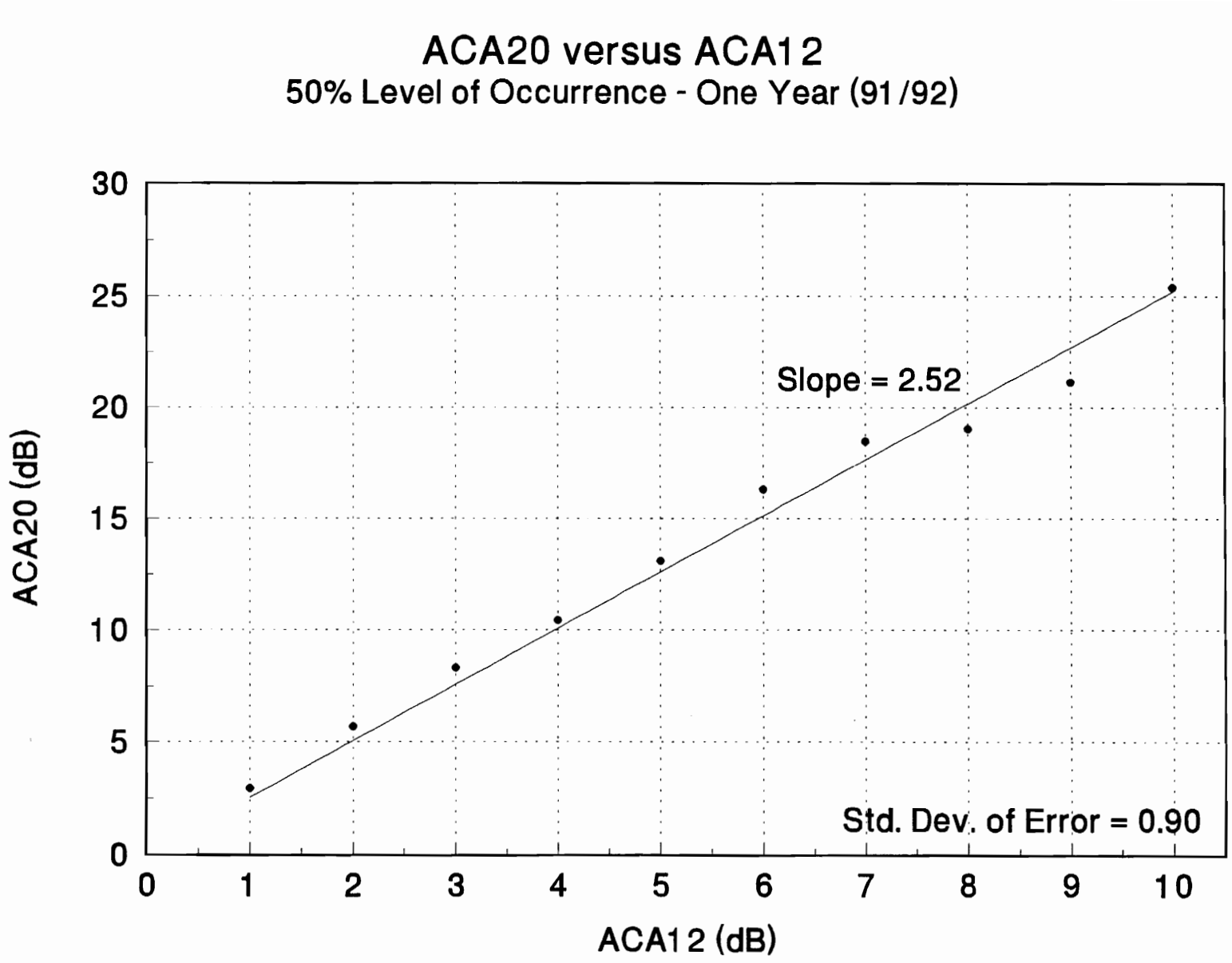

Figure 5.3-8 ACA20 vs. ACA12, 50% Level of Occurrence - One Year (91/92)

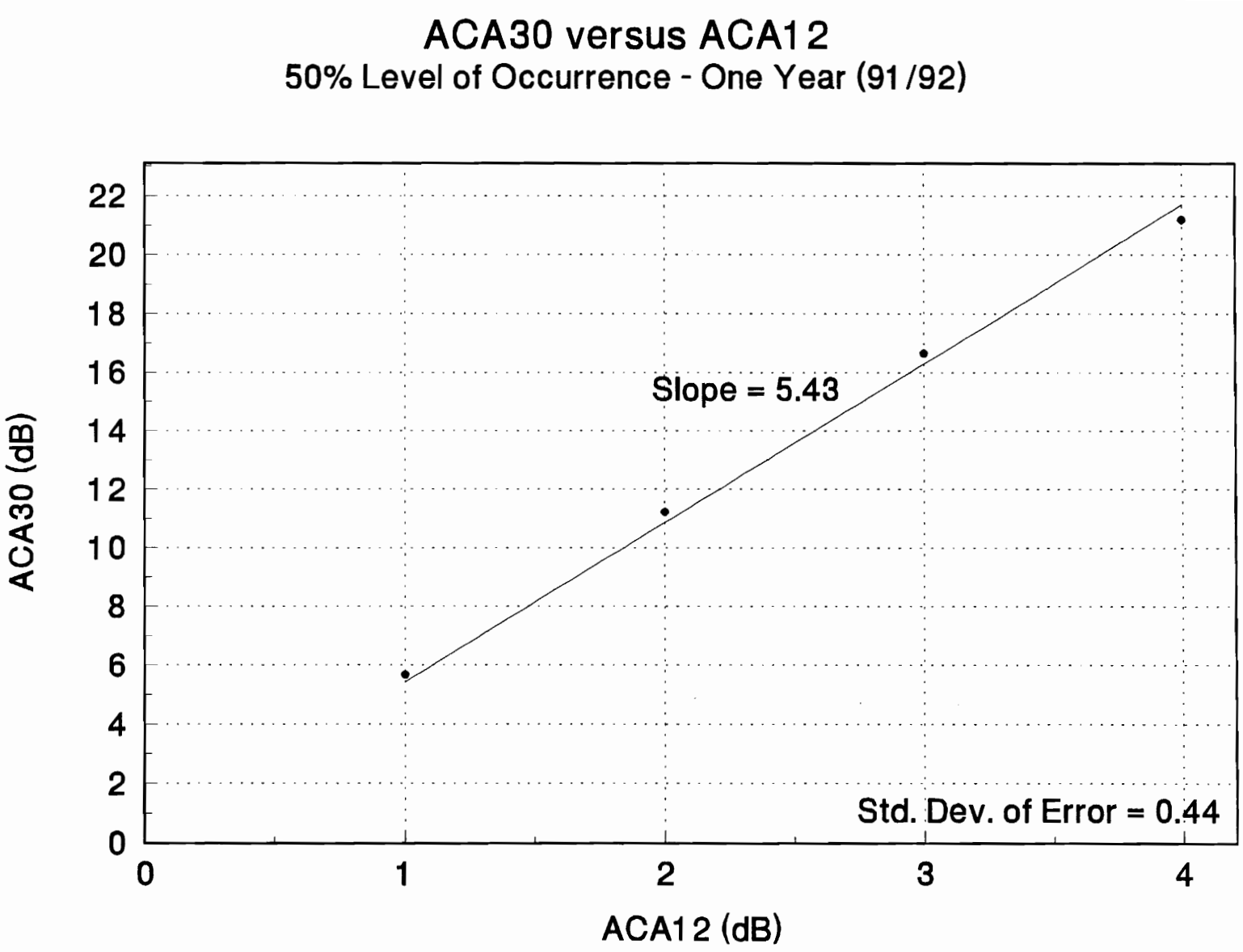

Figure 5.3-9 ACA30 vs. ACA12, 50% Level of Occurrence - One Year (91/92)

5.3.3 Reliability of the attenuation ratio

Attenuation ratio statistics can be skewed by the widely different attenuation values over the large frequency range of this experiment. Because rain produces much larger attenuation at 30 GHz than at 12 GHz, or at even 20 GHz, the 30 GHz and 20 GHz receivers will become saturated (at approximately 35 dB) while the lower frequency receivers will not. Attenuation ratio statistics will be biased if they include data points with the upper frequency attenuation saturated [2].

One way to handle saturation bias is to eliminate *RA* data points if the attenuation on either frequency is above a threshold level. Based on a constant attenuation ratio (in this case, the square law relation), and knowing the saturation point for each receiver, one can calculate a threshold for the base frequency attenuation. Stutzman, *et al.*, [2] employed this method and obtained the values in Table 5.3-4.

Table 5.3-4

Attenuation Ratio Data Limits [2]

Frequencies (GHz)		(1)	(2)	(3)
Upper	Lower	Upper Frequency *ACA* Maximum for Saturation [dB]	Expected Ratio (based on CCIR model)	Theoretical Lower Freq. *ACA* Limit = (1)/(2) [dB]
30	20	35	1.96	17.9
20	12	35	2.19	16.0
30	12	35	4.28	8.2

For example, for the 30/20 frequency pair from Table 5.3-4, virtually no saturation on ACA30 occurs for ACA20 < 17.9 dB. In practice, the threshold is somewhat lower than theory suggests. Table 5.3-5 shows the thresholds for those months in which saturation of the receivers occurs. The threshold for the year for each ratio is also tabulated. The percentage of saturation in the month of occurrence and for the whole year is also given.

Table 5.3-5

Saturation in the Data Set by Months and Year

Months *RA* for 30/20	Value of $ACA(20)$ when $ACA(30)$ Begins to Saturate	% Saturation in Month (ACA30 > 34 dB)
June 1992	14-15 dB	0.0711
July 1992	15-16 dB	0.1270
December 1991	15-16 dB	0.0237
Months *RA* for 20/12	Value of $ACA(12)$ when $ACA(20)$ Begins to Saturate	% Saturation in Month (ACA20 > 34 dB)
June 1992	12-13 dB	0.0014
July 1992	10-11 dB	0.0125
Months for *RA* for 30/12	Value of $ACA(12)$ when $ACA(30)$ Begins to Saturate	% Saturation in Month (ACA30 > 34 dB)
June 1992	3-4 dB	0.0711
July 1992	4-5 dB	0.1270
December 1991	5-6 dB	0.0237
RA frequencies for One Year (91/92)	Value of $ACA(f_L)$ when $ACA(f_U)$ begins to Saturate	% Saturation in Year
30/20	14-15 dB	0.02915
20/12	10-11dB	0.00119
30/12	3-4 dB	0.01880

For data sets biased by saturation, plots of *RA* vs. % Time Exceeded are slightly unreliable because of saturation at the higher attenuations. Plots of *RA* vs. Base

Attenuation are reliable below the base frequency attenuation value where the upper frequency receiver saturates (tabulated in Table 5.3-5). Beyond this saturation value, the *RA* vs Base Attenuation curve is pulled down by the saturation.

5.3.4 Probability of occurrence of *RA*

Attenuation ratio (that is, the "instantaneous" *RA* value) has been observed to vary throughout a precipitation event (e.g. a hysteresis effect is documented in Section 3.3.2.1). Both the Japanese and COMSAT experiments [1] report that the attenuation ratio is not constant, but neither address its variability. This indicates that *RA* is not solely a function of frequency because, if it were, *RA* would be constant. Since *RA* is plotted as a cumulative distribution over time (i.e., *RA* vs. % Time Exceeded), it is of interest to plot a probability distribution function (PDF) of *RA* to quantify the variation. Examples of PDFs for January 1991 are given in Figures 5.3-10 through 5.3-15 for a base frequency attenuation greater than 1 dB and for a base frequency attenuation range of 1 dB to 2 dB for the considered frequency ratios. In general, the PDFs show the range over which *RA* can vary, and they also show the most probable values for *RA*. Other PDFs for January 1991 are included in Appendix A.3.5. Since only January has been examined and since January experienced low rain fall, reliable conclusions cannot be drawn without comparison to other months. PDFs for the analysis year would be of interest, but they are not included in this report.

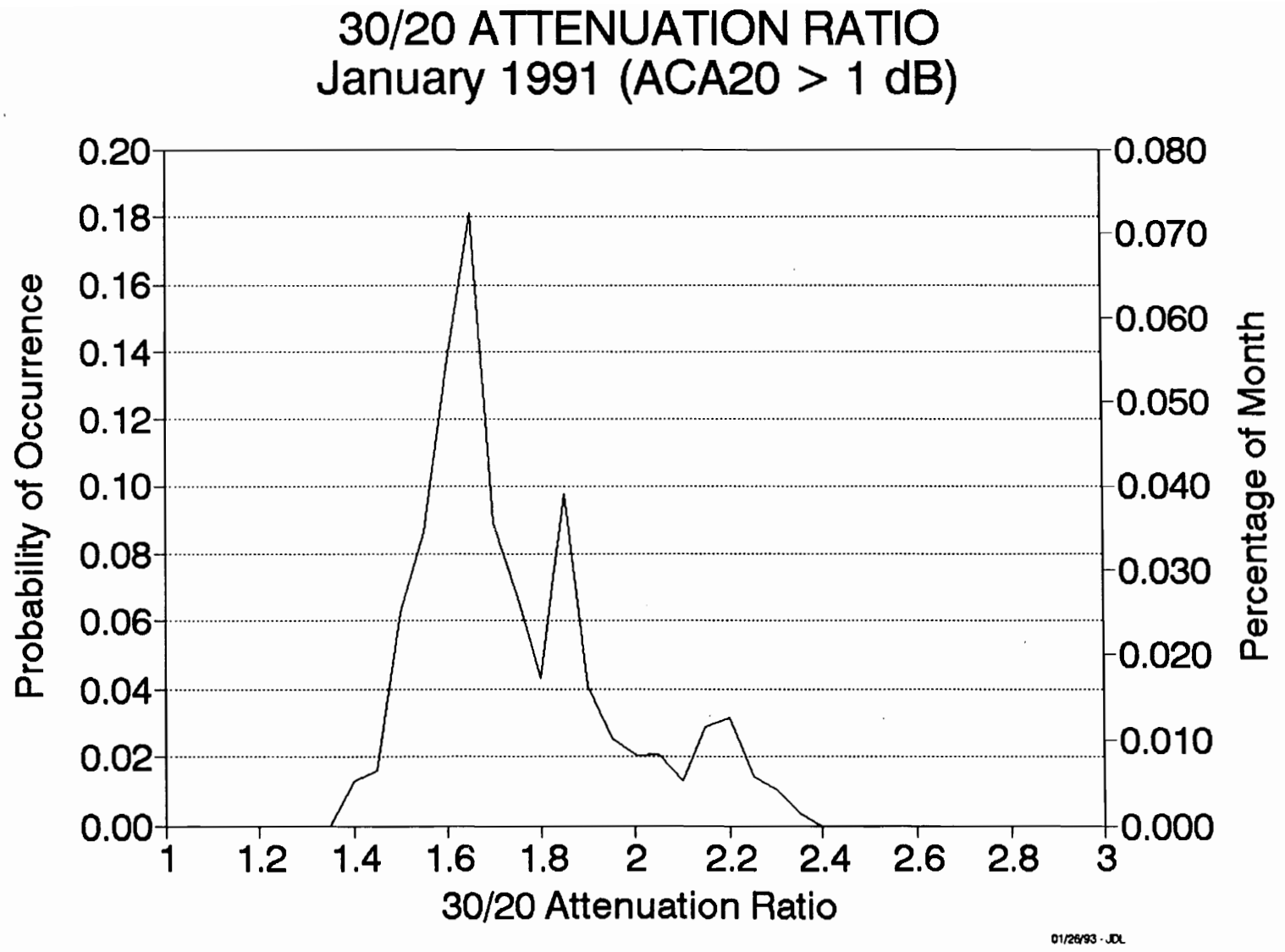

Figure 5.3-10 PDF of 30/20 *RA* for January 1991 - ACA(20) > 1 dB

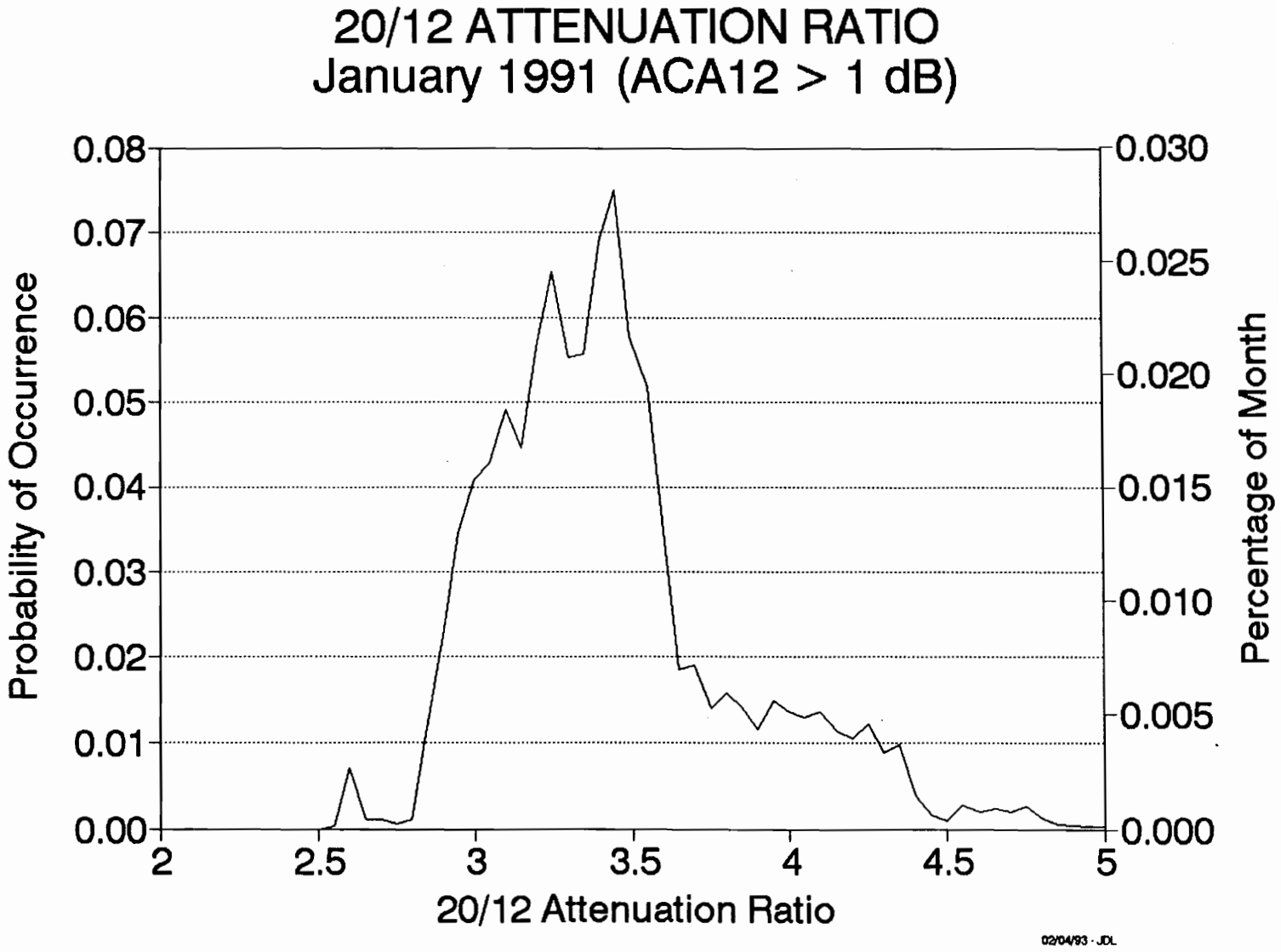

Figure 5.3-11 PDF of 20/12 *RA* for January 1991 - ACA(12) > 1 dB

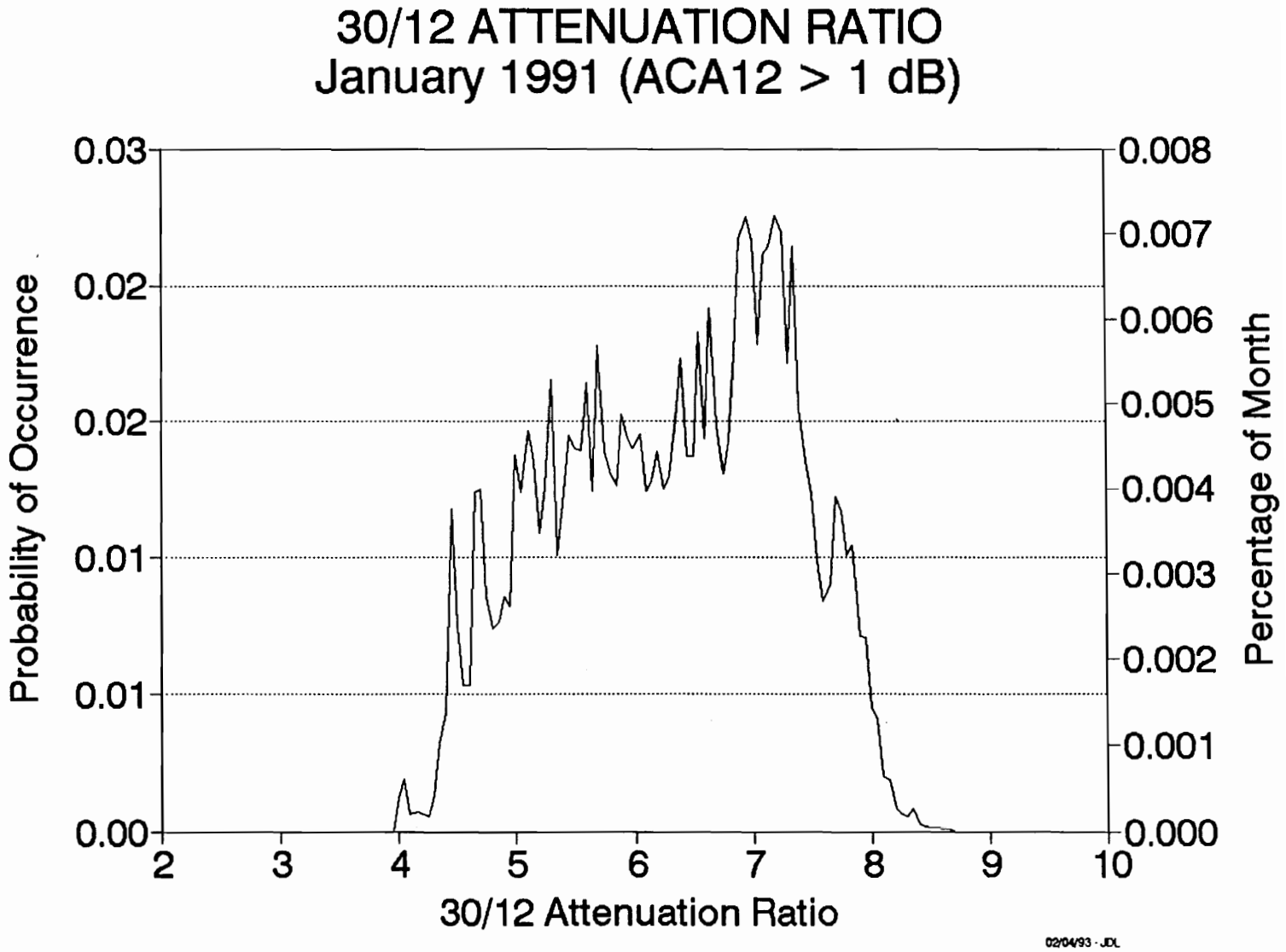

Figure 5.3-12 PDF of 30/12 *RA* for January 1991 - ACA(12) > 1 dB

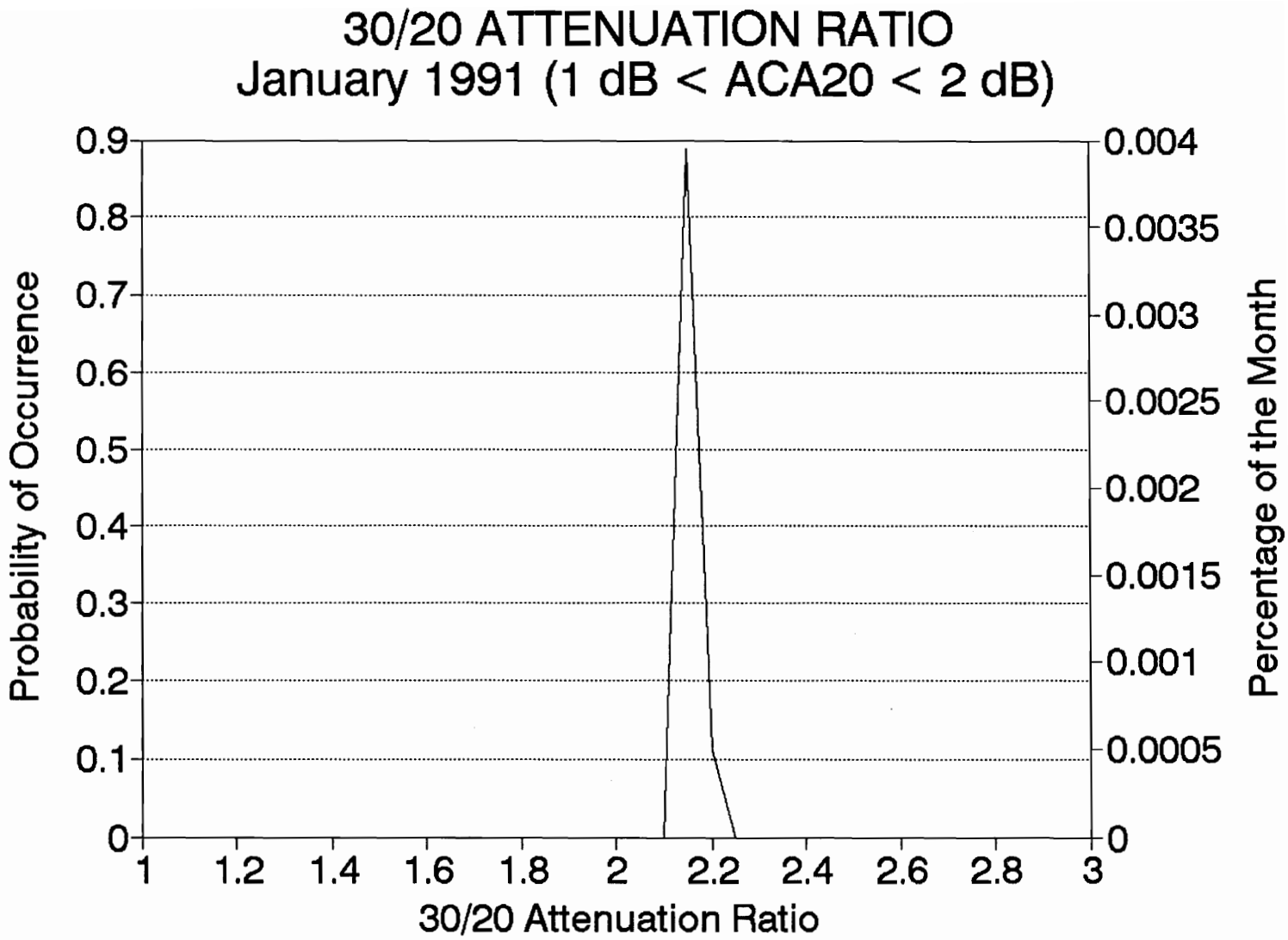

Figure 5.3-13 PDF of 30/20 *RA* for January 1991 - (1 dB < ACA(20) < 2 dB)

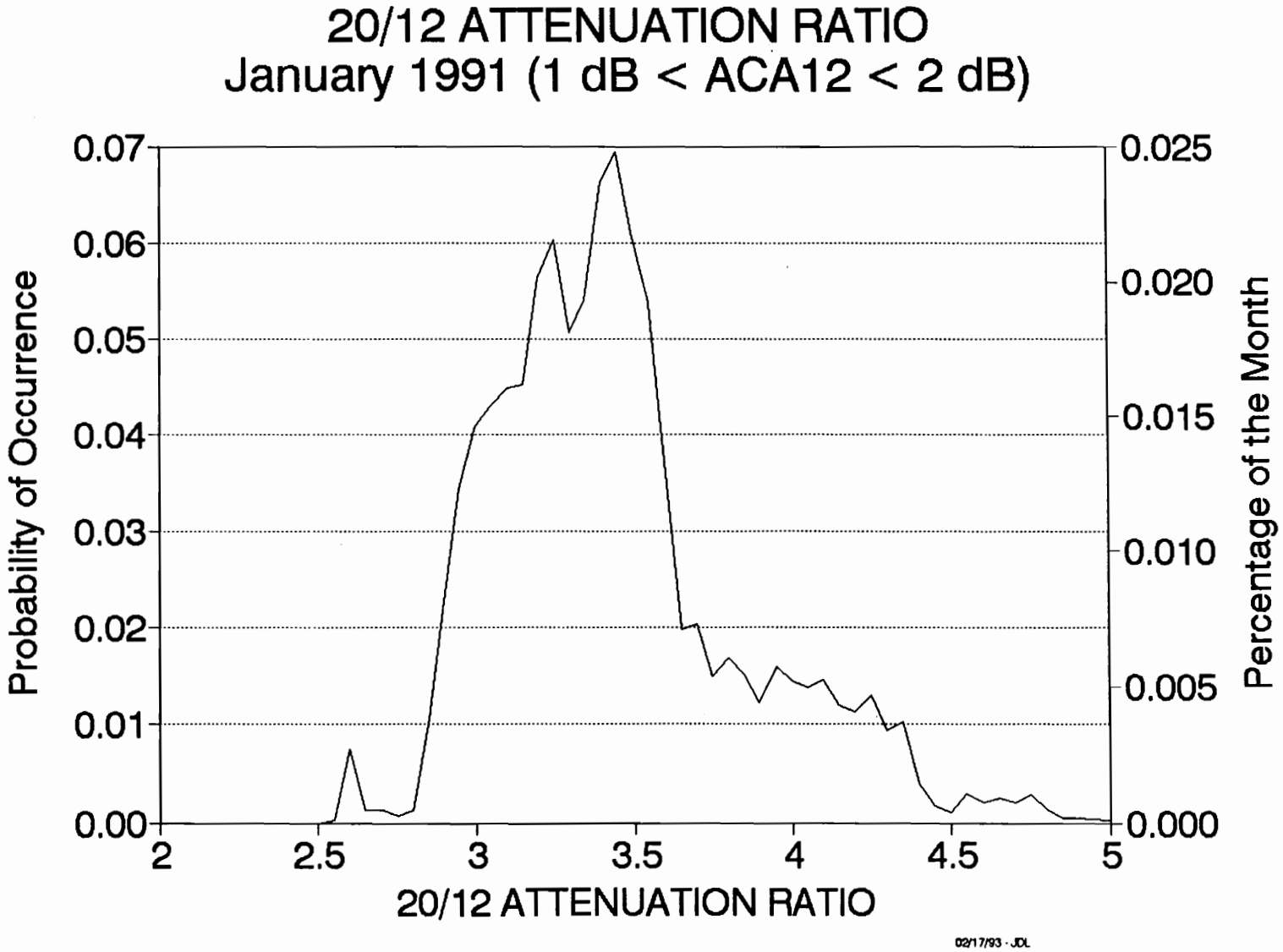

Figure 5.3-14 PDF of 20/12 *RA* for January 1991 - (1 dB < ACA(20) < 2 dB)

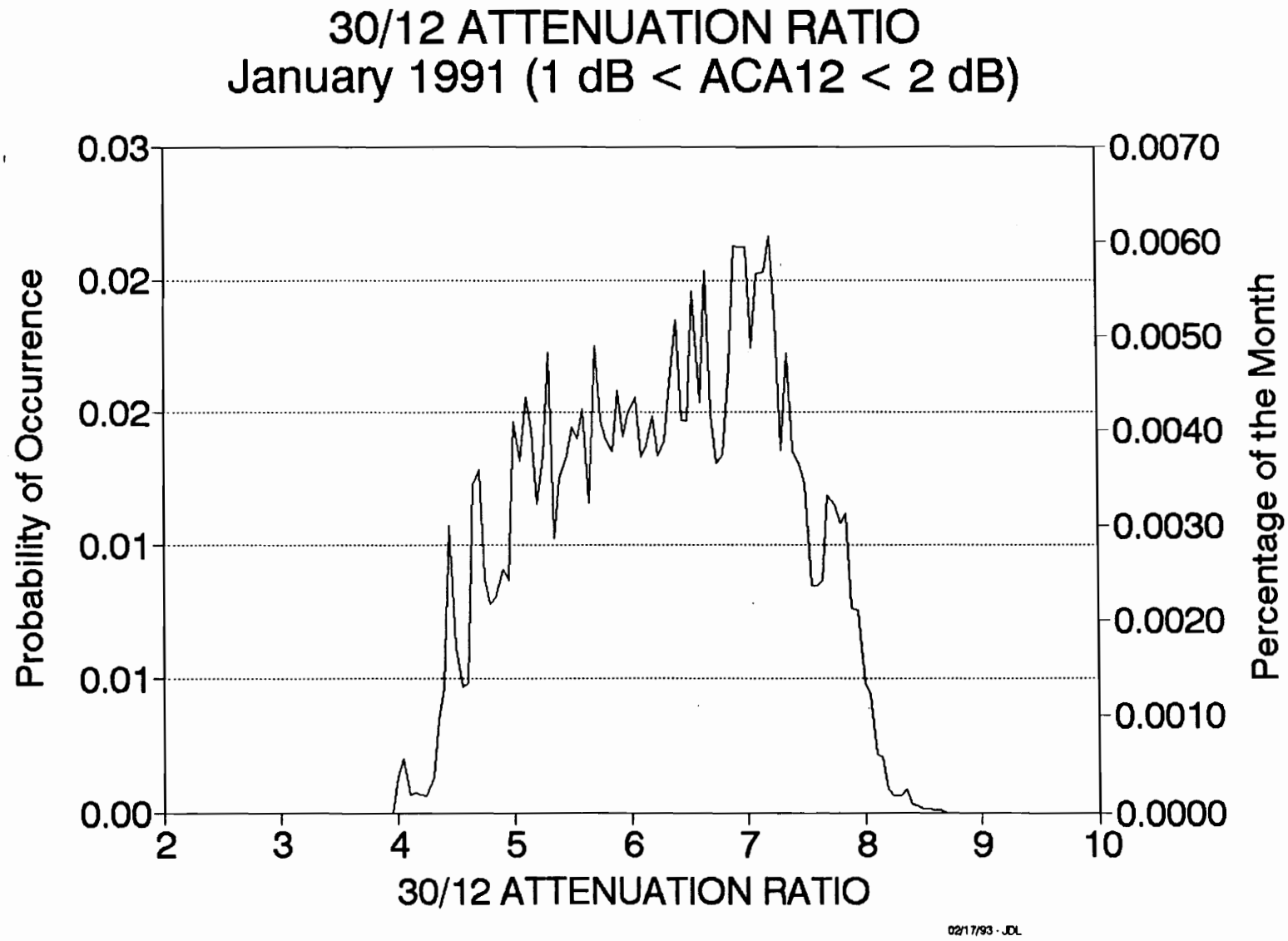

Figure 5.3-15 PDF of 30/12 *RA* for January 1991 - (1 dB < ACA(20) < 2 dB)

5.3.5 Time variation of *RA* for a representative rain event

Though cumulative distributions and probability distributions of *RA* are valuable, the behavior of *RA* in real time is of particular interest. In the following figures, a representative rain event (occurring on May 14, 1991) is examined in some detail with respect to attenuation scaling. Attenuation with Respect to Clear Air (*ACA*) for 30 GHz and 20 GHz are plotted against each other in Figure 5.3-16 (i.e., ACA30 versus ACA20, in dB).

The 10-Hz *ACA* data (10 *ACA* sample points per second) are averaged using the 30-s moving average of (3.1-2), and then each fiftieth (50th) point is plotted to produce the following figures. The moving average is used to filter out some of the scintillation effects. Figure 5.3-17 shows ACA30 versus ACA20 without the moving average, again with each fiftieth point plotted.

A linear regression was performed to derive a "best fit" line through approximately one hour of attenuation data for the event. The slope of the line represents an average *RA* for the event, $RA_{ave(event)}$. The slope values in Table 5.3-6 show that the slope is the same with the moving average and without the moving average for 30/20 which indicates that scintillation is symmetrical about $RA_{ave(event)}$.

The statistics for the event, with and without a moving average used, allow a direct comparison in Table 5.3-7. The higher error statistics from the plot without the moving average are due primarily to the inclusion of scintillation effects. Scintillation causes greater deviation (spread) from the mean value of the ratio of the upper frequency attenuation and the lower (base) frequency attenuation.

Table 5.3-6

Linear Regression Slope for Ratio Pairs for May 14, 1991 Rain Event

Ratio pairs	Slope of Linear Regression
30/20 - 30 sec moving average	2.27
30/20 - no moving average	2.27
20/12 - 30 sec moving average	2.48
30/12 - 30 sec moving average	5.65

The standard deviation of error, s, is usually defined as

$$s = \sqrt{E\left(\left|ACA(f_U)_{predicted} - ACA(f_U)_{measured}\right|^2\right)} \qquad \text{[dB]} \qquad (5.3\text{-}1a)$$

$$ACA(f_U)_{predicted} = ACA(f_L)_{measured} \bullet (\text{Slope of Linear Regress.}) \qquad (5.3\text{-}1b)$$

where $E(\cdot)$ is the expected value. For example, ACA30 versus ACA20 during the May 14, 1991 rain event, (5.3-1) is written as

$$s = \sqrt{E\left(\left|2.27\,ACA20_{measured} - ACA30_{measured}\right|^2\right)} \qquad \text{[dB]} \qquad (5.3\text{-}2)$$

One can further quantify the variation of the error by generating statistics of the absolute difference between the predicted and measured attenuation (without squaring the difference as in (5.3-1) and (5.3-2)). This error is denoted E.

$$E = \left|ACA(f_U)_{predicted} - ACA(f_U)_{measured}\right| \qquad \text{[dB]} \qquad (5.3\text{-}3)$$

For example, for ACA30 versus ACA20, the mean of (5.3-3) can be considered to be the average distance of measured ACA30 from the predicted value of ACA30 on the

"best fit" line, given a particular value of ACA20. Statistics for all three ratios are tabulated in Table 5.3-7.

Table 5.3-7

Error Statistics for Attenuation Ratio Pairs for May 14, 1991 Rain Event

Error equation	*E* from (5.3-3)				*s* from (5.3-2)
Error statistics	minimum	maximum	mean	median	stand.dev
30/20, moving avg.	0.00	4.13	1.78	1.82	1.98
30/20, no moving avg.	0.01	5.66	1.84	1.78	2.11
20/12, moving avg.	0.00	2.76	0.55	0.43	0.73
30/12, moving avg.	0.00	6.41	1.80	1.66	2.14

ACA20 is plotted in Figure 5.3-18 against ACA12 (i.e., against *ACA* at 12 GHz). Figure 5.3-19 shows ACA30 versus ACA12.

It is very interesting to examine the dynamic variations of *RA* during the course of an event. This behavior impacts directly on the utility of adaptive fade countermeasures. Attenuation ratio for 30/20 for a typical rain event is plotted as a function of time in Figure 5.3-20. Attenuation with respect to clear air (*ACA*) is included for both frequencies in Figure 5.3-21. *RA* remains fairly constant (around 2) except as the base frequency attenuation (ACA20 in this example) approaches small values ($\leq$ 1 dB). The relationship between *RA* and the base frequency attenuation is seen more readily in Figure 5.3-22 where *RA* strays away to a value of 5 as ACA20 approaches 1 dB. This high deviation in *RA* is due in part to the small values of *ACA* used to calculate *RA*; that is, a small change in a small *ACA* value can result in a large change in *RA* when a ratio is formed.

A proper perspective on this fluctuation in *RA* is obtained by examining Figure 5.3-16. At low values for ACA20, the standard deviation of error is only about 2 dB.

The high scaling ratios (found at low base frequency attenuations) do not necessarily translate into high upper frequency attenuations precisely because of the low base frequency attenuation values. This degree of error can be well compensated by the typical margin of a earth-space link.

Similar results are found in Figures 5.3-23 through 5.3-25 and Figures 5.3-26 through 5.3-28 which show *RA* vs. time and *RA* vs. base frequency attenuation for 20/12 and 30/12, respectively.

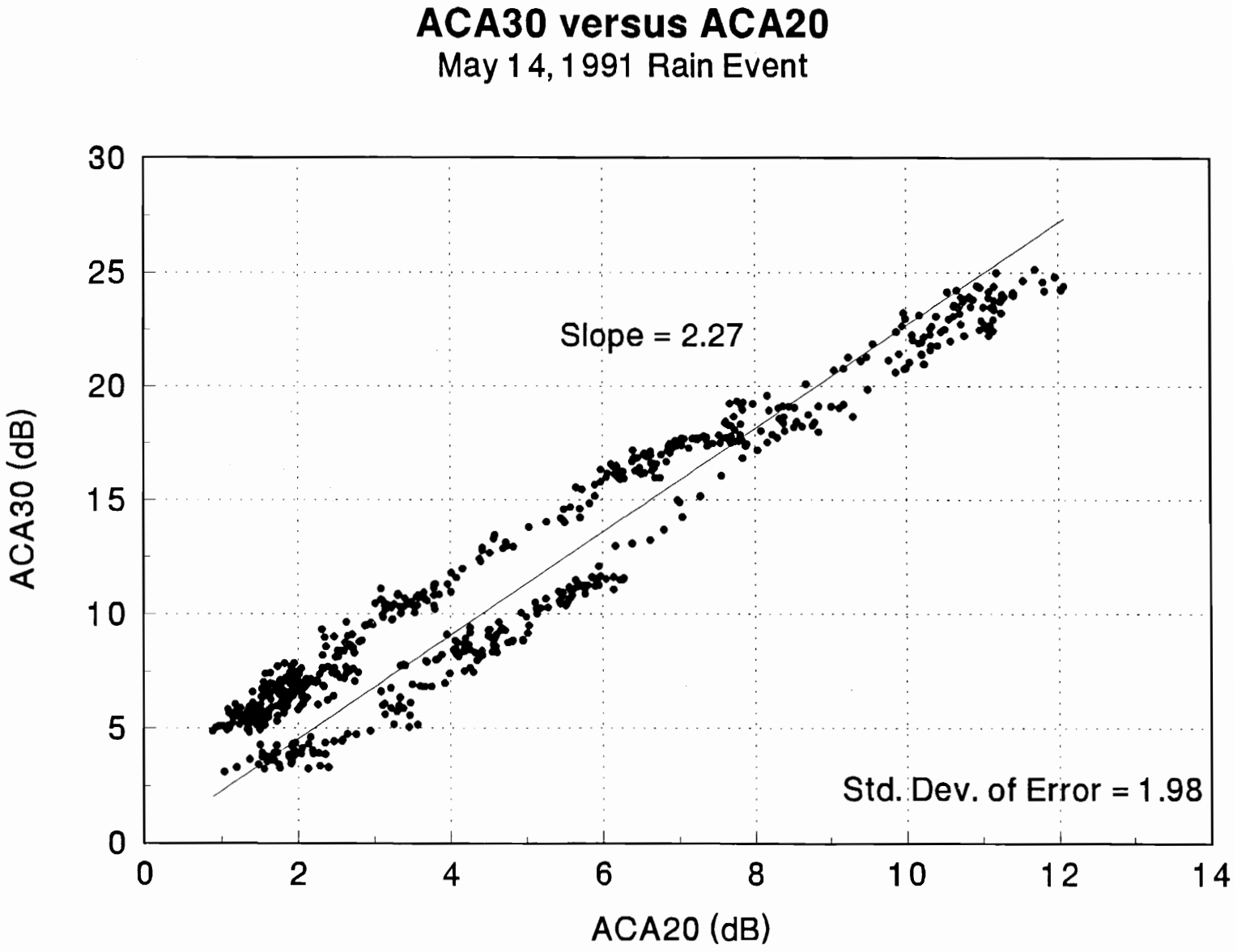

Figure 5.3-16 ACA30 vs. ACA20, May 14, 1991 Rain Event

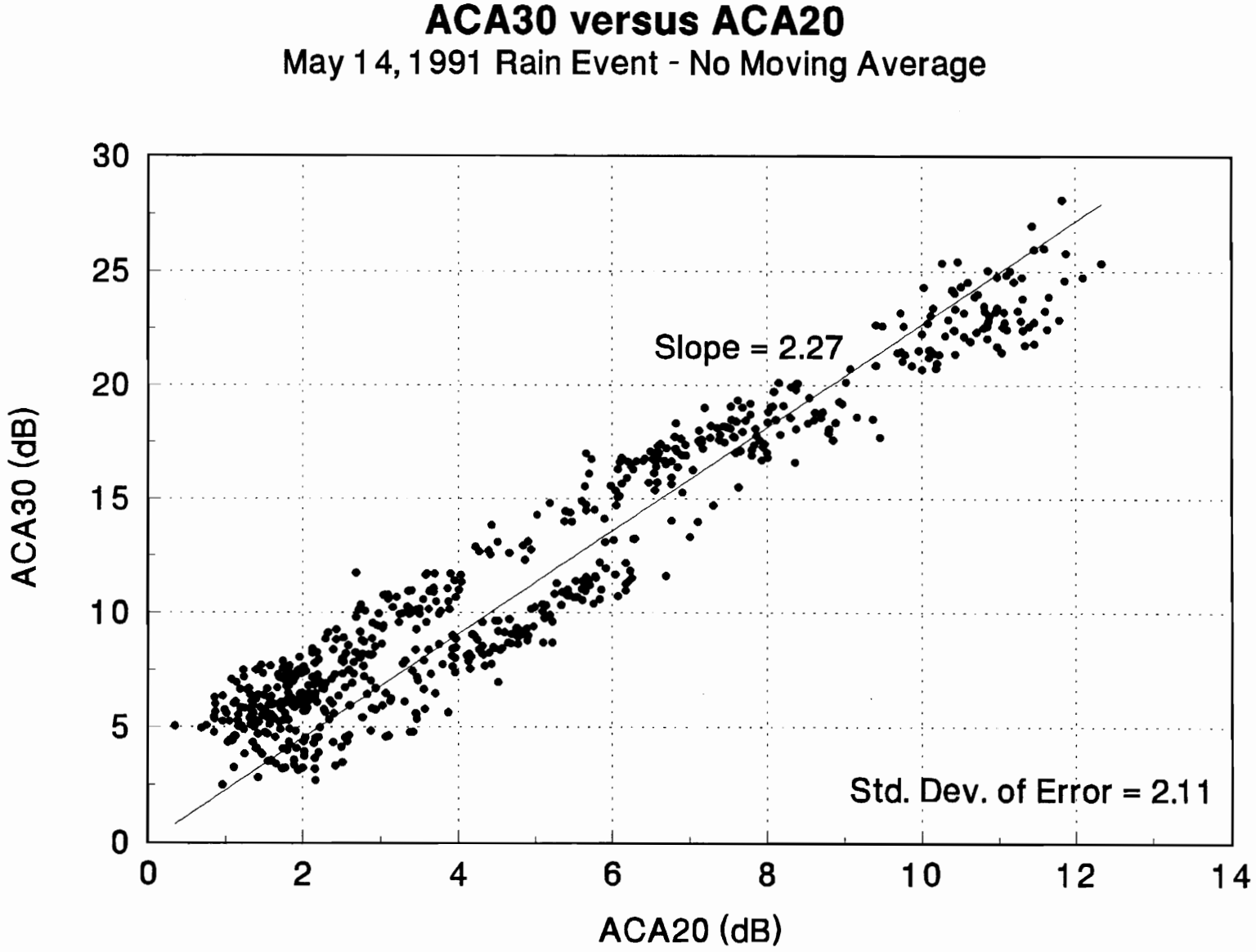

Figure 5.3-17 ACA30 vs. ACA20, May 14, 1991 Rain Event, no moving average

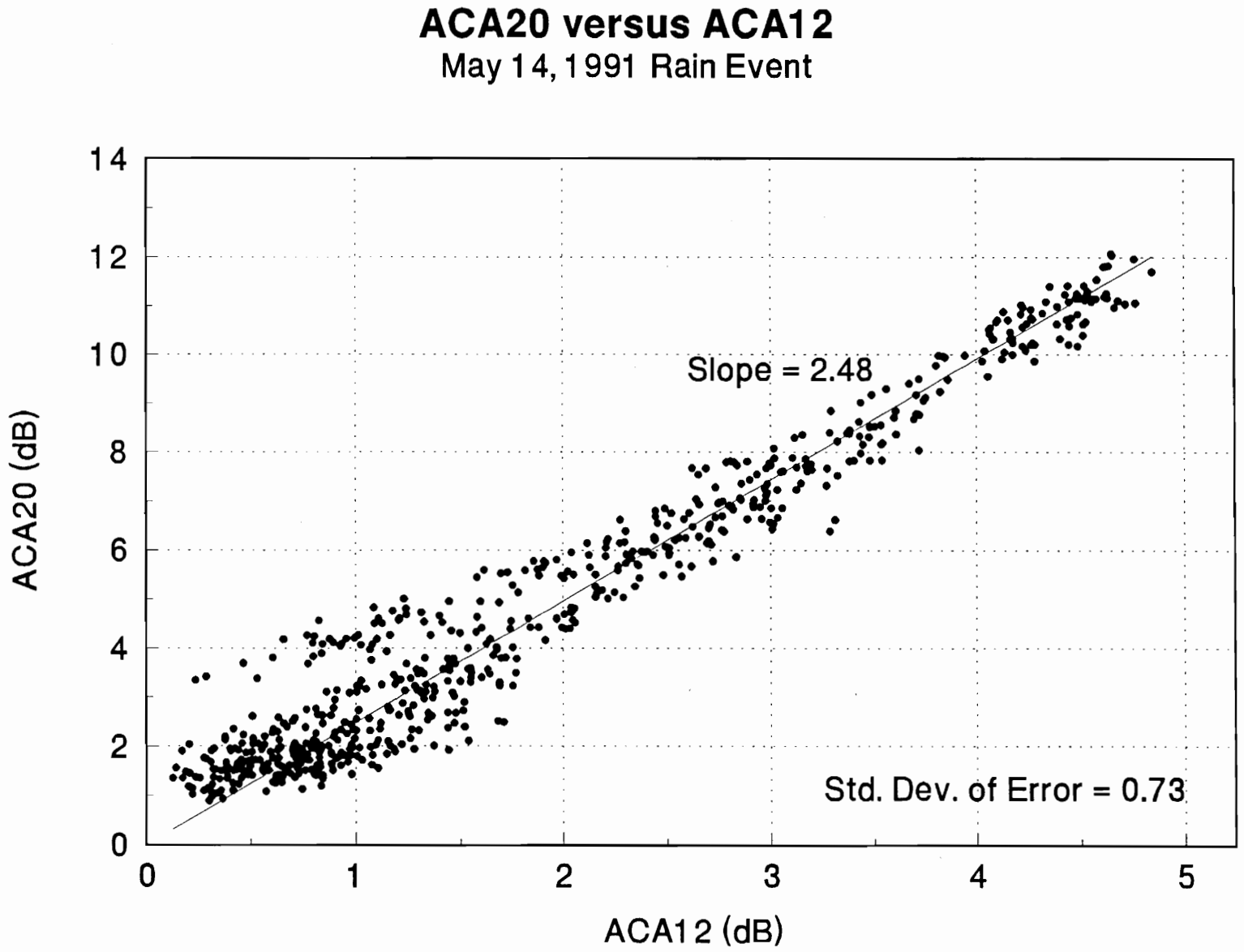

Figure 5.3-18 ACA20 vs. ACA12, May 14, 1991 Rain Event

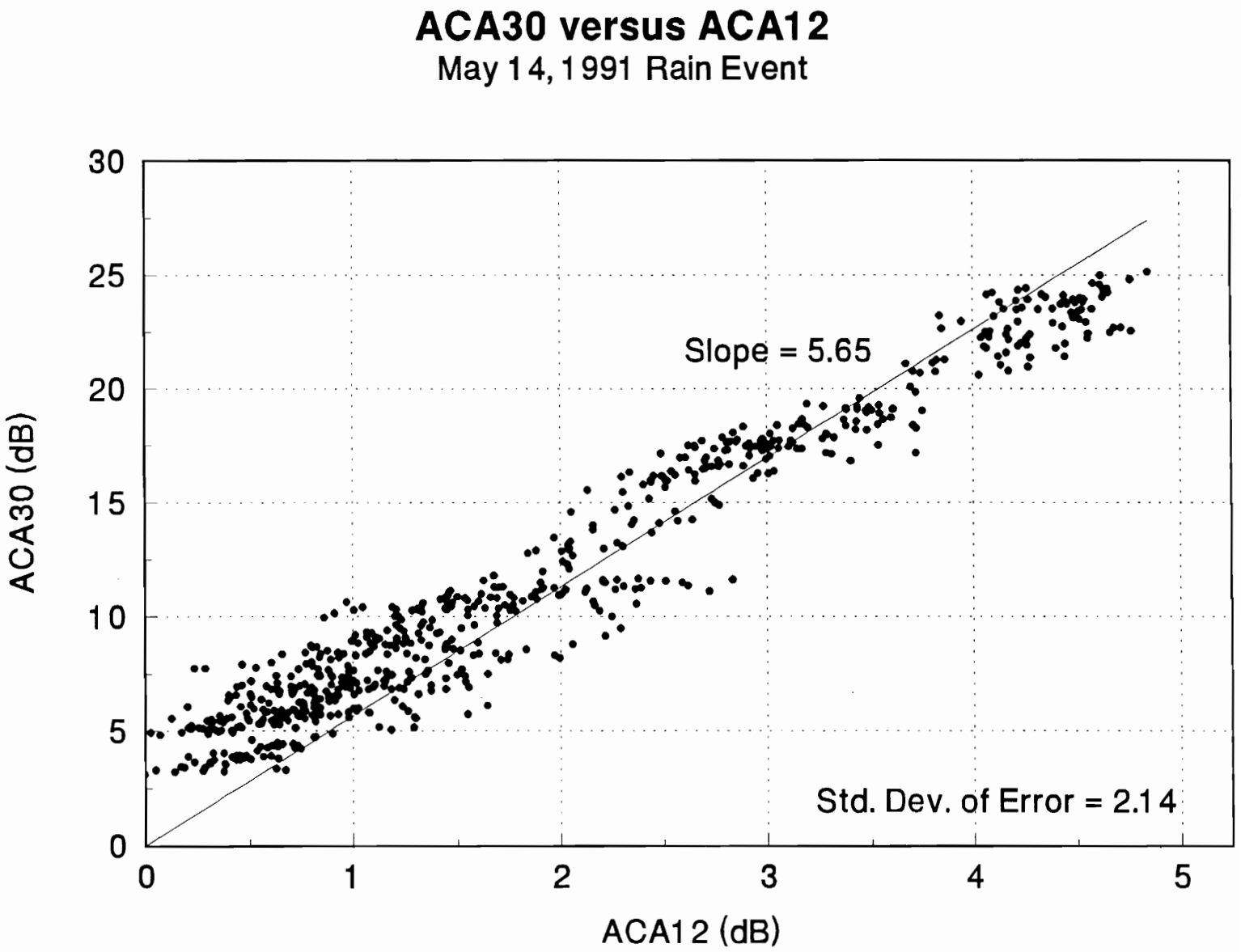

Figure 5.3-19 ACA30 vs. ACA12, May 14, 1991 Rain Event

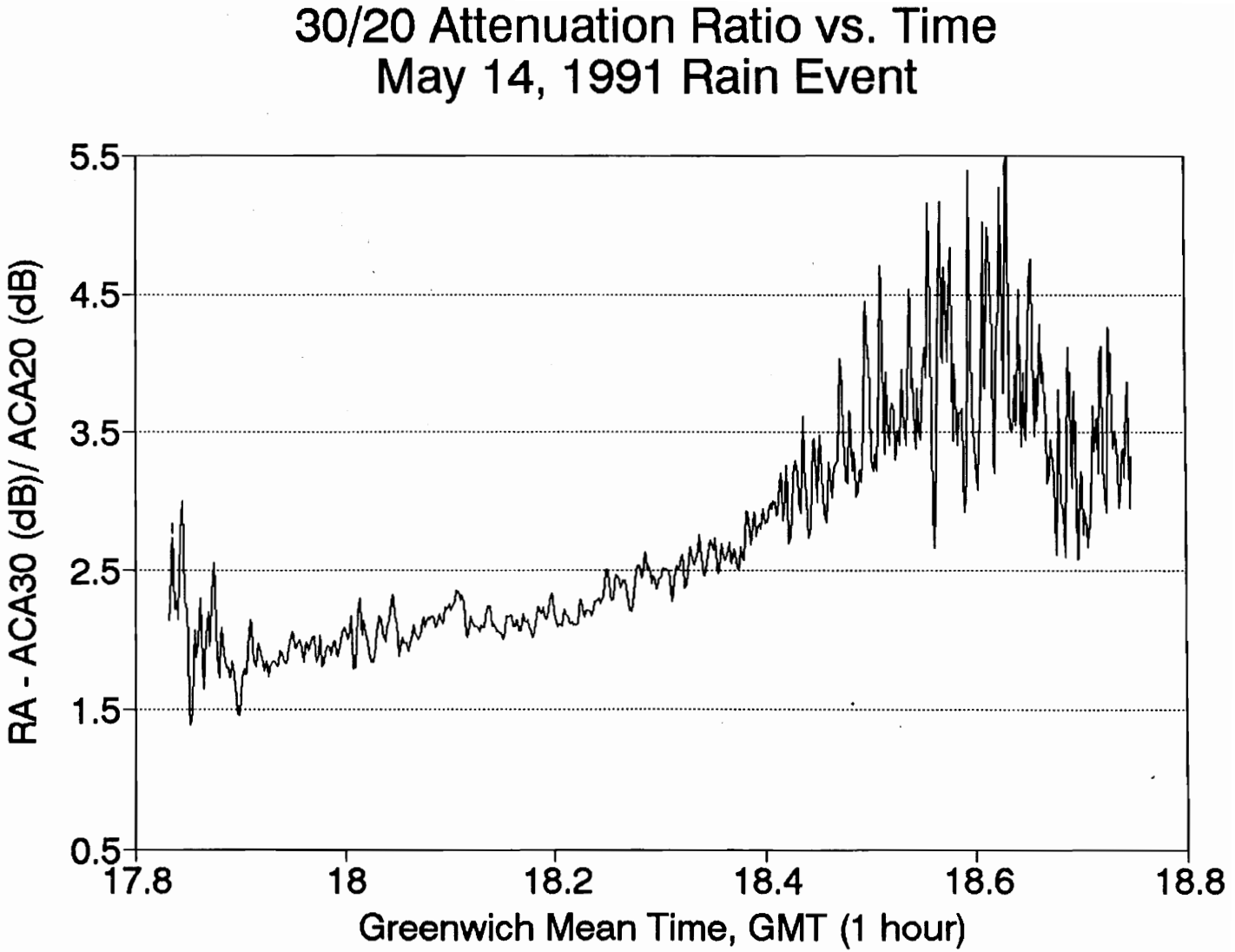

Figure 5.3-20 30/20 Attenuation Ratio vs. Time, May 14, 1991 Rain Event

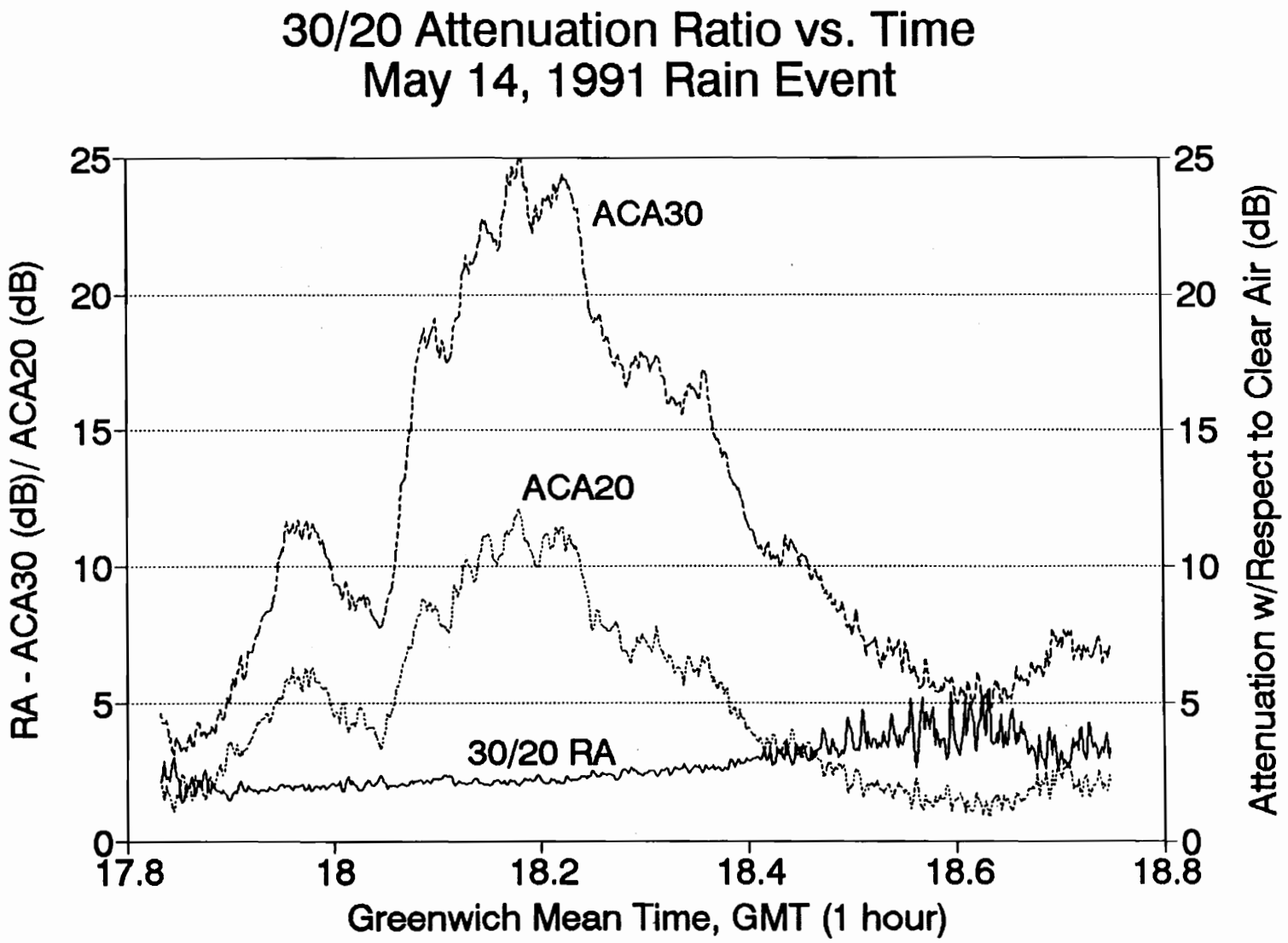

Figure 5.3-21 30/20 Attenuation Ratio vs. Time (with ACA30 & ACA20), May 14, 1991

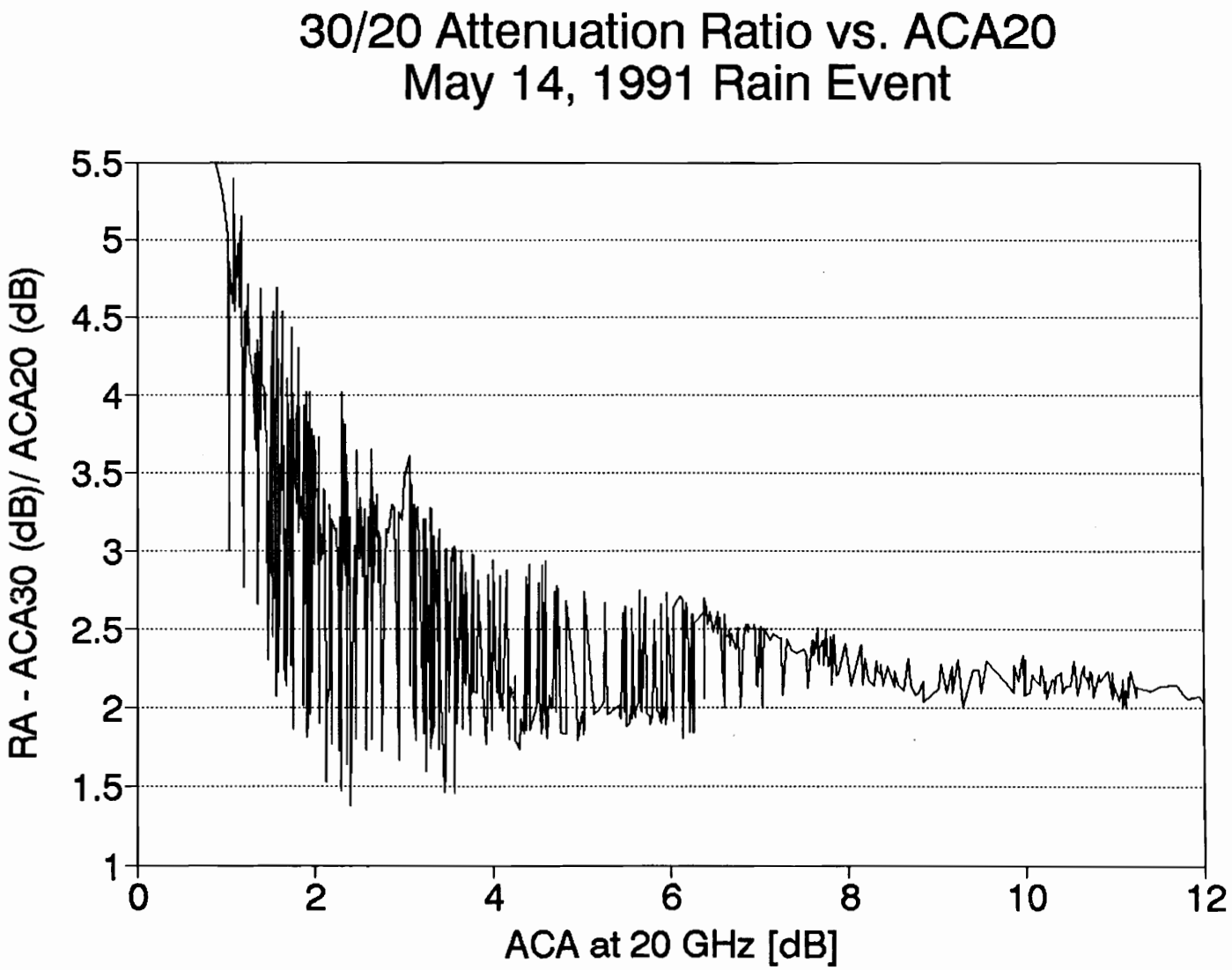

Figure 5.3-22 30/20 Attenuation Ratio vs. ACA20, May 14, 1991 Rain Event

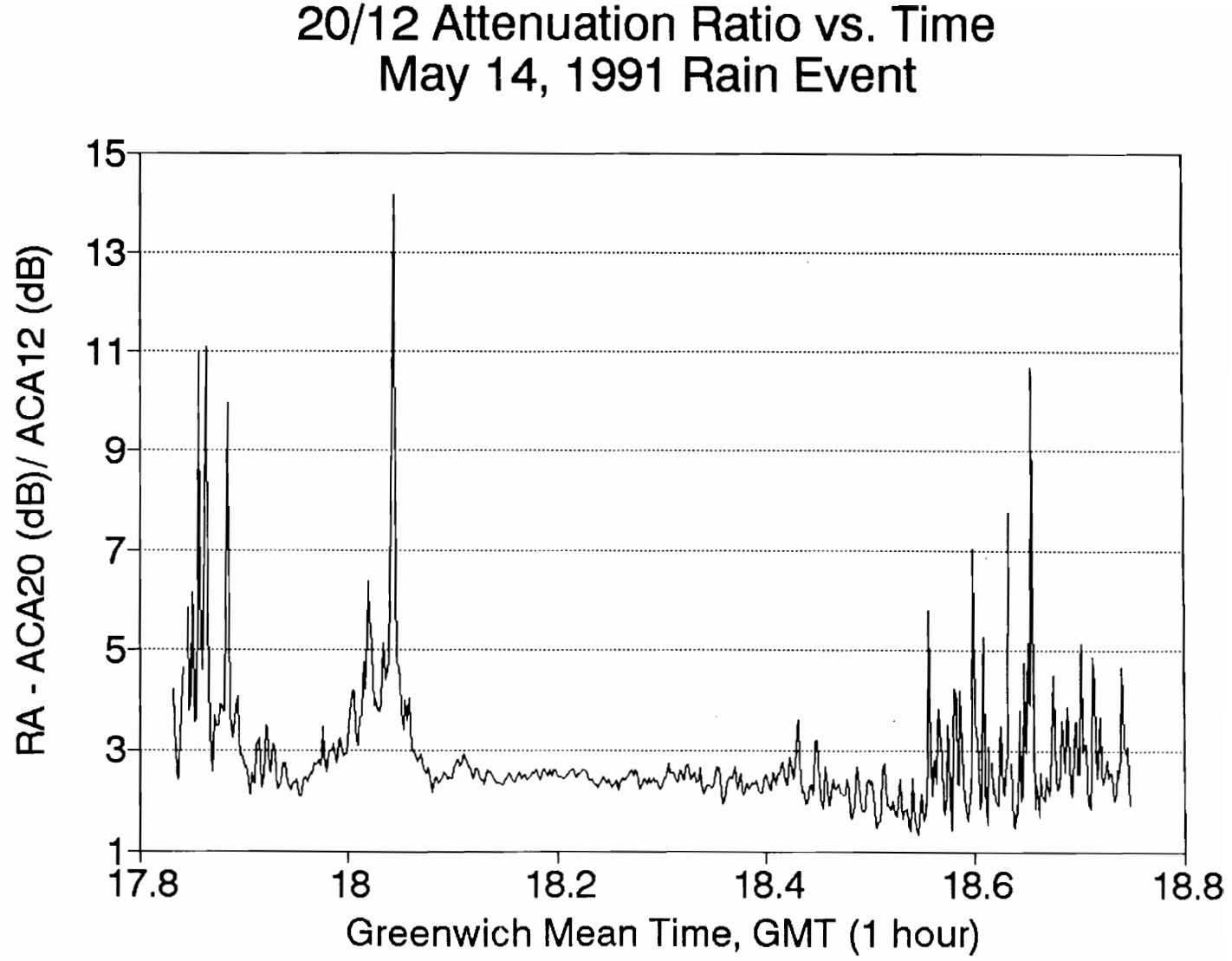

Figure 5.3-23 20/12 Attenuation Ratio vs. Time, May 14, 1991 Rain Event

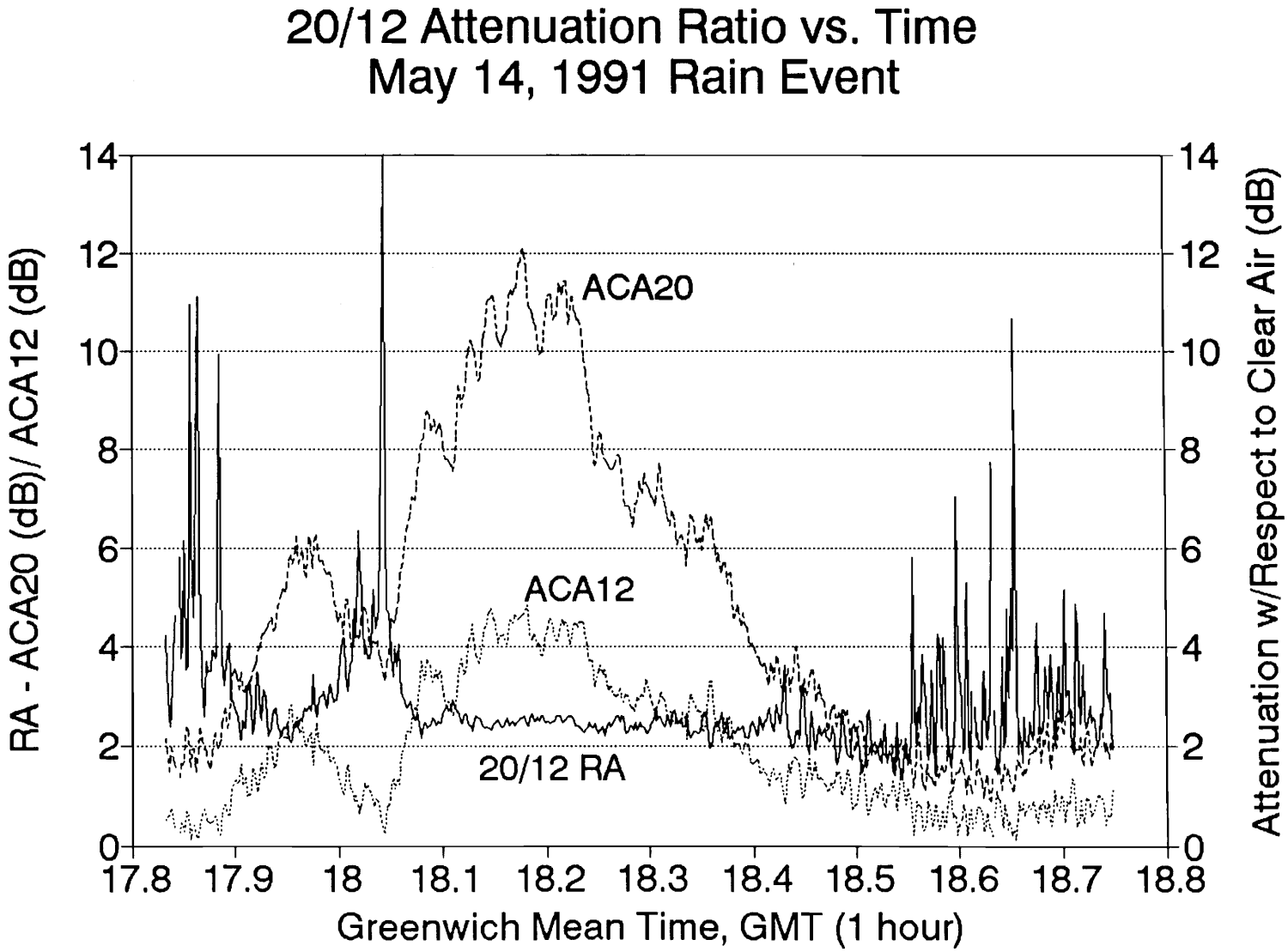

Figure 5.3-24 20/12 Attenuation Ratio vs. Time (with ACA20 & ACA12), May 14, 1991

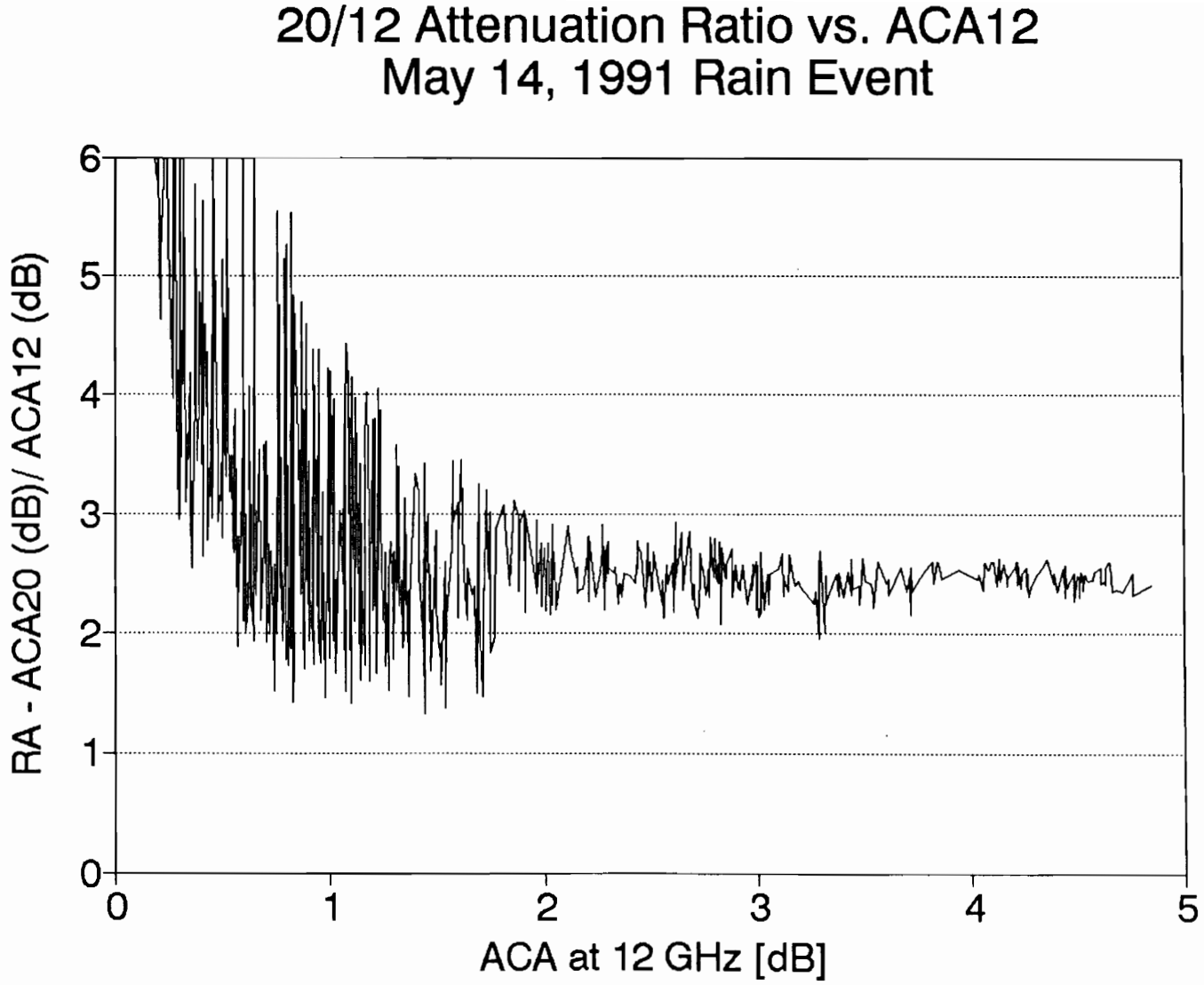

Figure 5.3-25 20/12 Attenuation Ratio vs. ACA12, May 14, 1991 Rain Event

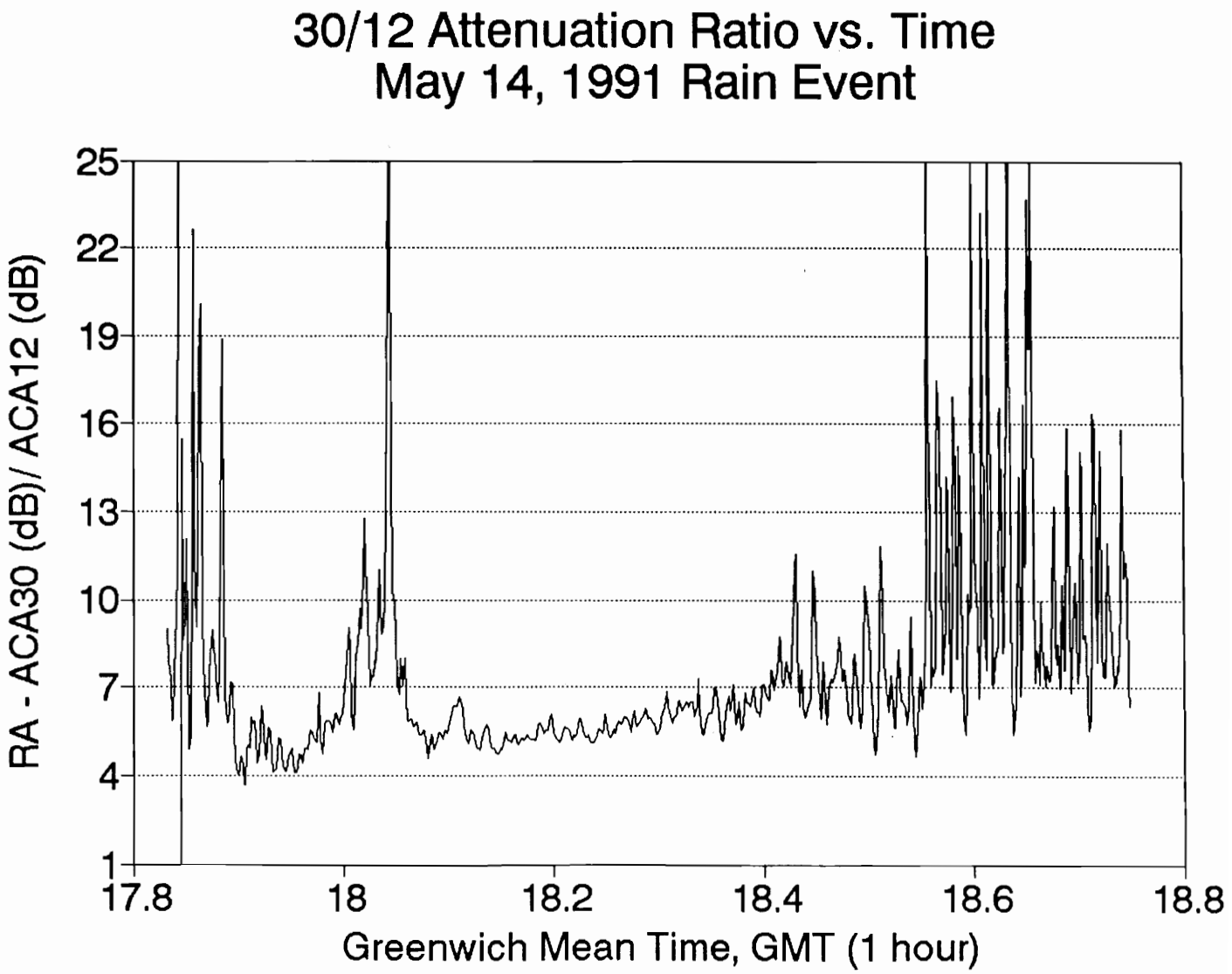

Figure 5.3-26 30/12 Attenuation Ratio vs. Time, May 14, 1991 Rain Event

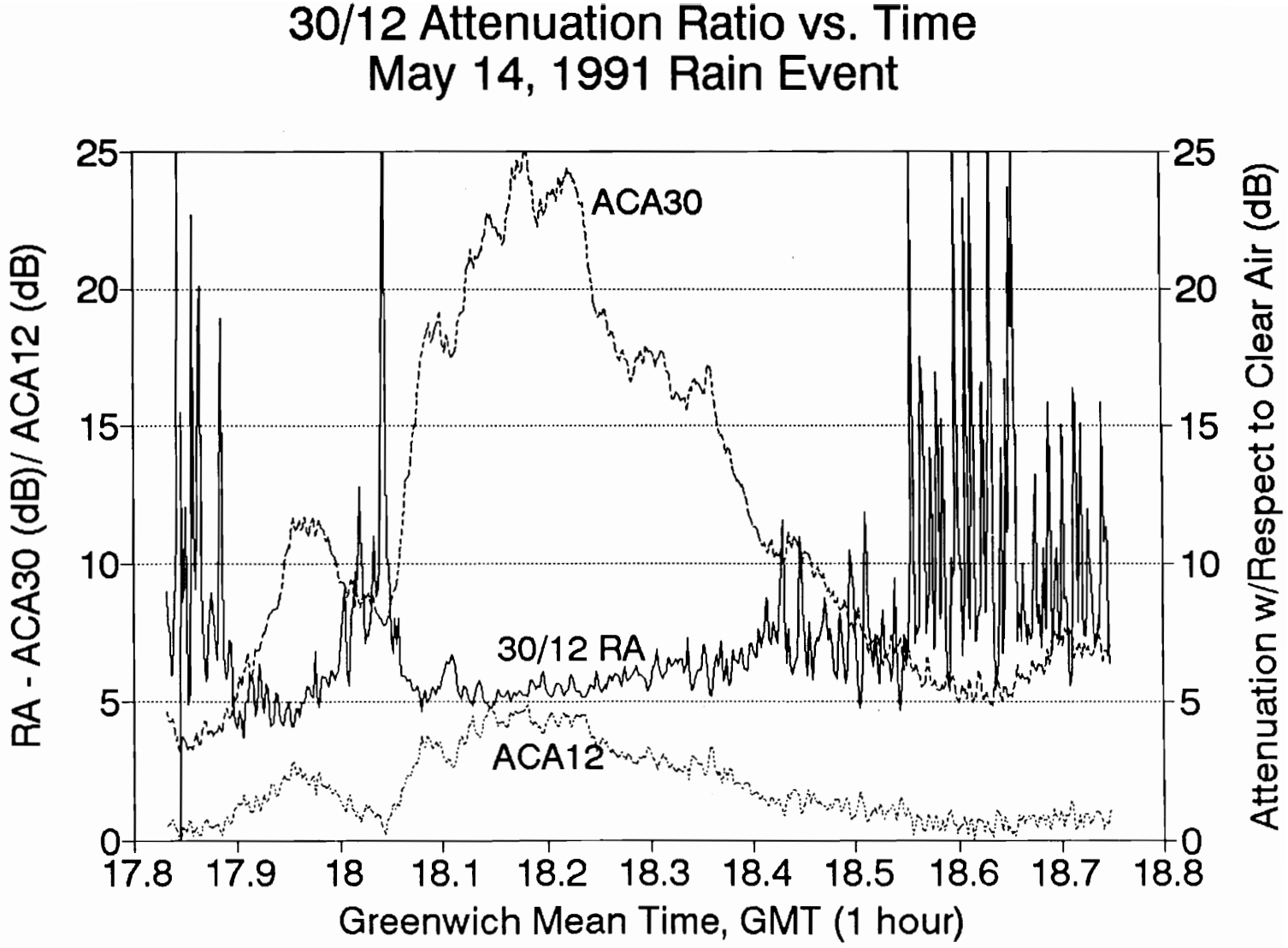

Figure 5.3-27 30/12 Attenuation Ratio vs. Time (with ACA30 & ACA12), May 14, 1991

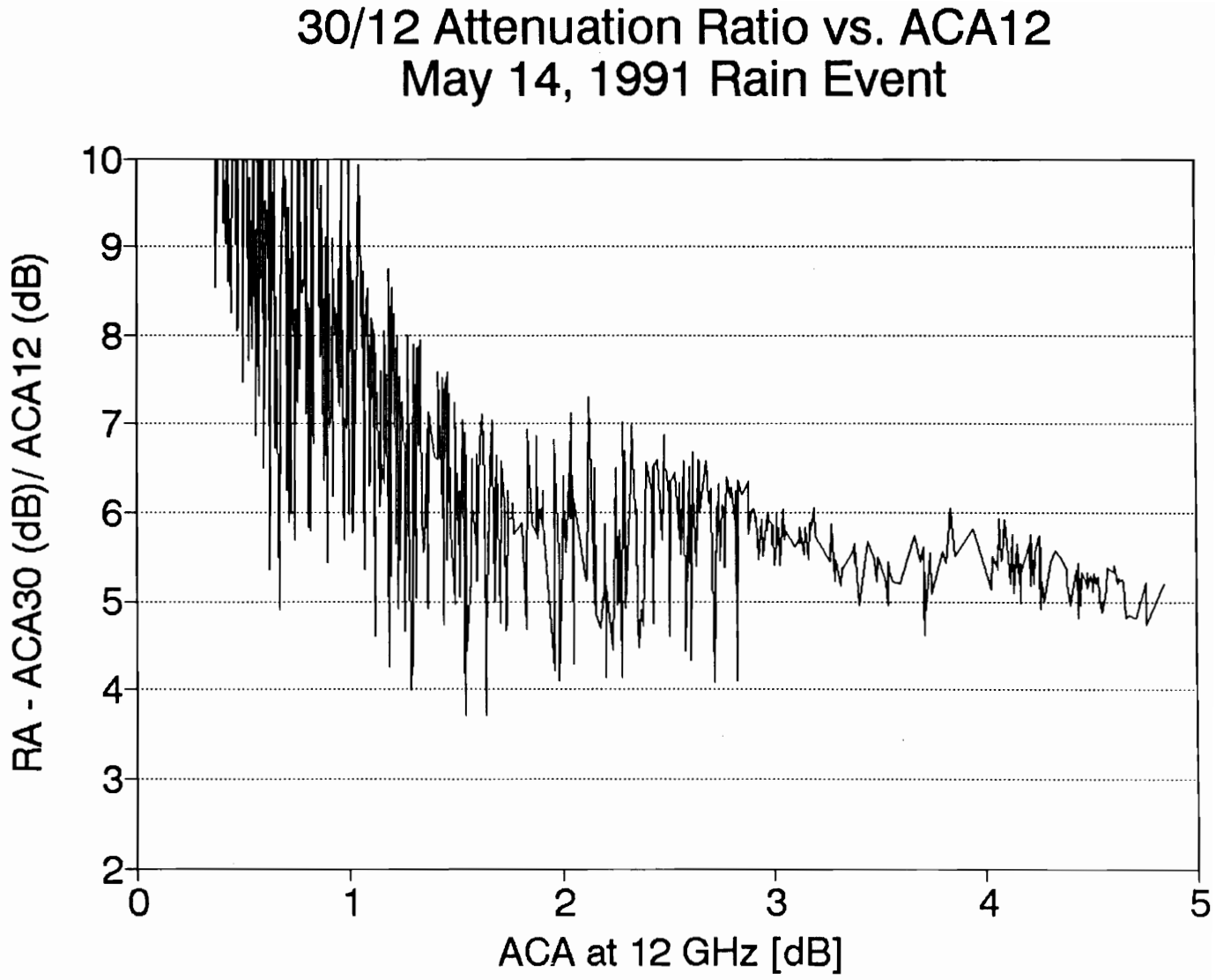

Figure 5.3-28 30/12 Attenuation Ratio vs. ACA12, May 14, 1991 Rain Event

5.4 Statistical Scaling (Statistical Attenuation Ratio)

In this section, we examine statistical attenuation ratio; *RAS* from (3.2-1) is the quotient of two statistical values of *ACA* (i.e., *ACAS*), at an upper and lower frequency, respectively. *RAS* is a much easier quantity to obtain. It is found directly from attenuation statistics in contrast to the statistics of *RA* which are found from instantaneous *RA* values for the entire period. Plots can be generated showing the percentage of time that the statistical attenuation ratio, *RAS*, exceeds a specific value. Again, Statistical *ACA* values and *RAS* are tabulated in Table 5.4-1 for the percentage of time exceeded. It should be noted that *RAS* values for low base frequency attenuations ($A(f_L) < 1$ dB) are not as reliable because of roundoff errors (i.e., the base frequency attenuation is binned only to two decimal places in dB). In Table 5.4-1, these low base frequency attenuations are marked off from the other data by a thin line.

The monthly time bases for attenuation ratio, *RA*, include only *RA* values where the base frequency attenuation exceeds 1 dB and are given in Table 5.3-1. The time bases for statistical attenuation ratio, *RAS*, are given in Table 5.2-1. Because of the different time bases, it is almost meaningless to compare *RA* and *RAS* for same the percentage of time. However, meaningful comparison can be made between *RA* and *RAS* with respect to the base frequency attenuation. Plots for *RAS* vs. Base Attenuation for the year are given in Figure 5.4-1, 5.4-2, and 5.4-3. To facilitate comparison, the 50% level for *RA*, RA_{med_i}, vs. Base Attenuation is included in these plots. The figures show that *RAS* agrees very well with the median *RA*, indicating the possibility of using attenuation statistics to predict the median instantaneous ratio as a function of base

frequency attenuation. Plots of *RAS* vs. Base Attenuation for individual months are included in Appendix A.4.1.

Table 5.4-1

ACA Values (in dB), RAS, and % Time Exceeded for One Year (91/92)

% Time Exceedance	ACA20	ACA30	RAS 30/20	ACA12	ACA20	RAS 20/12	ACA12	ACA30	RAS 30/12
50.000	0.04	0.04	1.00	0.01	0.04	4.00	0.01	0.04	4.00
30.000	0.16	0.19	1.19	0.10	0.17	1.70	0.10	0.20	2.00
20.000	0.28	0.33	1.18	0.17	0.31	1.82	0.17	0.36	2.12
10.000	0.60	0.74	1.23	0.31	0.65	2.10	0.31	0.82	2.65
5.000	1.13	1.69	1.50	0.51	1.22	2.39	0.51	1.89	3.71
3.000	1.75	3.03	1.73	0.71	1.88	2.65	0.71	3.33	4.69
2.000	2.37	4.45	1.88	0.94	2.55	2.71	0.94	4.76	5.06
1.000	3.83	7.26	1.90	1.42	4.08	2.87	1.41	7.69	5.45
0.500	5.51	10.85	1.97	2.06	5.86	2.84	2.03	11.38	5.61
0.300	7.03	14.16	2.01	2.66	7.48	2.81	2.59	14.84	5.73
0.200	8.39	17.16	2.05	3.22	9.05	2.81	3.11	17.95	5.77
0.100	11.42	23.03	2.02	4.64	12.66	2.73	4.39	23.98	5.46
0.050	15.58	30.46	1.96	6.48	17.19	2.65	6.14	31.49	5.13
0.030	18.76	34.94	1.86	7.68	19.84	2.58	7.45	35.67	4.79
0.020	20.77	37.61	1.81	8.92	22.16	2.48			
0.010				11.10	27.15	2.45			
0/005				13.01	31.75	2.44			
0.003				14.00	34.54	2.47			
0.002				14.66	36.54	2.49			
0.001									

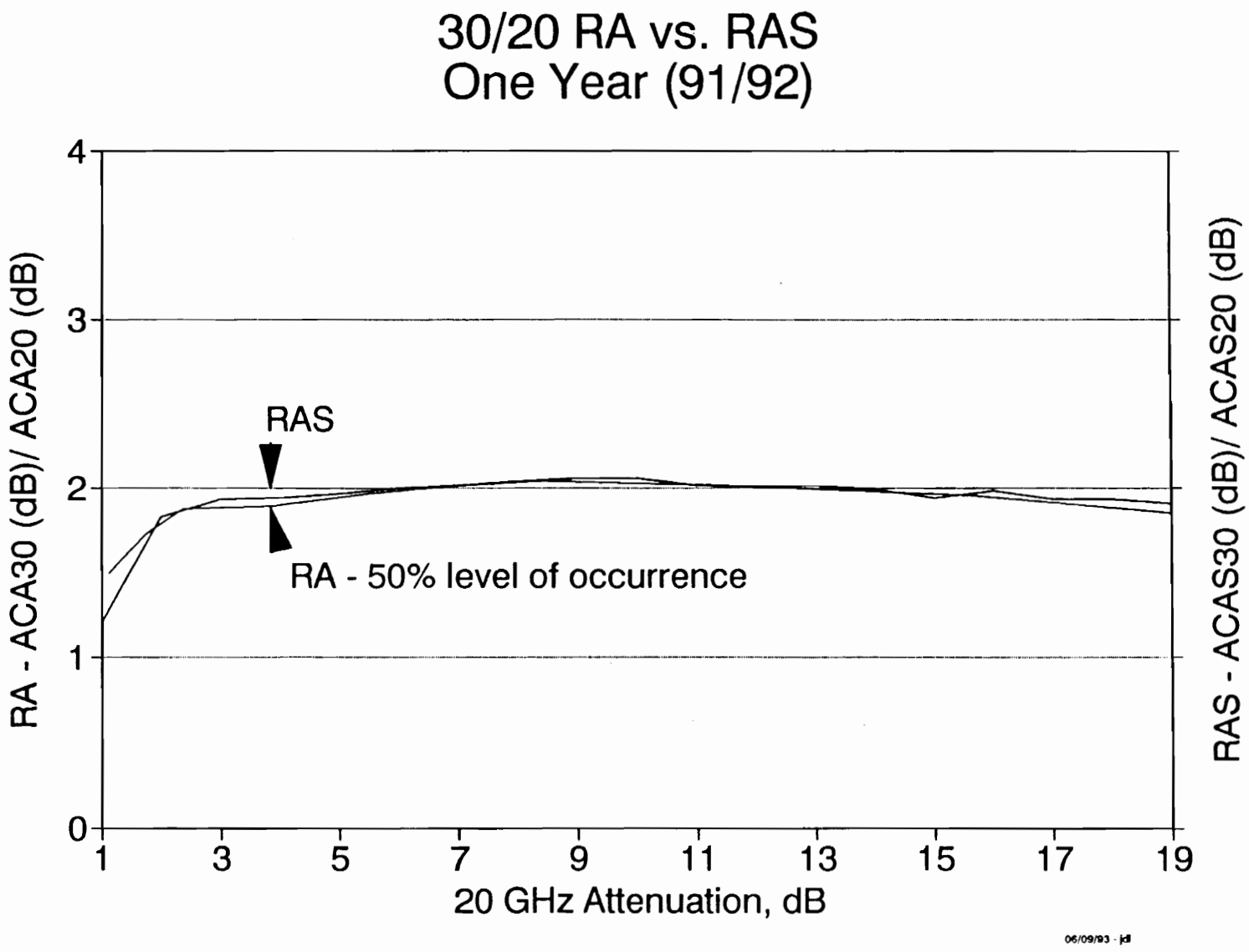

Figure 5.4-1 30/20 *RA* 50% Level of Occurrence & *RAS* vs. ACA20 - One Year (91/92)

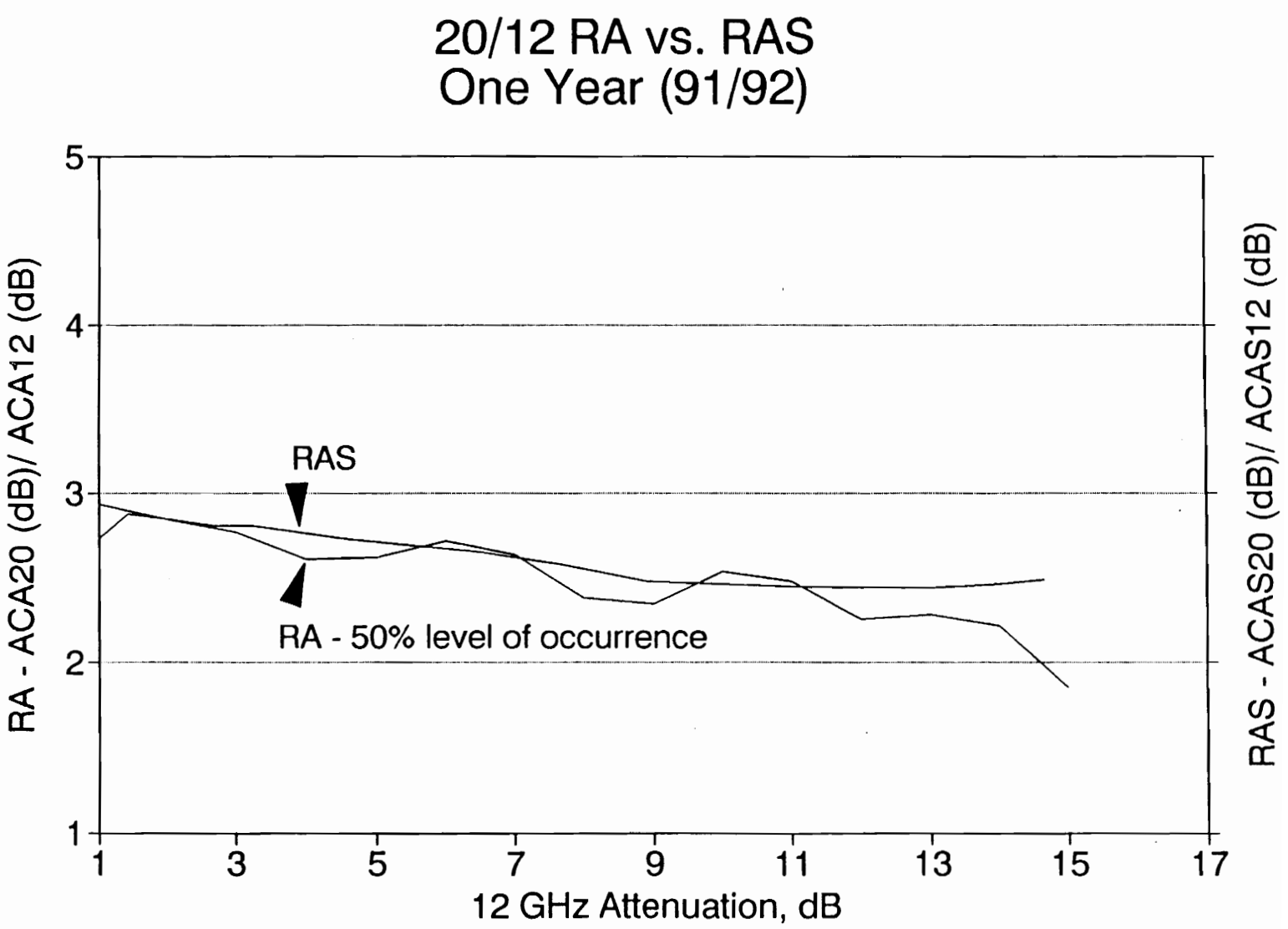

Figure 5.4-2 20/12 *RA* 50% Level of Occurrence & *RAS* vs. ACA12 - One Year (91/92)

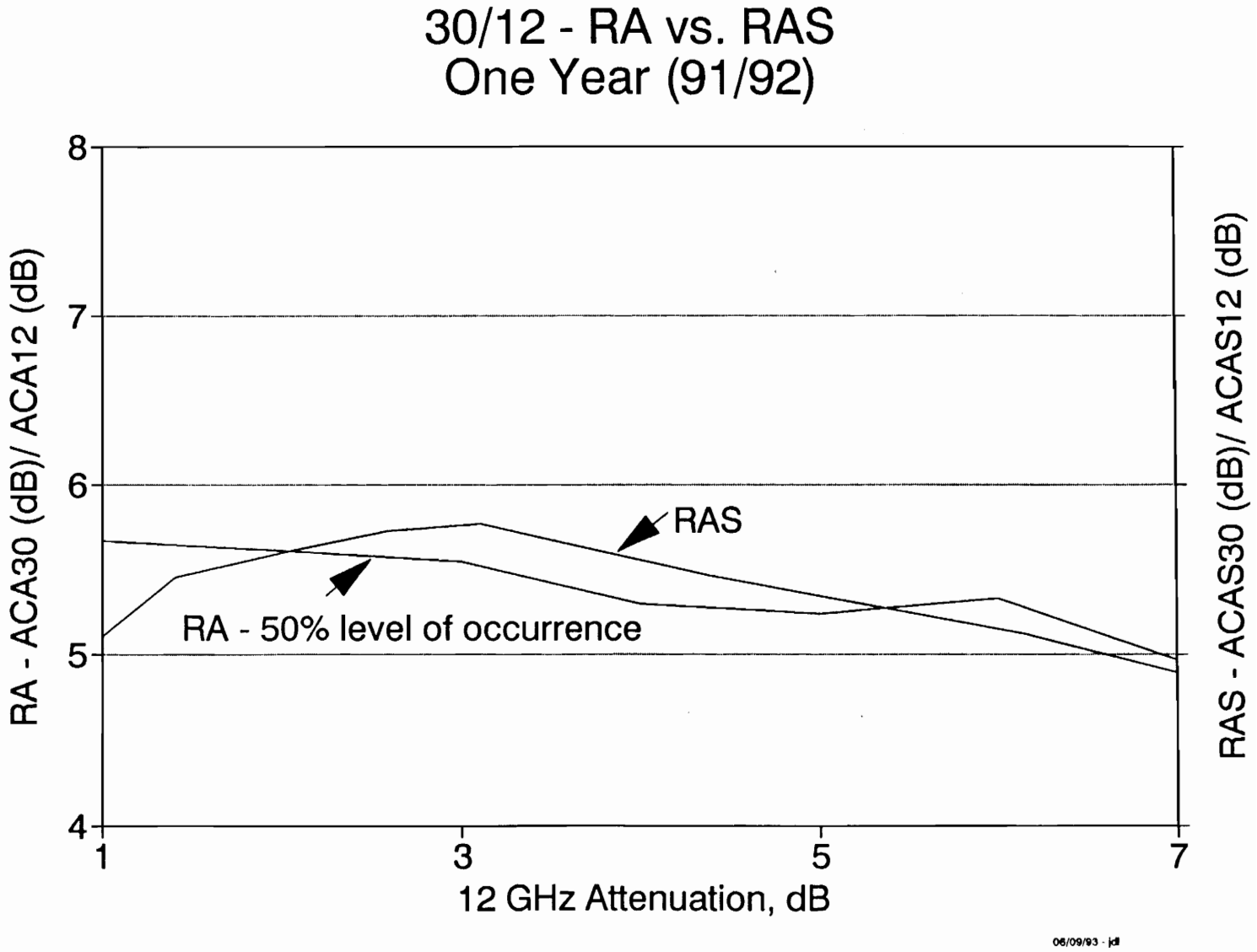

Figure 5.4-3 30/12 *RA* 50% Level of Occurrence & *RAS* vs. ACA12 - One Year (91/92)

5.5 References

1. Sweeney, D.G., "Adaptive Power Control as a Fade Countermeasure on Satellite Links," Unpublished doctoral dissertation, Report EESATCOM 93-2, Virginia Polytechnic Institute & State University, Department of Electrical Engineering, Blacksburg, VA, January 1993, p. 53.

2. Stutzman, W.L., *et al.*, "Communications and propagation experiments using the OLYMPUS spacecraft - Analysis of OLYMPUS Propagation Data for the Period January to May 1991," Report EESATCOM 92-5, Virginia Polytechnic Institute & State University, Department of Electrical Engineering, Blacksburg, VA, JPL Contract No. 958435, November 1991, p. 48.

CHAPTER 6

EVALUATION OF MODELS USING OLYMPUS DATA

6.1 Scaling of Instantaneous and Statistical Attenuation

6.1.1 Scaling as a function of % time exceeded

The models presented in Chapter 3 quantify the behavior of average instantaneous attenuation ratio RA_{ave} and statistical attenuation ratio *RAS*. Values of *RA* predicted, RA_{pred}, from some of the simpler models are plotted in Figures 6.1-1 to 6.1-3 against percentage of time exceeded. This is the percentage of time that *RA* exceeds some specific value. The data are based on the time for which the base frequency attenuation exceeds 1 dB (e.g., ACA20 > 1 dB for 30/20 ratio); these time bases are tabulated in Table 5.3-1. Also shown for comparison are the Virginia Tech *RA* data. The measured data are not constant with frequency. The 50% level for *RA*, RA_{med}, (defined in Section 5.3.1) is marked on the plots. *RA* is level dependent which in turn may be a function of the rain drop size distribution [5]. Several of the models used for comparison of *RA* versus percentage of time in Figures 6.1-1 to 6.1-3 are ratio models and are constants (as discussed in Section 3.1).

Curves for models based on the power law (Eq. (3.2-3); see Section 3.2.1.1.2) with various n values are included in Figures 6.1-1 to 6.1-3 as follows

- Dintelmann [1] $n = 1.8$
- Owolabi & Ajayi [2] $n = 2$
- Drufuca [2] $n = 1.72$

Also included in Figures 6.1-1 to 6.1-3 are

- Battesti's model [2] (3.2-4, 3.2-5, 3.2-6) (see Section 3.2.1.1.3)
- CCIR's model [3] (3.2-2) (see Section 3.2.1.1.1)

A comparison of RA_{pred} from the models and Va. Tech's measured data are given in Table 6.1-1. Missing values in the table correspond to situations where the model does not apply.

Table 6.1-1

Measured Median RA, RA_{med}, Compared to Model Predictions for OLYMPUS

Model or Data	Frequencies, f_U / f_L		
	30/20	20/12	30/12
RA_{med} data	1.93	2.86	5.56
RA_{ave} data (see Section 5.3.2)	2.01	2.52	5.43
Battesti model	2.01	2.12	4.23
CCIR model	1.96	2.18	4.28
Dintelmann model	2.07	---	4.74
Drufuca model	---	2.20	---
Owolabi/Ajayi model	2.25	2.50	5.63

Examination of Table 6.1-1 reveals that existing models do not satisfactorily predict the measured median RA values. Some models come close for individual frequency pairs such as Battesti, CCIR, and Dintelmann for 30/20 and Owolabi/Ajayi for 20/12 and 30/12. But no models are accurate across the Ku/Ka band.

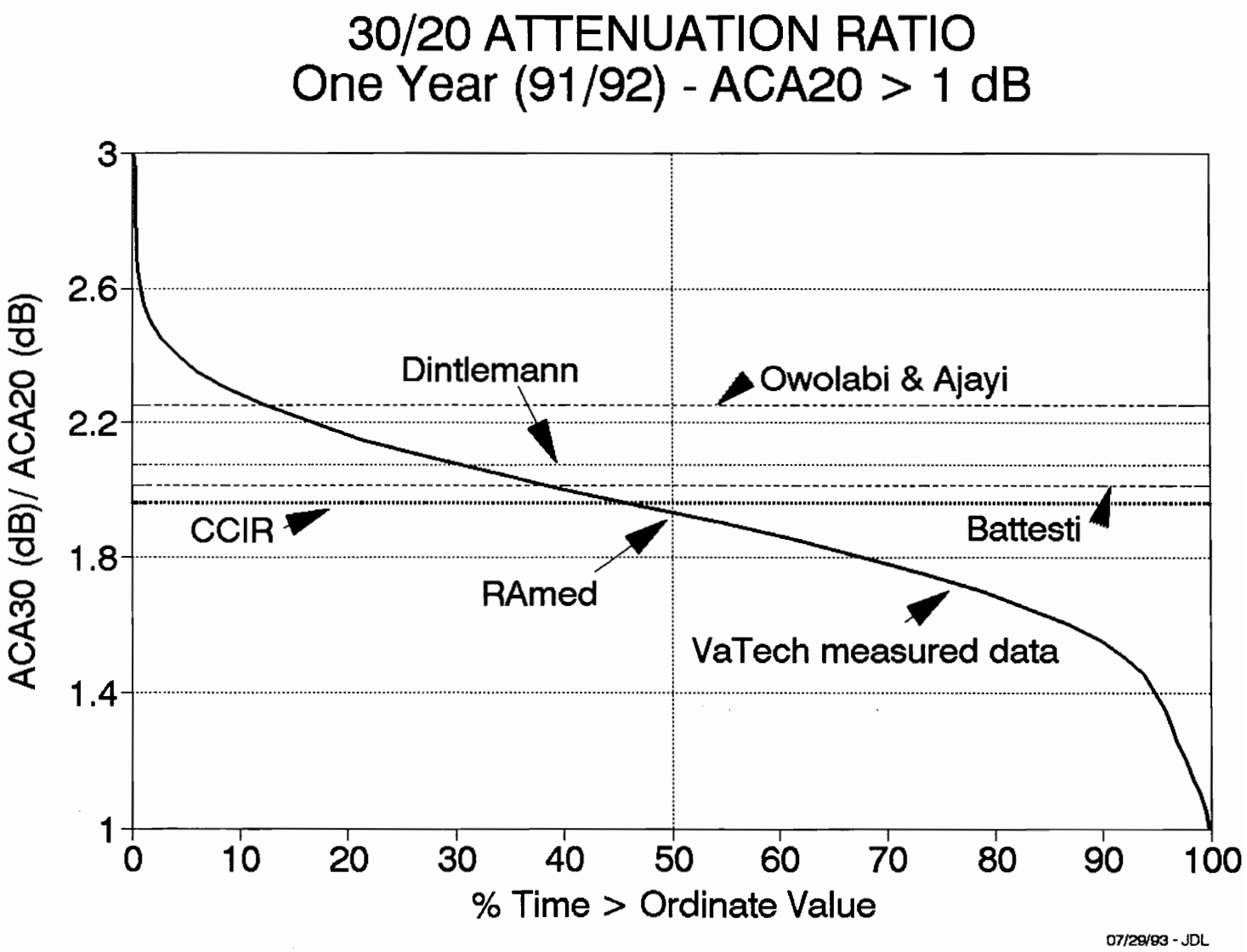

Figure 6.1-1 30/20 *RA* (with various models) vs. % Time - One Year (91/92)

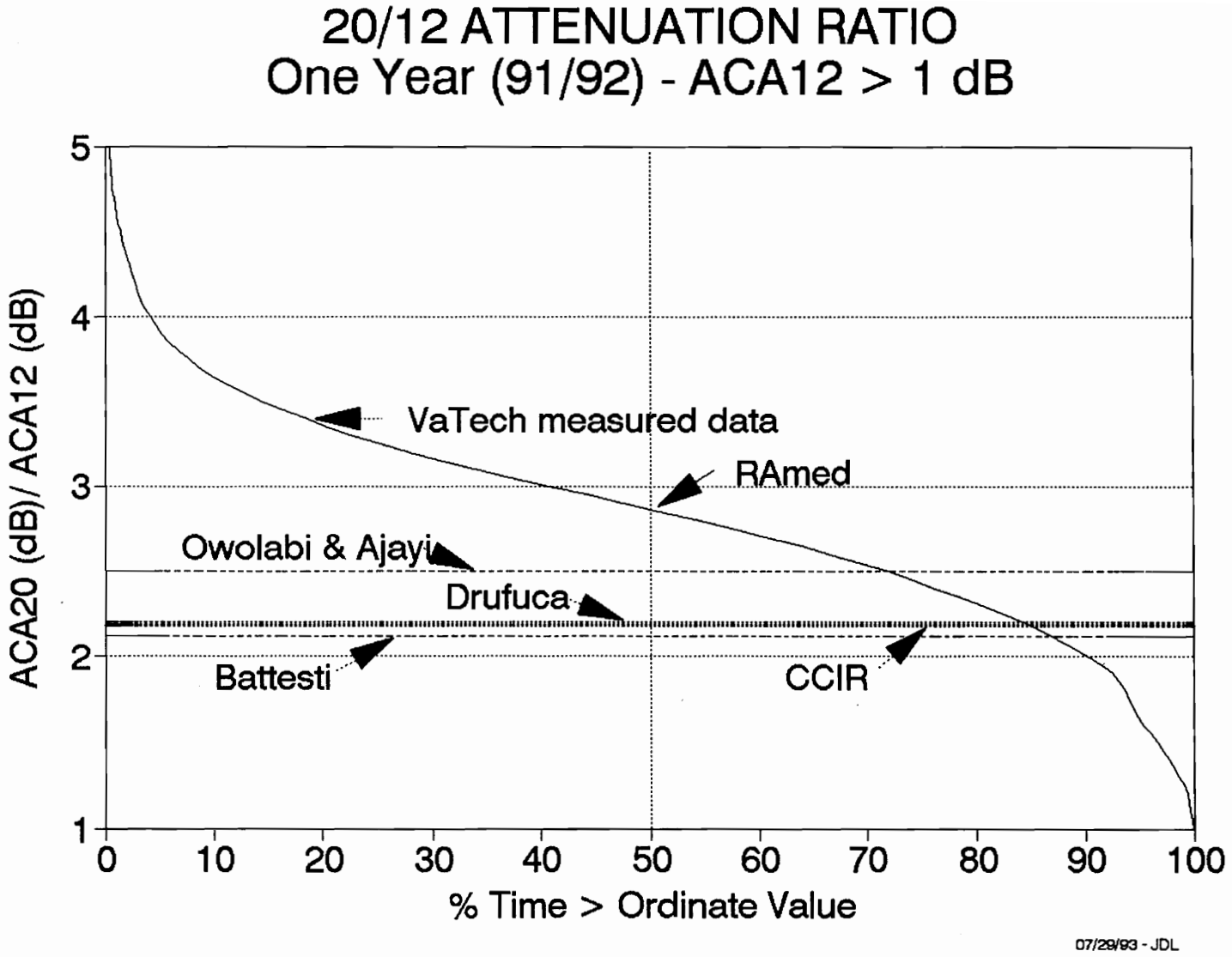

Figure 6.1-2 20/12 *RA* (with various models) vs. % Time - One Year (91/92)

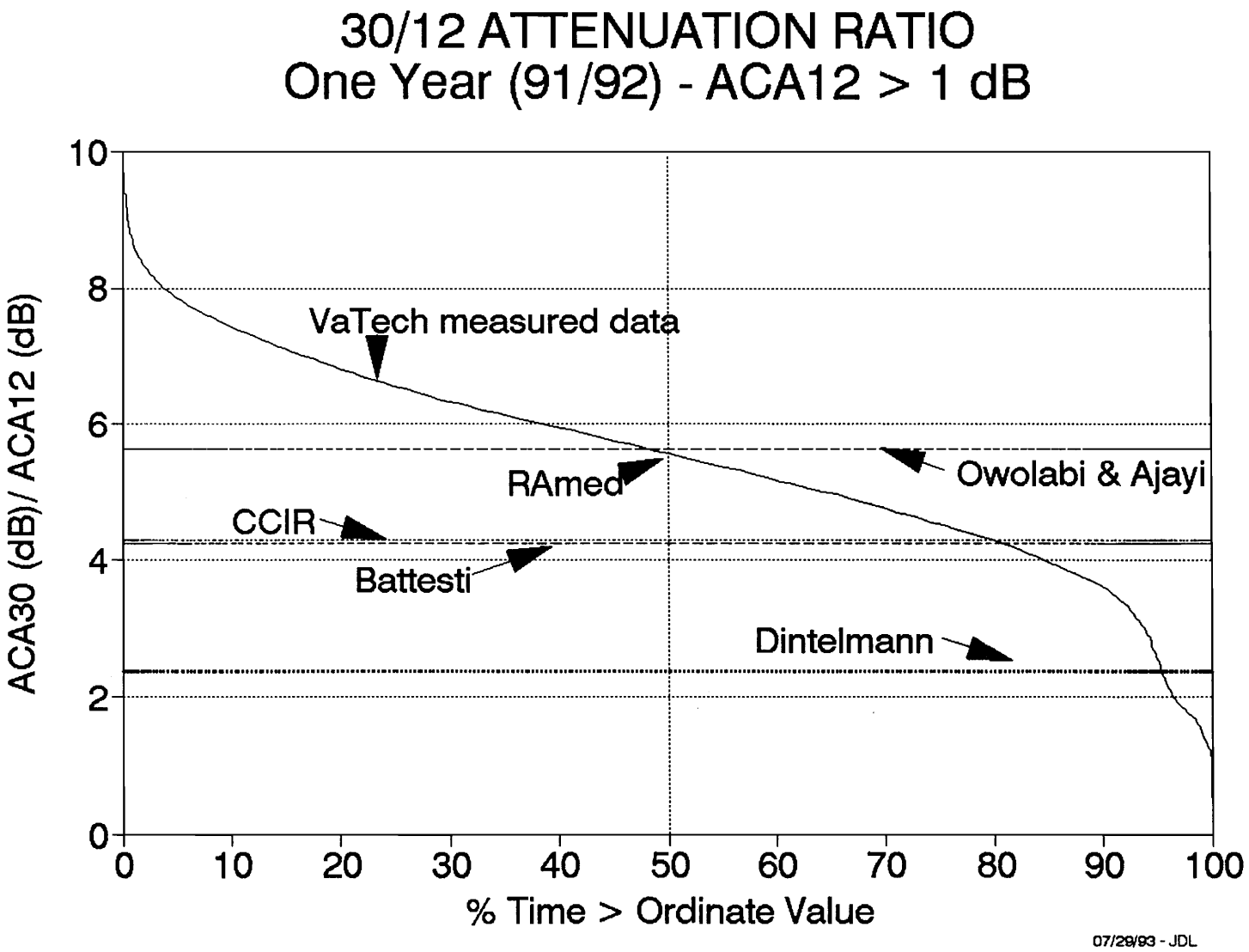

Figure 6.1-3 30/12 *RA* (with various models) vs. % Time - One Year (91/92)

6.1.2 Attenuation ratio dependence on base frequency attenuation

RA_{med_i} (see Section 5.3.2) and *RAS* are plotted as a function of base frequency attenuation in Figures 6.1-4 to 6.1-6. Also shown are measured values and values predicted from ratio models discussed in Section 6.1.1. The non-ratio model of Boithias (Eq. (3.2-22); see Section 3.2.2.1.1) is also plotted [3,4].

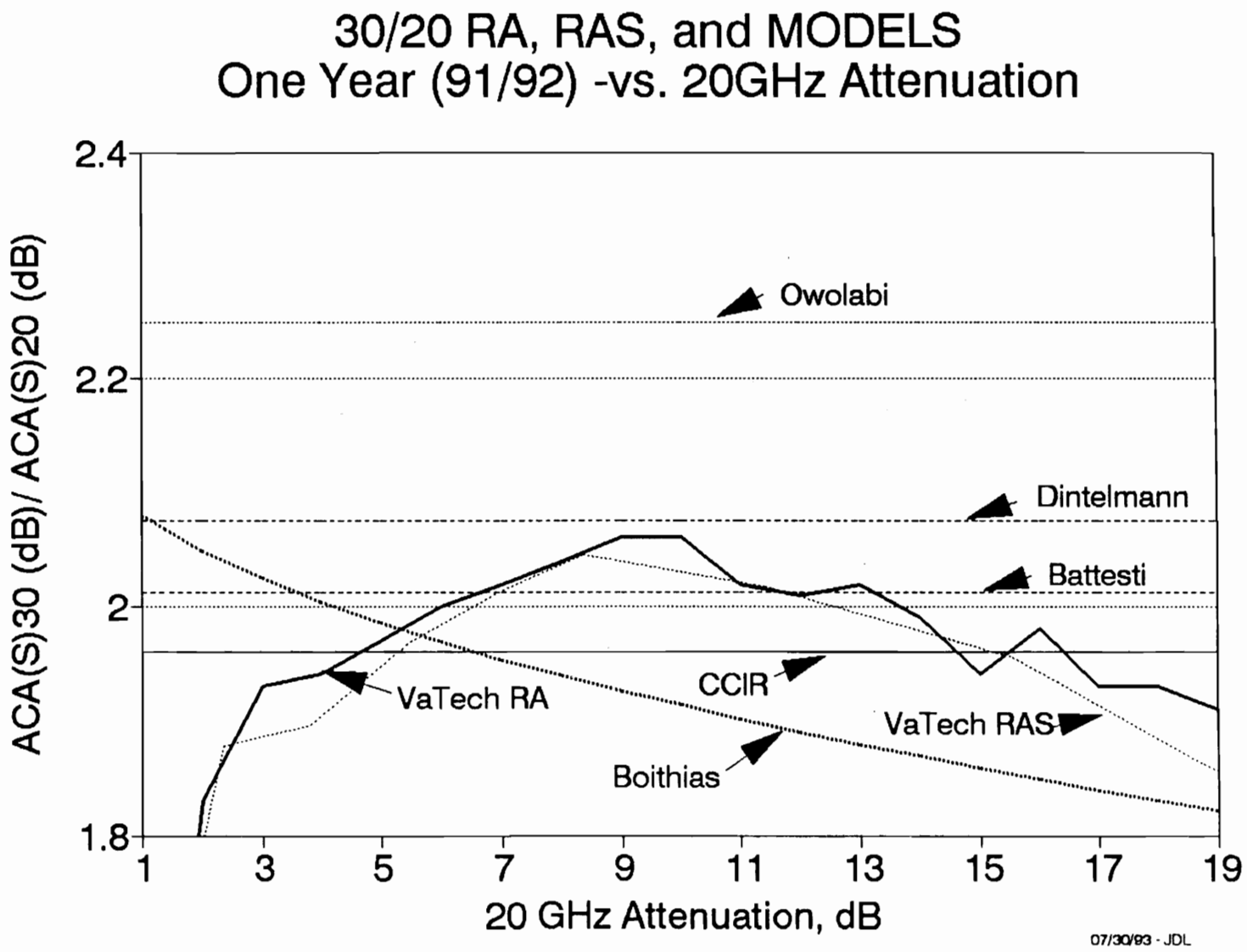

Figure 6.1-4 30/20 *RA*, *RAS*, and Models vs. ACA20 - One Year (91/92)

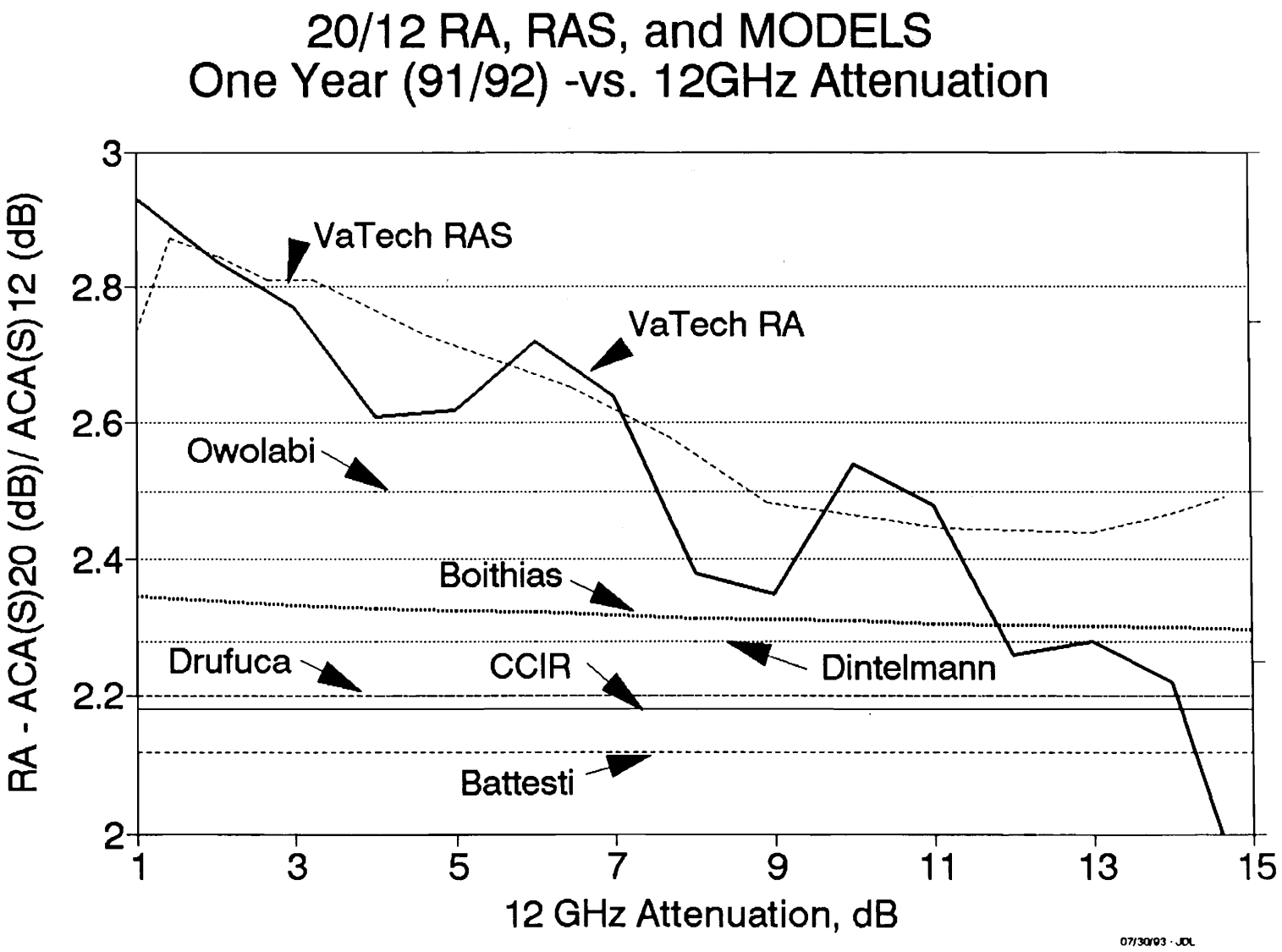

Figure 6.1-5 20/12 *RA*, *RAS*, and Models vs. ACA12 - One Year (91/92)

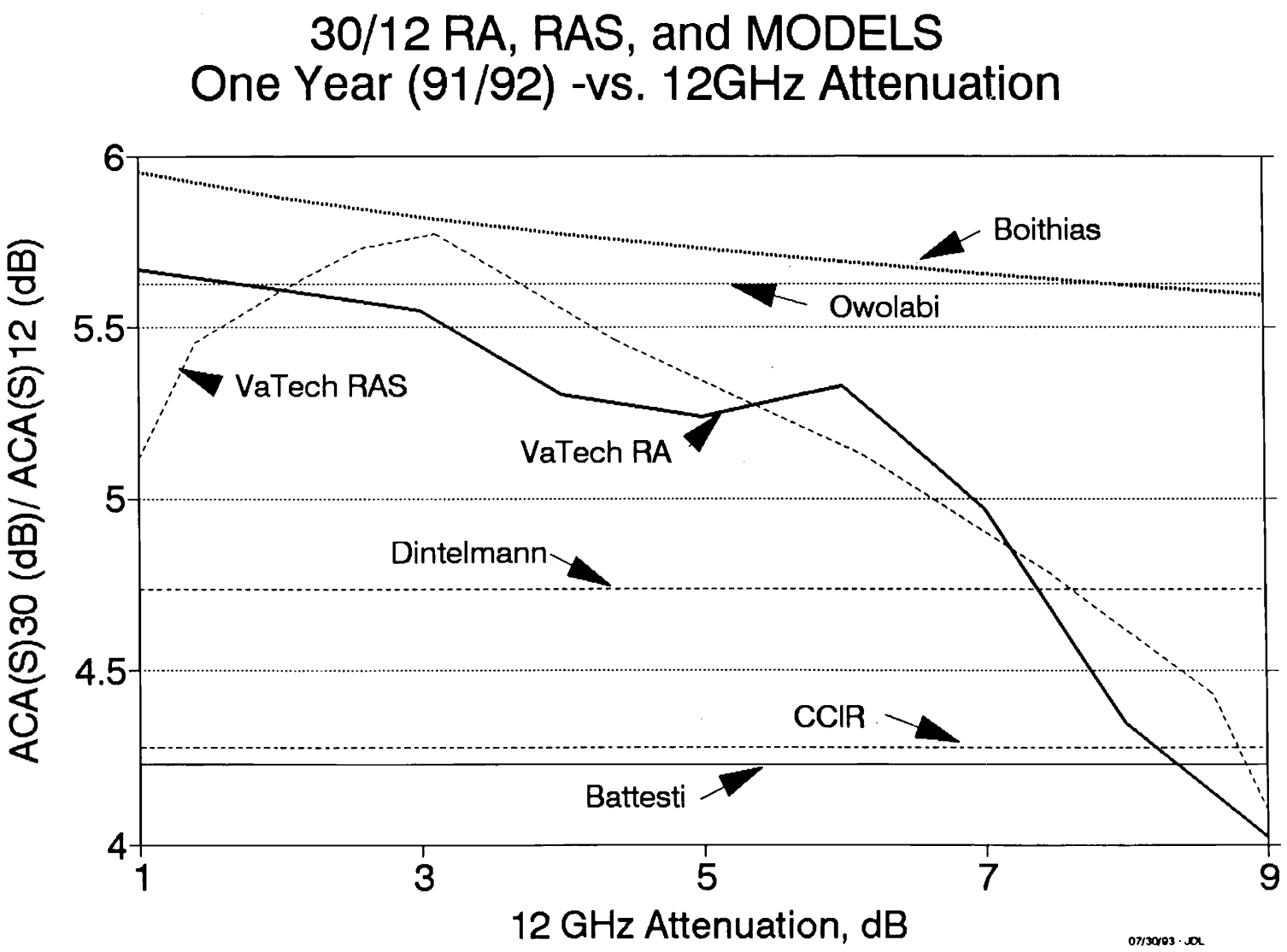

Figure 6.1-6 30/12 *RA*, *RAS*, and Models vs. ACA12 - One Year (91/92)

Again, an examination of the Table 6.1-1 indicates that existing models do not satisfactorily predict RA_{med_i} (i.e., the measured median *RA* values as a function of base frequency attenuation).

6.1.3 *RAS* from attenuation models

As indicated in Section 3.2.1.2, *RAS* can be derived from attenuation models such as the Stutzman's Simple Attenuation Model (SAM). SAM predicts *RAS* values at each percentage of time exceeded and can be compared to the statistics of *RA*. SAM values (for Blacksburg, VA) for 30 and 20 GHz and the resulting ratio are given in Table 6.1-2 as an example.

Table 6.1-2

Measured & Predicted (from the SAM Model) Values

of ACA30, ACA20, & Their Ratio

% Time Exceeded	SAM ACA20	Measured ACA20	SAM ACA30	Measured ACA30	SAM RAS	Measured *RAS*
1.0	2.13	4.04	5.00	7.69	2.35	1.90
0.3	7.07	7.31	15.26	14.28	2.16	1.95
0.1	13.96	11.93	28.78	23.87	2.06	2.00
0.03	21.84	19.12	43.12	35.50	1.97	1.86
0.01	32.09	26.43	62.56	---	1.95	---
0.003	45.64	34.27	86.45	---	1.89	---
0.001	58.93	---	109.21	---	1.85	---

The attenuation predictions deviate somewhat from the measured *ACA* values, but this may be due to the use of the CCIR rain model in SAM rather than actual rain

statistics. Nevertheless, the SAM model produces fairly accurate attenuation ratio results. Further investigation is needed.

6.2 Power Law Model Fits to Measured Data

6.2.1 Statistical attenuation scaling

The power law model of (3.2-3) assumes that rain attenuation $A(f)$ at a given frequency can be expressed as the product of some constant A_o and the given frequency raised to a power of n:

$$A(f) = A_o f^n \tag{6.2-1}$$

Attenuation ratio based on this attenuation model is (see also Eq. (3.2-3))

$$RA = \frac{A_U}{A_L} = \left(\frac{f_U}{f_L}\right)^n \tag{6.2-2}$$

In Virginia Tech's measured data, RA and RAS vary over time and as a function of the base frequency attenuation. The values for n computed from (6.2-2) using RA_{med} and RA_{ave} values from Table 6.1-1 are given in Table 6.2-1. Again, RA_{med} is the overall median RA, and RA_{ave} is the average of the medians for 1-dB binned values of base frequency attenuation. Both, RA_{med} and RA_{ave} represent the 50% level of occurrence for the time that the base frequency attenuation exceeds 1 dB (as given in Table 5.3-1 for the months and experimental year).

Table 6.2-1

Powers, n, for Power Law Fits to Median and Average Measured Attenuation Ratio

	Frequencies f_U / f_L			
	30/20	20/12	30/12	Average n
Power n for RA_{med}	1.62	2.29	1.99	1.97
Power n for RA_{ave}	1.72	2.02	1.96	1.90

The average values of n for a power law fit over the three frequency pairs are also given in Table 6.2-1 and are 1.97 and 1.90 for the median and average *RA*s, respectively. The deviation from these average powers is as high as 17%. This is reasonable and leads to about 2 dB error out of 20 dB. Based on these results, a value of $n_{ave} = 1.90$ is recommended for 10-30 GHz frequency range. However, better results are obtained by using the power law values in Table 6.2-1 if the desired frequency pair corresponds to a pair in the table.

6.2.2 Instantaneous scaling

An important issue is whether statistical models can be applied to events. In this section, we apply the power law relation to the instantaneous data for the May 14, 1991 rain event. The "best fit" lines (i.e., least rms error) are plotted (in Figures 5.3-16, 5.3-18, and 5.3-19) to scatter plots of the upper frequency attenuation versus the base frequency attenuation for 30/20, 20/12, and 30/12 frequency pairs for the event of May 14, 1991. The slopes from these fits correspond to the values of n shown in Table 6.2-2. Note that the power law with $n = 2.0$ applies to all frequency pairs. This is

probably due to the particular nature of this storm. The data base of all rain storms in the experimental year yields the results in Table 6.2-1.

Table 6.2-2

Comparison of Power Law Model Predictions to Attenuation Data for the Rain Event of May 14, 1991

	Frequencies, f_U / f_L		
	30/20	20/12	30/12
Slope of Regression Line	2.27	2.48	5.65
Power n, for a power law fit	2.02	1.98	2.00

6.3 Virginia Tech Models

6.3.1 Prediction of Median Attenuation (for $A(f_L) > 1$ dB)

It is apparent from the figures and tables that none of the existing models accurately reflect the measured data for all frequency pairs. Clearly compromises are in order. In addition, models for application to specific frequencies will be better than those for general use over wide frequency ranges. If a model that only depends on frequency (ratio relationship) is acceptable, a linear fit to the variations with fade level must be chosen. If one wishes to characterize the variance of the attenuation ratios, then a non-ratio relationship must be employed. Boithias [4] proposes a non-ratio relationship, but his formula is inaccurate when compared to the measured data.

Measured *RA* data are plotted in Figures 5.3-4 to 5.3-6 against base frequency attenuation for various percentages of time exceeded (1%, 10%, 50%, 90%, and 99%). In light of the good results tabulated in Table 6.2-1, a power law relation with $n = 1.9$ is recommended for RA_{ave} (which is the average of the medians for a 50% level of occurrence across the range of the base frequency attenuation):

$$RA_{ave} \approx \left(\frac{f_U}{f_L} \right)^{1.9} \tag{6.3-1}$$

where f_U and f_L are the upper and lower frequencies, respectively. Values for the frequency ratio for the frequency pairs in this experiment are given in Table 6.3-1.

Table 6.3-1

Frequency Ratio Values for 30/20, 20/12, and 30/12
Computed from the Power Law Model with $n = 1.9$

Frequencies, f_U / f_L	30/20	20/12	30/12
Value of f_U / f_L	1.5003	1.5816	2.3728
Predicted RA_{ave} with $n = 1.9$	2.16	2.39	5.16

6.3.2 Prediction of Attenuation Exceeded 99% of the Time

Equation (6.3-1) only predicts that average value of *RA*. We are also interested in the excursions from the average behavior. This can only be obtained directly from the data. Second-order polynomials of (6.3-2) were fitted to the 99% level of occurrence plots of *RA* in Figures 5.3-4 through 5.3-6. The 99% occurrence level of *RA* is 99% of the time that the base frequency attenuation exceeds 1 dB, which is about

1.23% of the year for 30/20, 20/12, and 30/12. For 99% of 1.23% of the year, *RA* can be expected to be below the plotted values. This means that *RA* can be above what is expected for 1% of 1.23% of the year, or about 68 minutes out of a year. Furthermore, because the 99% level is for each 1-dB bin of base frequency attenuations, the time involved is even less. For example, if the base frequency attenuation is between 9 and 10 dB on 30/20 for 60 minutes in the year (likely a high estimate), then the amount of uncertainty in *RA* is for only 1% of 60 minutes, or about 36 seconds in the year.

In contrast to the nearly flat 50% level plots, the 99% level plots curve downward with increasing base frequency attenuation. As long as the upper frequency attenuation is below the point where the receiver begins to saturate, this downward trend is valid. *RA* was first modeled as a second-order polynomial function of the base attenuation frequency:

$$A(f_U) = \alpha A(f_L) - \beta A(f_L)^2 \tag{6.3-2}$$

where $A(f_U)$ and $A(f_L)$ are attenuations at the upper and lower frequencies, and where α and β are coefficients of the second-order polynomial. This second order polynomial was fitted to the 99% level plots of Figures 5.3-4 to 5.3-6 with the following results for the OLYMPUS frequency pairs:

For 99% 30/20, for (1 dB $\leq ACA20 \leq$ 14 dB)

$$ACA30 = 2.75 * ACA20 - 0.02 * ACA20^2 \tag{6.3-3}$$

For 99% 20/12, for (1 dB $\leq ACA12 \leq$ 10 dB)

$$ACA20 = 3.94 * ACA12 - 0.08 * ACA12^2 \tag{6.3-4}$$

For 99% 30/12, for (1 dB $\leq ACA12 \leq$ 4 dB)

$$ACA30 = 9.32 * ACA12 - 0.39 * ACA12^2 \qquad (6.3\text{-}5)$$

where ACA30, ACA20, and ACA12 are the attenuations at 30, 20, and 12 GHz, respectively, and the ranges over which the empirical formulas are valid are given with each equation. These coefficient values are also given in Table 6.3-2. The scaling factors tend to be over predicted because the deviations caused by scintillation effects are included.

Table 6.3-2

Coefficients and Error for Modeling 99% Level *RA*

Ratio (Freq. Pairs)	α	β	Valid Range	Standard Dev.
30/20	2.75	0.02	1 dB ≤ ACA20 ≤ 14 dB	0.32
20/12	3.94	0.08	1 dB ≤ ACA12 ≤ 10 dB	0.93
30/12	9.32	0.39	1 dB ≤ ACA12 ≤ 4 dB	0.23

Since there is interest in scaling across the Ku/Ka band for any frequency pair, an attempt has been made to model the 99% level *RA* behavior across the Ku/Ka band. Using the α and β values in Table 6.3-2, a general relation that approximates (6.3-3), (6.3-4), and (6.3-5) was derived by curve-fitting through α and β and the respective values of the frequency pairs (i.e., f_U / f_L given in Table 6.3-1). The general relation is as follows:

$$A(f_U)_{99\%} = \left(\frac{f_2}{f_1}\right)^{2.65} A(f_L) - 0.00138\left(\frac{f_2}{f_1}\right)^{6.98} A(f_L)^2 \qquad (6.3\text{-}6)$$

Equation (6.3-6) has a standard deviation of error of 0.83 dB, based on all three pairs of the Virginia Tech measured data for the experiment year. Attenuation $A(f_U)$ derived from (6.3-6) is plotted in Figures 6.3-1, 6.3-2, and 6.3-3 as a function of $A(f_L)$ together with the measured 99% level of occurrence for *RA*. ACA30 versus ACA20 is overestimated, ACA20 versus ACA12 is underestimated, and ACA30 versus ACA12 is very accurate. The curve fit splits between 30/20 and 20/12, and the deviation of these pairs is understandable considering that 20 GHz is close to a water vapor absorption band (at 22.3 GHz). A higher than normal attenuation would be expected around 20 GHz, which would result in (6.3-6) overestimating upper frequency attenuation for a frequency pair with the base frequency around 20 GHz. On the other hand, if the upper frequency is around 20 GHz, then (6.3-6) would underestimate the upper frequency attenuation.

As a final example, we apply the nonlinear model of (6.3-6) to the Milstar frequencies of 20 GHz and 44 GHz. A moderate amount of attenuation data are available at 20 GHz, whereas very little is available at 44 GHz. Inserting these approximate frequencies into (6.3-1) and (6.3-6) yields for following relations for the 44/20 frequency scaling ratio.

50%:
$$RA_{ave} = \frac{ACA(44)}{ACA(20)} = \left(\frac{44}{20}\right)^{1.9} = 4.47 \qquad (6.3\text{-}7)$$

99%:
$$ACA(44) = 8.08\,ACA(20) - 0.34\,ACA(20)^2 \qquad (6.3\text{-}8)$$

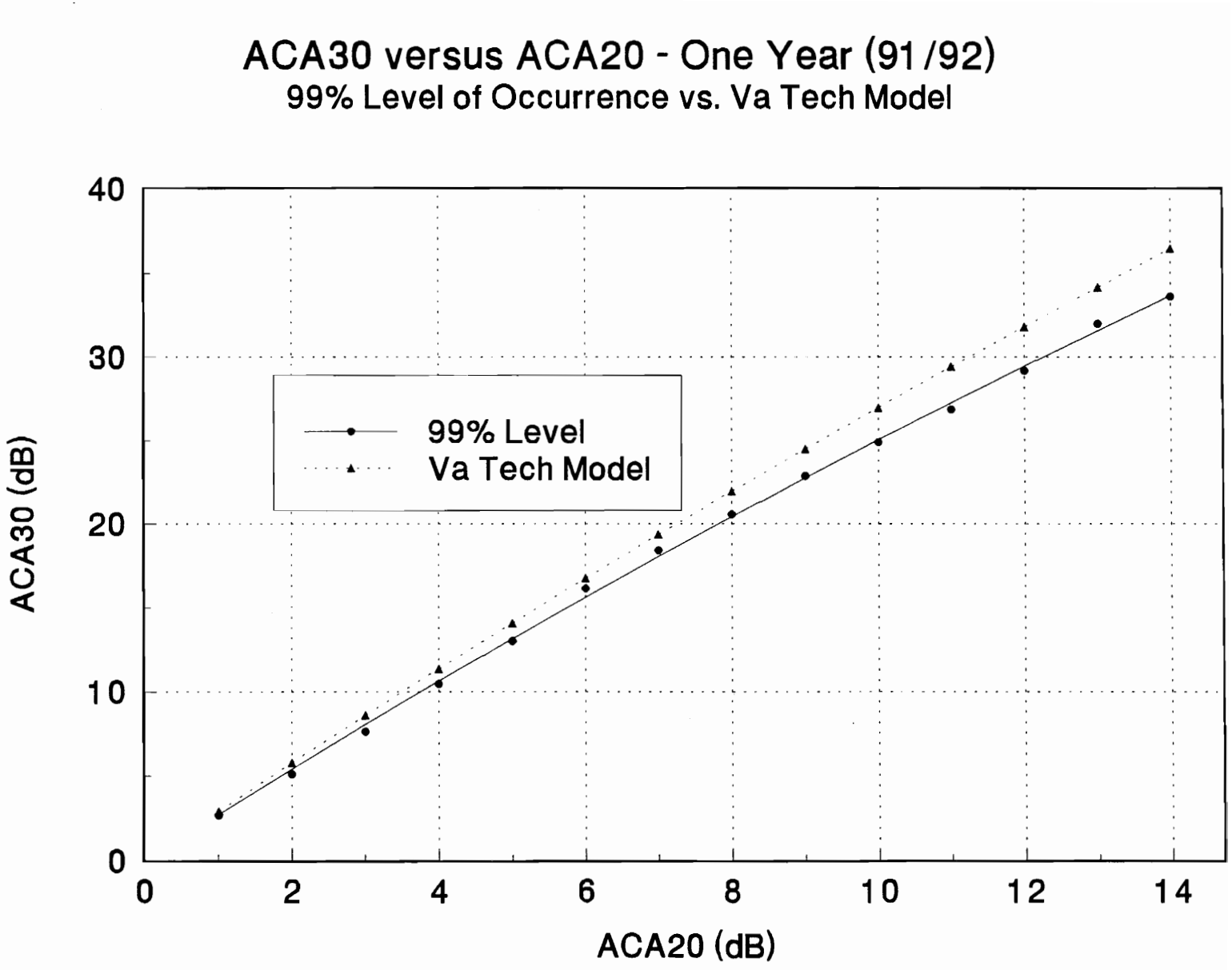

Figure 6.3-1 99% Level, 30/20 Measured vs. VT Ku/Ka Model (6.3-6) - One Year (91/92)

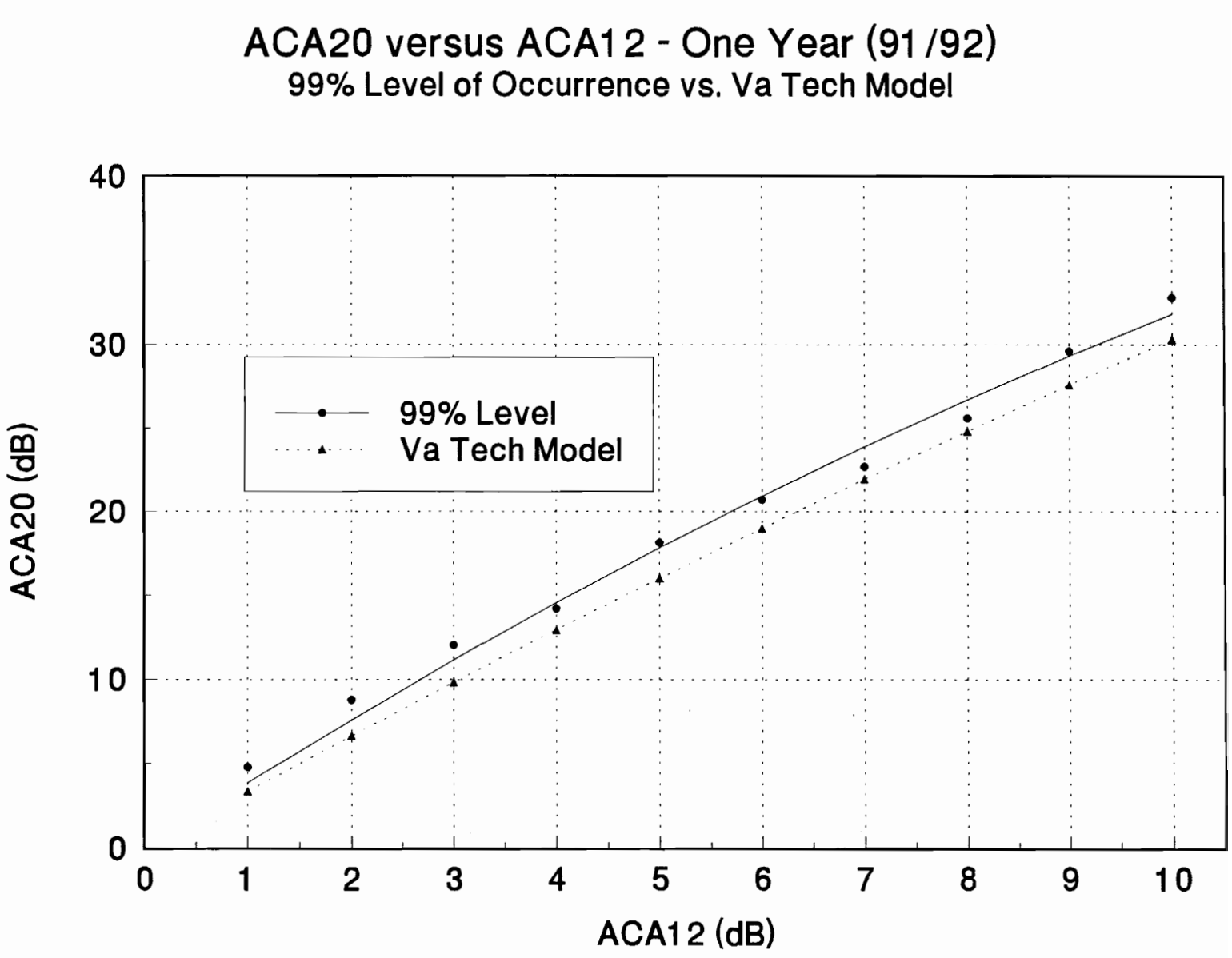

Figure 6.3-2 99% Level, 20/12 Measured vs. VT Ku/Ka Model (6.3-6) - One Year (91/92)

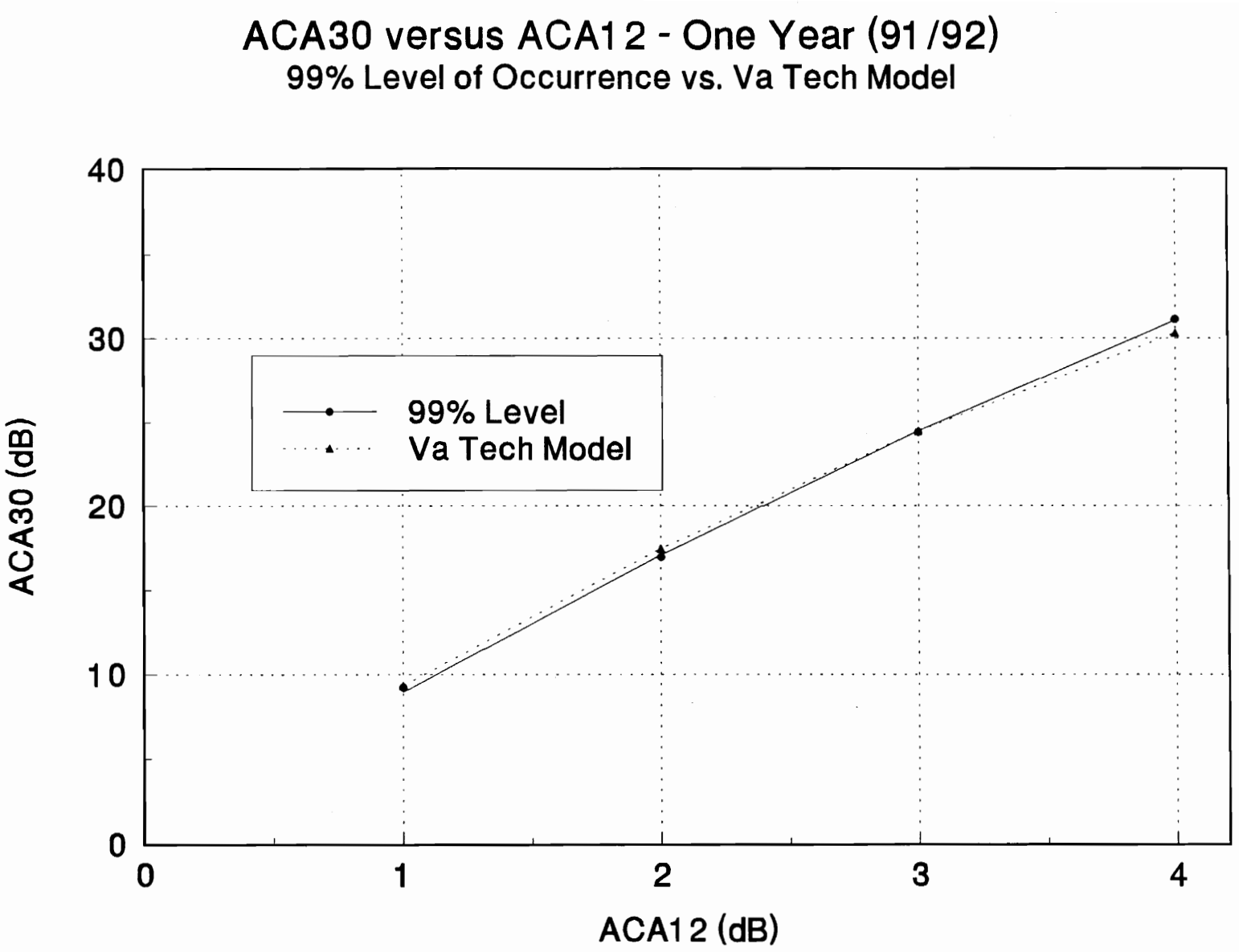

Figure 6.3-3 99% Level, 30/12 Measured vs. VT Ku/Ka Model (6.3-6) - One Year (91/92)

6.4 References

1. Dintelmann, F., Ortgies, G., Rücker, and Jakoby, R., "Results From 12 to 30 GHz German Propagation Experiments Carried out with Radiometers and the OLYMPUS Satellite," Research Centre, Deutsche Bundespost Telekom, Darmstadt, Germany, 1992.
2. Cited in Segal, B., "Rain Attenuation Statistics for Terrestrial Microwave Links in Canada," Communications Research Centre Report No. 1351-E, Ottawa, Canada, January 1982, p. 14.
3. "Attenuation by Hydrometeors, in Precipitation, and Other Atmospheric Particles," CCIR Report 721-3, *Propagation in Non-Ionized Media*, Vol. 5, ITU, Geneva, 1990.
4. Boithias, Lucien, "Similitue en frequence pour l'affaiblissement par la pluie," *Ann. Telecommun.*, 44, No. 3-4, 1986, pp.186-191 (cited in Sweeney, D.G., "Adaptive Power Control as a Fade Countermeasure on Satellite Links," Unpublished doctoral dissertation, Report EESATCOM 93-2, Virginia Polytechnic Institute & State University, Department of Electrical Engineering, Blacksburg, VA, January 1993, p. 53).
5. Sweeney, D.G., "Adaptive Power Control as a Fade Countermeasure on Satellite Links," Unpublished doctoral dissertation, Report EESATCOM 93-2, Virginia Polytechnic Institute & State University, Department of Electrical Engineering, Blacksburg, VA, January 1993.

CHAPTER 7

CONCLUSIONS

Accurate prediction of rain attenuation is of interest because of the need to exploit Ku and Ka frequency bands for satellite communcations. Essential to the prediction of rain attenuation is the ability to scale attenuation data from one frequency to another. Reliable models are needed to facilitate system design for frequency scaling of both rain attenuation statistics and instantaneous rain attenuation values. Frequency scaling of attenuation statistics uses existing attenuation statistics to predict attenuation at frequencies where data are unavailable. Frequency scaling of instantaneous attenuation data is important for adaptive fade countermeasures.

The data from the OLYMPUS satellite experiment at Virginia Tech were used in a comprehensive study of frequency scaling of both instantaneous and statistical attenuation. First, we examined the statistics of attenuation at 12, 20, and 30 GHz for the analysis year of January-May 1991, June-August 1992, and September-December 1991 (summarized in Section 7.1). The attenuation statistics were used to compute statistical attenuation ratio (denoted *RAS*) for each frequency pair (30/20, 20/12, and 30/12 GHz); *RAS* results are summarized in Section 7.2. Next we processed the year of data to calculate attenuation ratio (denoted *RA*) for each frequency pair. *RA* is the ratio of attenuation at each sample time; the statistics of *RA* are summarized in Section 7.3. A rain event was also examined to determined the time dependence of *RA* (summarized in Section 7.4). We examined the application of our results to other climate zones (see Section 7.5), and we compared our findings to the work of other researchers (see Section 7.6). Major findings are summarized in Section 7.7. Areas for future research are suggested in Section 7.8.

7.1 Attenuation Statistics

Some of the most important results of the OLYMPUS experiment are the attenuation statistics. These data include cumulative (or "exceedance") statistics for attenuation with respect to clear air, ACA, (refer to Section 2.2.3). The most important data sets are those for which data exist simultaneously at different pairs of frequencies (plotted in Figures 5.2.1 to 5.2-4 and tabulated in Tables 5.2-1 and 5.2-2). This permits direct comparison of signal quantities on different frequencies, including the ratio of attenuations at two different frequencies. We found the expected result that rain attenuation and scintillation fading become increasingly severe as frequency increases through the Ku/Ka bands.

Rain is responsible for the majority of attenuation with respect to clear air, ACA. It is both the extent of rain along the path and the intensity of the rain (or rain rate) which affect attenuation. A rain gauge was placed at our receiving site to monitor rain rate continuously. Figures 5.1-1 and 5.1-2 and Table 5.1-1 show the annual statistics from the tipping bucket rain gauge. The rain accumulation, based on rain gauge data and a nearby National Weather Service observer, equaled that of our annual average of 1067 mm. However, the fall of the analysis year was much dryer than normal while the summer was much wetter. Thus, there was greater than average amount of thunderstorm type rain during the analysis year.

7.2 Frequency Scaling of Instantaneous Attenuation Ratio

The ratio of attenuations for each frequency pair were computed for each sample instant (0.1 s apart) and stored as a function of time. Both instantaneous *RA*

and the statistics of *RA* were examined. The statistics of *RA* are the statistics of instantaneous attenuation ratio, in contrast to *RAS* which is the ratio of statistical attenuations.

7.2.1 The average and median of *RA* for frequency pairs

RA_{ave} is the average of median *RA* values over the 1-dB binned values of base frequency attenuation. RA_{med} is the median value of *RA* over all sampling times. RA_{ave} weights the fade levels equally, and RA_{med} pools all data.

We recommend the power law relation of (equation (6.2-2); repeated here for convenience) for average attenuation ratio RA_{ave}:

$$RA_{ave} = \frac{A(f_U)}{A(f_L)} = \left(\frac{f_U}{f_L}\right)^n \qquad (7.2\text{-}1)$$

Measured RA_{ave} values are given in Table 7.2-1. Using the exact OLYMPUS frequencies (see Table 6.3-1), the values for *n* derived by evaluating (7.2-1) for the individual frequency pairs are repeated in Table 7.2-2 for convenience.

A power law relation is also recommended for RA_{med}. Measured RA_{med} values are given in Table 7.2-1. Using the exact OLYMPUS frequencies (see Table 6.3-1), the values for *n* derived by evaluating (7.2-1) for the individual frequency pairs are repeated in Table 7.2-2 for convenience.

Table 7.2-1

Measured Average and Median *RA* Scale Factors
For the OLYMPUS Experiment Analysis Year of Data

	Frequencies f_U / f_L		
	30/20	20/12	30/12
RA_{ave}	1.93	2.86	5.56
RA_{med}	2.01	2.52	5.43

Table 7.2-2
Powers, n, for Power Law Fits to Measured Average & Median *RA*
From the OLYMPUS Experiment Analysis Year of Data

	Frequencies f_U / f_L			
	30/20	20/12	30/12	n_{ave}
Power n for RA_{ave}	1.72	2.02	1.96	1.90
Power n for RA_{med}	1.62	2.29	1.99	1.97

7.2.2 The average and median of *RA* across the Ku/Ka band

A power law relation with $n_{ave} = 1.9$ is a good approximation for frequency scaling of average (or mean) attenuation across the Ku/Ka band; it is found by averaging the powers of n for the three frequency pairs in Table 7.2-2. Table 7.2-2 reveals that RA_{ave} for 20/12 will be underpredicted and RA_{ave} for 30/20 will be overpredicted by a power law relation with $n = 1.9$ (also, RA_{ave} for 30/12 is slightly underpredicted).

For frequency scaling of overall median attenuation across the Ku/Ka band, RA_{med} follows a power law relation with n_{ave} = 1.97 found by averaging the powers of n for the three frequency pairs in Table 7.2-2. This is close to the square law relation (i.e., a power law relation with n = 2), which is a commonly used model (implying that rain attenuation in dB increases approximately as the square of the operating frequency).

7.2.3 Worst case models of *RA* for frequency pairs

Use of the constant scaling values of RA_{ave} and RA_{med} is convenient, but only predict "average" type behavior. It is also important to quantify the deviations from average behavior. A 99% level of occurrence of *RA* (shown in Figures 5.3-4 to 5.3-6) can be used as worst case model to quantify the deviation of *RA* from the average. The time base for the 99% level of occurrence of *RA* represents the product of 1.23% of the experiment year (given in Table 5.3-1) and the percentage of yearly up-time for an individual frequency pair (given in Table 5.2-1). The 99% level of occurrence means that the upper frequency attenuation can be expected to be at or below its value for 99% of the time that the base frequency attenuation is at a particular level (binned in 1-dB increments). The 1% of uncertainty is on the order of minutes and even seconds out of the entire year, depending the amount of time represented by a 1-dB bin of base frequency attenuation.

The 99% levels of occurrence of *RA* for 30/20, 20/12, and 30/12 depend on fade level, indicating that the relationship between the upper frequency attenuation and the lower (base) frequency attenuation cannot be well approximated by a constant attenuation ratio for these frequency pairs. Existing models are not adequate for prediction of the variation in $ACA(f_U)$ with $ACA(f_L)$. The 99% level of occurrence

quantifies the variation for 99% of the time. The 99% level can be approximated by a second order polynomial as given in (6.3-3), (6.3-4), and (6.3-5) for 30/20, 20/12, and 30/12, respectively. RA_{pred} is no longer a ratio yielding a constant for all base frequency attenuations (refer to (3.2-1)), but is a function of base frequency attenuation as is given by

$$RA_{pred} = A(f_U) / A(f_L) = \alpha - \beta A(f_L) \qquad (7.2\text{-}2)$$

7.2.4 Worst case model of *RA* across the Ku/Ka band

Because the empirical formulas differ for the individual frequency pairs, a more general model is needed to quantify the deviation of *RA* across the Ku/Ka band. Existing models across the Ku/Ka band do not adequately predict the Virginia Tech measured data. We propose the general formula of (6.3-6) for frequency scaling of attenuation across the Ku/Ka band. This empirical formula was derived by curve fitting the empirical formula parameters from Table 6.3-2 (i.e., α, β, and the frequency ratio values). One only need recognize that the Virginia Tech general formula of (6.3-6) slightly overestimates upper frequency attenuation when the base frequency is approximately 22.3 GHz (a water absorption band) and that (6.3-6) slightly underestimates upper frequency attenuation when the upper frequency is approximately 22.3 GHz (refer to Figures 6.3-1 to 6.3-3).

7.3 Frequency Scaling of Attenuation Statistics

Statistical attenuation ratio, *RAS*, is computed from the attenuation statistics at each frequency by the taking the ratio of $A(f_U)$ and $A(f_L)$ for a common percentage of time (see Section 2.4). An important result of this experiment is that *RAS* tracks the 50% level of occurrence for instantaneous ratio *RA*, RA_{med_i}, as a function of the base frequency attenuation (that is, *RAS* tracks RA_{med_i}). This indicates that existing attenuation statistics can be used in system design to predict the median instantaneous ratio as a function of base frequency attenuation.

7.4 Event Analysis

A representative rain event on May 14, 1991, was examined in Section 5.3.5 to see how well frequency scaling relations developed from the annual statistics apply to an individual event. The average attenuation ratio for the event, $RA_{ave_{event}}$, which is the slope of a "best fit" line through a scatter plot of $A(f_U)$ versus $A(f_L)$, was evaluated for each frequency pair. The results were very close to that of a frequency squared power law relation. It was found that a square law relation (i.e., a power law relation with $n = 2$) approximated the behavior of average attenuation ratio for the frequency pairs for this rain event.

Figures 5.3-16 and 5.3-17 show that scintillation causes deviation (spread) from the mean value of the ratio of $A(f_U)$ versus $A(f_L)$. In addition, the slope of a "best fit" line is the same with the moving average and without the moving average for 30/20, indicating that scintillation is symmetrical about $RA_{ave_{event}}$ for the frequency pair 30/20.

Examination of individual events (see Section 5.3.5 and Section 3.3.2.1) showed what others [5,6] have found about the time dynamics of rain storms. *RA* tends to be smaller at the beginning of a storm and larger at the end of a storm. This hysteresis effect is observed to begin at 1 dB for the base frequency attenuation on 30/20 for this rain event. For the events that Sweeney examined, the hysteresis effect begins at a base frequency attenuation of about 6 dB (i.e., at about $A(f_{20}) = 6$ dB).

7.5 Universality of Results

Since the Virginia Tech experiment is the only long term measurement program to span all of the Ku/Ka band frequencies simultaneously, it is important to speculate on its application to other situations, such as different climate zones. We comment on the application of our results to other climates and elevation angles.

Locations with a climate similar to Virginia Tech's should expect similar attenuation scaling behavior. Year to year variation of attenuation statistics within a climate zone can be large, but attenuation ratio is largely insensitive to such variations. Climate is important because of the variation of attenuation ratio within a rain event. This variation seems to be due to changes in the rain drop size distribution during the rain event. For example, climatic regions such as tropical areas experience more intense rainfall than is experienced in CCIR Zone K (e.g. at Virginia Tech). More intense rainfall translates into different average rain drop size distribution and likely results in different attenuation ratio statistics. Further research is needed in other climates to validate this prediction and quantify *RA* behavior.

Attenuation statistics can be translated from one elevation angle to another using (3.5-1) and (3.5-2) for a common frequency. We would like to compare Va Tech's

attenuation ratio statistics to that of other OLYMPUS experimenters at elevation angles different from that of Va Tech. In ratio models of attenuation scaling (see Section 3.2.1), there is no elevation angle dependence. Consequently, ratio models, such as the power law relation, are independent of elevation angle, so that Va Tech's *RA* statistics can be meaningfully compared to *RA* statistics of other OLYMPUS experimenters who have different elevation angles.

Non-ratio models (see Section 3.2.2), however, require that elevation scaling be performed. In contrast to ratio models, the elevation scaling factors do not cancel out for common frequencies when one scales from one elevation angle to another. This means that elevation angle scaling must be performed when applying non-ratio models such as Va Tech's 99% models to a location with a elevation angle different from Va Tech's (i.e., 14°). Elevation angle scaling can be performed fairly reliably (see Section 3.4).

7.6 Comparison to European OLYMPUS Results

The Virginia Tech measured results for one year and proposed models were compared to those from European OLYMPUS experiments.

British Telecom Labs [3] published average *RA* values for the OLYMPUS frequency pairs, where their average *RA* is slope of a best fit line through a scatter plot of $A(f_U)$ versus $A(f_L)$ for 136 rain events (taken from two years of measured data). This is similar to our RA_{ave} defined in Section 5.3.2. The results are given in Table 7.6-1. Their average *RA* values are less than Va Tech values for all frequency pairs.

Dintelmann, *et al.* [4] examined one year of data from their OLYMPUS experiment in Germany and found that a power law relation with $n = 1.8$ is an

adequate frequency scaling relation for the OLYMPUS frequencies. This is close to the power law relation with $n = 1.9$ derived from the Virginia Tech data. Using a $n = 1.8$ power law relation, RA_{ave} scaling factors are calculated for the German data in Table 7.6-1 (refer also to Table 6.1-1). Compared to Virginia Tech values, average *RA* values based on data from Germany are higher on 30/20 and lower on 20/12 and 30/12.

Table 7.6-1

Comparison of Attenuation Ratio Values for Three Long Term Experiments Using OLYMPUS

	Frequencies f_U / f_L		
	30/20	20/12	30/12
BT Labs (best fit slope of $A(f_U)$ vs. $A(f_L)$)	1.8	2.5	4.3
Dintelmann (*RA* computed with $n = 1.8$)	2.07	2.28	4.28
Virginia Tech Measured RA_{ave}	2.01	2.52	5.43

Ortgies, *et al.*, [5] found from the German OLYMPUS experiments that instantaneous frequency scaling of attenuation (*RA*) exhibits a hysteresis effect, which they attributed to variations of the drop size distribution and the effective path length through rain, as well as antenna effects [6]. They maintain that the hysteresis effect begins at much lower base attenuation values than that observed by Sweeney, *et al.* [7]. Our findings agree with Ortgies, *et al.* that the hysteresis effect can begin at attenuations as low as 1 dB for $A(f_L)$

The slight differences between European and Virginia Tech results could be due to the slight differences in climate between the localities. Attenuation ratio seems to

vary with rain drop size distribution. If a location consistently experiences stratiform rain while another location experiences more thunderstorm rain, the attenuation ratio statistics are likely to differ. The statistical nature of rain events in terms of rain drop size distribution varies yearly and is difficult to quantify.

7.7 Summary of Major Findings

(1) We found the expected result that rain attenuation and scintillation fading become increasingly severe as frequency increases through the Ku/Ka bands.

(2) For frequency scaling across the Ku/Ka band, average instantaneous attenuation ratio, RA_{ave}, which is the average of RA_{med_i} for all of the ith 1-dB bins, follows a power law relation with a power of $n = 1.9$.

(3) For frequency scaling across the Ku/Ka band, median instantaneous attenuation ratio, RA_{med}, which is the the median value of RA over all sampling times, follows a power law relation with $n = 1.97$.

(4) The excellent agreement between 50% level of occurrence for RA and RAS indicates that RAS, which is easily computed from separate attenuation exceedance statistics, is an accurate predictor of median instantaneous ratio as a function of base frequency attenuation.

(5) For individual rain events, hysteresis effects are observed where attenuation ratios at the beginning of a storm are different from those at the end for the same base frequency attenuation. Hysteresis begins at about 1 dB on $A(f_L)$.

7.8 Areas for Future Research

As discussed in Sections 3.2.1 and 6.1.3, attenuation models can be used to compute attenuation ratio, *RAS*. Attenuation models, such as SAM and others, could be examined to determine their validity as estimators of *RAS*.

Many data sets include the effects of scintillation, and researchers have attempted to filter out scintillation by taking moving averages of the data. In the May 14, 1991 rain event, the presence of scintillation (no moving average on the data) causes the data to spread away from the mean value, when compared to data filtered with a 30-s moving average (Section 5.3.5). The overall effects of scintillation need to be examined in more detail. Haidara [2] has characterized much of the behavior of scintillation, but her work needs to be expanded. The effects of applying moving averages to the data also needs to be quantified for the scaling relations under consideration in this paper.

Elevation angle scaling of attenuation (Section 3.4) is worthy of further investigation. This can be investigated by comparing the data and results of other OLYMPUS experimenters to the data and results of Virginia Tech's OLYMPUS experiment. Or better, Virginia Tech COMSAT experiment data could be compared to Virginia Tech's OLYMPUS data. The comparison would need to scale the differing elevation angles. The propagation frequencies and the climate are the same. A valid elevation scaling model would allow extrapolation of the previous results to new

satellites with differing elevation angles. Frequency scaling models could then be used if the new satellite had frequencies different from those of one's measured data.

Attenuation scaling from two frequencies (discussed in Section 3.2.2.2) can be investigated with the OLYMPUS data to see if two-frequency scaling yields better results than one-frequency scaling. The limited application of a two-frequency model, however, calls into question whether such an investigation is worthwhile.

7.9. References

1. Sweeney, D.G., "Adaptive Power Control as a Fade Countermeasure on Satellite Links," Unpublished doctoral dissertation, Report EESATCOM 93-2, Virginia Polytechnic Institute & State University, Department of Electrical Engineering, Blacksburg, VA, January 1993, p. 53.
2. Haidara, Fatim, "Characterization of Tropospheric Scintillations on Earth-Space Paths in the Ku and Ka Frequency Bands Using the Results from the Virginia Tech OLYMPUS Experiment," Unpublished doctoral dissertation, Report EESATCOM 93-11, Virginia Polytechnic Institute & State University, Department of Electrical Engineering, Blacksburg, VA, May 1993
3. Howell, R.G., Stucky, R.L., and Harris, J.W., "The BT Laboratories slant-path measurement complex," *BT Technology Journal*, 10, No. 4, October 1992.
4. Dintelmann, F., Ortgies, G., Rücker, and Jakoby, R., "Results From 12 to 30 GHz German Propagation Experiments Carried out with Radiometers and the OLYMPUS Satellite," Research Centre, Deutsche Bundespost Telekom, Darmstadt, Germany, 1992.
5. Ortgies, G., Rücker, F., and Dintelmann, F., "Some aspects of attenuation frequency scaling," *North American Radio Science Meeting and Internat IEEE/AP-S, Symposium*, London, Canada, 1991.
6. Ortgies, G. Rücker, F., Dintelmann, F., and Jakoby, R., "Effect-specific analysis of propagation parameters," *Proc. of the 16th NASA Propagation Experimenters Meeting (NAPEX XVI) and ACTS Propagation Studies Miniworkshop*, Houston, USA, 1992, pp. 143-154.
7. Sweeney, D.G., Pratt, T., and Bostian, C.W., "Hysteresis Effects in Instantaneous Frequency Scaling of Attenuation on 20 and 30 GHz Satellite Links," *Electronic Letters*, 2nd January 1992, Vol. 28, No. 1.

APPENDIX A

OTHER RESULTS FROM THE OLYMPUS EXPERIMENT

A.3.5 Probability of Occurrence of *RA*

A.3.5.1 30/20 for various thresholds
A.3.5.2 20/12 for various thresholds
A.3.5.3 30/12 for various thresholds
A.3.5.4 30/20 for various ranges
A.3.5.5 20/12 for various ranges
A.3.5.6 30/12 for various ranges

A.4 Statistical Scaling (Statistical Attenuation Ratio)

A.4.1 *RAS* vs. Base Attenuation

A.4.1.1 30/20 (ACAS20 > 1 dB) by months
A.4.1.2 20/12 (ACAS12 > 1 dB) by months
A.4.1.3 30/12 (ACAS12 > 1 dB) by months

MEASURED RAIN RATE AT BLACKSBURG, VA
January 1991 (Gauges 1 & 2 combined)

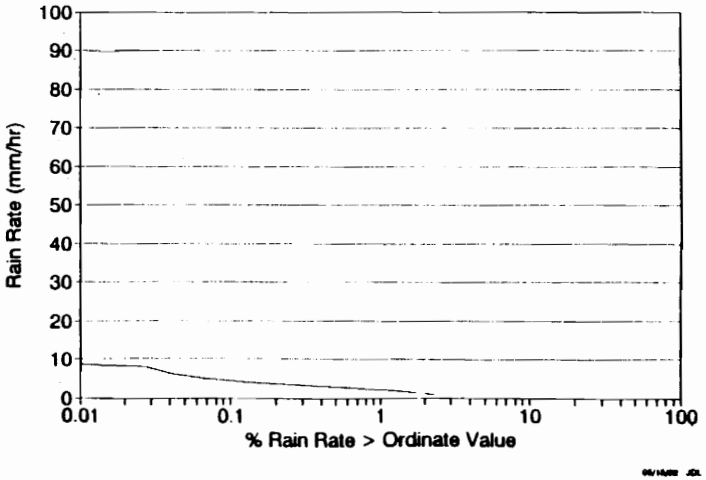

MEASURED RAIN RATE AT BLACKSBURG, VA
March 1991 (Gauges 1 & 2 combined)

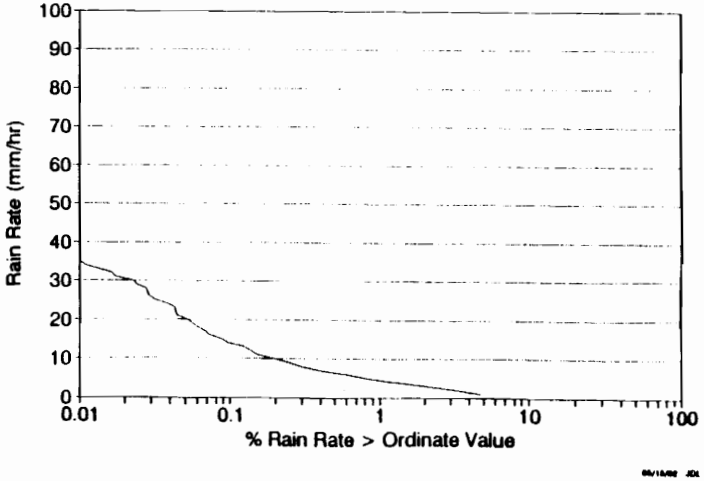

MEASURED RAIN RATE AT BLACKSBURG, VA
February 1991 (Gauges 1 & 2 combined)

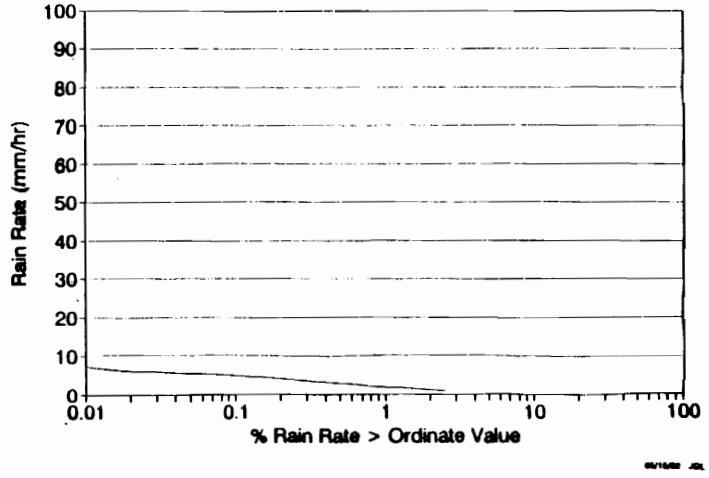

MEASURED RAIN RATE AT BLACKSBURG, VA
April 1991 (Gauge 1)

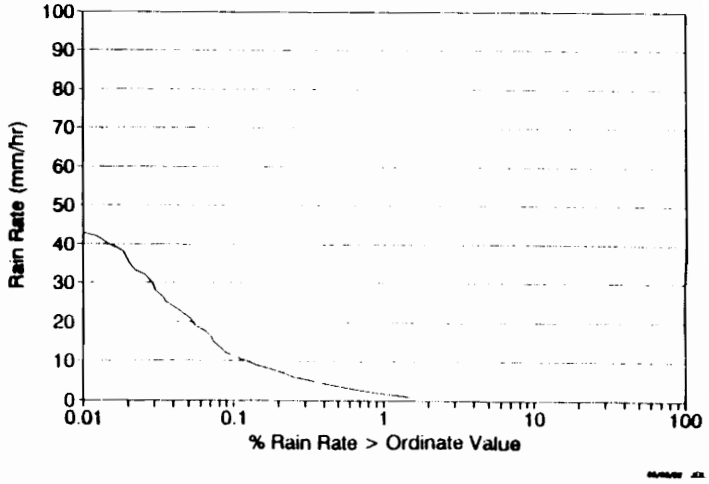

MEASURED RAIN RATE AT BLACKSBURG, VA
May 1991 (Gauge 1)

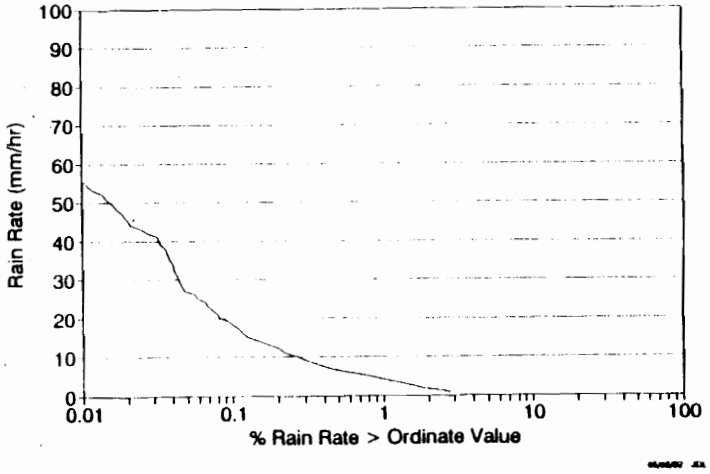

MEASURED RAIN RATE AT BLACKSBURG, VA
October 1991 (Gauge 1)

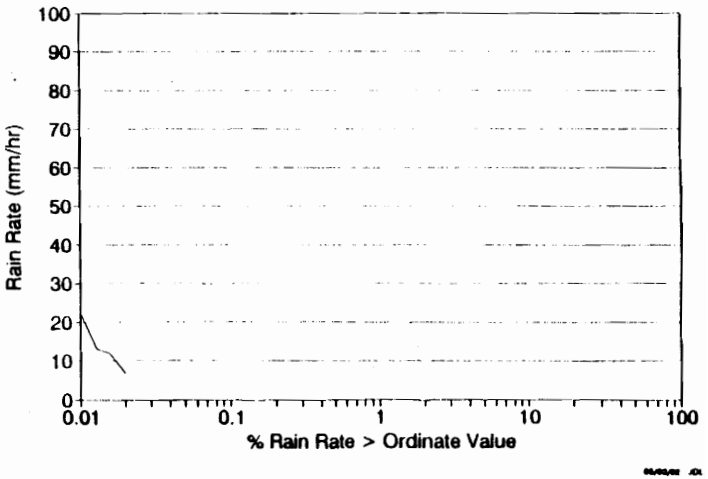

MEASURED RAIN RATE AT BLACKSBURG, VA
September 1991 (Gauge 1)

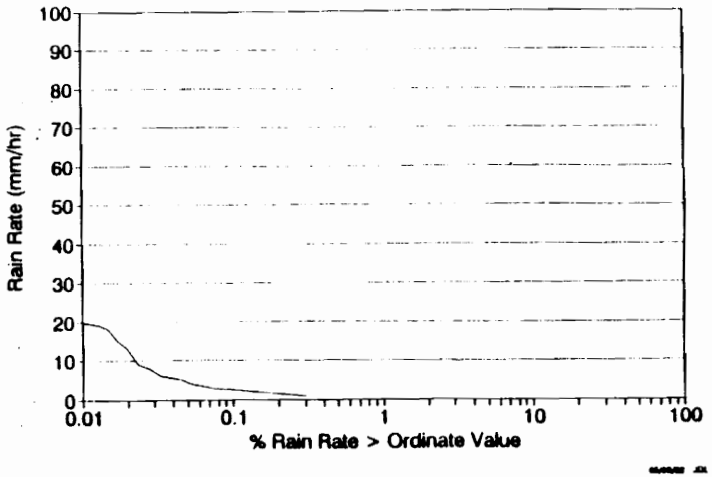

MEASURED RAIN RATE AT BLACKSBURG, VA
November 1991 (Gauge 1)

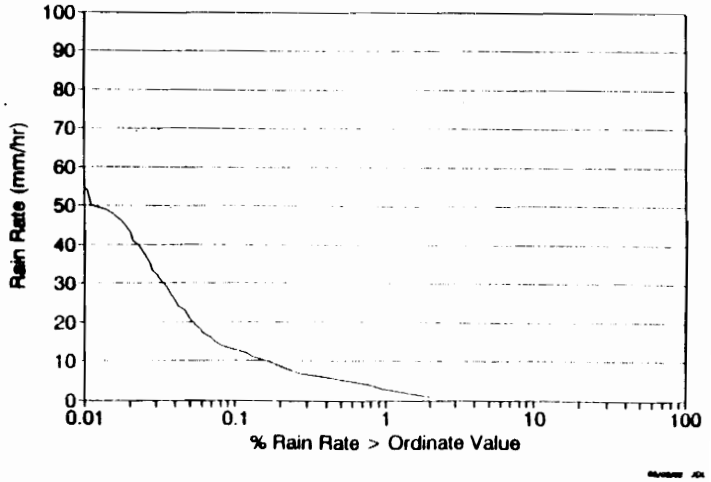

MEASURED RAIN RATE AT BLACKSBURG, VA
December 1991 (Gauge 1)

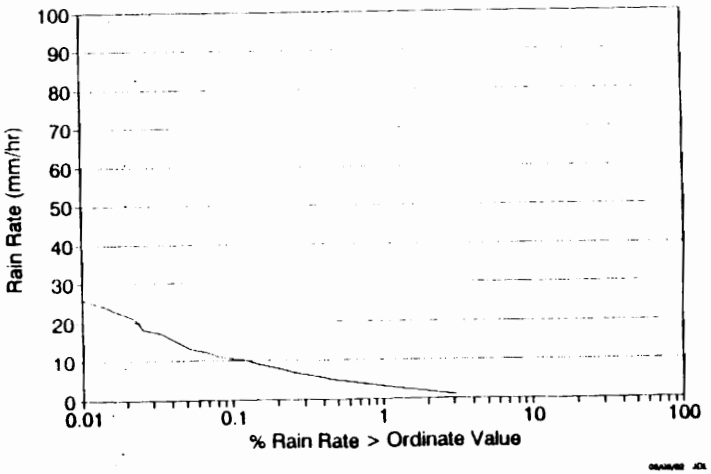

MEASURED RAIN RATE AT BLACKSBURG, VA
July 1992

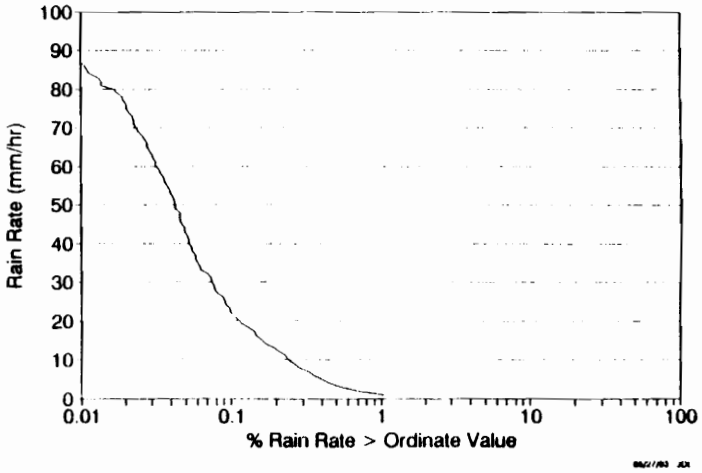

MEASURED RAIN RATE AT BLACKSBURG, VA
June 1992

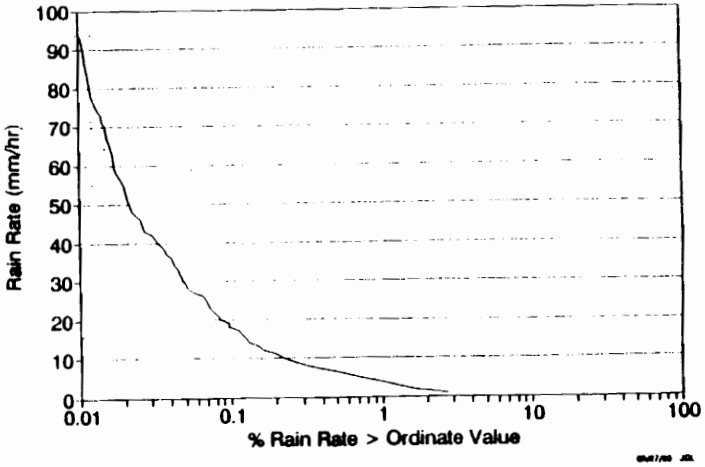

MEASURED RAIN RATE AT BLACKSBURG, VA
August 1992

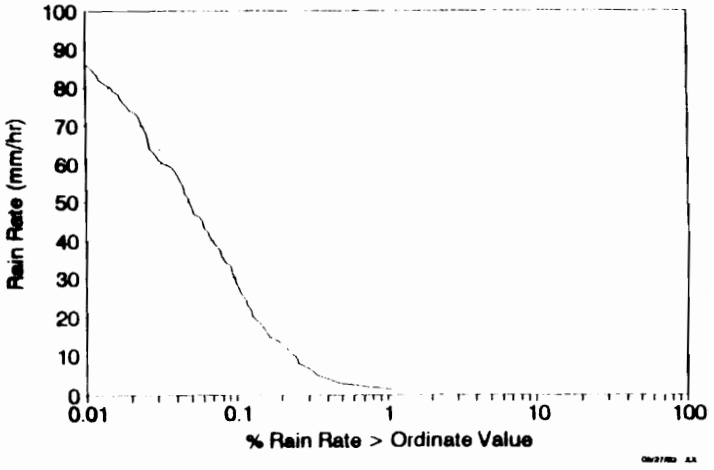

ATTENUATION WITH RESPECT TO CLEAR AIR
20 & 30 GHz - January 1991

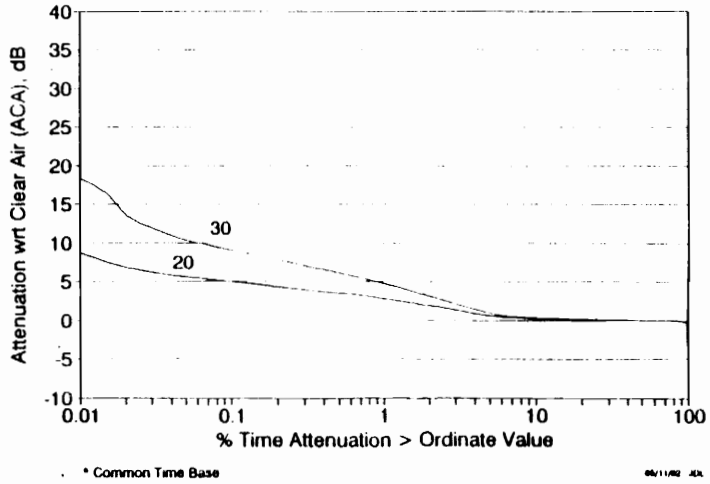

* Common Time Base

ATTENUATION WITH RESPECT TO CLEAR AIR
20 & 30 GHz - March 1991

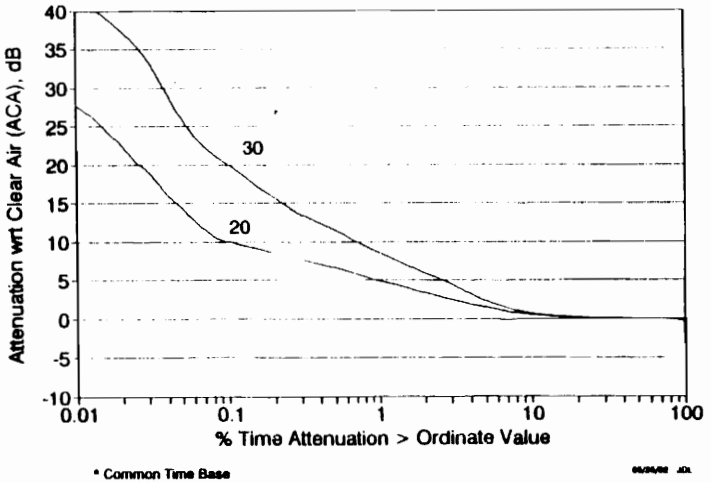

* Common Time Base

ATTENUATION WITH RESPECT TO CLEAR AIR
20 & 30 GHz - February 1991

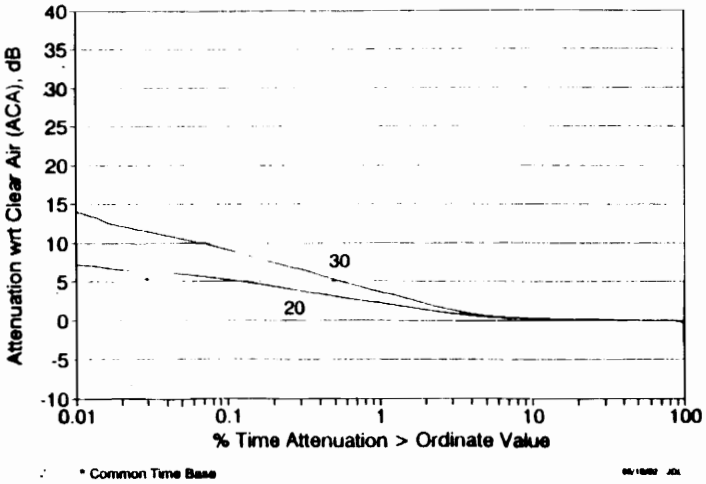

* Common Time Base

ATTENUATION WITH RESPECT TO CLEAR AIR
20 & 30 GHz - April 1991

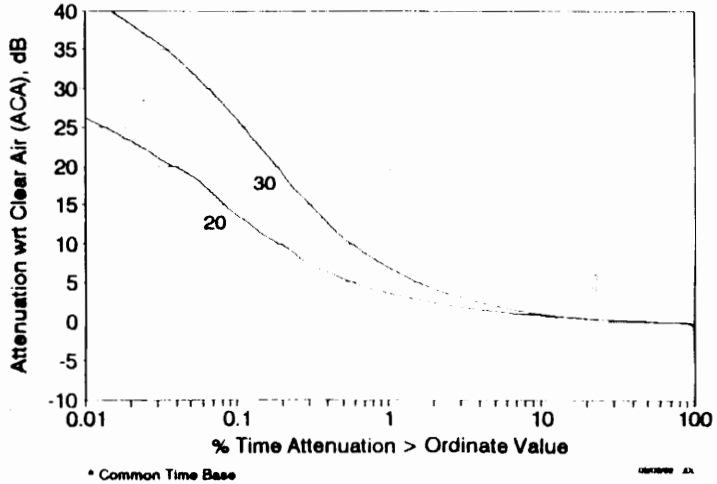

* Common Time Base

ATTENUATION WITH RESPECT TO CLEAR AIR
20 & 30 GHz - May 1991

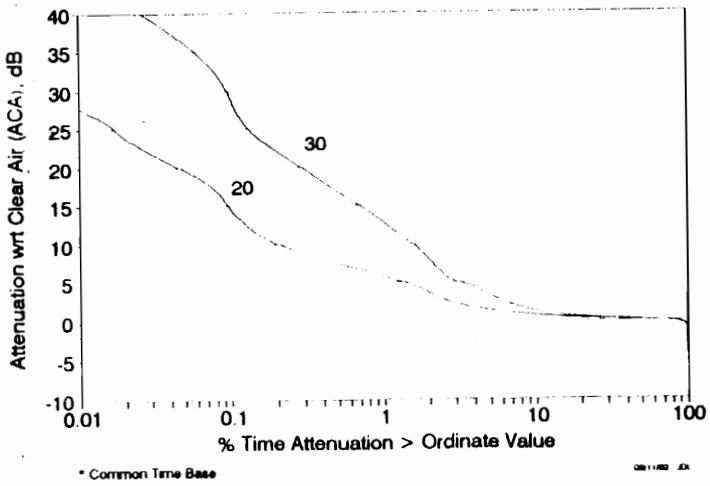

ATTENUATION WITH RESPECT TO CLEAR AIR
20 & 30 GHz - October 1991

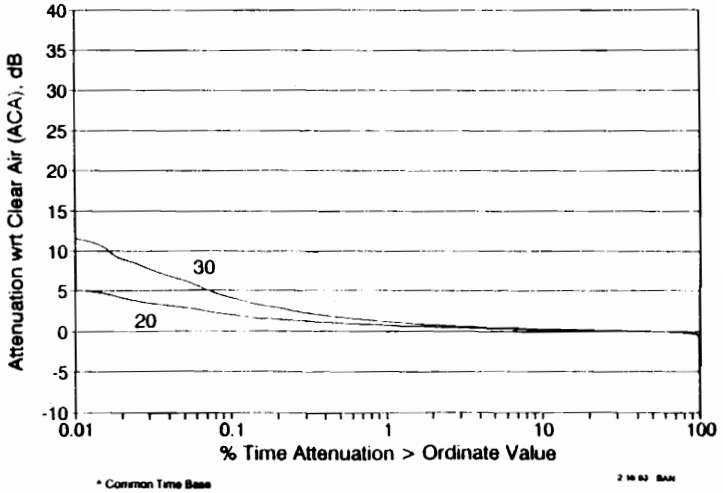

ATTENUATION WITH RESPECT TO CLEAR AIR
20 & 30 GHz - September 1991

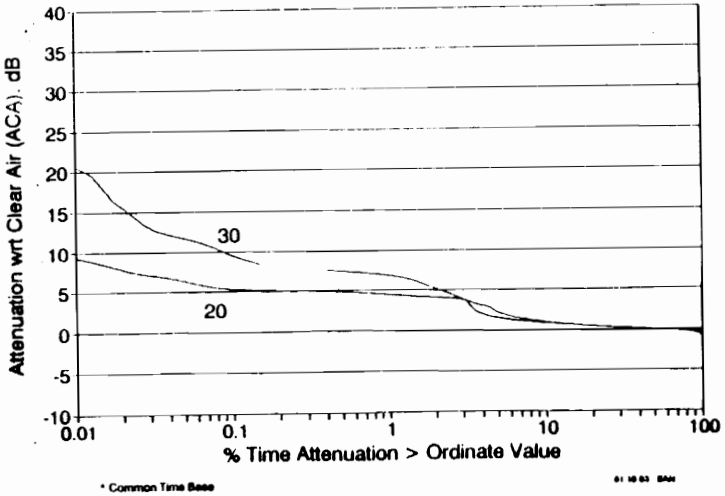

ATTENUATION WITH RESPECT TO CLEAR AIR
20 & 30 GHz - November 1991

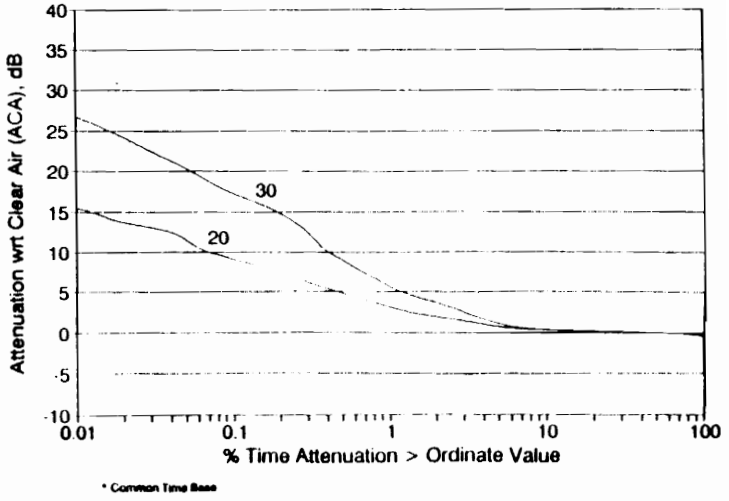

ATTENUATION WITH RESPECT TO CLEAR AIR
20 & 30 GHz - December 1991

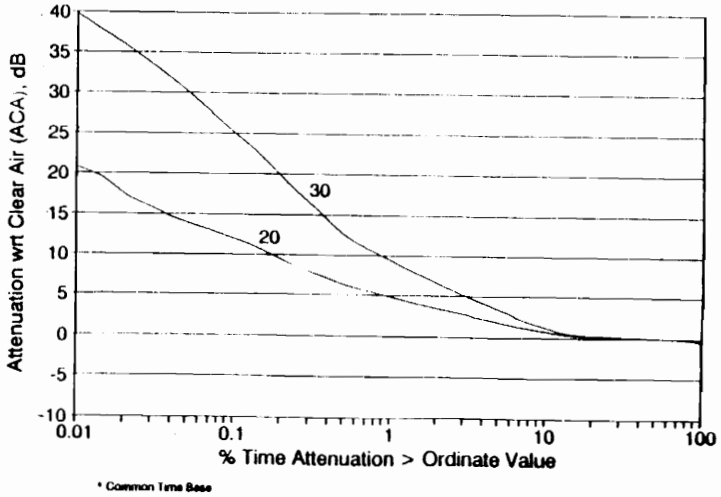

ATTENUATION WITH RESPECT TO CLEAR AIR
20 & 30 GHz - July 1992

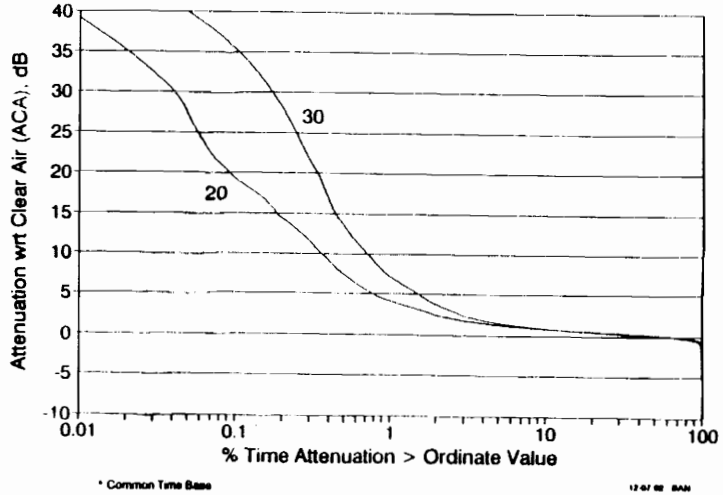

ATTENUATION WITH RESPECT TO CLEAR AIR
20 & 30 GHz - June 1992

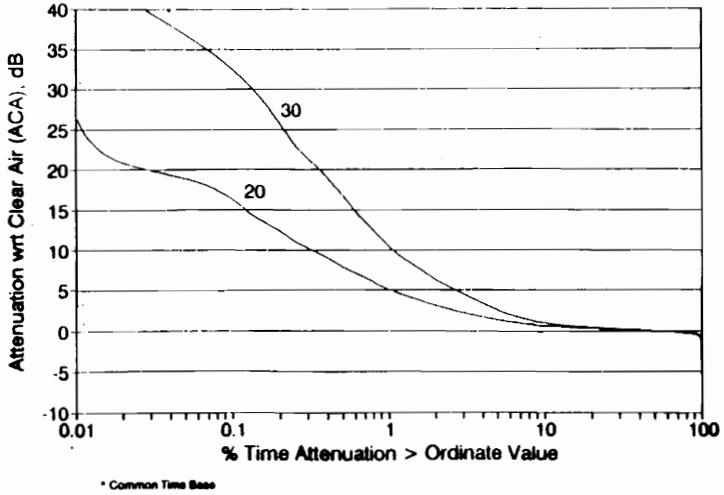

ATTENUATION WITH RESPECT TO CLEAR AIR
20 & 30 GHz - August 1992

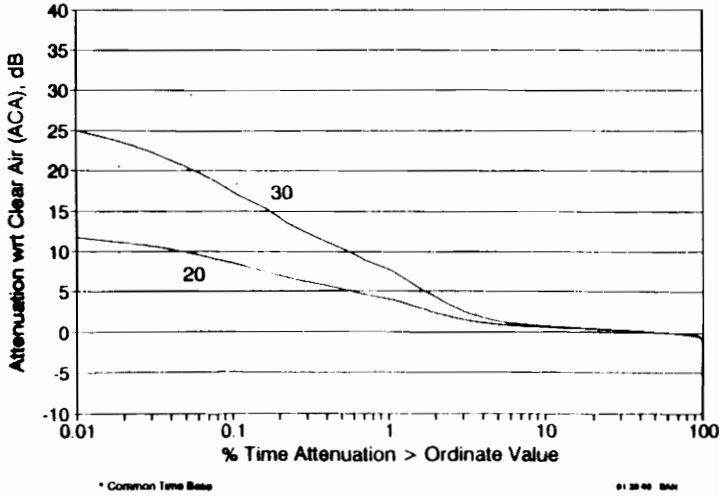

ATTENUATION WITH RESPECT TO CLEAR AIR
12 & 20 GHz - January 1991

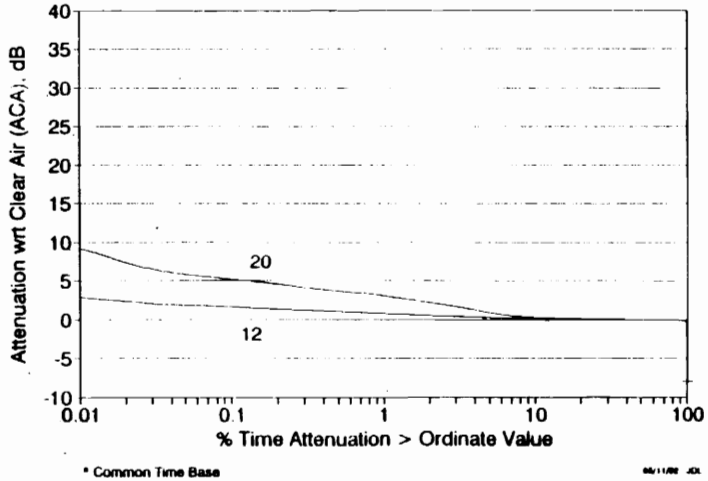

ATTENUATION WITH RESPECT TO CLEAR AIR
12 & 20 GHz - March 1991

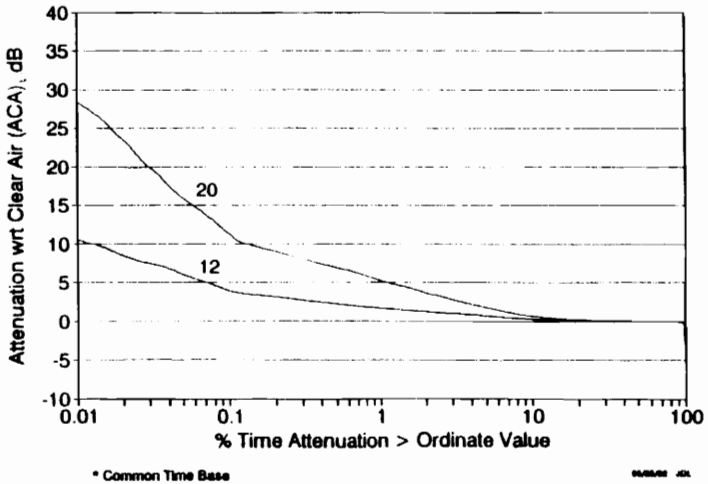

ATTENUATION WITH RESPECT TO CLEAR AIR
12 & 20 GHz - February 1991

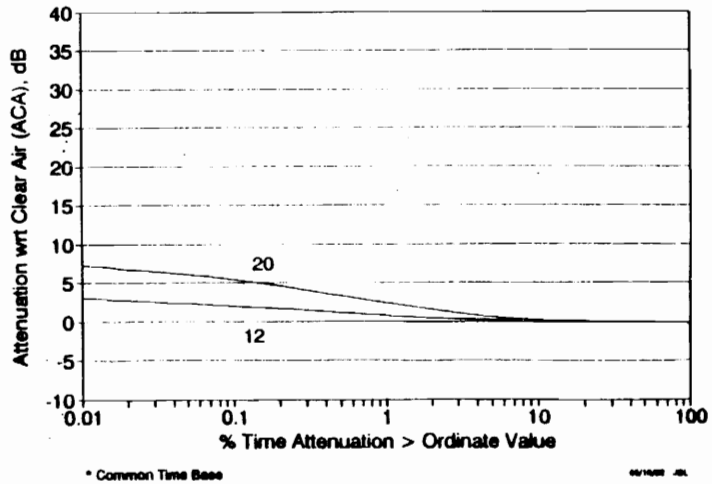

ATTENUATION WITH RESPECT TO CLEAR AIR
12 & 20 GHz - April 1991

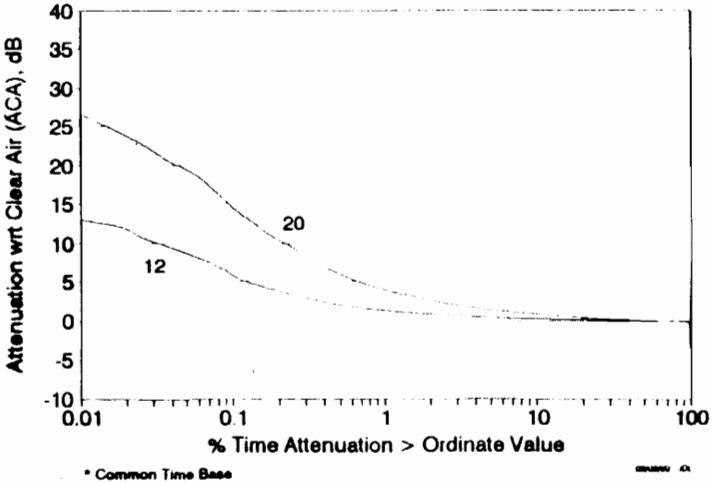

ATTENUATION WITH RESPECT TO CLEAR AIR
12 & 20 GHz - May 1991

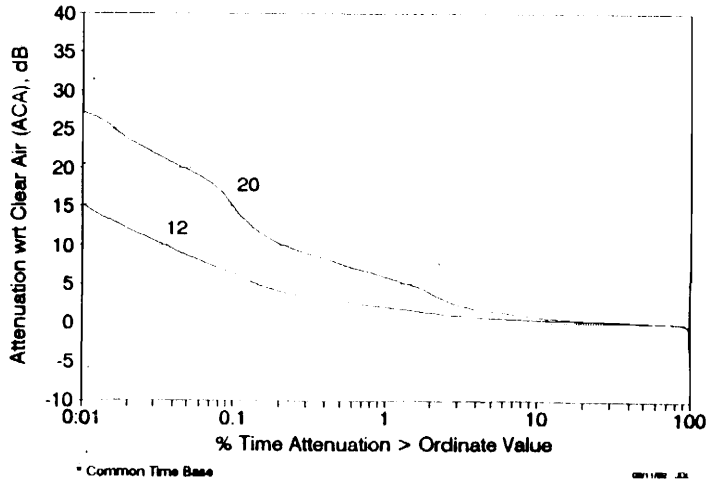

ATTENUATION WITH RESPECT TO CLEAR AIR
12 & 20 GHz - October 1991

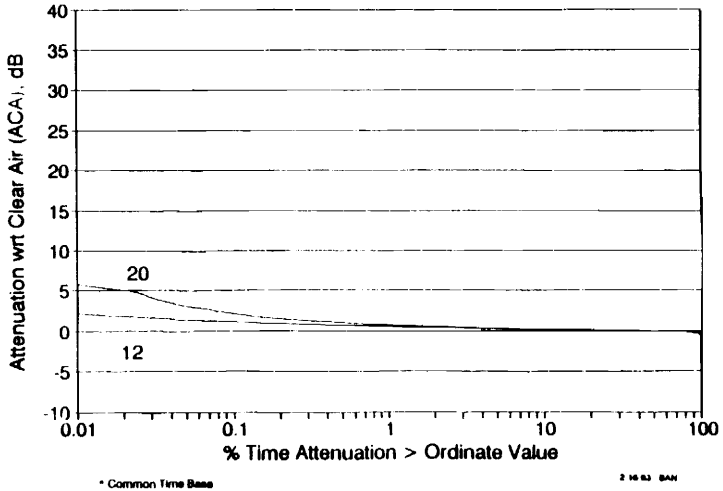

ATTENUATION WITH RESPECT TO CLEAR AIR
12 & 20 GHz - September 1991

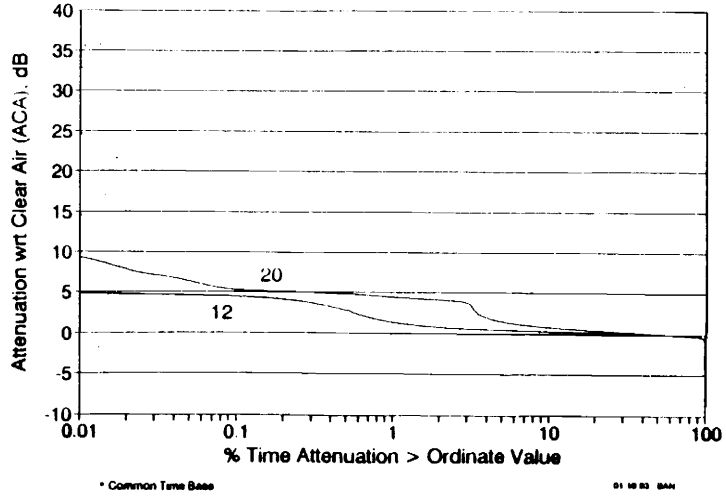

ATTENUATION WITH RESPECT TO CLEAR AIR
12 & 20 GHz - November 1991

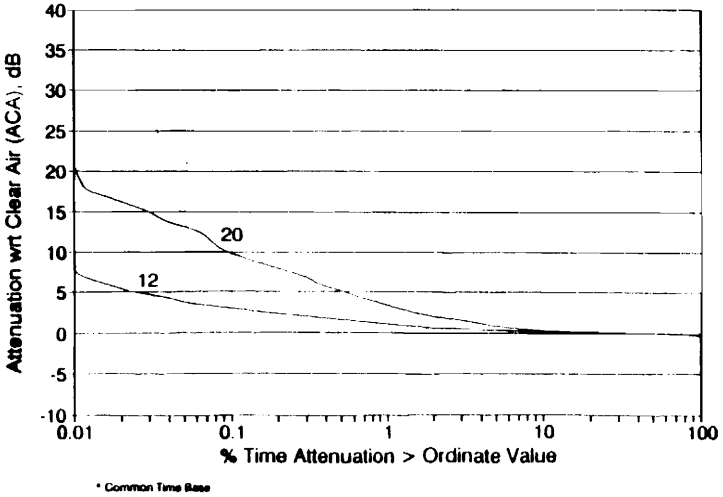

ATTENUATION WITH RESPECT TO CLEAR AIR
12 & 20 GHz - December 1991

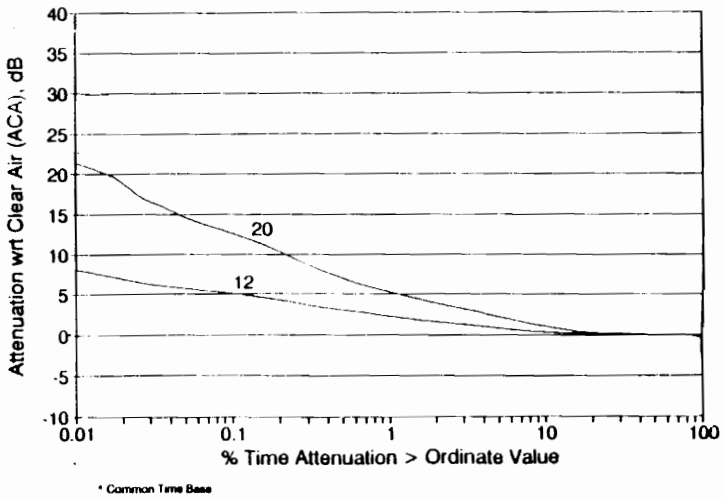

ATTENUATION WITH RESPECT TO CLEAR AIR
12 & 20 GHz - July 1992

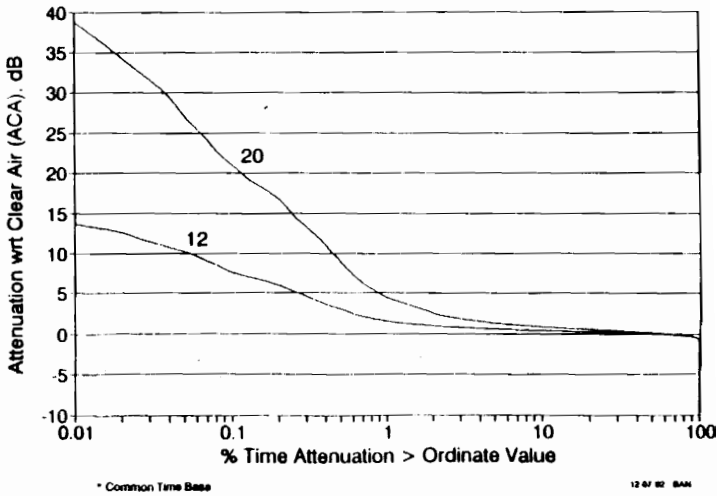

ATTENUATION WITH RESPECT TO CLEAR AIR
12 & 20 GHz - June 1992

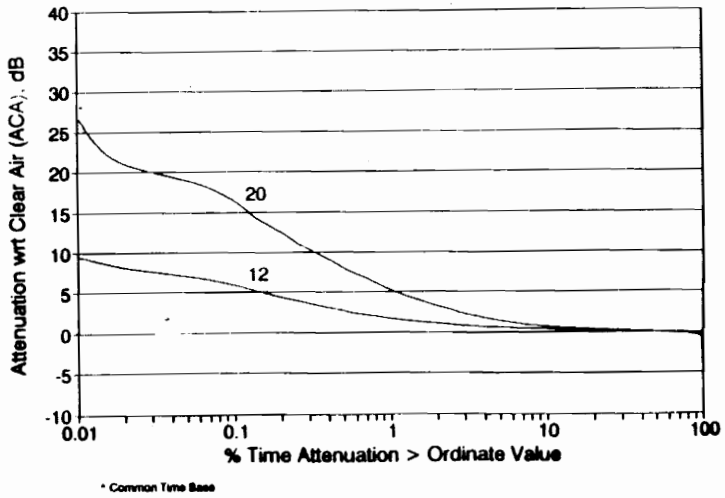

ATTENUATION WITH RESPECT TO CLEAR AIR
12 & 20 GHz - August 1992

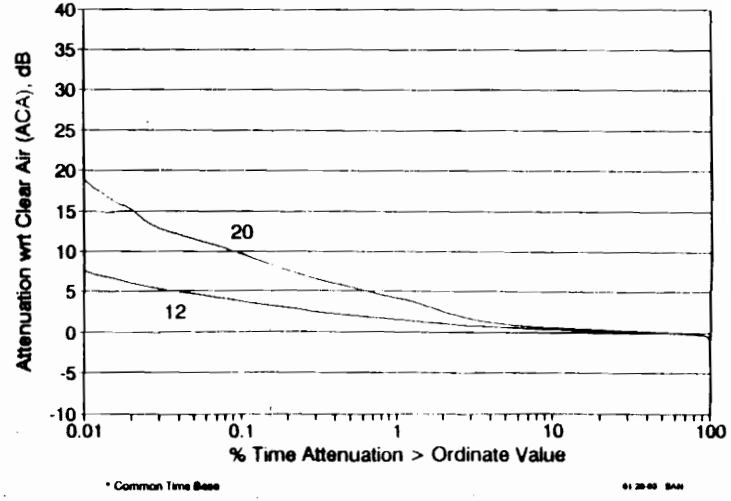

ATTENUATION WITH RESPECT TO CLEAR AIR
12 & 30 GHz - January 1991

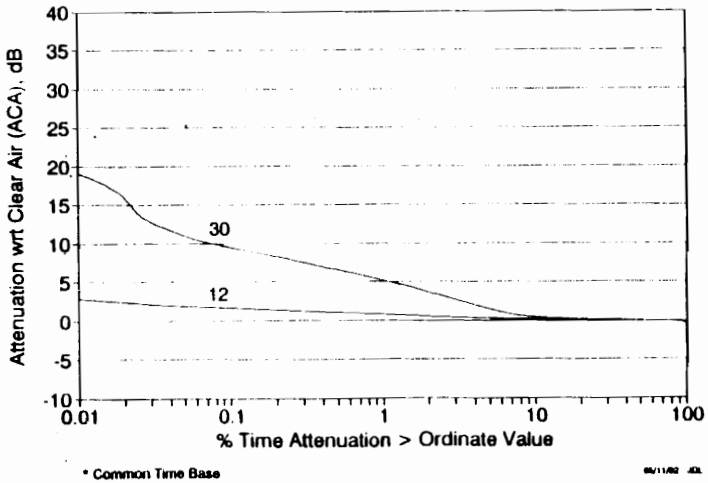

ATTENUATION WITH RESPECT TO CLEAR AIR
12 & 30 GHz - March 1991

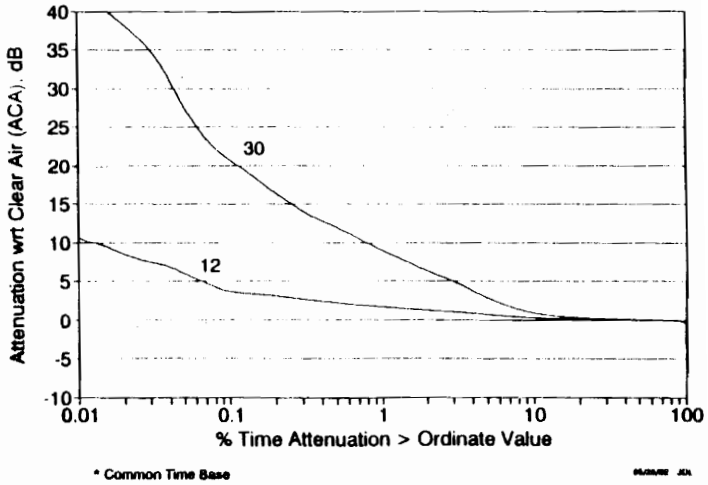

ATTENUATION WITH RESPECT TO CLEAR AIR
12 & 30 GHz - February 1991

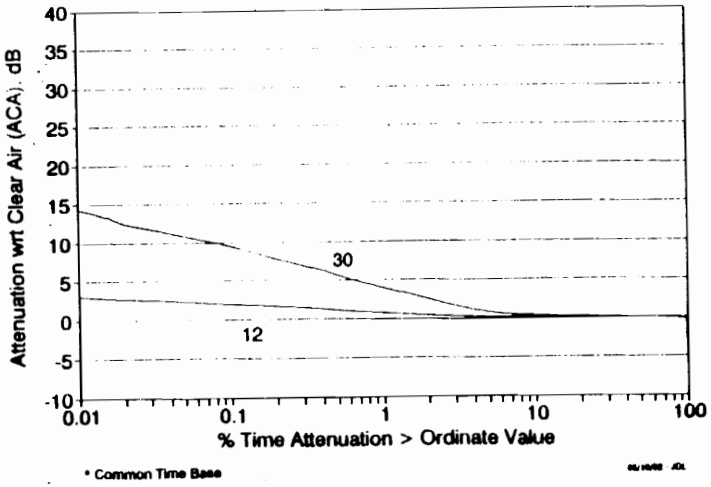

ATTENUATION WITH RESPECT TO CLEAR AIR
12 & 30 GHz - April 1991

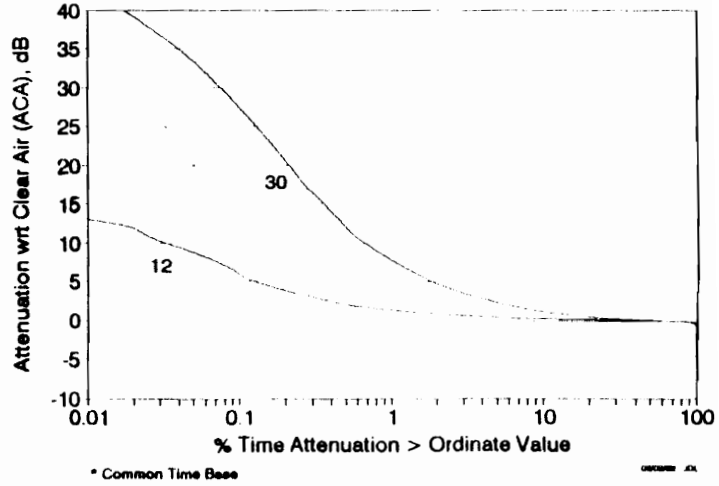

ATTENUATION WITH RESPECT TO CLEAR AIR
12 & 30 GHz - May 1991

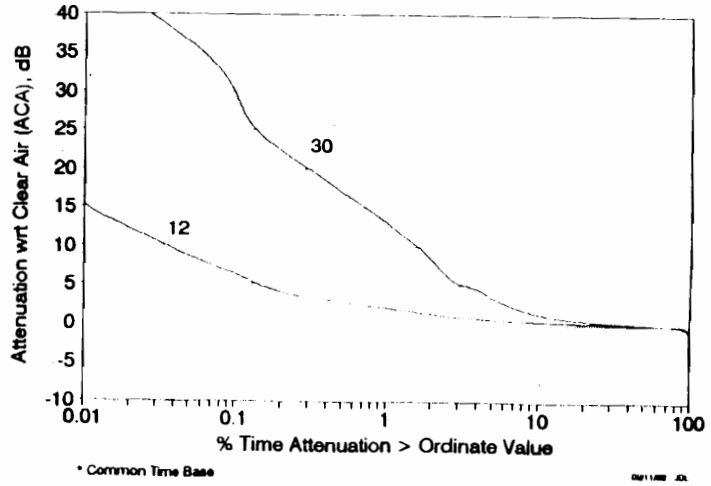

ATTENUATION WITH RESPECT TO CLEAR AIR
12 & 30 GHz - October 1991

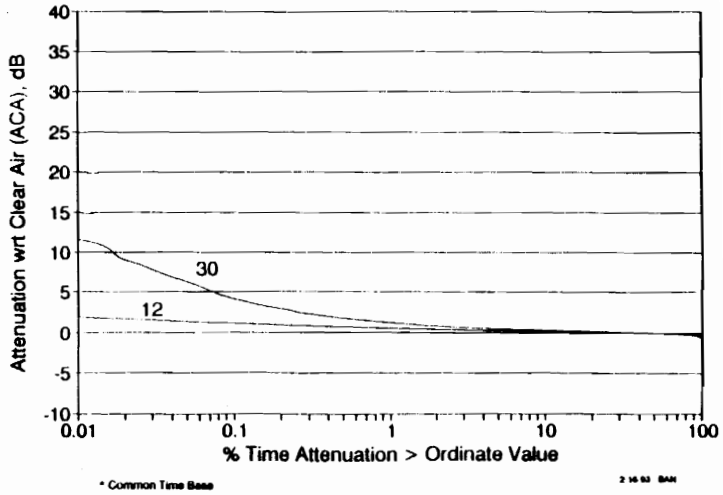

ATTENUATION WITH RESPECT TO CLEAR AIR
12 & 30 GHz - September 1991

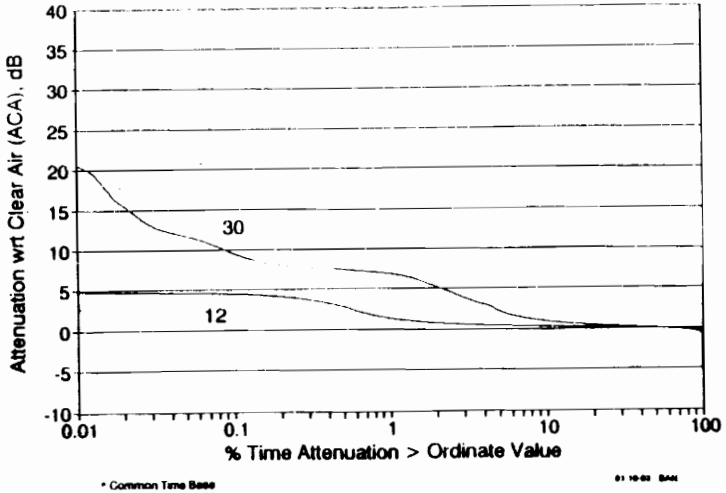

ATTENUATION WITH RESPECT TO CLEAR AIR
12 & 30 GHz - November 1991

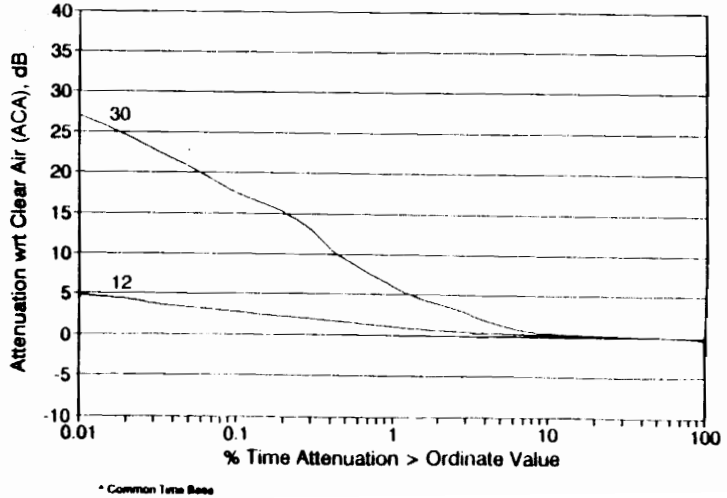

ATTENUATION WITH RESPECT TO CLEAR AIR
12 & 30 GHz - December 1991

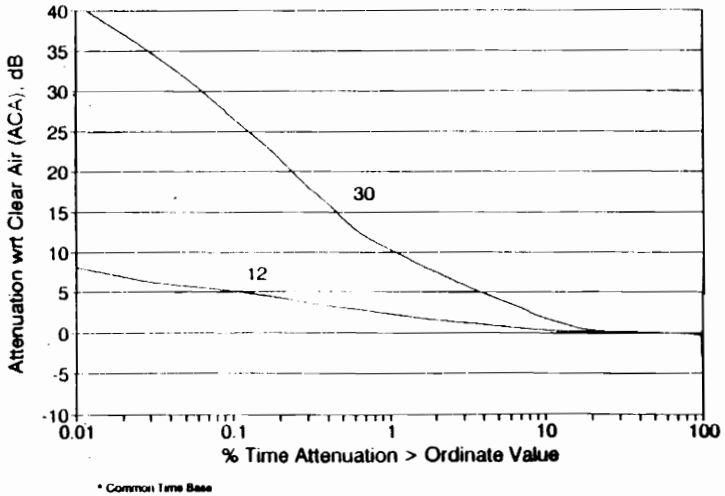

ATTENUATION WITH RESPECT TO CLEAR AIR
12 & 30 GHz - July 1992

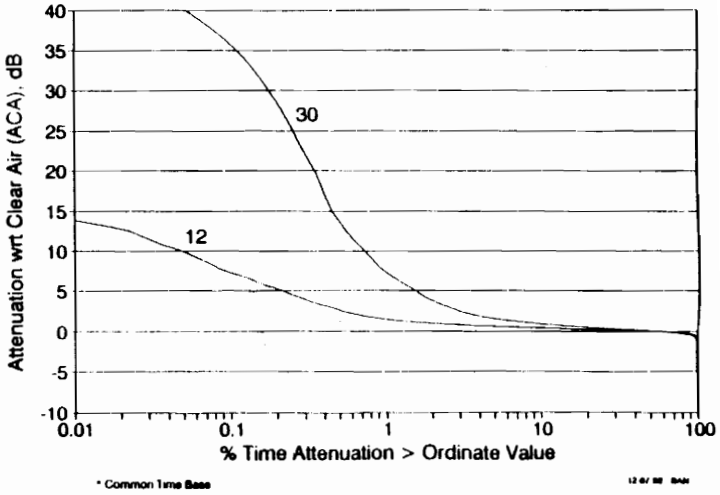

ATTENUATION WITH RESPECT TO CLEAR AIR
12 & 30 GHz - June 1992

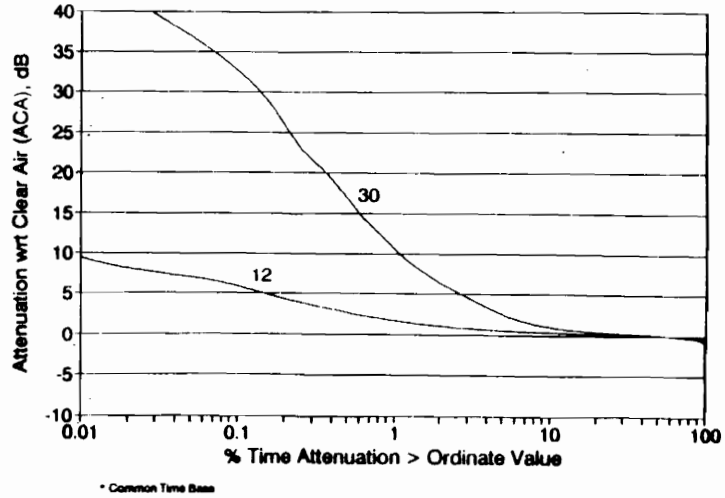

ATTENUATION WITH RESPECT TO CLEAR AIR
12 & 30 GHz - August 1992

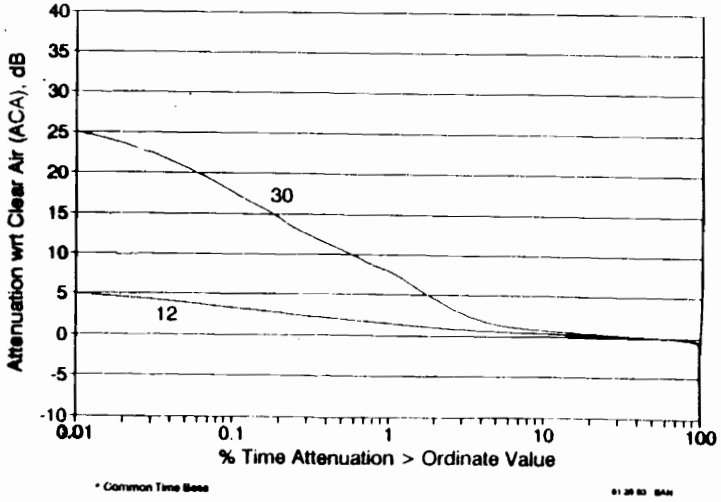

30/20 ATTENUATION RATIO
January 1991 (ACA20 > 1 dB)

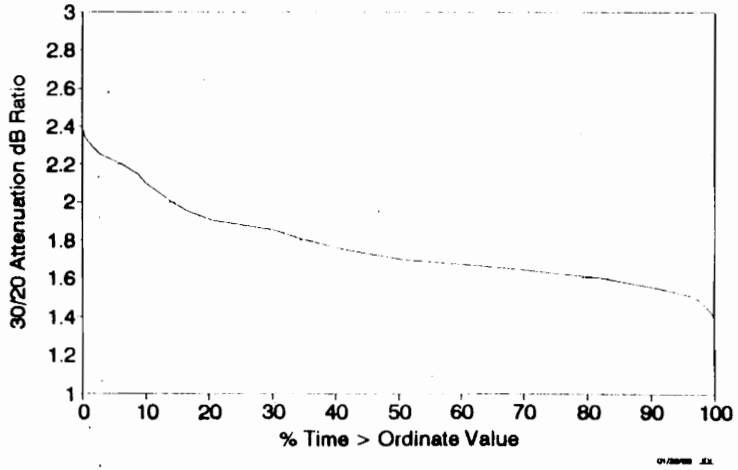

30/20 ATTENUATION RATIO
March 1991 (Exceeding 1 dB)

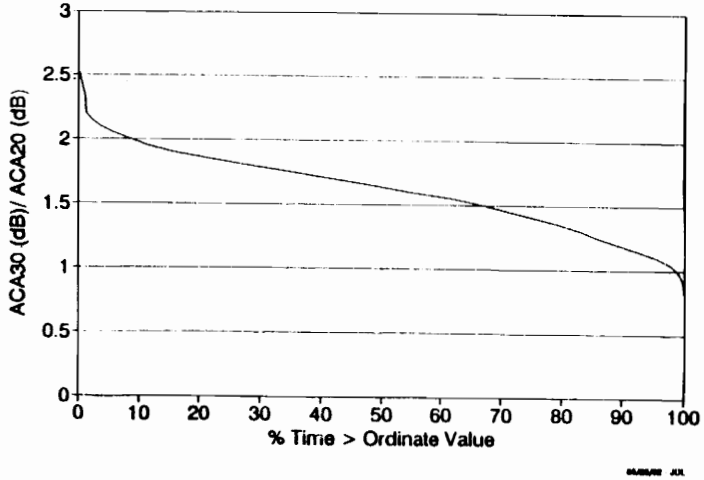

30/20 ATTENUATION RATIO
February 1991 (Exceeding 1 dB)

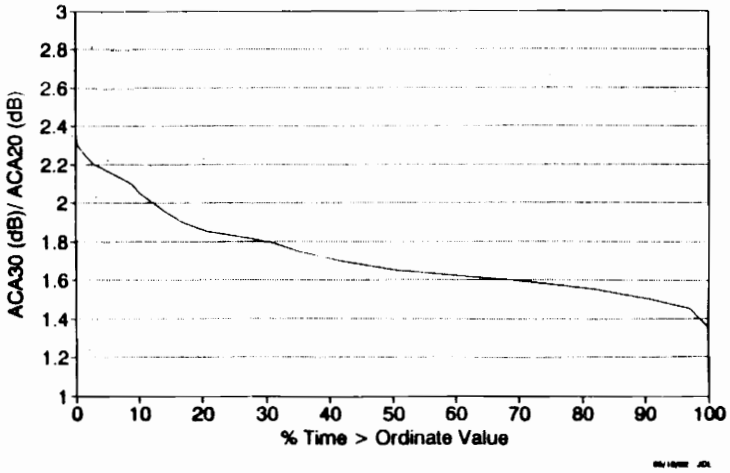

30/20 ATTENUATION RATIO
April 1991 (Exceeding 1 dB)

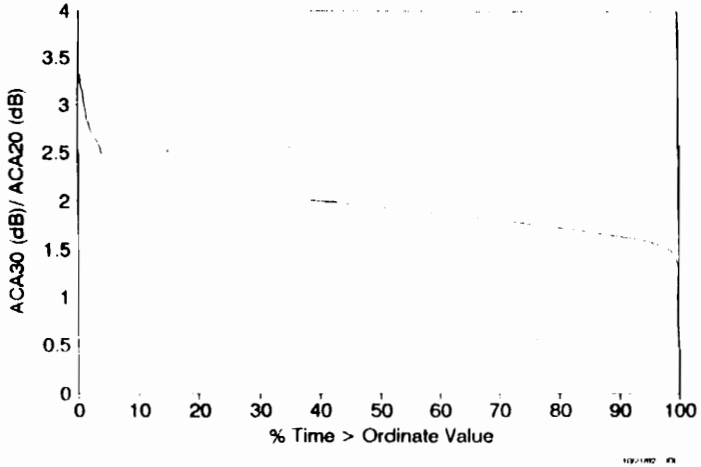

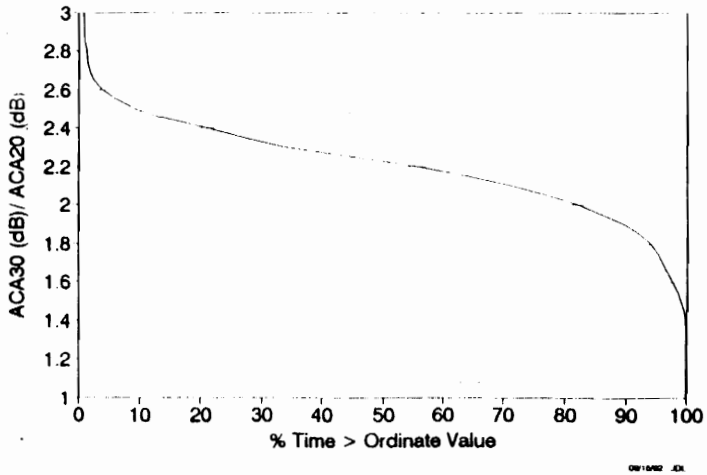
30/20 ATTENUATION RATIO
May 1991 (Exceeding 1 dB)
ACA30 (dB)/ ACA20 (dB)
% Time > Ordinate Value

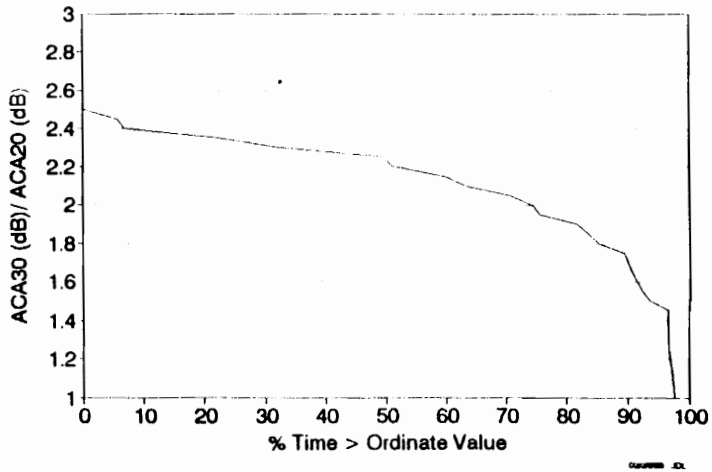
30/20 ATTENUATION RATIO
October 1991 (ACA20 > 1 dB)
ACA30 (dB)/ ACA20 (dB)
% Time > Ordinate Value

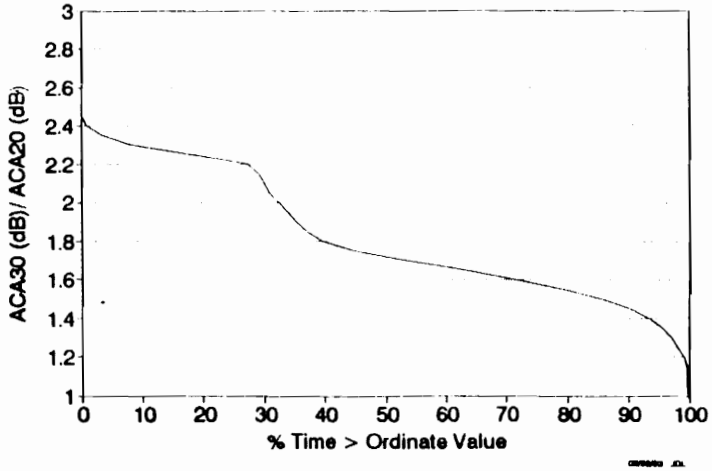
30/20 ATTENUATION RATIO
September 1991 (ACA20 > 1 dB)
ACA30 (dB)/ ACA20 (dB)
% Time > Ordinate Value

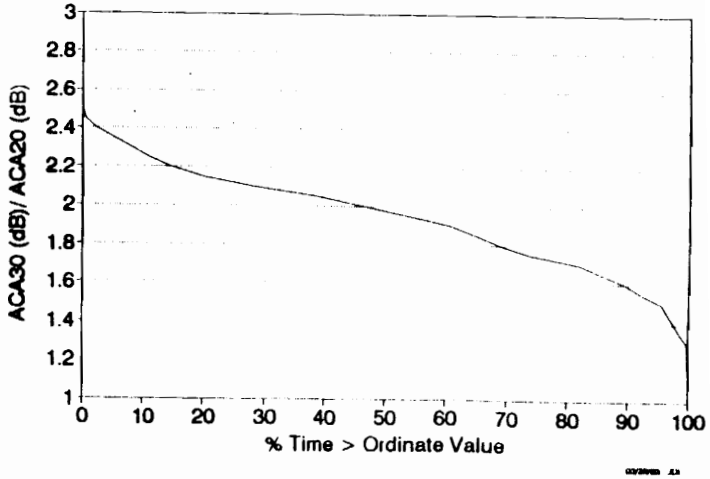
30/20 ATTENUATION RATIO
November 1991 (ACA20 > 1 dB)
ACA30 (dB)/ ACA20 (dB)
% Time > Ordinate Value

30/20 ATTENUATION RATIO
December 1991 (ACA20 > 1 dB)

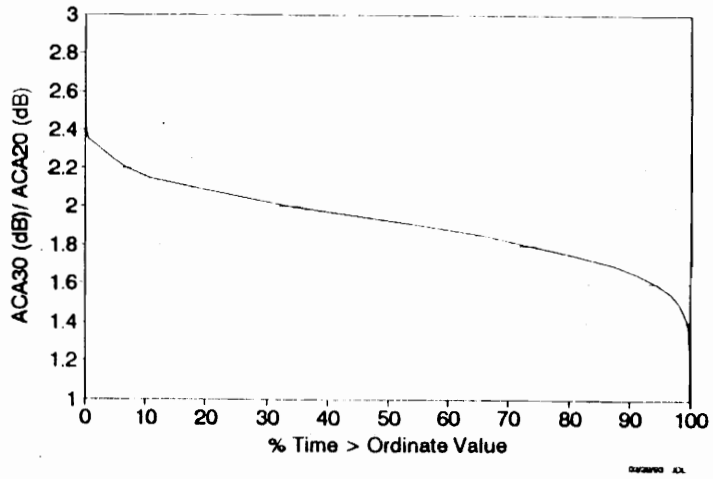

30/20 ATTENUATION RATIO
July 1992 (ACA20 > 1 dB)

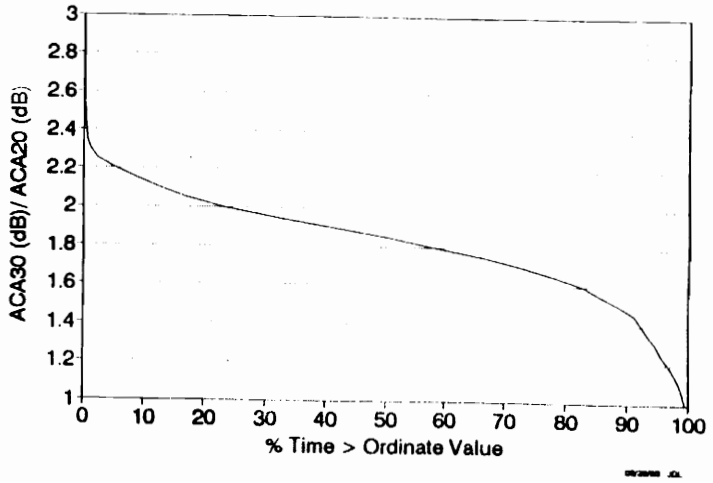

30/20 ATTENUATION RATIO
June 1992 (ACA20 > 1 dB)

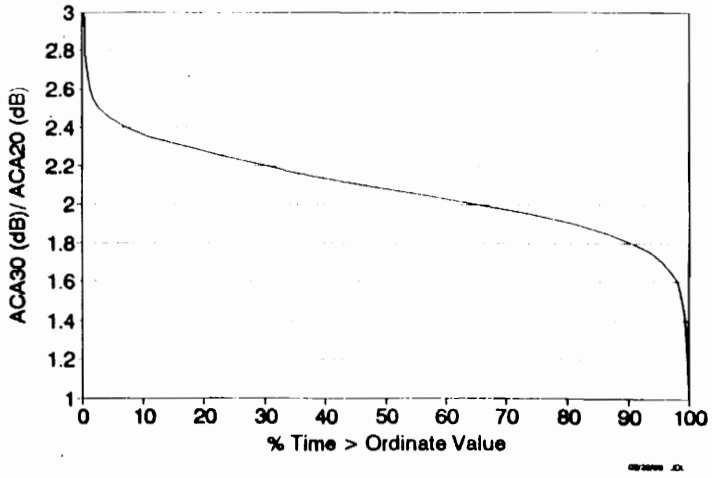

30/20 ATTENUATION RATIO
August 1992 (ACA20 > 1 dB)

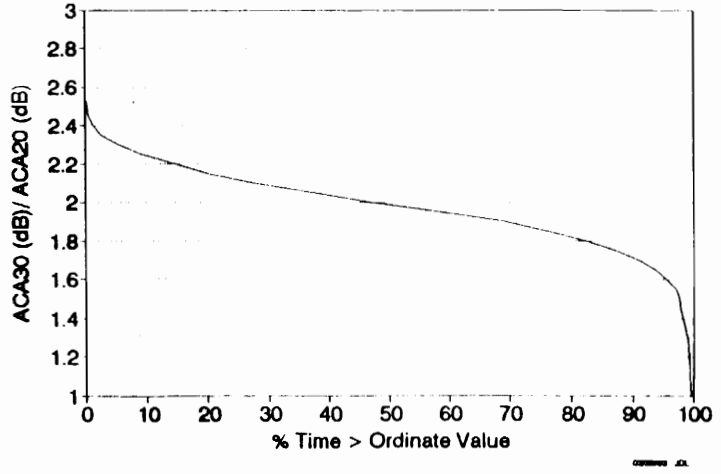

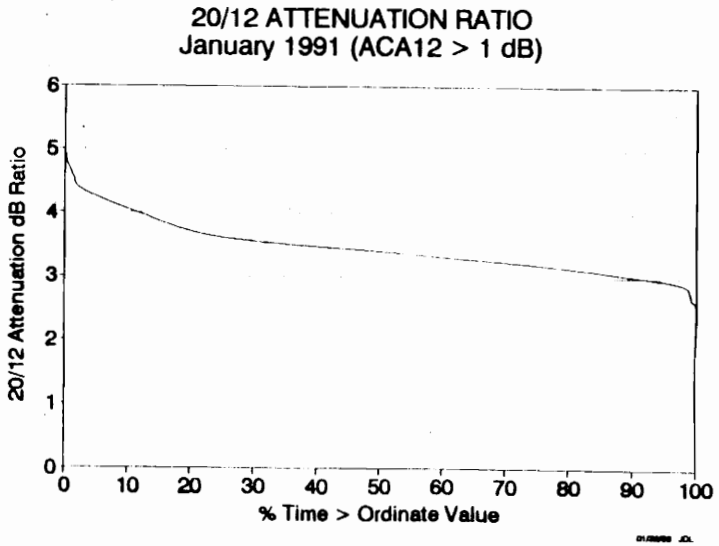
20/12 ATTENUATION RATIO
January 1991 (ACA12 > 1 dB)
20/12 Attenuation dB Ratio
% Time > Ordinate Value

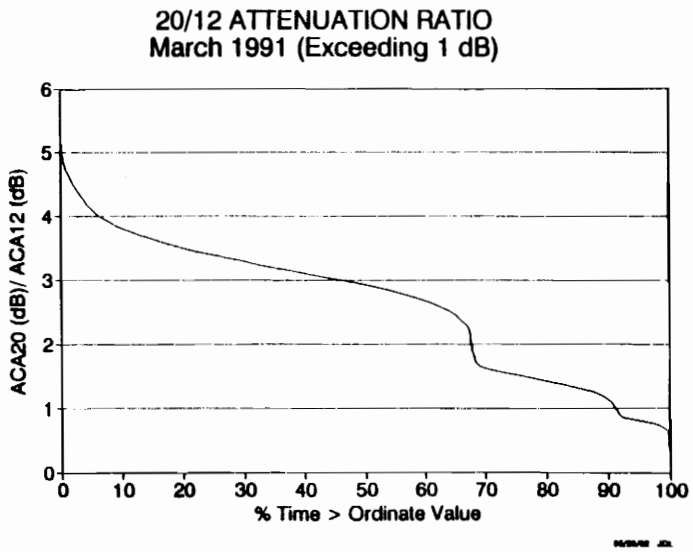
20/12 ATTENUATION RATIO
March 1991 (Exceeding 1 dB)
ACA20 (dB)/ ACA12 (dB)
% Time > Ordinate Value

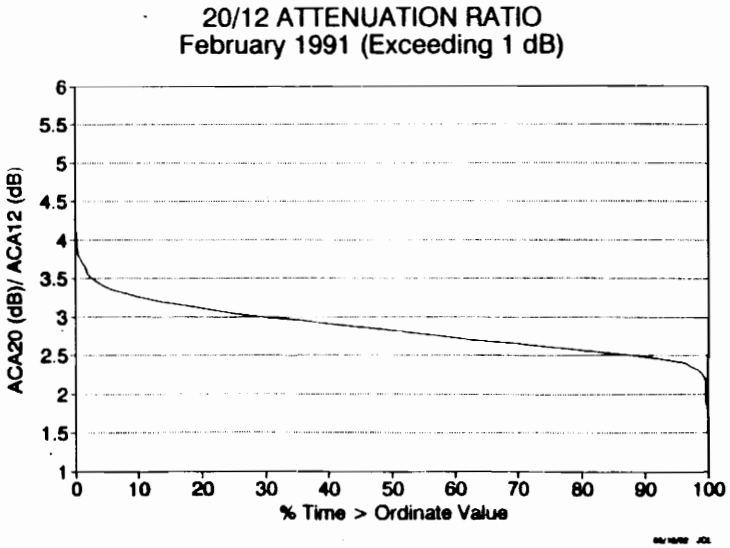
20/12 ATTENUATION RATIO
February 1991 (Exceeding 1 dB)
ACA20 (dB)/ ACA12 (dB)
% Time > Ordinate Value

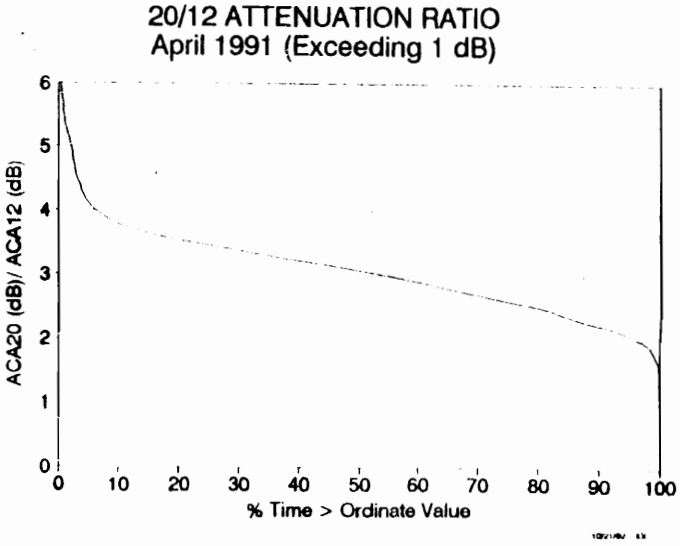
20/12 ATTENUATION RATIO
April 1991 (Exceeding 1 dB)
ACA20 (dB)/ ACA12 (dB)
% Time > Ordinate Value

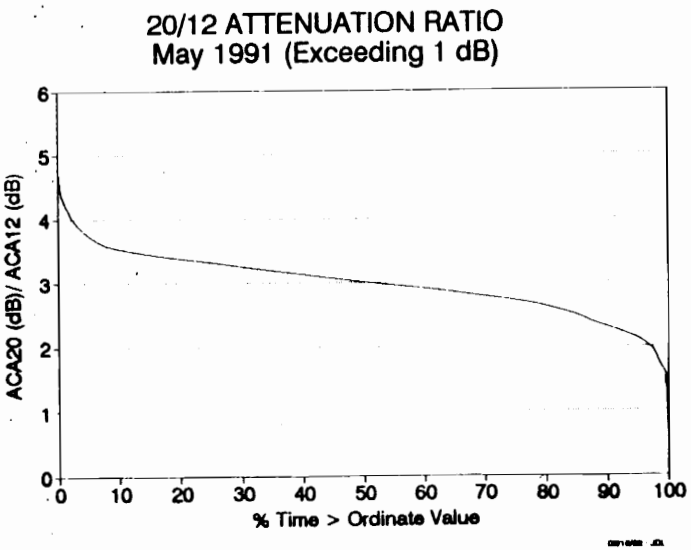
20/12 ATTENUATION RATIO
May 1991 (Exceeding 1 dB)
ACA20 (dB)/ ACA12 (dB)
0
1
2
3
4
5
6
0
10
20
30
40
50
60
70
80
90
100
% Time > Ordinate Value

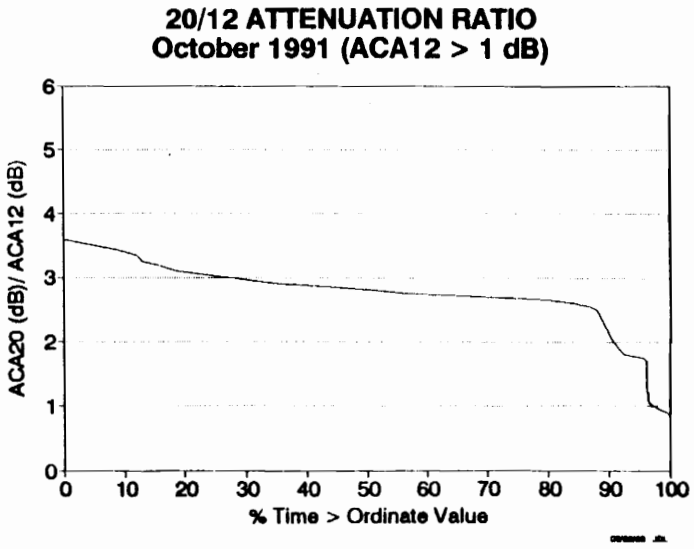
20/12 ATTENUATION RATIO
October 1991 (ACA12 > 1 dB)
ACA20 (dB)/ ACA12 (dB)
0
1
2
3
4
5
6
0
10
20
30
40
50
60
70
80
90
100
% Time > Ordinate Value

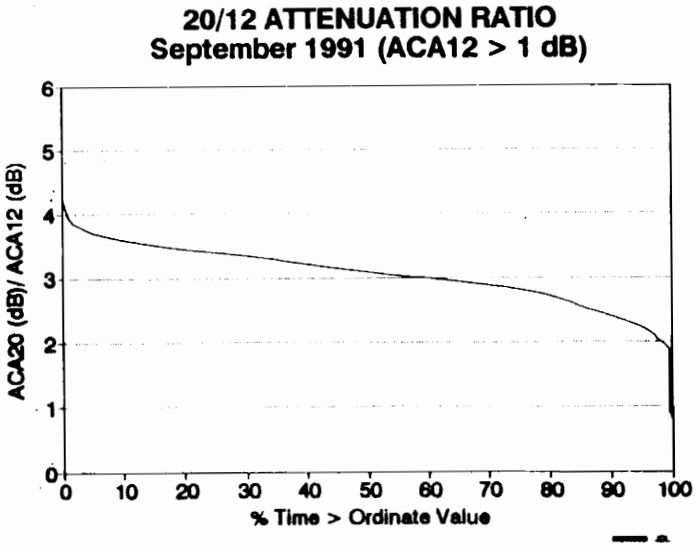
20/12 ATTENUATION RATIO
September 1991 (ACA12 > 1 dB)
ACA20 (dB)/ ACA12 (dB)
0
1
2
3
4
5
6
0
10
20
30
40
50
60
70
80
90
100
% Time > Ordinate Value

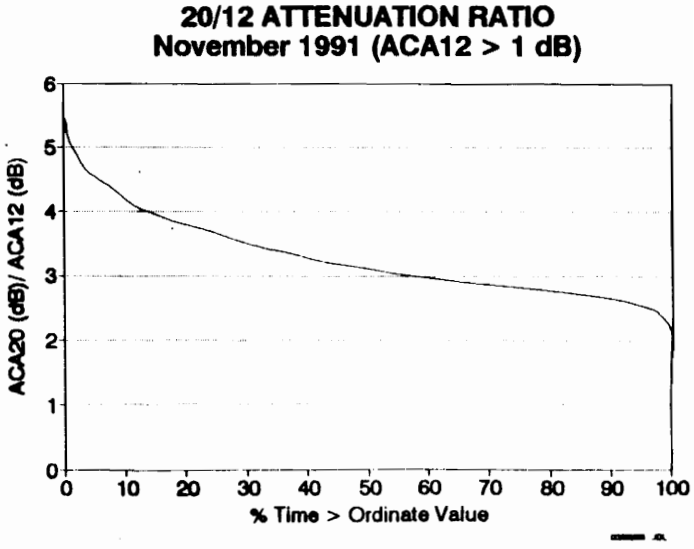
20/12 ATTENUATION RATIO
November 1991 (ACA12 > 1 dB)
ACA20 (dB)/ ACA12 (dB)
0
1
2
3
4
5
6
0
10
20
30
40
50
60
70
80
90
100
% Time > Ordinate Value

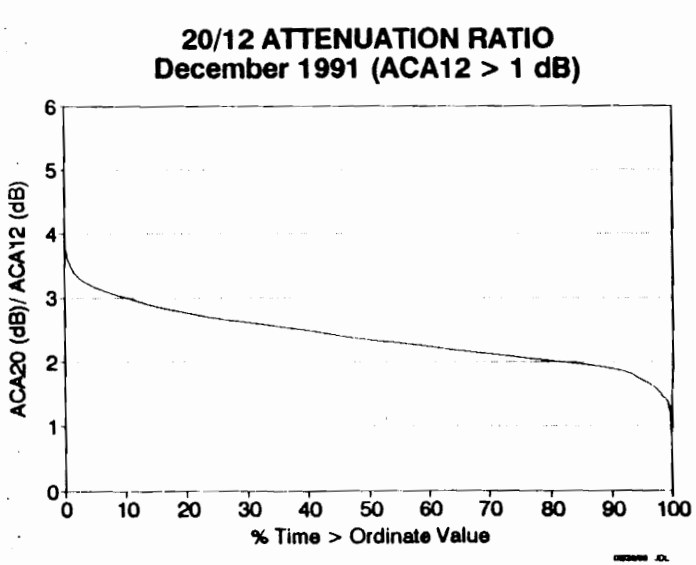
20/12 ATTENUATION RATIO
December 1991 (ACA12 > 1 dB)
ACA20 (dB)/ ACA12 (dB)
0
1
2
3
4
5
6
0 10 20 30 40 50 60 70 80 90 100
% Time > Ordinate Value

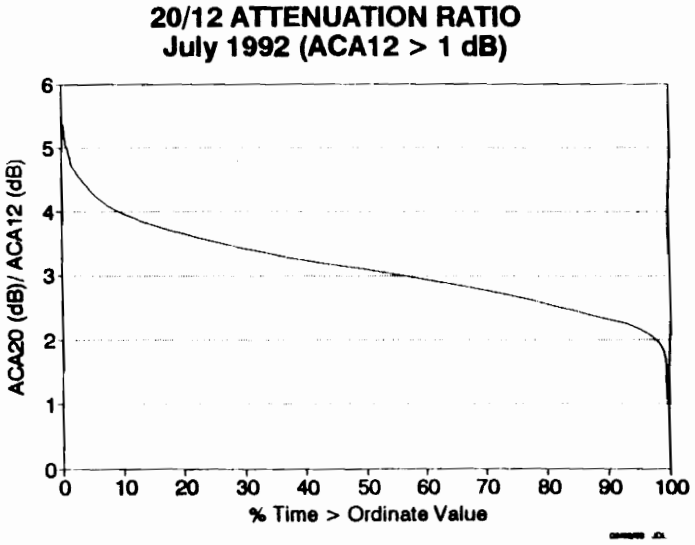
20/12 ATTENUATION RATIO
July 1992 (ACA12 > 1 dB)
ACA20 (dB)/ ACA12 (dB)
0
1
2
3
4
5
6
0 10 20 30 40 50 60 70 80 90 100
% Time > Ordinate Value

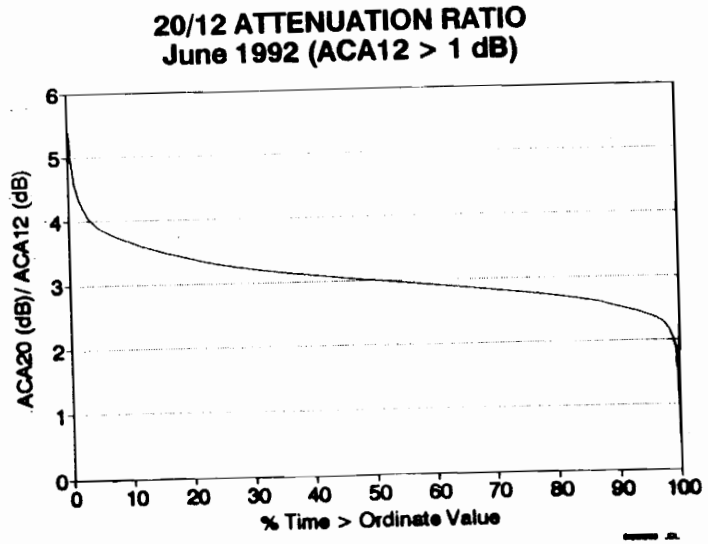
20/12 ATTENUATION RATIO
June 1992 (ACA12 > 1 dB)
ACA20 (dB)/ ACA12 (dB)
0
1
2
3
4
5
6
0 10 20 30 40 50 60 70 80 90 100
% Time > Ordinate Value

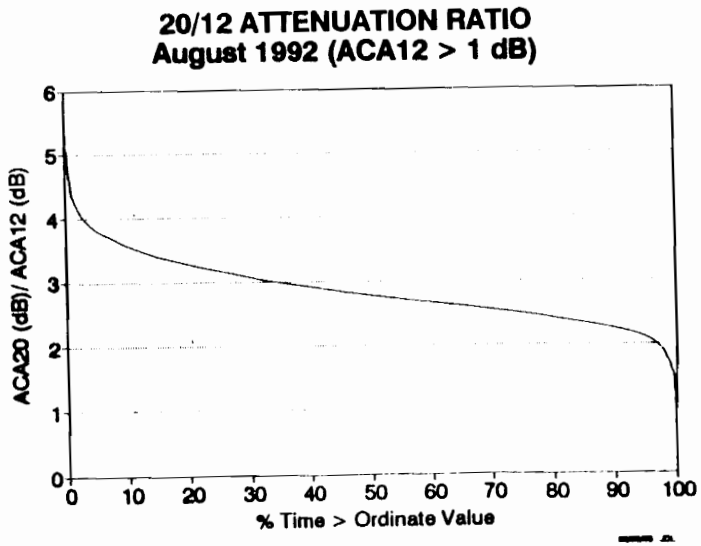
20/12 ATTENUATION RATIO
August 1992 (ACA12 > 1 dB)
ACA20 (dB)/ ACA12 (dB)
0
1
2
3
4
5
6
0 10 20 30 40 50 60 70 80 90 100
% Time > Ordinate Value

30/12 ATTENUATION RATIO
January 1991 (ACA12 > 1 dB)

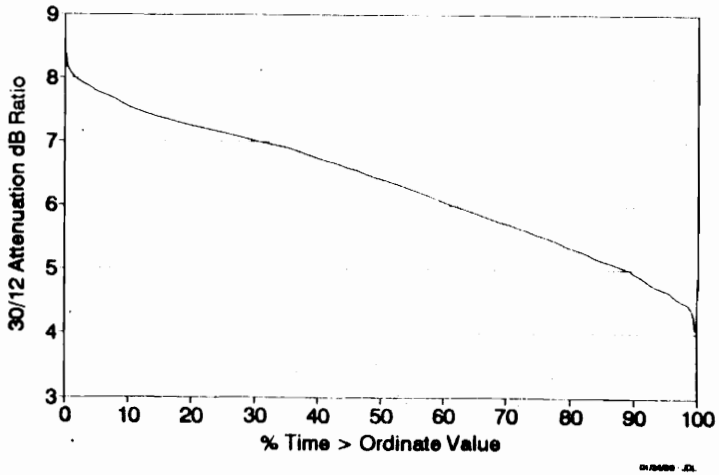

30/12 ATTENUATION RATIO
March 1991 (Exceeding 1 dB)

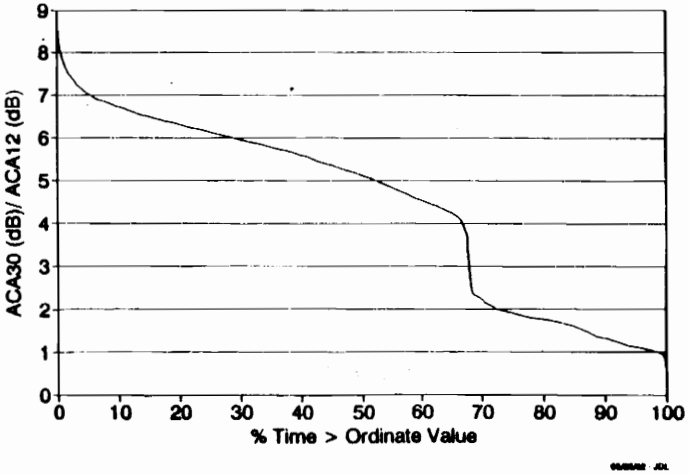

30/12 ATTENUATION RATIO
February 1991 (Exceeding 1 dB)

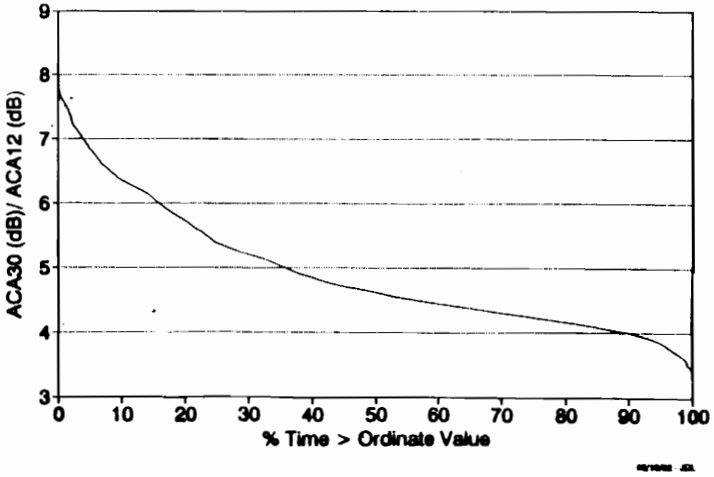

30/12 ATTENUATION RATIO
April 1991 (Exceeding 1 dB)

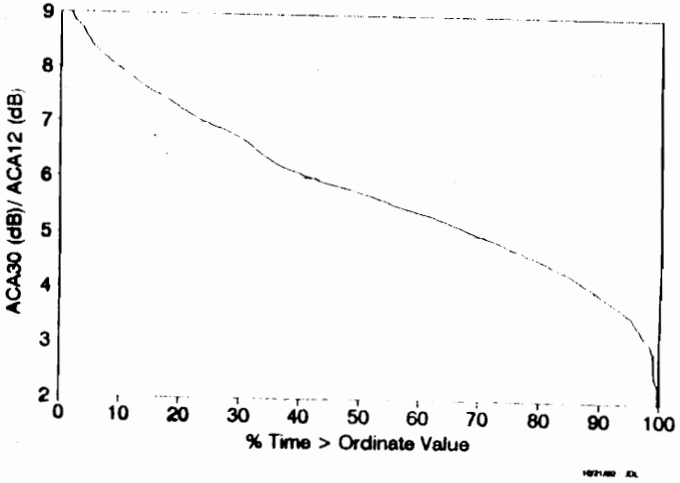

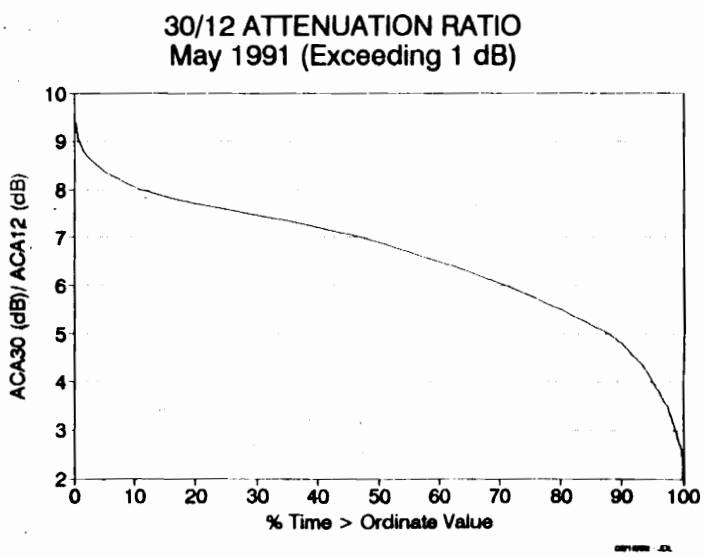
30/12 ATTENUATION RATIO
May 1991 (Exceeding 1 dB)
ACA30 (dB)/ ACA12 (dB)
% Time > Ordinate Value

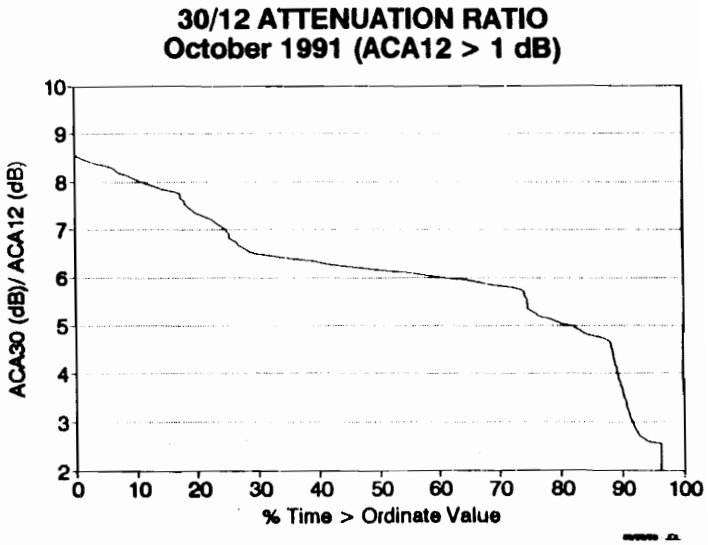
30/12 ATTENUATION RATIO
October 1991 (ACA12 > 1 dB)
ACA30 (dB)/ ACA12 (dB)
% Time > Ordinate Value

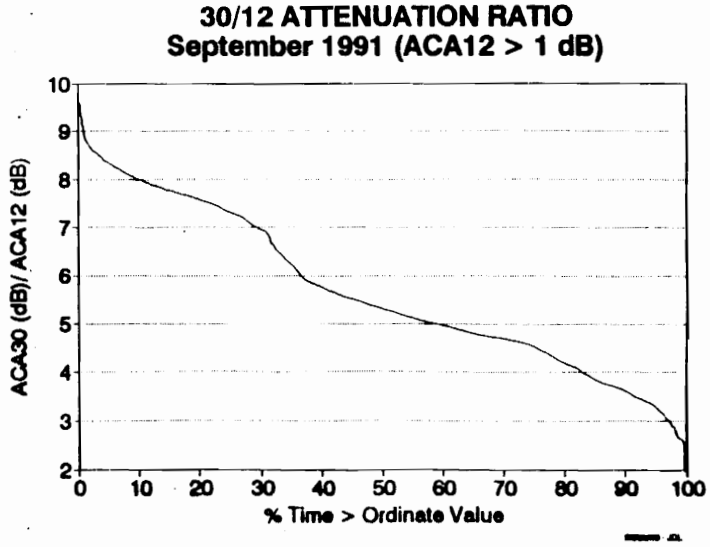
30/12 ATTENUATION RATIO
September 1991 (ACA12 > 1 dB)
ACA30 (dB)/ ACA12 (dB)
% Time > Ordinate Value

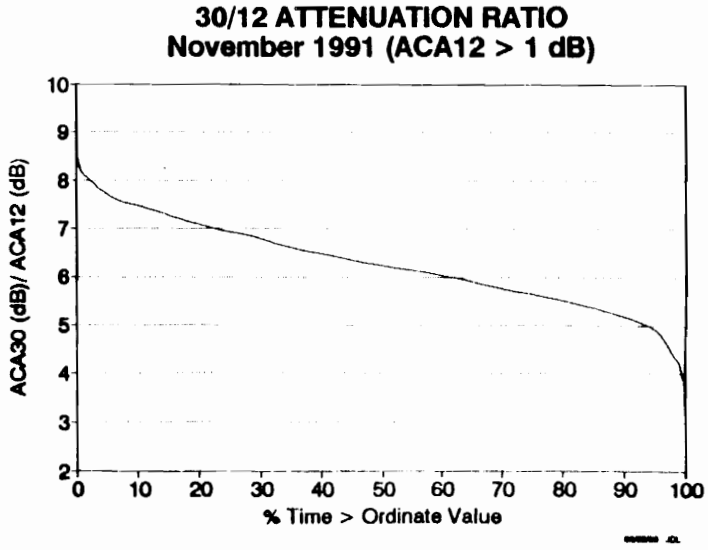
30/12 ATTENUATION RATIO
November 1991 (ACA12 > 1 dB)
ACA30 (dB)/ ACA12 (dB)
% Time > Ordinate Value

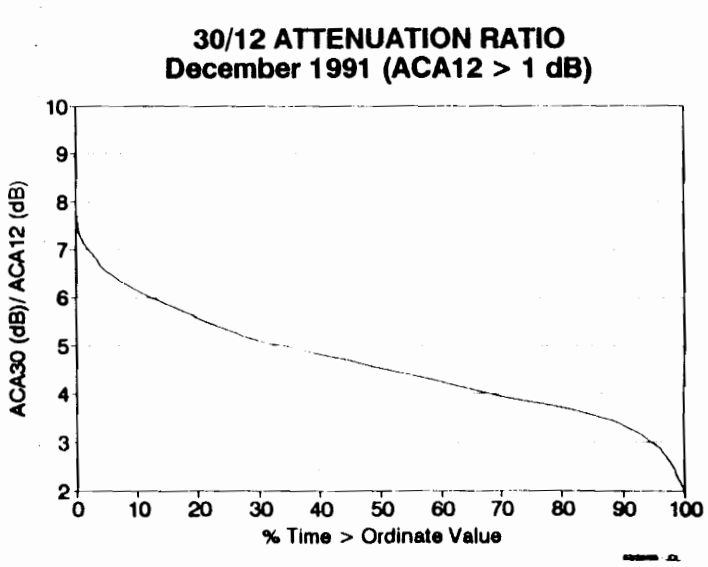
30/12 ATTENUATION RATIO
December 1991 (ACA12 > 1 dB)
ACA30 (dB)/ ACA12 (dB)
% Time > Ordinate Value

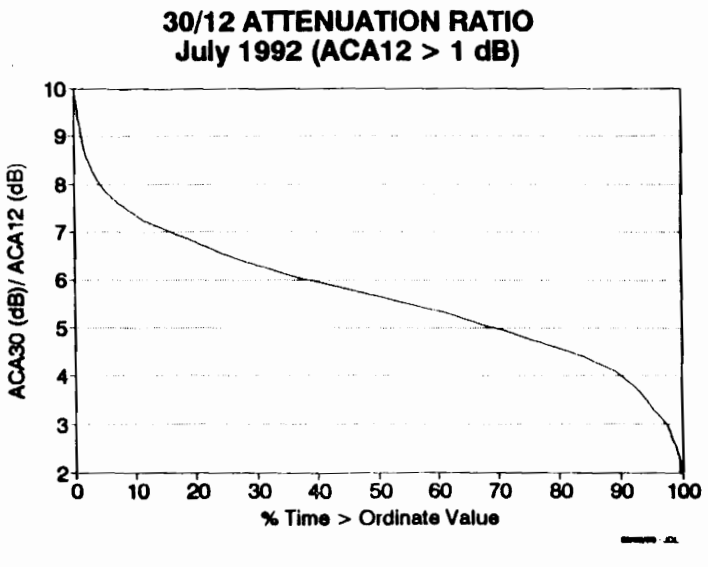
30/12 ATTENUATION RATIO
July 1992 (ACA12 > 1 dB)
ACA30 (dB)/ ACA12 (dB)
% Time > Ordinate Value

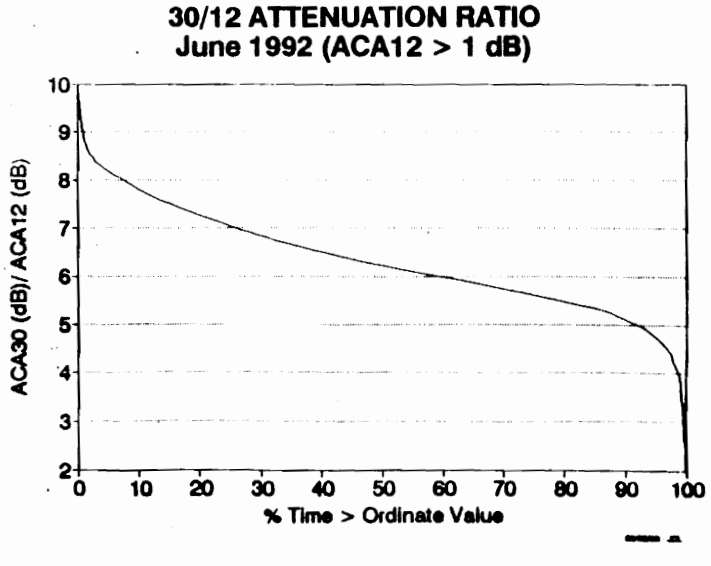
30/12 ATTENUATION RATIO
June 1992 (ACA12 > 1 dB)
ACA30 (dB)/ ACA12 (dB)
% Time > Ordinate Value

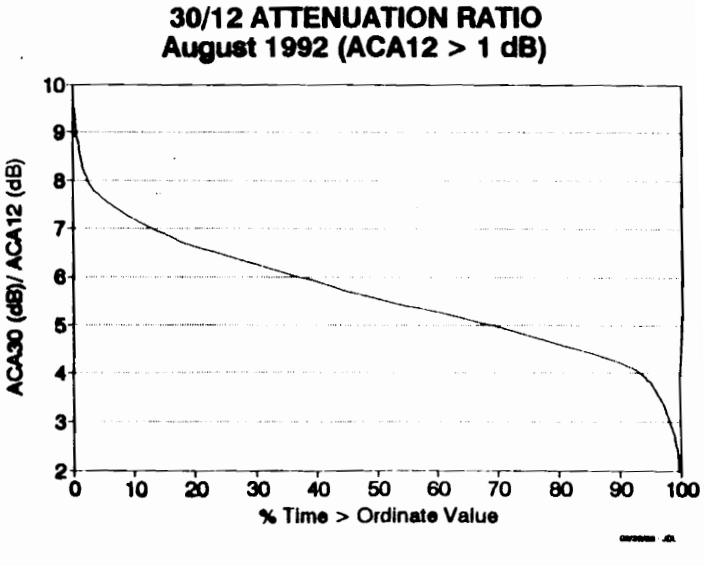
30/12 ATTENUATION RATIO
August 1992 (ACA12 > 1 dB)
ACA30 (dB)/ ACA12 (dB)
% Time > Ordinate Value

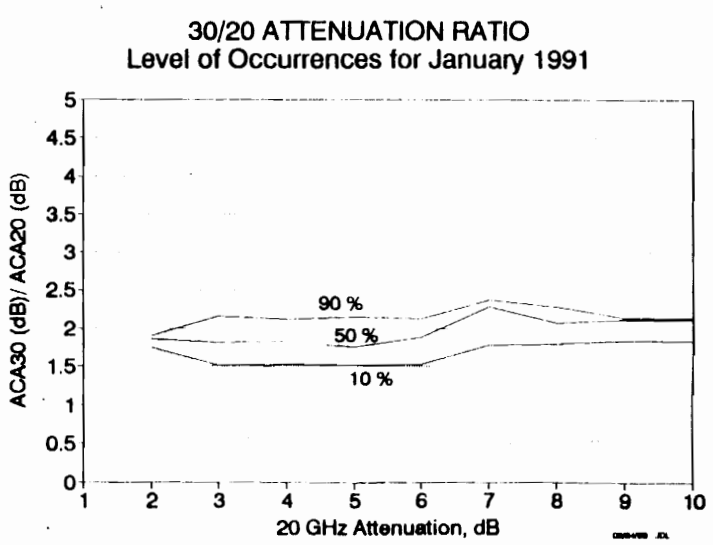
30/20 ATTENUATION RATIO
Level of Occurrences for January 1991
ACA30 (dB)/ ACA20 (dB)
20 GHz Attenuation, dB
90 %
50 %
10 %

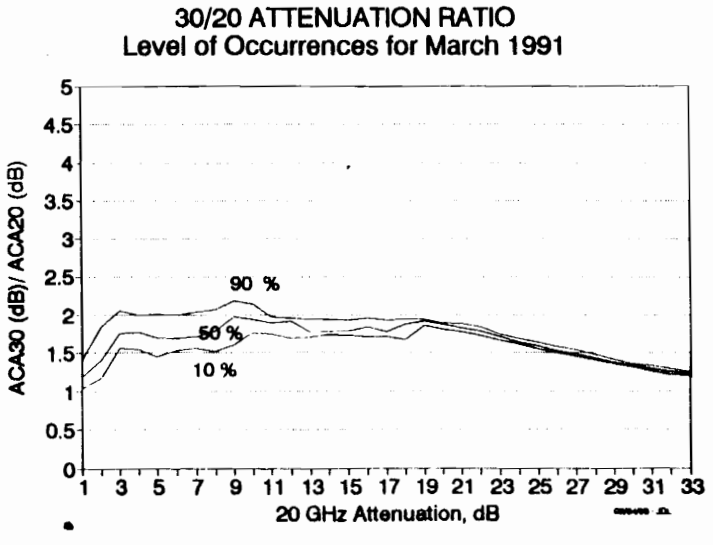
30/20 ATTENUATION RATIO
Level of Occurrences for March 1991
ACA30 (dB)/ ACA20 (dB)
20 GHz Attenuation, dB
90 %
50 %
10 %

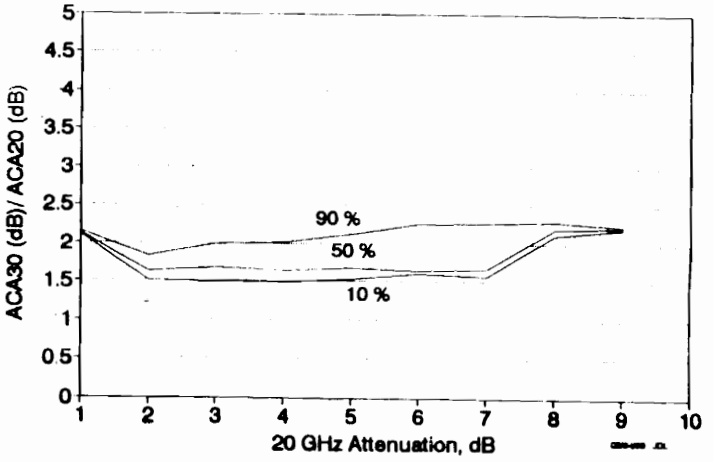
30/20 ATTENUATION RATIO
Level of Occurrences for February 1991
ACA30 (dB)/ ACA20 (dB)
20 GHz Attenuation, dB
90 %
50 %
10 %

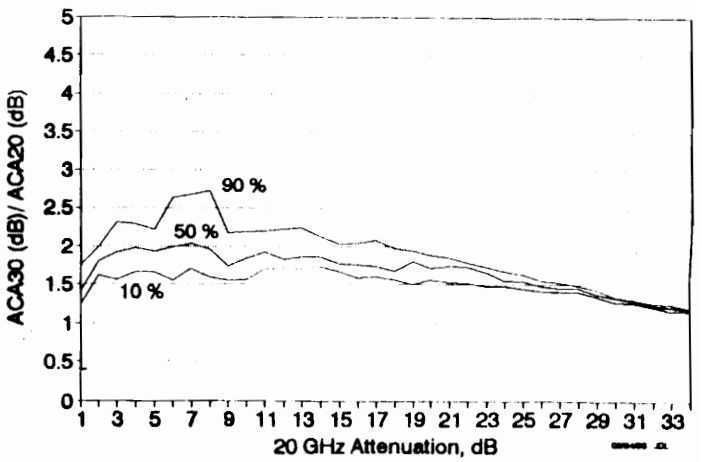
30/20 ATTENUATION RATIO
Level of Occurrences for April 1991
ACA30 (dB)/ ACA20 (dB)
20 GHz Attenuation, dB
90 %
50 %
10 %

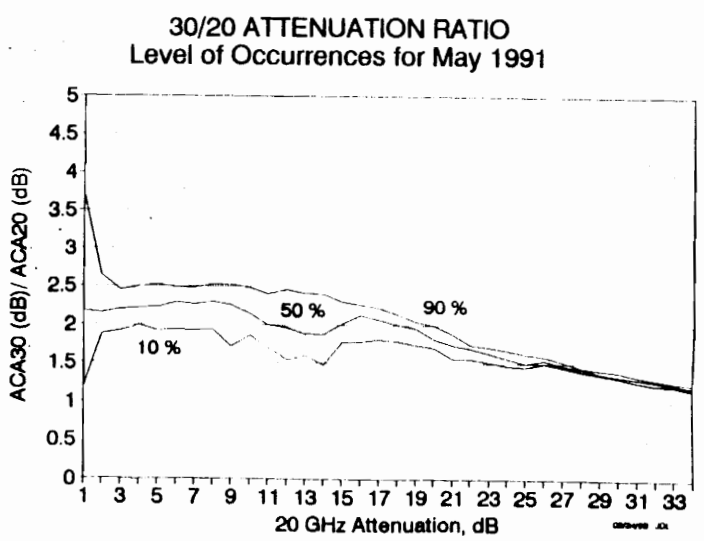
30/20 ATTENUATION RATIO
Level of Occurrences for May 1991
ACA30 (dB)/ ACA20 (dB)
20 GHz Attenuation, dB
10 %
50 %
90 %

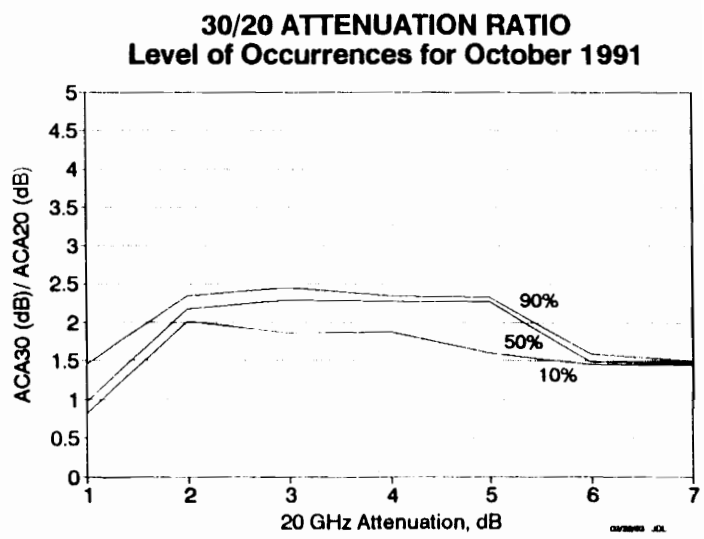
30/20 ATTENUATION RATIO
Level of Occurrences for October 1991
ACA30 (dB)/ ACA20 (dB)
20 GHz Attenuation, dB
90%
50%
10%

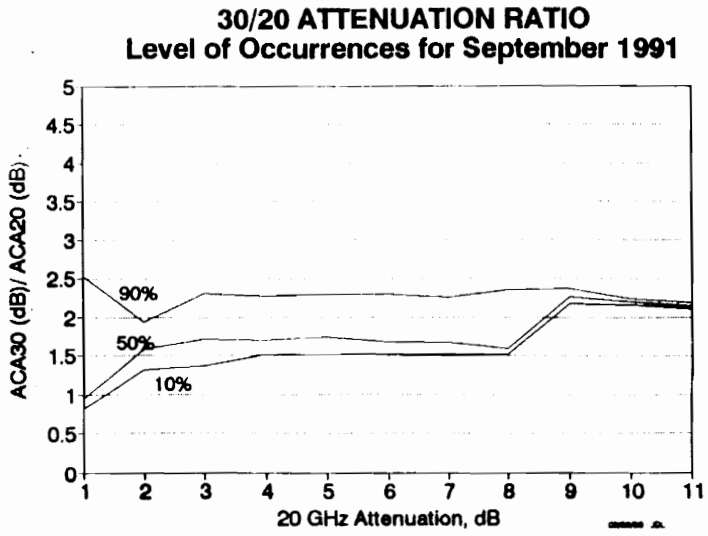
30/20 ATTENUATION RATIO
Level of Occurrences for September 1991
ACA30 (dB)/ ACA20 (dB)
20 GHz Attenuation, dB
90%
50%
10%

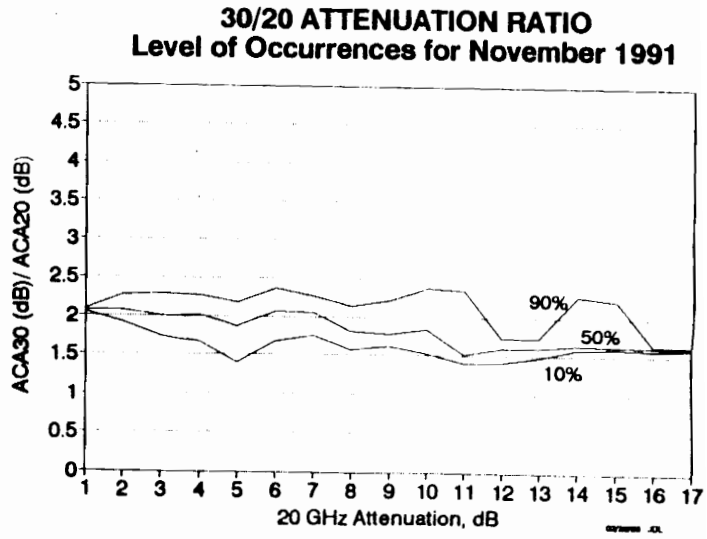
30/20 ATTENUATION RATIO
Level of Occurrences for November 1991
ACA30 (dB)/ ACA20 (dB)
20 GHz Attenuation, dB
90%
50%
10%

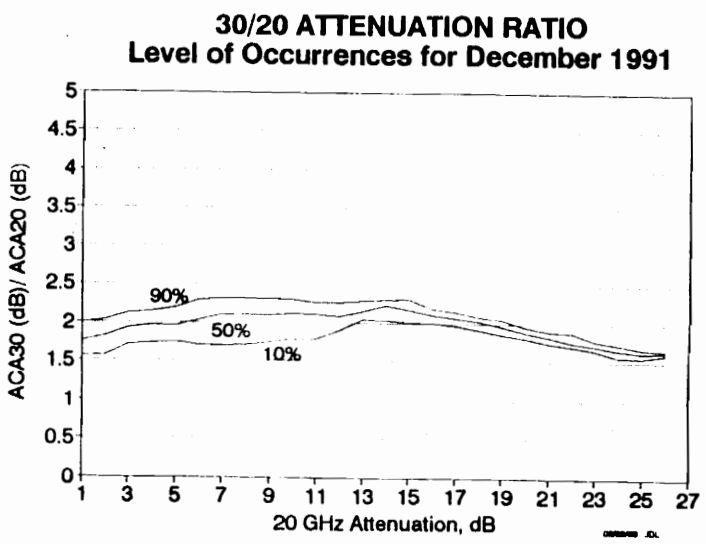
30/20 ATTENUATION RATIO
Level of Occurrences for December 1991
ACA30 (dB)/ ACA20 (dB)
90%
50%
10%
20 GHz Attenuation, dB

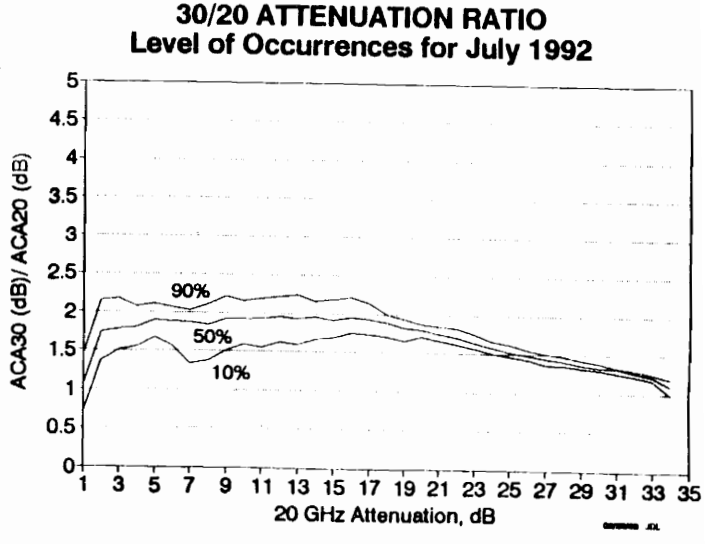
30/20 ATTENUATION RATIO
Level of Occurrences for July 1992
ACA30 (dB)/ ACA20 (dB)
90%
50%
10%
20 GHz Attenuation, dB

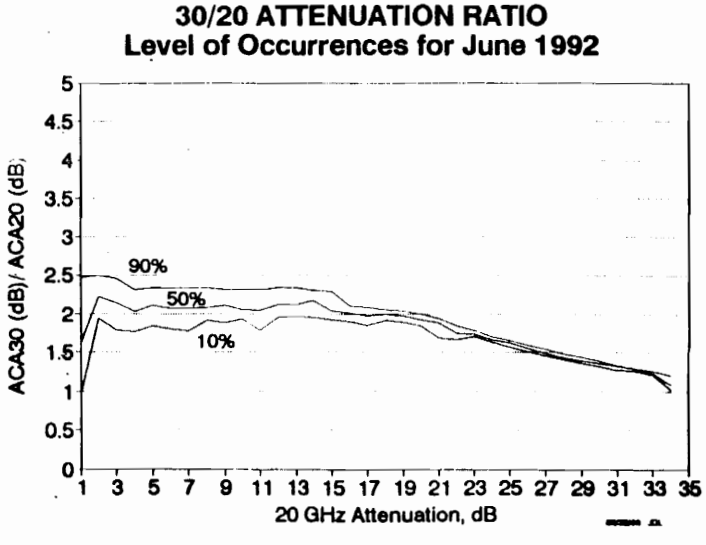
30/20 ATTENUATION RATIO
Level of Occurrences for June 1992
ACA30 (dB)/ ACA20 (dB)
90%
50%
10%
20 GHz Attenuation, dB

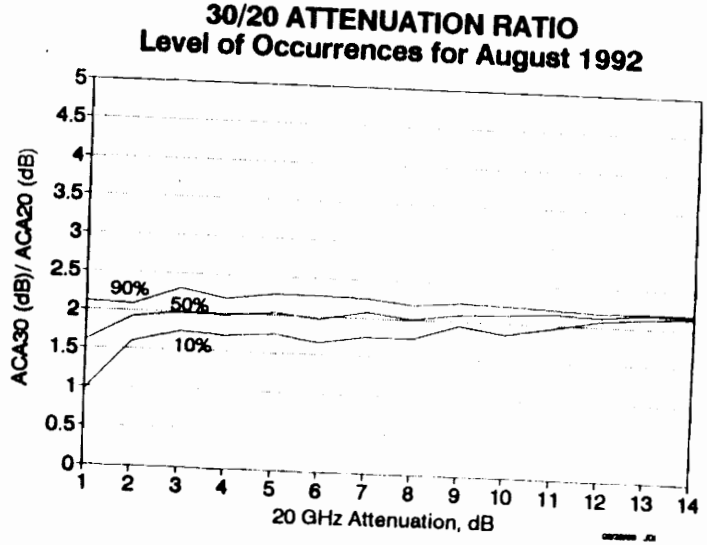
30/20 ATTENUATION RATIO
Level of Occurrences for August 1992
ACA30 (dB)/ ACA20 (dB)
90%
50%
10%
20 GHz Attenuation, dB

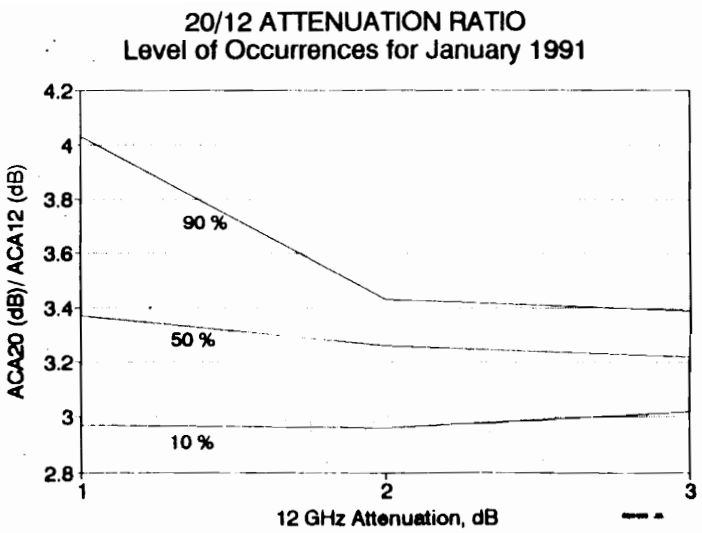
20/12 ATTENUATION RATIO
Level of Occurrences for January 1991
ACA20 (dB)/ ACA12 (dB)
4.2
4
3.8
3.6
3.4
3.2
3
2.8
90 %
50 %
10 %
1
2
3
12 GHz Attenuation, dB

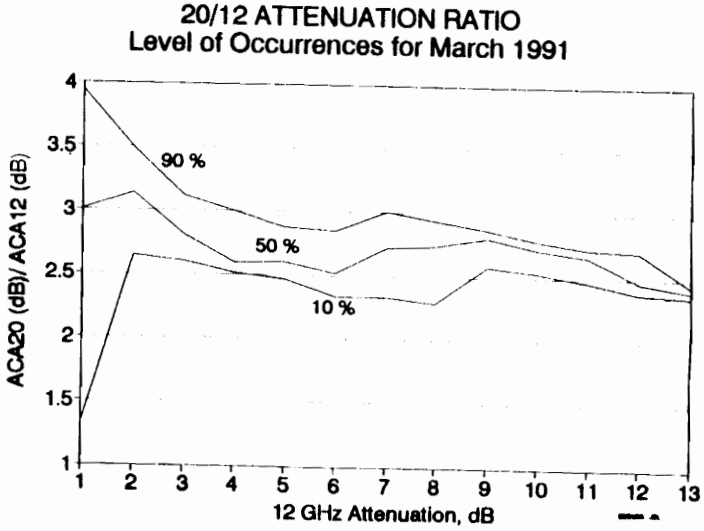
20/12 ATTENUATION RATIO
Level of Occurrences for March 1991
ACA20 (dB)/ ACA12 (dB)
4
3.5
3
2.5
2
1.5
1
90 %
50 %
10 %
1 2 3 4 5 6 7 8 9 10 11 12 13
12 GHz Attenuation, dB

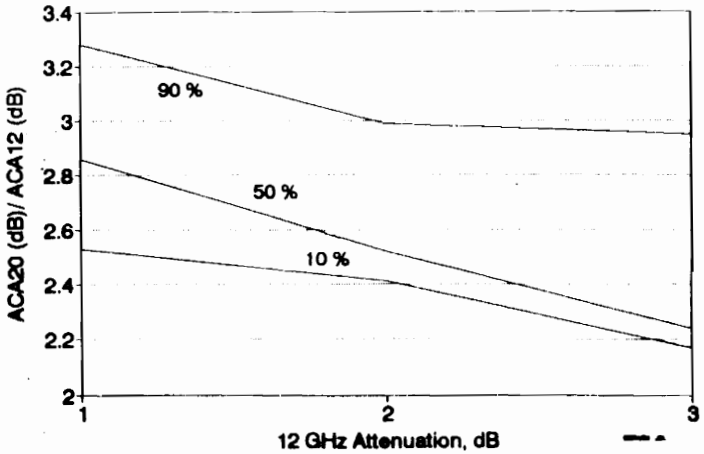
20/12 ATTENUATION RATIO
Level of Occurrences for February 1991
ACA20 (dB)/ ACA12 (dB)
3.4
3.2
3
2.8
2.6
2.4
2.2
2
90 %
50 %
10 %
1
2
3
12 GHz Attenuation, dB

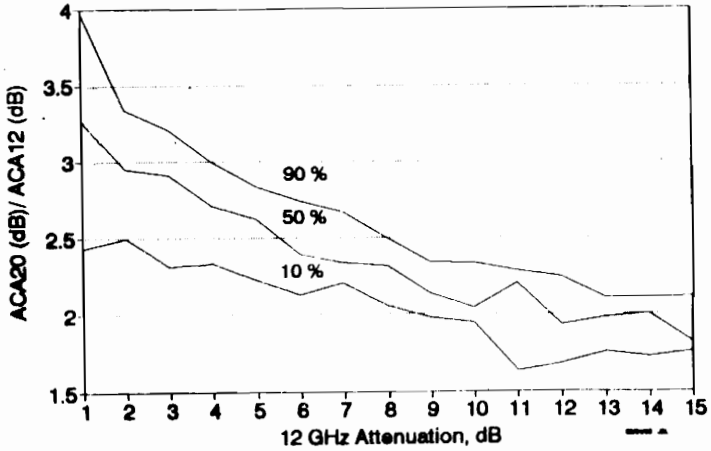
20/12 ATTENUATION RATIO
Level of Occurrences for April 1991
ACA20 (dB)/ ACA12 (dB)
4
3.5
3
2.5
2
1.5
90 %
50 %
10 %
1 2 3 4 5 6 7 8 9 10 11 12 13 14 15
12 GHz Attenuation, dB

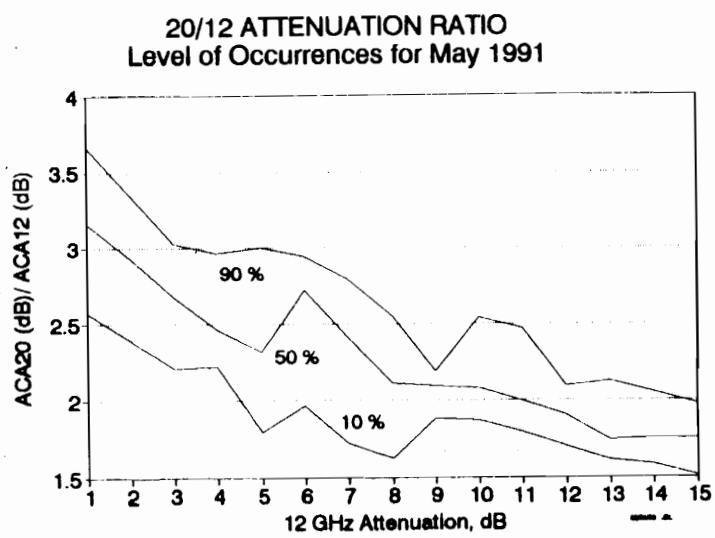
20/12 ATTENUATION RATIO
Level of Occurrences for May 1991
ACA20 (dB)/ ACA12 (dB)
90 %
50 %
10 %
12 GHz Attenuation, dB

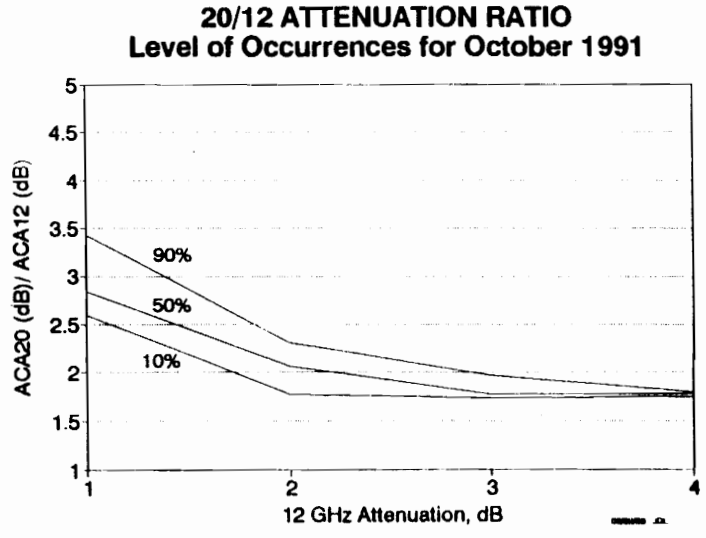
20/12 ATTENUATION RATIO
Level of Occurrences for October 1991
ACA20 (dB)/ ACA12 (dB)
90%
50%
10%
12 GHz Attenuation, dB

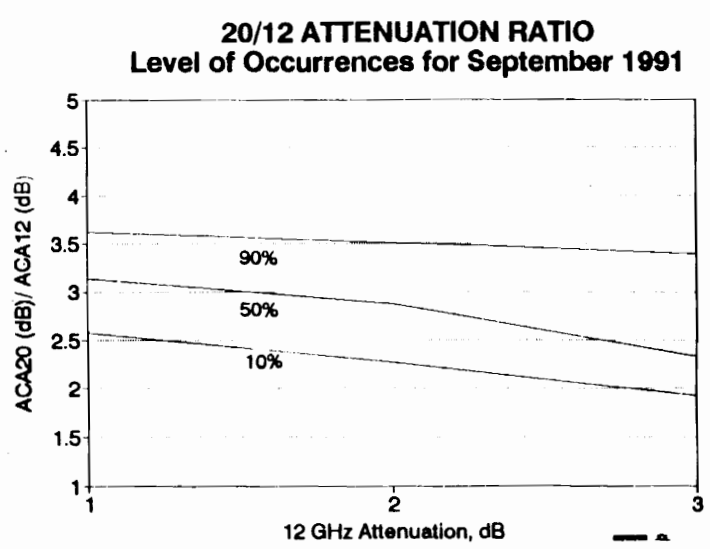
20/12 ATTENUATION RATIO
Level of Occurrences for September 1991
ACA20 (dB)/ ACA12 (dB)
90%
50%
10%
12 GHz Attenuation, dB

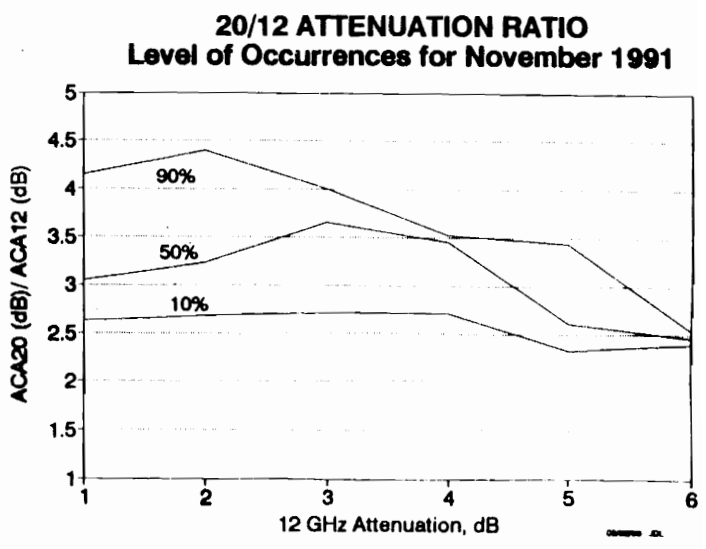
20/12 ATTENUATION RATIO
Level of Occurrences for November 1991
ACA20 (dB)/ ACA12 (dB)
90%
50%
10%
12 GHz Attenuation, dB

20/12 ATTENUATION RATIO
Level of Occurrences for December 1991

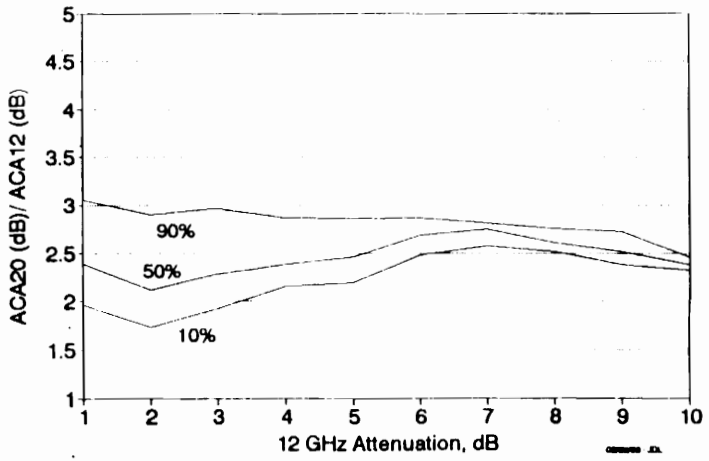

20/12 ATTENUATION RATIO
Level of Occurrences for July 1992

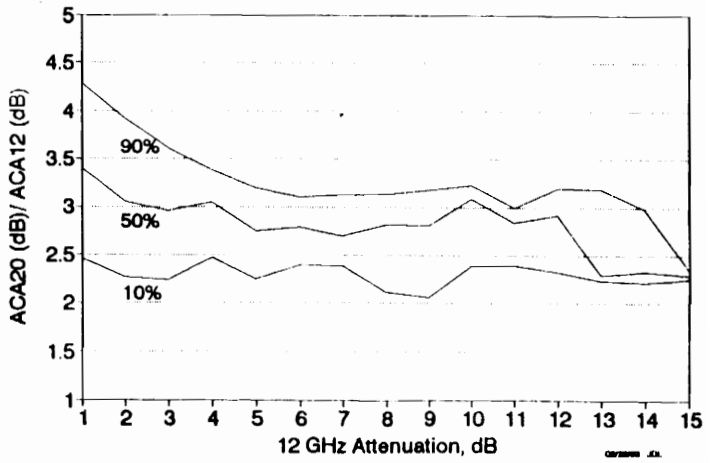

20/12 ATTENUATION RATIO
Level of Occurrences for June 1992

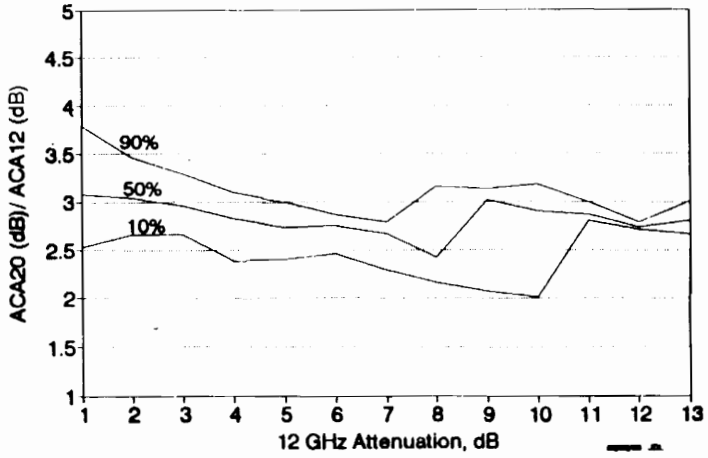

20/12 ATTENUATION RATIO
Level of Occurrences for August 1992

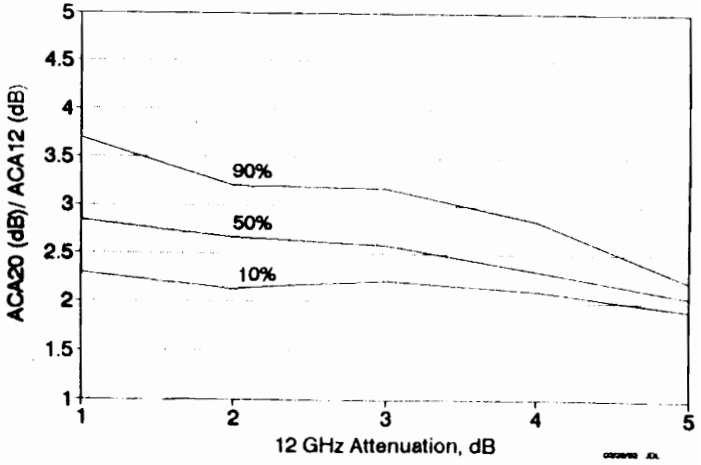

30/12 ATTENUATION RATIO
Level of Occurrences for January 1991

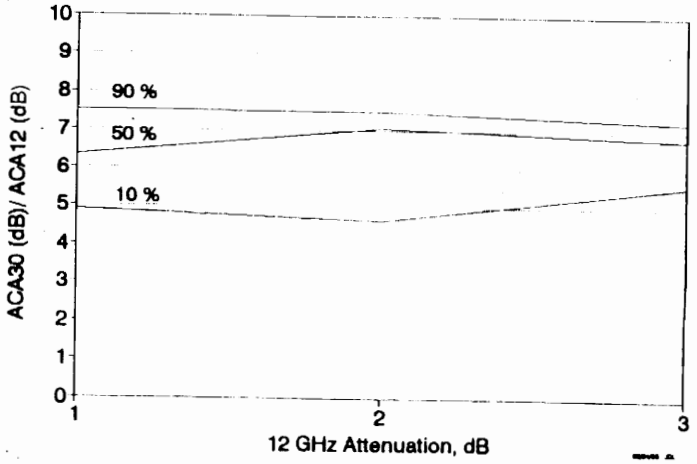

30/12 ATTENUATION RATIO
Level of Occurrences for March 1991

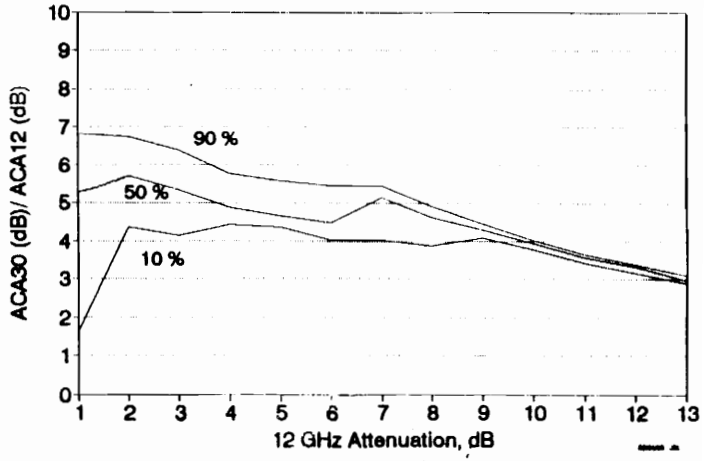

30/12 ATTENUATION RATIO
Level of Occurrences for February 1991

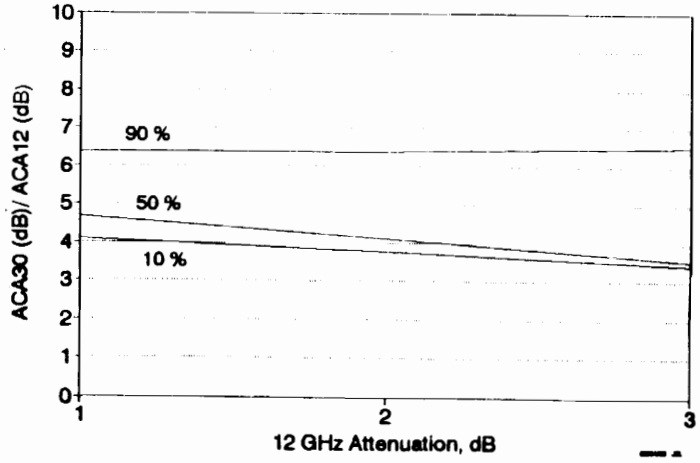

30/12 ATTENUATION RATIO
Level of Occurrences for April 1991

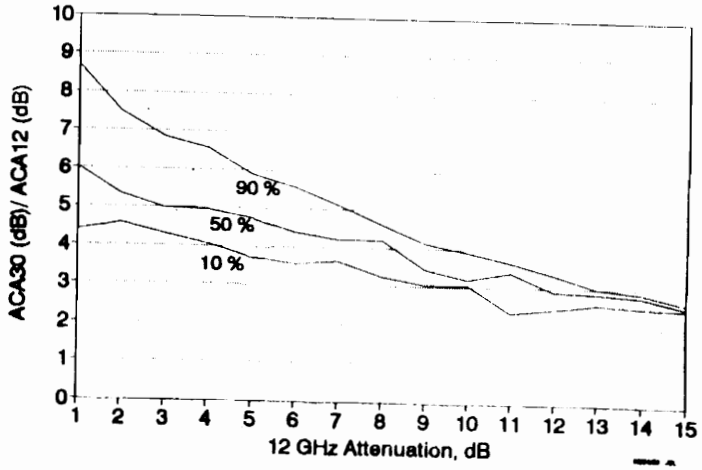

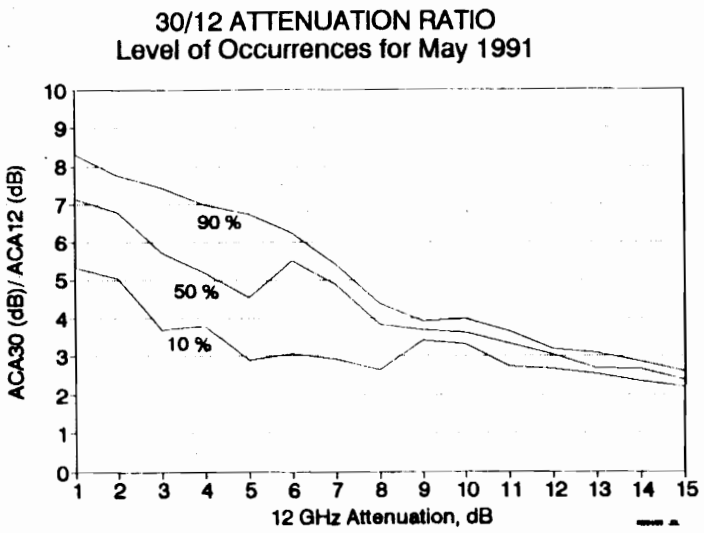
30/12 ATTENUATION RATIO
Level of Occurrences for May 1991
ACA30 (dB)/ ACA12 (dB)
90 %
50 %
10 %
12 GHz Attenuation, dB

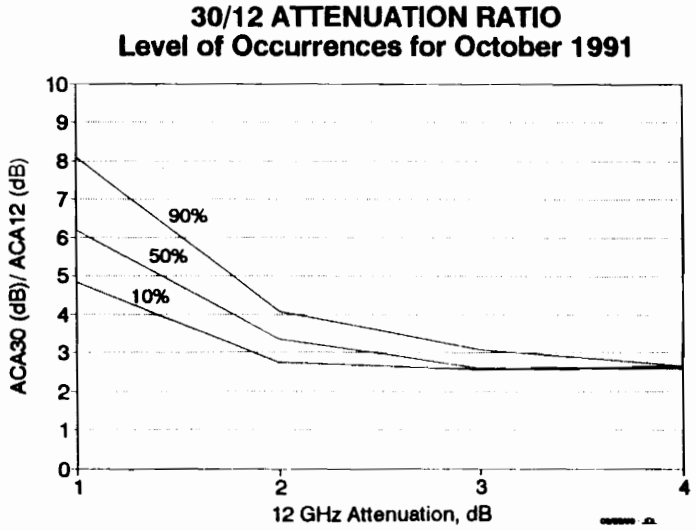
30/12 ATTENUATION RATIO
Level of Occurrences for October 1991
ACA30 (dB)/ ACA12 (dB)
90%
50%
10%
12 GHz Attenuation, dB

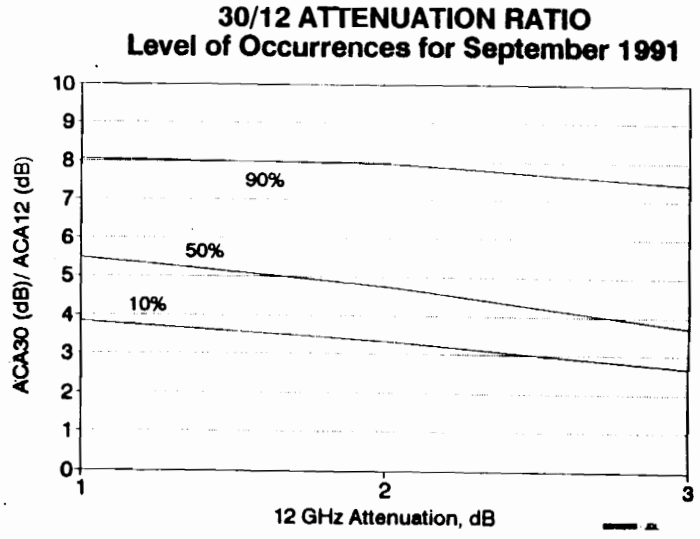
30/12 ATTENUATION RATIO
Level of Occurrences for September 1991
ACA30 (dB)/ ACA12 (dB)
90%
50%
10%
12 GHz Attenuation, dB

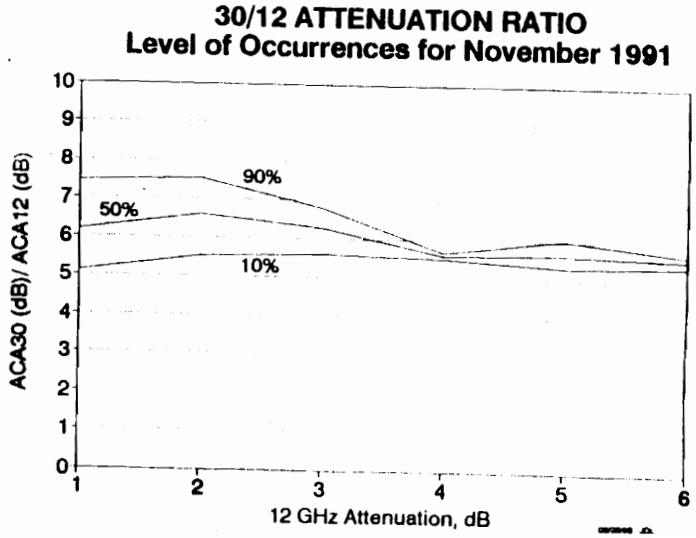
30/12 ATTENUATION RATIO
Level of Occurrences for November 1991
ACA30 (dB)/ ACA12 (dB)
90%
50%
10%
12 GHz Attenuation, dB

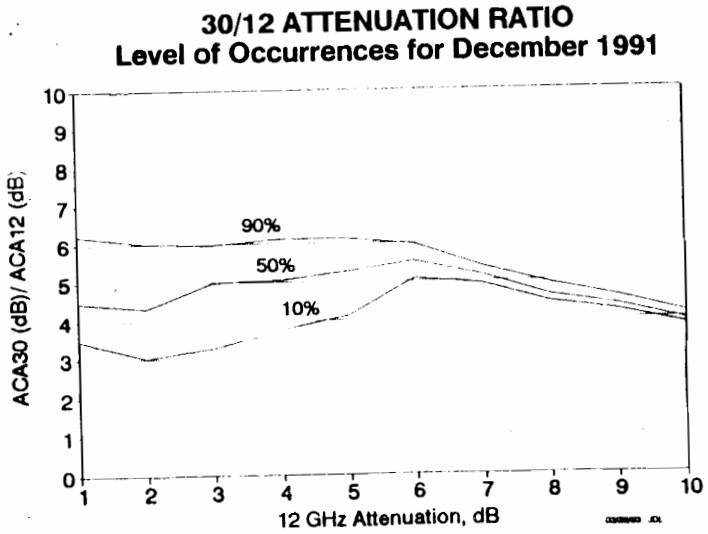
30/12 ATTENUATION RATIO
Level of Occurrences for December 1991
ACA30 (dB)/ ACA12 (dB)
90%
50%
10%
12 GHz Attenuation, dB

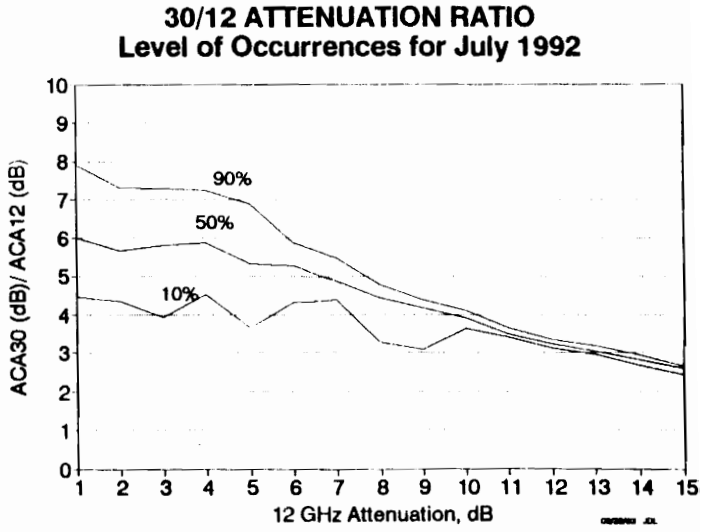
30/12 ATTENUATION RATIO
Level of Occurrences for July 1992
ACA30 (dB)/ ACA12 (dB)
90%
50%
10%
12 GHz Attenuation, dB

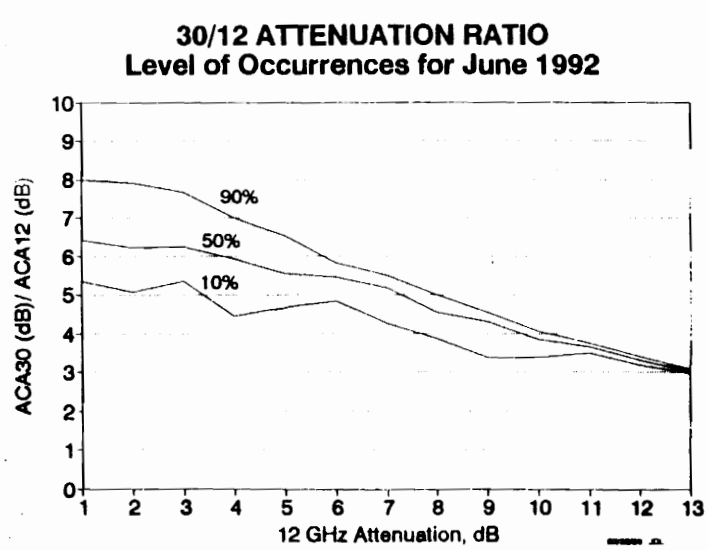
30/12 ATTENUATION RATIO
Level of Occurrences for June 1992
ACA30 (dB)/ ACA12 (dB)
90%
50%
10%
12 GHz Attenuation, dB

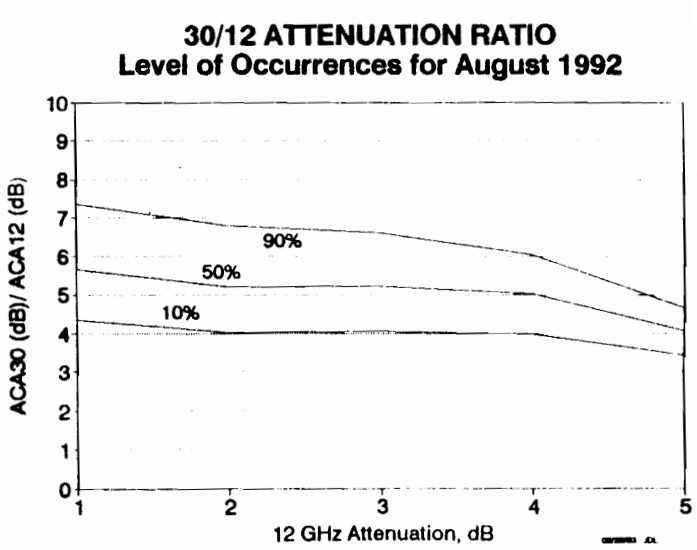
30/12 ATTENUATION RATIO
Level of Occurrences for August 1992
ACA30 (dB)/ ACA12 (dB)
90%
50%
10%
12 GHz Attenuation, dB

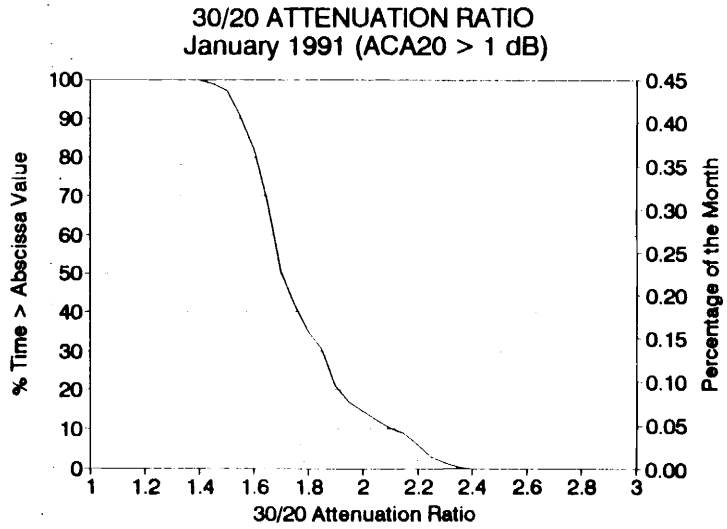
30/20 ATTENUATION RATIO
January 1991 (ACA20 > 1 dB)
% Time > Abscissa Value
Percentage of the Month
30/20 Attenuation Ratio

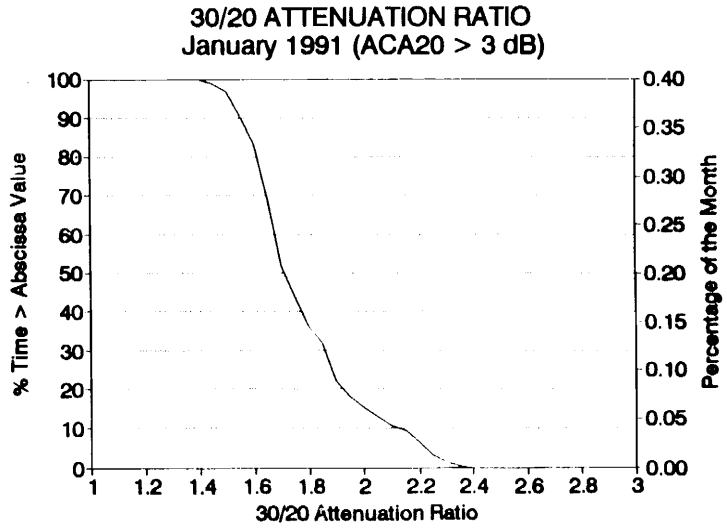
30/20 ATTENUATION RATIO
January 1991 (ACA20 > 3 dB)
% Time > Abscissa Value
Percentage of the Month
30/20 Attenuation Ratio

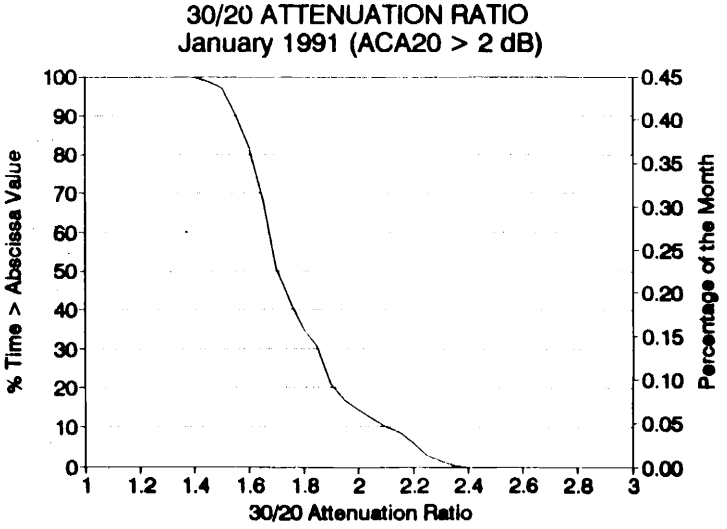
30/20 ATTENUATION RATIO
January 1991 (ACA20 > 2 dB)
% Time > Abscissa Value
Percentage of the Month
30/20 Attenuation Ratio

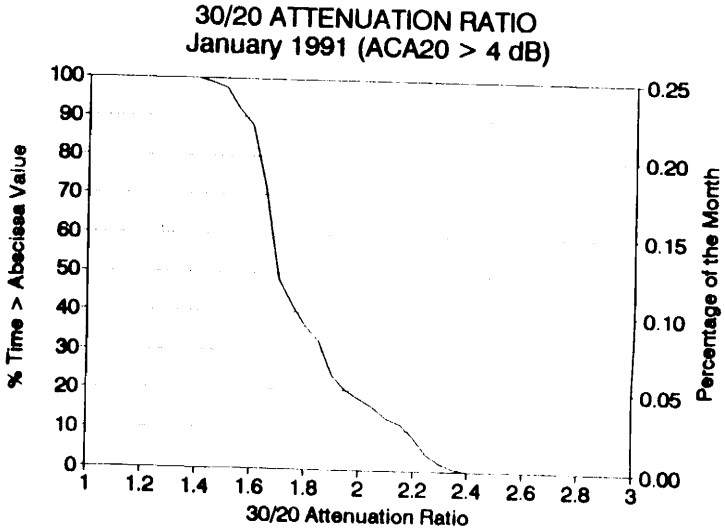
30/20 ATTENUATION RATIO
January 1991 (ACA20 > 4 dB)
% Time > Abscissa Value
Percentage of the Month
30/20 Attenuation Ratio

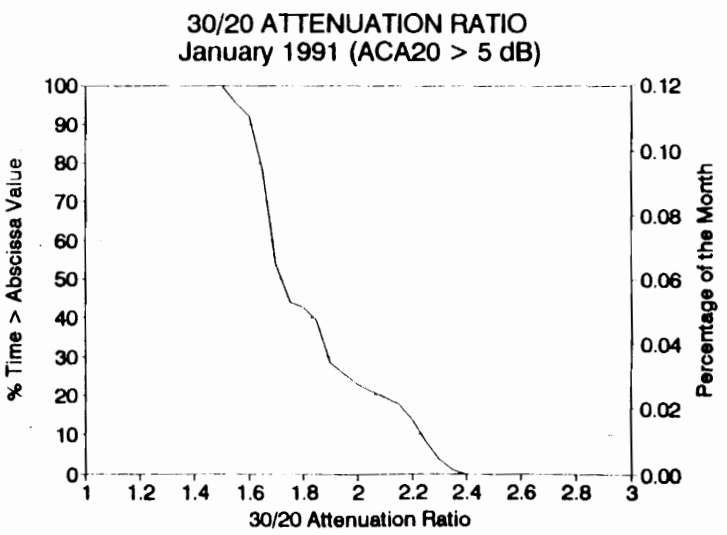
30/20 ATTENUATION RATIO
January 1991 (ACA20 > 5 dB)
% Time > Abscissa Value
Percentage of the Month
30/20 Attenuation Ratio
100
90
80
70
60
50
40
30
20
10
0
0.12
0.10
0.08
0.06
0.04
0.02
0.00
1
1.2
1.4
1.6
1.8
2
2.2
2.4
2.6
2.8
3

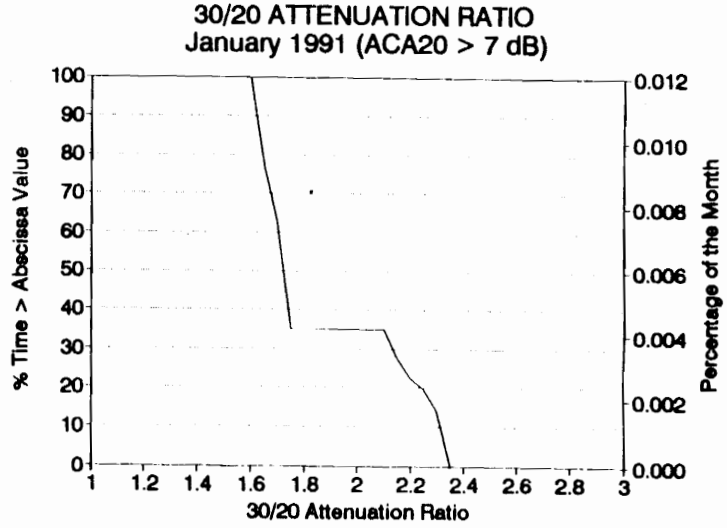
30/20 ATTENUATION RATIO
January 1991 (ACA20 > 7 dB)
% Time > Abscissa Value
Percentage of the Month
30/20 Attenuation Ratio
100
90
80
70
60
50
40
30
20
10
0
0.012
0.010
0.008
0.006
0.004
0.002
0.000
1
1.2
1.4
1.6
1.8
2
2.2
2.4
2.6
2.8
3

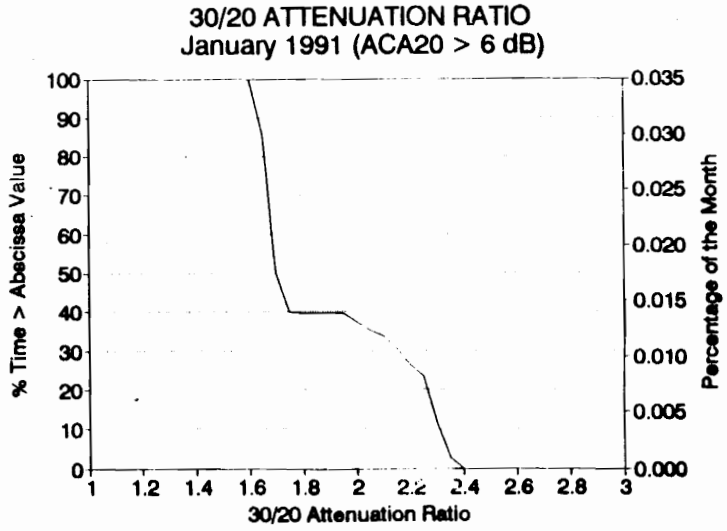
30/20 ATTENUATION RATIO
January 1991 (ACA20 > 6 dB)
% Time > Abscissa Value
Percentage of the Month
30/20 Attenuation Ratio
100
90
80
70
60
50
40
30
20
10
0
0.035
0.030
0.025
0.020
0.015
0.010
0.005
0.000
1
1.2
1.4
1.6
1.8
2
2.2
2.4
2.6
2.8
3

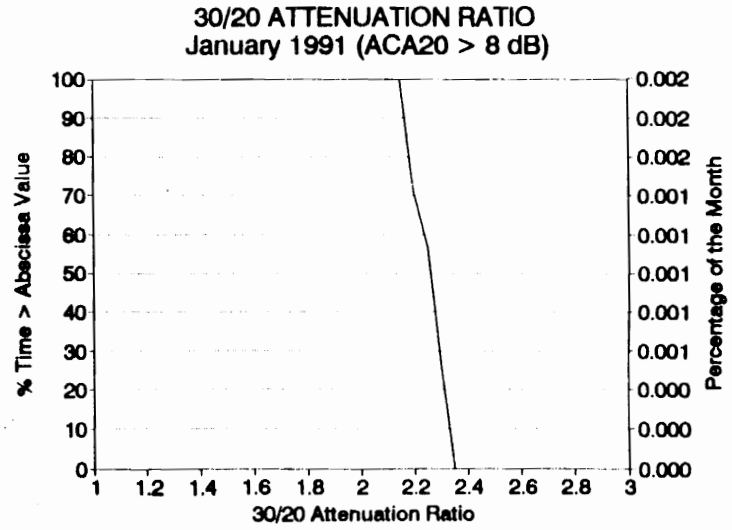
30/20 ATTENUATION RATIO
January 1991 (ACA20 > 8 dB)
% Time > Abscissa Value
Percentage of the Month
30/20 Attenuation Ratio
100
90
80
70
60
50
40
30
20
10
0
0.002
0.002
0.002
0.001
0.001
0.001
0.001
0.000
0.000
0.000
1
1.2
1.4
1.6
1.8
2
2.2
2.4
2.6
2.8
3

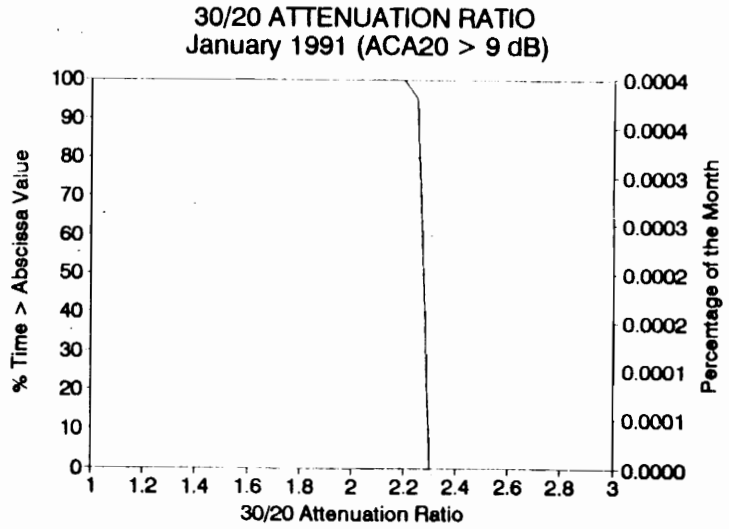
30/20 ATTENUATION RATIO
January 1991 (ACA20 > 9 dB)
% Time > Abscissa Value
Percentage of the Month
30/20 Attenuation Ratio
100
90
80
70
60
50
40
30
20
10
0
1
1.2
1.4
1.6
1.8
2
2.2
2.4
2.6
2.8
3
0.0004
0.0004
0.0003
0.0003
0.0002
0.0002
0.0001
0.0001
0.0000

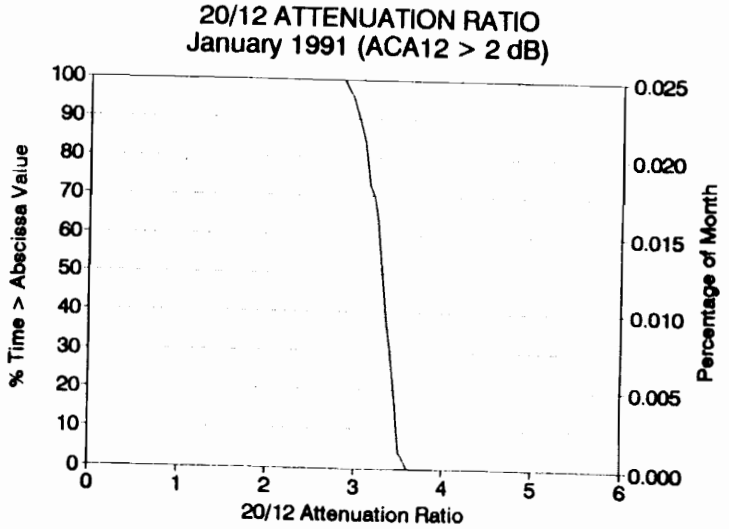
20/12 ATTENUATION RATIO
January 1991 (ACA12 > 2 dB)
% Time > Abscissa Value
Percentage of Month
20/12 Attenuation Ratio
100
90
80
70
60
50
40
30
20
10
0
0
1
2
3
4
5
6
0.025
0.020
0.015
0.010
0.005
0.000

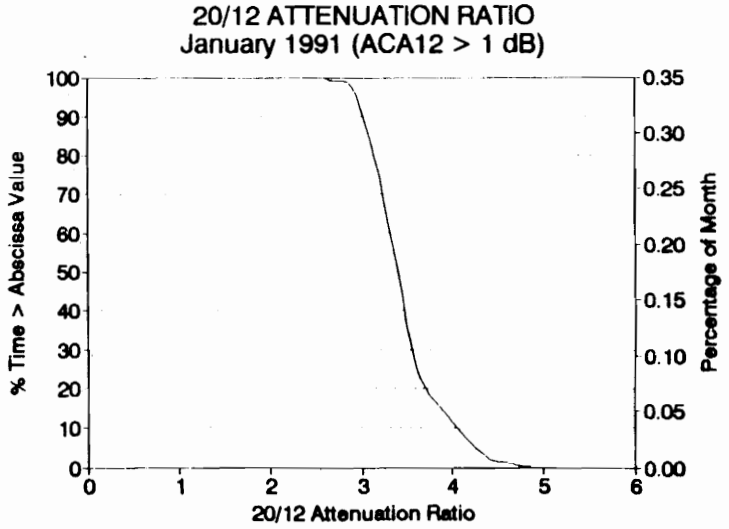
20/12 ATTENUATION RATIO
January 1991 (ACA12 > 1 dB)
% Time > Abscissa Value
Percentage of Month
20/12 Attenuation Ratio
100
90
80
70
60
50
40
30
20
10
0
0
1
2
3
4
5
6
0.35
0.30
0.25
0.20
0.15
0.10
0.05
0.00

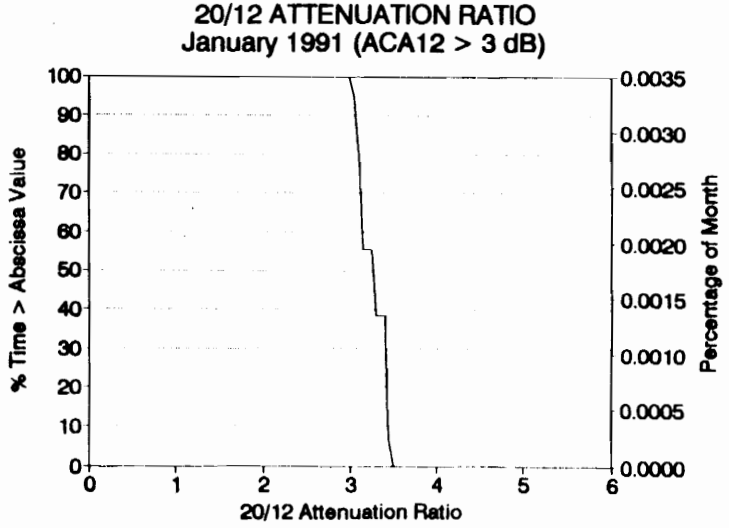
20/12 ATTENUATION RATIO
January 1991 (ACA12 > 3 dB)
% Time > Abscissa Value
Percentage of Month
20/12 Attenuation Ratio
100
90
80
70
60
50
40
30
20
10
0
0
1
2
3
4
5
6
0.0035
0.0030
0.0025
0.0020
0.0015
0.0010
0.0005
0.0000

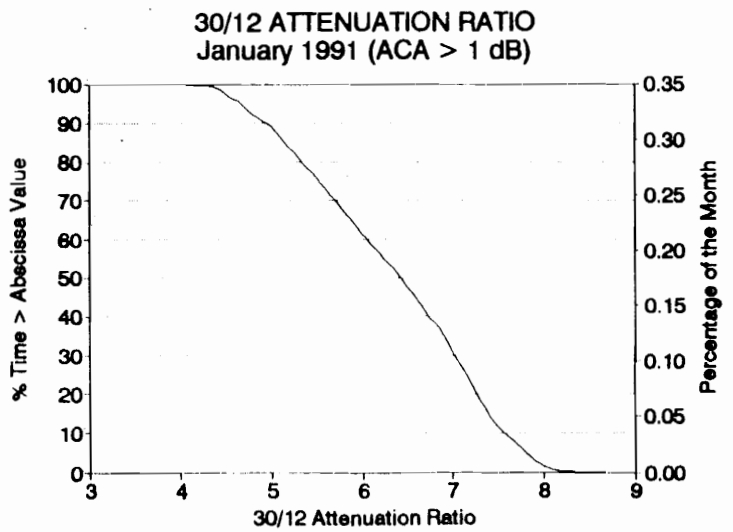
30/12 ATTENUATION RATIO
January 1991 (ACA > 1 dB)
% Time > Abcissa Value
Percentage of the Month
30/12 Attenuation Ratio

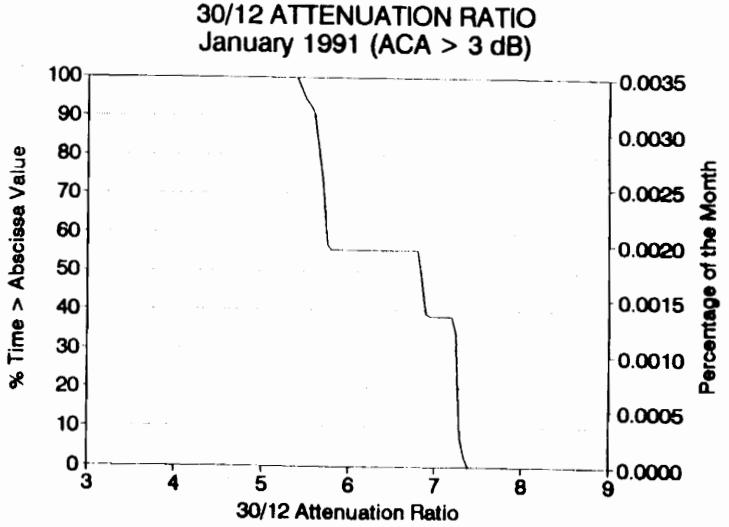
30/12 ATTENUATION RATIO
January 1991 (ACA > 3 dB)
% Time > Abcissa Value
Percentage of the Month
30/12 Attenuation Ratio

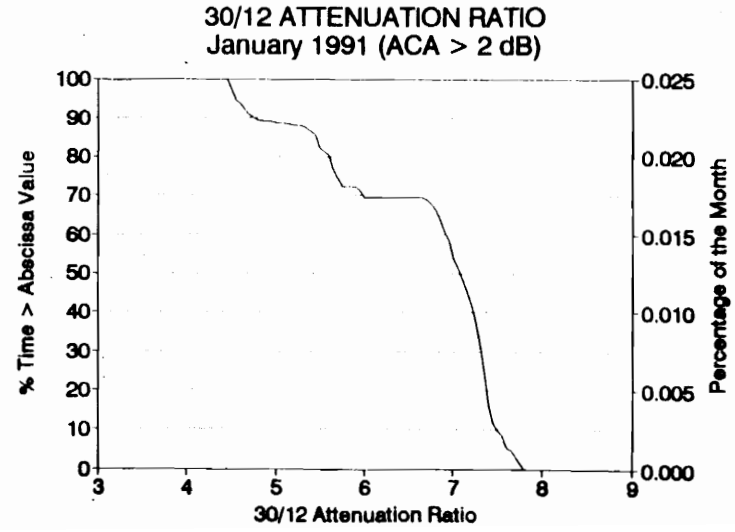
30/12 ATTENUATION RATIO
January 1991 (ACA > 2 dB)
% Time > Abcissa Value
Percentage of the Month
30/12 Attenuation Ratio

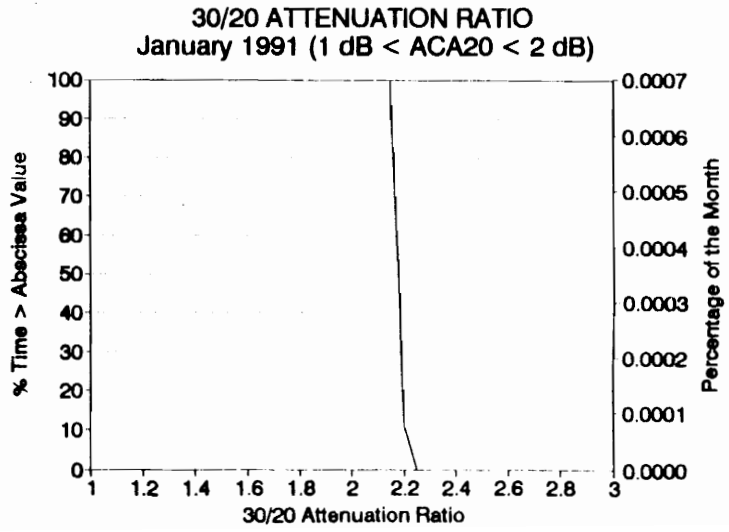
30/20 ATTENUATION RATIO
January 1991 (1 dB < ACA20 < 2 dB)
% Time > Abcissa Value
Percentage of the Month
30/20 Attenuation Ratio

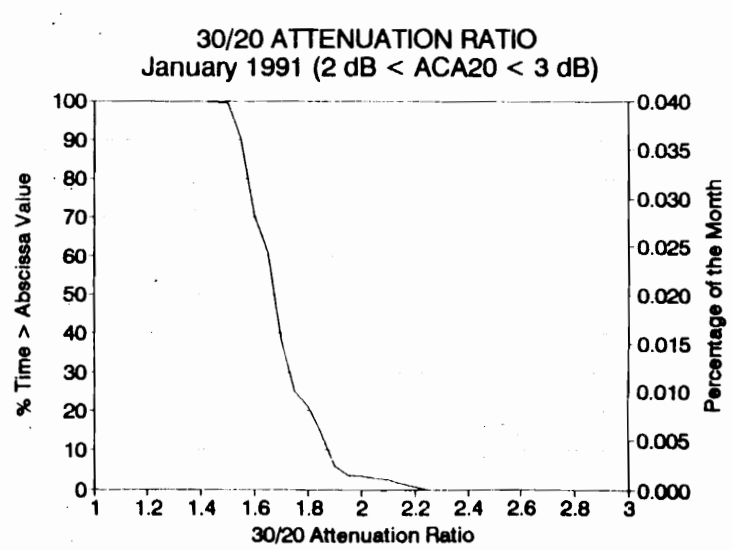
30/20 ATTENUATION RATIO
January 1991 (2 dB < ACA20 < 3 dB)
% Time > Abscissa Value
Percentage of the Month
30/20 Attenuation Ratio
100
90
80
70
60
50
40
30
20
10
0
0.040
0.035
0.030
0.025
0.020
0.015
0.010
0.005
0.000
1
1.2
1.4
1.6
1.8
2
2.2
2.4
2.6
2.8
3

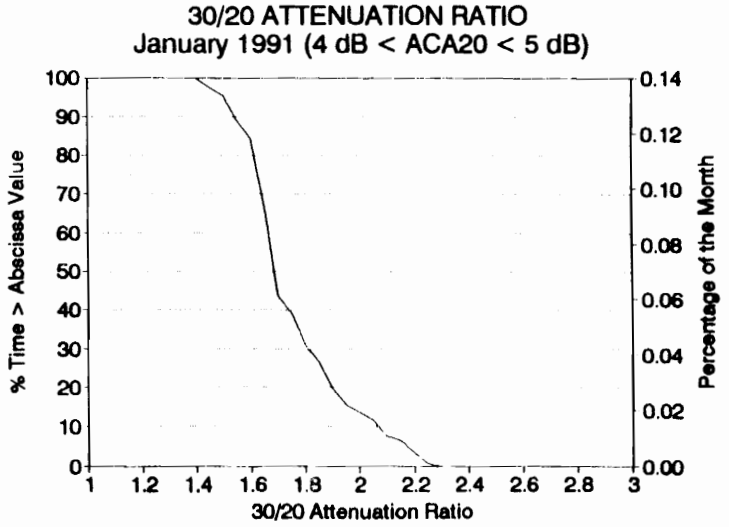
30/20 ATTENUATION RATIO
January 1991 (4 dB < ACA20 < 5 dB)
% Time > Abscissa Value
Percentage of the Month
30/20 Attenuation Ratio
100
90
80
70
60
50
40
30
20
10
0
0.14
0.12
0.10
0.08
0.06
0.04
0.02
0.00
1
1.2
1.4
1.6
1.8
2
2.2
2.4
2.6
2.8
3

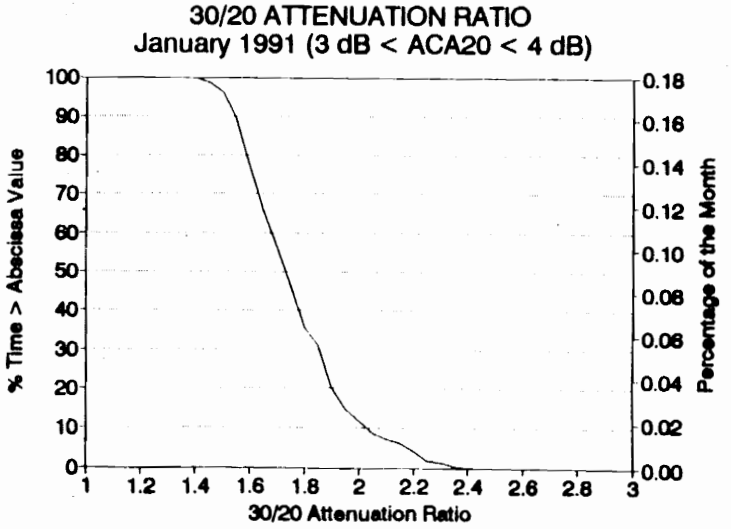
30/20 ATTENUATION RATIO
January 1991 (3 dB < ACA20 < 4 dB)
% Time > Abscissa Value
Percentage of the Month
30/20 Attenuation Ratio
100
90
80
70
60
50
40
30
20
10
0
0.18
0.16
0.14
0.12
0.10
0.08
0.06
0.04
0.02
0.00
1
1.2
1.4
1.6
1.8
2
2.2
2.4
2.6
2.8
3

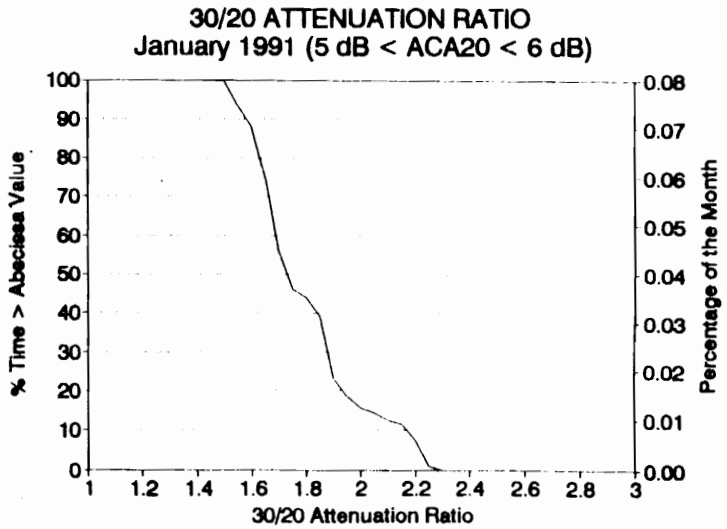
30/20 ATTENUATION RATIO
January 1991 (5 dB < ACA20 < 6 dB)
% Time > Abscissa Value
Percentage of the Month
30/20 Attenuation Ratio
100
90
80
70
60
50
40
30
20
10
0
0.08
0.07
0.06
0.05
0.04
0.03
0.02
0.01
0.00
1
1.2
1.4
1.6
1.8
2
2.2
2.4
2.6
2.8
3

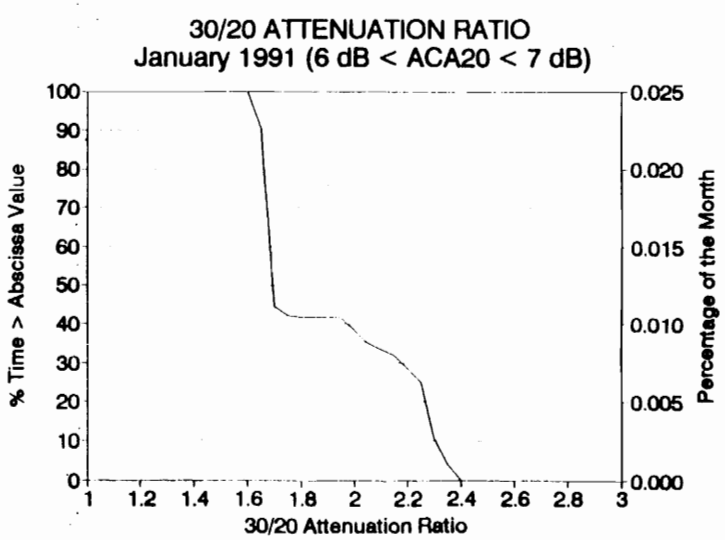
30/20 ATTENUATION RATIO
January 1991 (6 dB < ACA20 < 7 dB)
% Time > Abcissa Value
Percentage of the Month
30/20 Attenuation Ratio
100
90
80
70
60
50
40
30
20
10
0
0.025
0.020
0.015
0.010
0.005
0.000
1
1.2
1.4
1.6
1.8
2
2.2
2.4
2.6
2.8
3

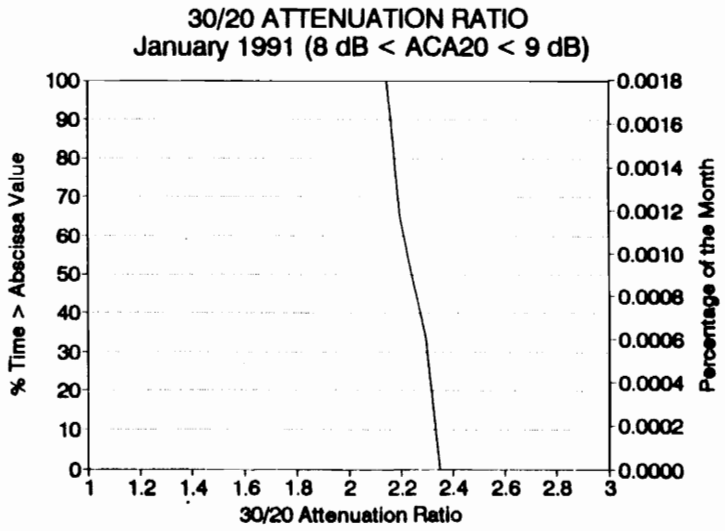
30/20 ATTENUATION RATIO
January 1991 (8 dB < ACA20 < 9 dB)
% Time > Abcissa Value
Percentage of the Month
30/20 Attenuation Ratio
100
90
80
70
60
50
40
30
20
10
0
0.0018
0.0016
0.0014
0.0012
0.0010
0.0008
0.0006
0.0004
0.0002
0.0000
1
1.2
1.4
1.6
1.8
2
2.2
2.4
2.6
2.8
3

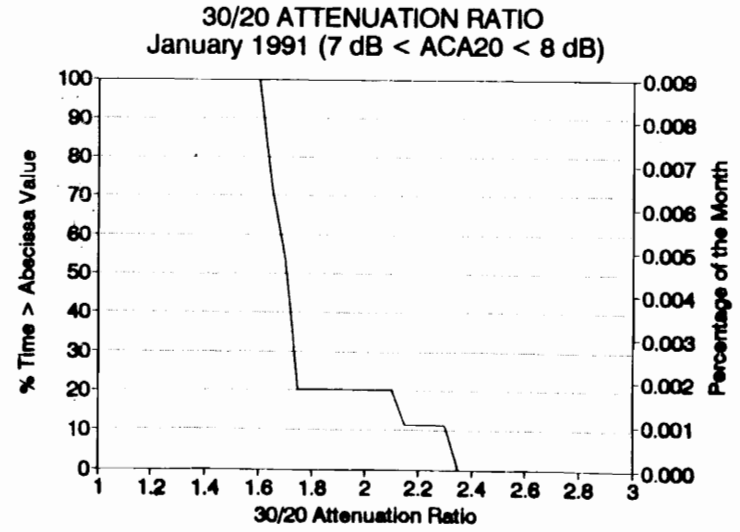
30/20 ATTENUATION RATIO
January 1991 (7 dB < ACA20 < 8 dB)
% Time > Abcissa Value
Percentage of the Month
30/20 Attenuation Ratio
100
90
80
70
60
50
40
30
20
10
0
0.009
0.008
0.007
0.006
0.005
0.004
0.003
0.002
0.001
0.000
1
1.2
1.4
1.6
1.8
2
2.2
2.4
2.6
2.8
3

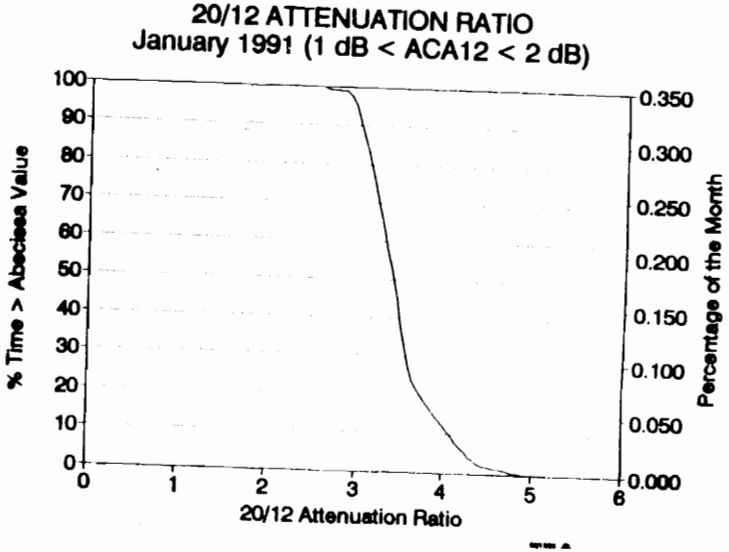
20/12 ATTENUATION RATIO
January 1991 (1 dB < ACA12 < 2 dB)
% Time > Abcissa Value
Percentage of the Month
20/12 Attenuation Ratio
100
90
80
70
60
50
40
30
20
10
0
0.350
0.300
0.250
0.200
0.150
0.100
0.050
0.000
0
1
2
3
4
5
6

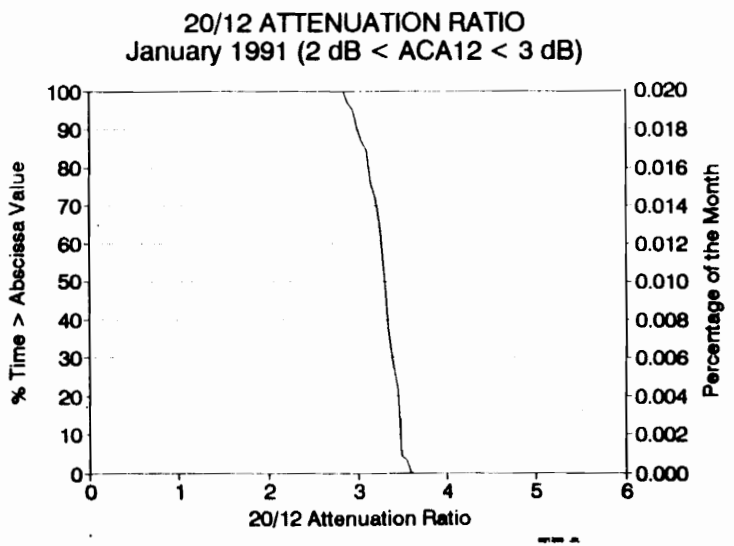
20/12 ATTENUATION RATIO
January 1991 (2 dB < ACA12 < 3 dB)
% Time > Abcissa Value
Percentage of the Month
20/12 Attenuation Ratio

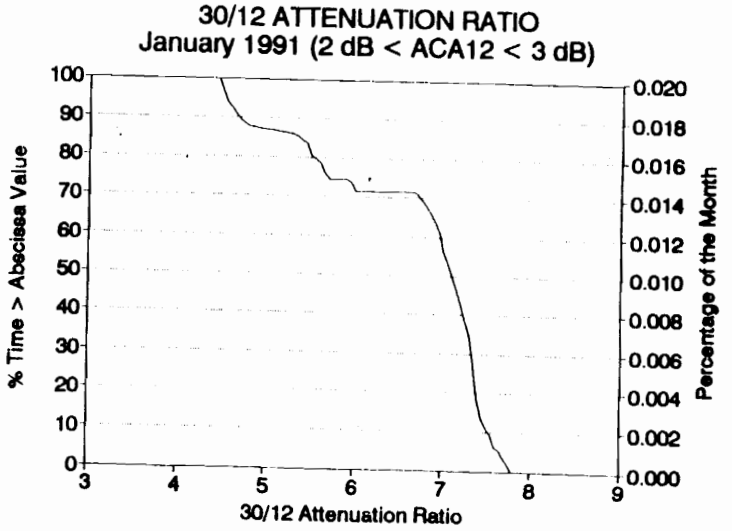
30/12 ATTENUATION RATIO
January 1991 (2 dB < ACA12 < 3 dB)
% Time > Abcissa Value
Percentage of the Month
30/12 Attenuation Ratio

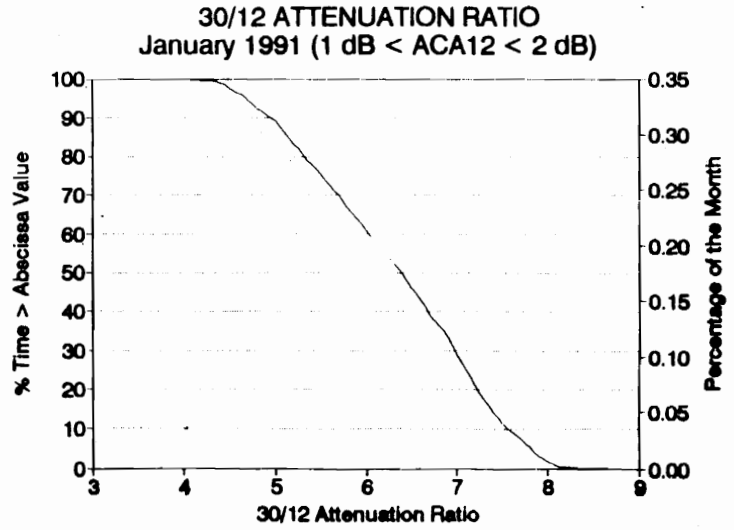
30/12 ATTENUATION RATIO
January 1991 (1 dB < ACA12 < 2 dB)
% Time > Abcissa Value
Percentage of the Month
30/12 Attenuation Ratio

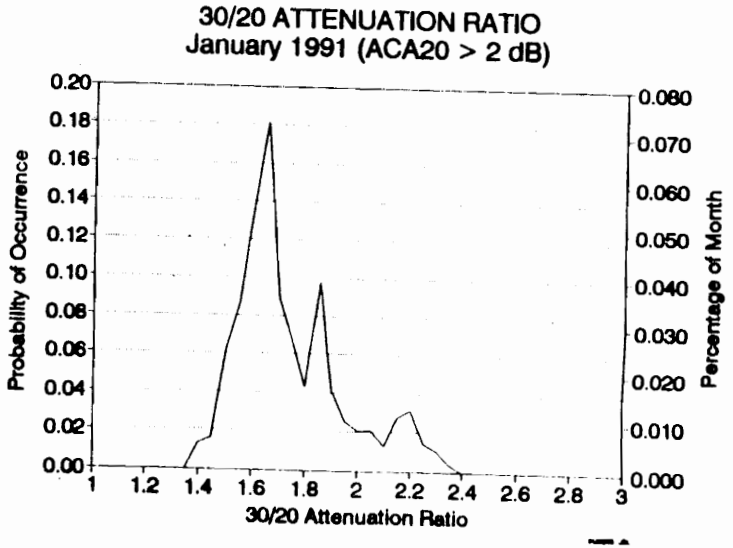
30/20 ATTENUATION RATIO
January 1991 (ACA20 > 2 dB)
Probability of Occurrence
Percentage of Month
30/20 Attenuation Ratio

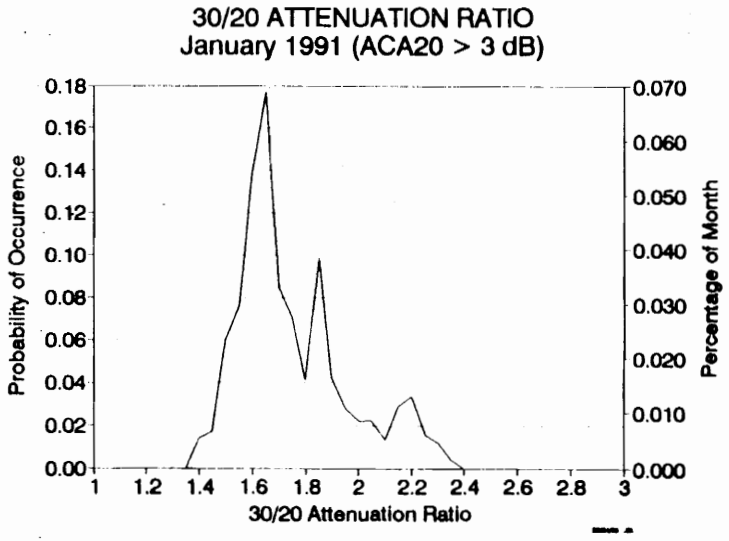
30/20 ATTENUATION RATIO
January 1991 (ACA20 > 3 dB)
Probability of Occurrence
Percentage of Month
30/20 Attenuation Ratio
0.18
0.16
0.14
0.12
0.10
0.08
0.06
0.04
0.02
0.00
0.070
0.060
0.050
0.040
0.030
0.020
0.010
0.000
1
1.2
1.4
1.6
1.8
2
2.2
2.4
2.6
2.8
3

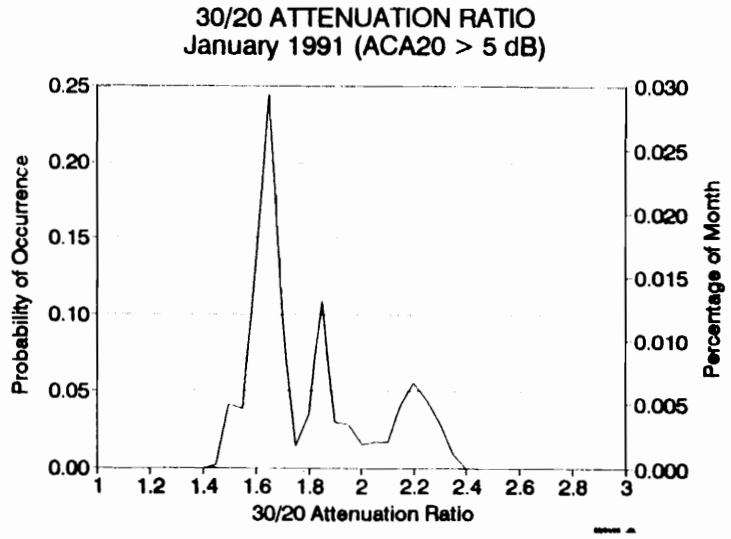
30/20 ATTENUATION RATIO
January 1991 (ACA20 > 5 dB)
Probability of Occurrence
Percentage of Month
30/20 Attenuation Ratio
0.25
0.20
0.15
0.10
0.05
0.00
0.030
0.025
0.020
0.015
0.010
0.005
0.000
1
1.2
1.4
1.6
1.8
2
2.2
2.4
2.6
2.8
3

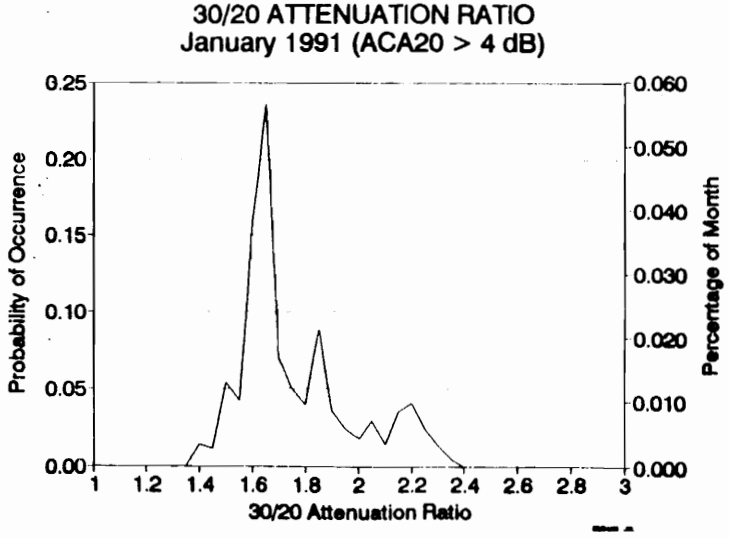
30/20 ATTENUATION RATIO
January 1991 (ACA20 > 4 dB)
Probability of Occurrence
Percentage of Month
30/20 Attenuation Ratio
0.25
0.20
0.15
0.10
0.05
0.00
0.060
0.050
0.040
0.030
0.020
0.010
0.000
1
1.2
1.4
1.6
1.8
2
2.2
2.4
2.6
2.8
3

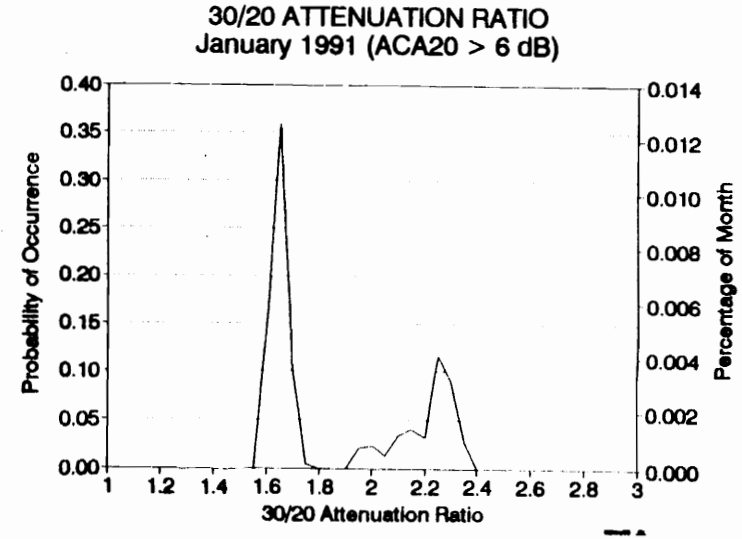
30/20 ATTENUATION RATIO
January 1991 (ACA20 > 6 dB)
Probability of Occurrence
Percentage of Month
30/20 Attenuation Ratio
0.40
0.35
0.30
0.25
0.20
0.15
0.10
0.05
0.00
0.014
0.012
0.010
0.008
0.006
0.004
0.002
0.000
1
1.2
1.4
1.6
1.8
2
2.2
2.4
2.6
2.8
3

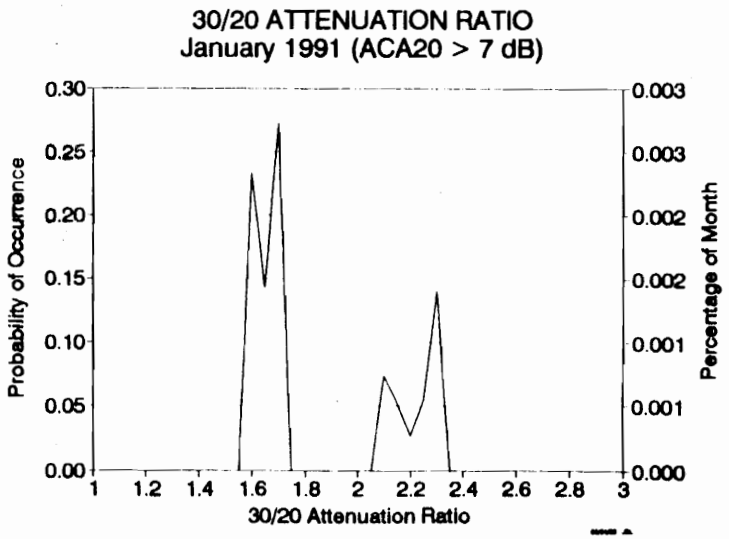
30/20 ATTENUATION RATIO
January 1991 (ACA20 > 7 dB)
Probability of Occurrence
Percentage of Month
30/20 Attenuation Ratio
0.30
0.25
0.20
0.15
0.10
0.05
0.00
0.003
0.003
0.002
0.002
0.001
0.001
0.000
1
1.2
1.4
1.6
1.8
2
2.2
2.4
2.6
2.8
3

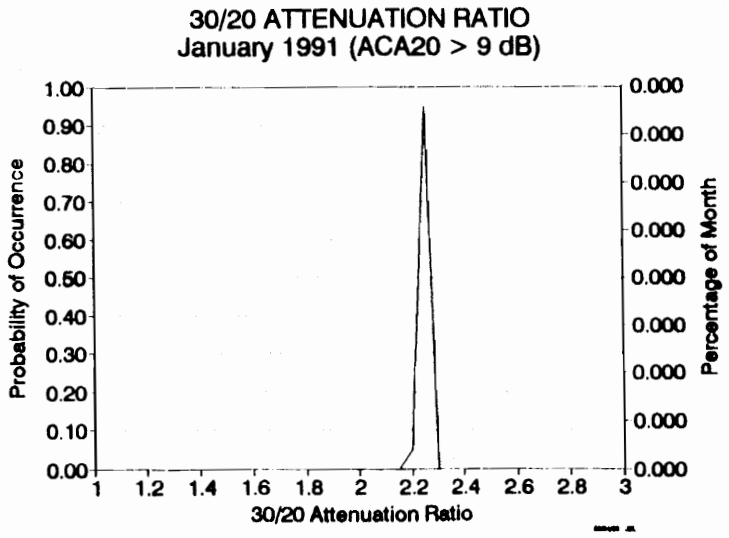
30/20 ATTENUATION RATIO
January 1991 (ACA20 > 9 dB)
Probability of Occurrence
Percentage of Month
30/20 Attenuation Ratio
1.00
0.90
0.80
0.70
0.60
0.50
0.40
0.30
0.20
0.10
0.00
0.000
0.000
0.000
0.000
0.000
0.000
0.000
0.000
1
1.2
1.4
1.6
1.8
2
2.2
2.4
2.6
2.8
3

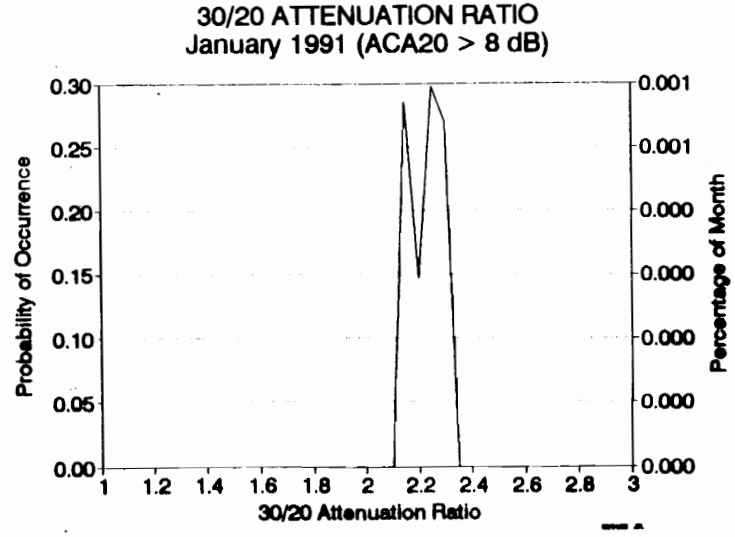
30/20 ATTENUATION RATIO
January 1991 (ACA20 > 8 dB)
Probability of Occurrence
Percentage of Month
30/20 Attenuation Ratio
0.30
0.25
0.20
0.15
0.10
0.05
0.00
0.001
0.001
0.000
0.000
0.000
0.000
0.000
1
1.2
1.4
1.6
1.8
2
2.2
2.4
2.6
2.8
3

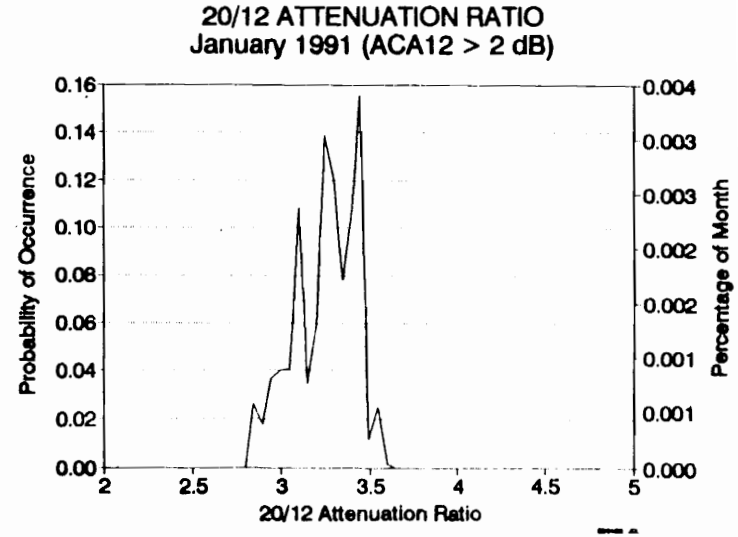
20/12 ATTENUATION RATIO
January 1991 (ACA12 > 2 dB)
Probability of Occurrence
Percentage of Month
20/12 Attenuation Ratio
0.16
0.14
0.12
0.10
0.08
0.06
0.04
0.02
0.00
0.004
0.003
0.003
0.002
0.002
0.001
0.001
0.000
2
2.5
3
3.5
4
4.5
5

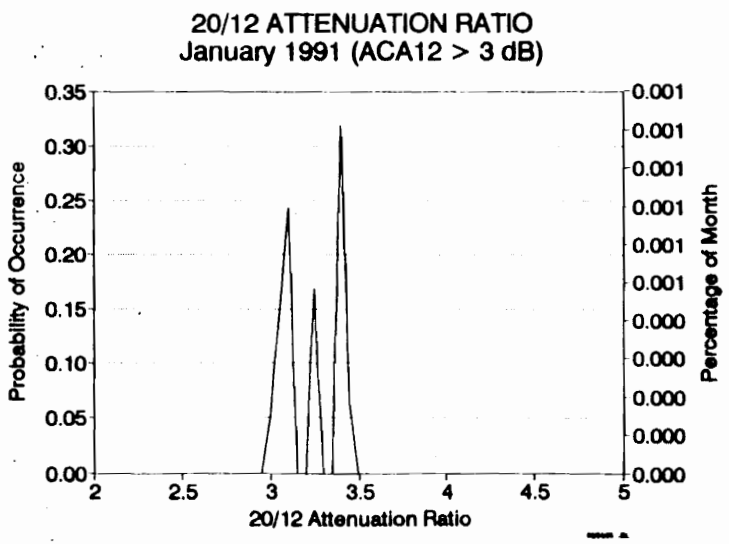
20/12 ATTENUATION RATIO
January 1991 (ACA12 > 3 dB)
Probability of Occurrence
Percentage of Month
20/12 Attenuation Ratio

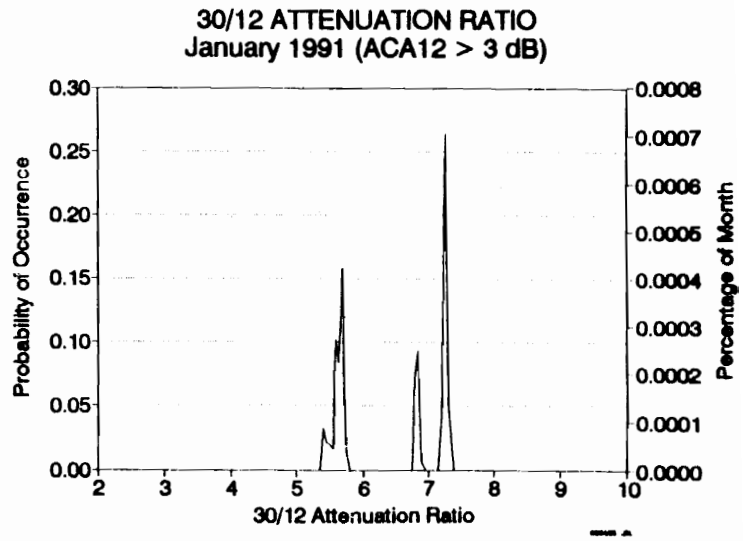
30/12 ATTENUATION RATIO
January 1991 (ACA12 > 3 dB)
Probability of Occurrence
Percentage of Month
30/12 Attenuation Ratio

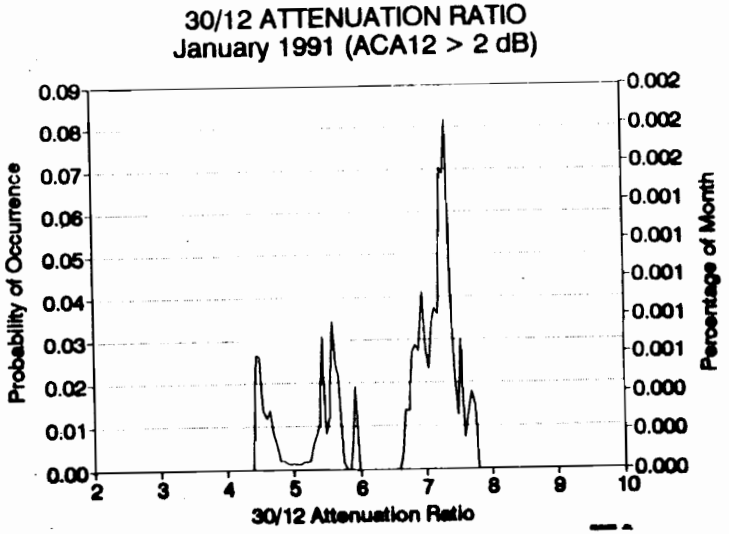
30/12 ATTENUATION RATIO
January 1991 (ACA12 > 2 dB)
Probability of Occurrence
Percentage of Month
30/12 Attenuation Ratio

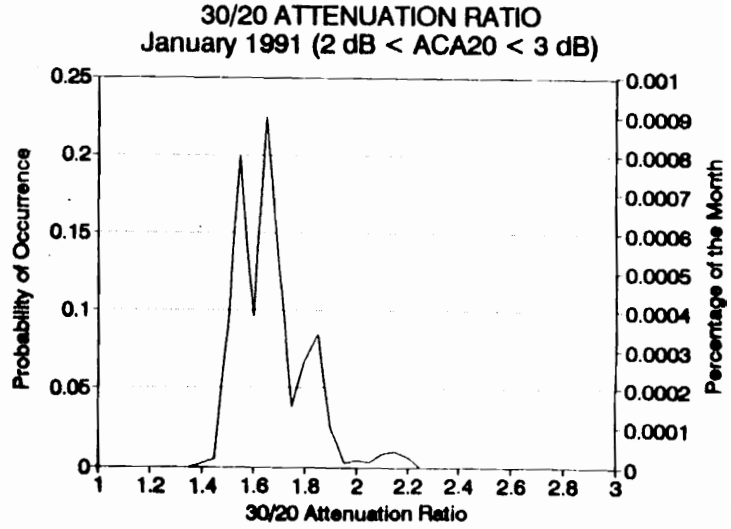
30/20 ATTENUATION RATIO
January 1991 (2 dB < ACA20 < 3 dB)
Probability of Occurrence
Percentage of the Month
30/20 Attenuation Ratio

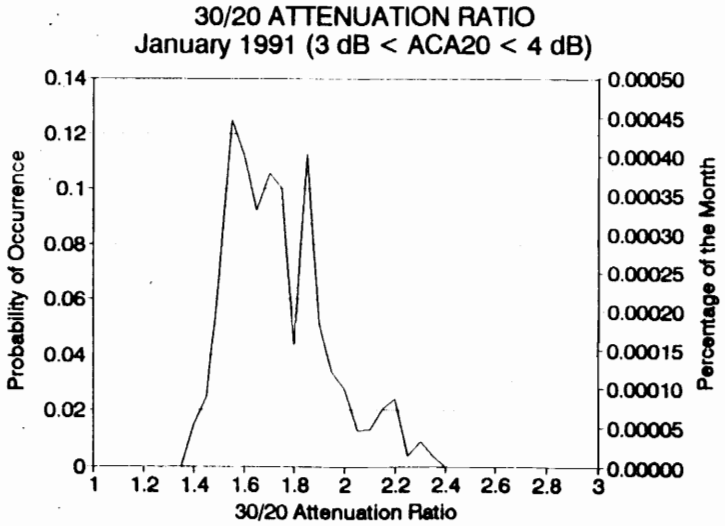
30/20 ATTENUATION RATIO
January 1991 (3 dB < ACA20 < 4 dB)
Probability of Occurrence
Percentage of the Month
30/20 Attenuation Ratio
0.14
0.12
0.1
0.08
0.06
0.04
0.02
0
0.00050
0.00045
0.00040
0.00035
0.00030
0.00025
0.00020
0.00015
0.00010
0.00005
0.00000
1
1.2
1.4
1.6
1.8
2
2.2
2.4
2.6
2.8
3

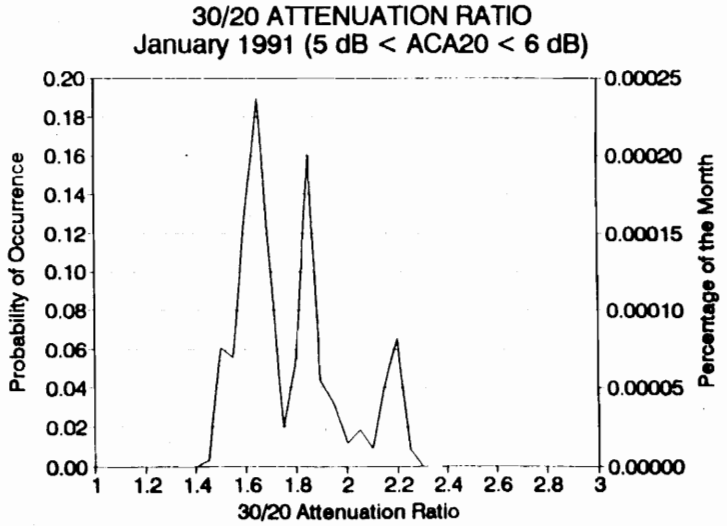
30/20 ATTENUATION RATIO
January 1991 (5 dB < ACA20 < 6 dB)
Probability of Occurrence
Percentage of the Month
30/20 Attenuation Ratio
0.20
0.18
0.16
0.14
0.12
0.10
0.08
0.06
0.04
0.02
0.00
0.00025
0.00020
0.00015
0.00010
0.00005
0.00000
1
1.2
1.4
1.6
1.8
2
2.2
2.4
2.6
2.8
3

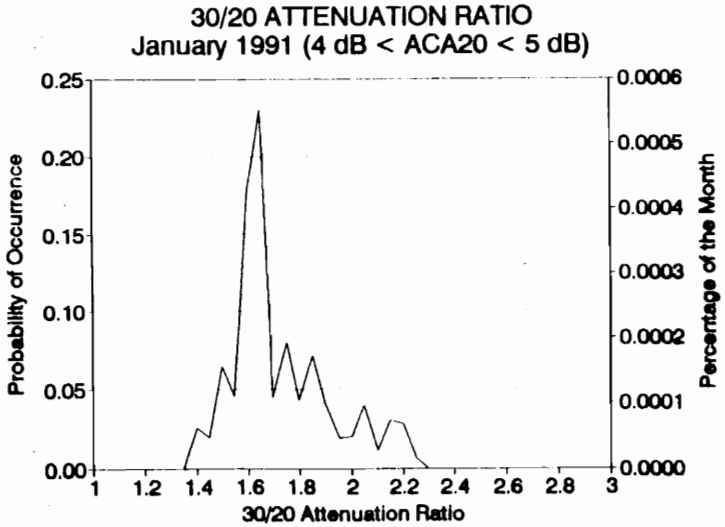
30/20 ATTENUATION RATIO
January 1991 (4 dB < ACA20 < 5 dB)
Probability of Occurrence
Percentage of the Month
30/20 Attenuation Ratio
0.25
0.20
0.15
0.10
0.05
0.00
0.0006
0.0005
0.0004
0.0003
0.0002
0.0001
0.0000
1
1.2
1.4
1.6
1.8
2
2.2
2.4
2.6
2.8
3

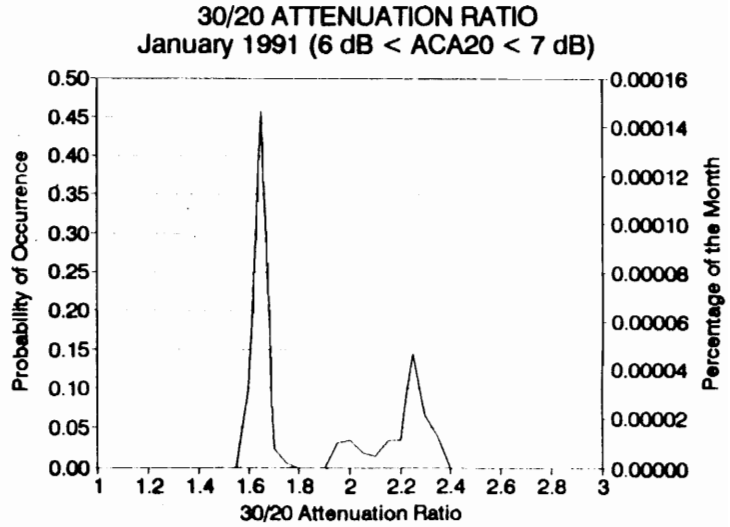
30/20 ATTENUATION RATIO
January 1991 (6 dB < ACA20 < 7 dB)
Probability of Occurrence
Percentage of the Month
30/20 Attenuation Ratio
0.50
0.45
0.40
0.35
0.30
0.25
0.20
0.15
0.10
0.05
0.00
0.00016
0.00014
0.00012
0.00010
0.00008
0.00006
0.00004
0.00002
0.00000
1
1.2
1.4
1.6
1.8
2
2.2
2.4
2.6
2.8
3

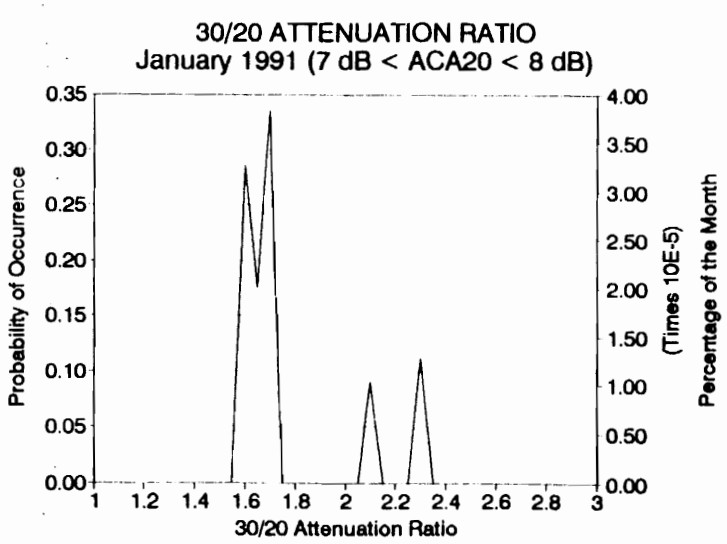
30/20 ATTENUATION RATIO
January 1991 (7 dB < ACA20 < 8 dB)
Probability of Occurrence
Percentage of the Month
(Times 10E-5)
30/20 Attenuation Ratio

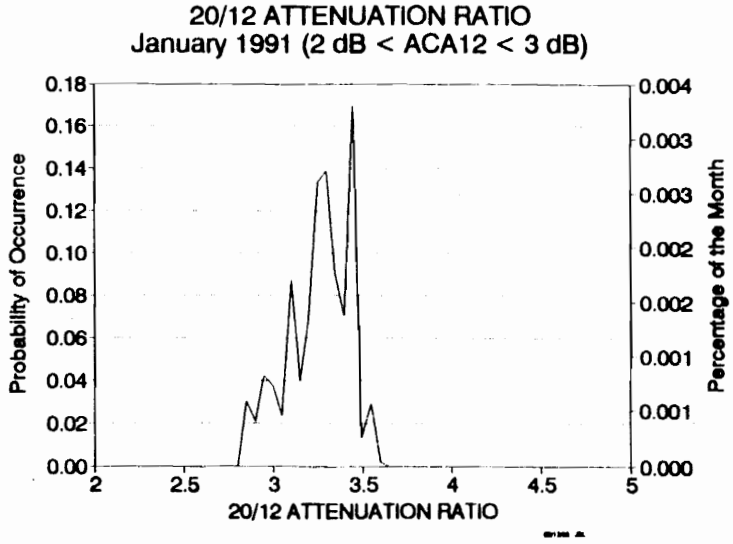
20/12 ATTENUATION RATIO
January 1991 (2 dB < ACA12 < 3 dB)
Probability of Occurrence
Percentage of the Month
20/12 ATTENUATION RATIO

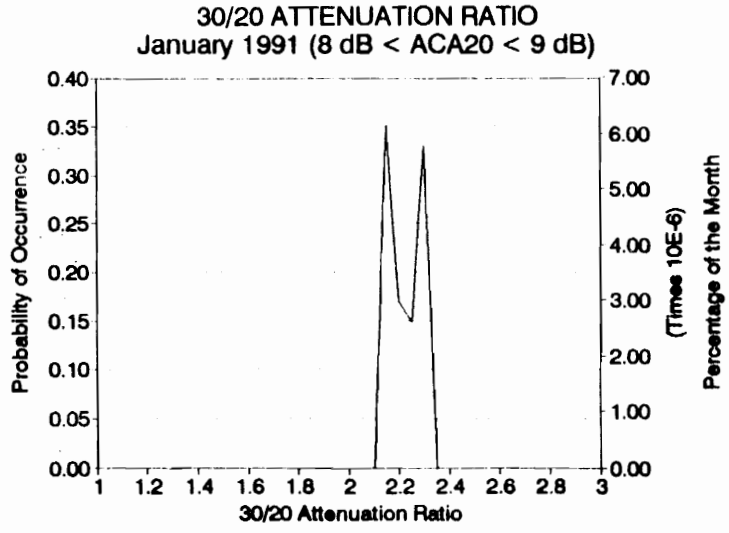
30/20 ATTENUATION RATIO
January 1991 (8 dB < ACA20 < 9 dB)
Probability of Occurrence
Percentage of the Month
(Times 10E-6)
30/20 Attenuation Ratio

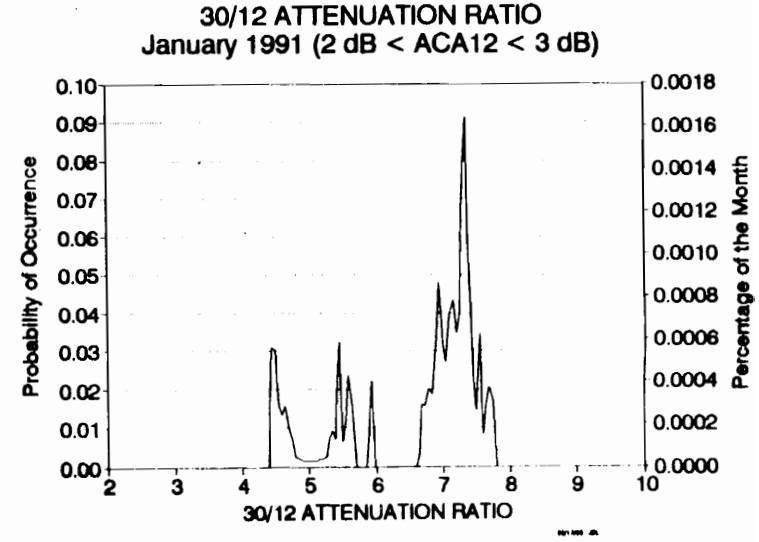
30/12 ATTENUATION RATIO
January 1991 (2 dB < ACA12 < 3 dB)
Probability of Occurrence
Percentage of the Month
30/12 ATTENUATION RATIO

30/20 STATISTICAL ATTENUATION RATIO
January 1991 (ACAS20 > 1 dB)

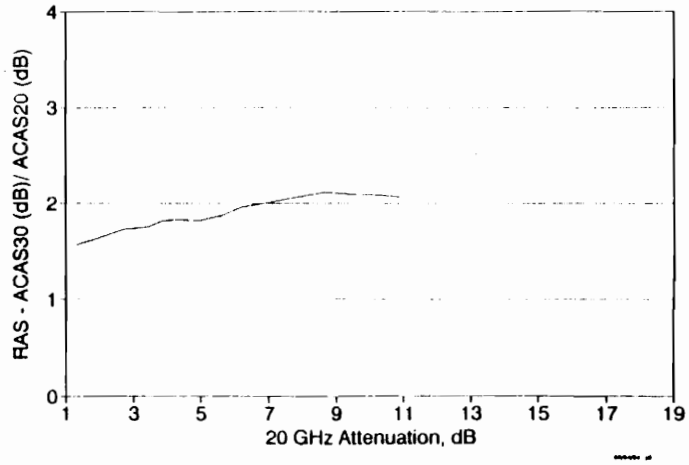

30/20 STATISTICAL ATTENUATION RATIO
March 1991 (ACAS20 > 1 dB)

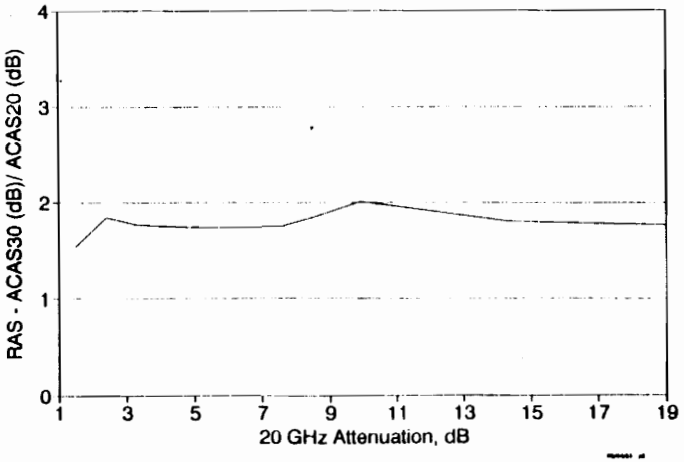

30/20 STATISTICAL ATTENUATION RATIO
February 1991 (ACAS20 > 1 dB)

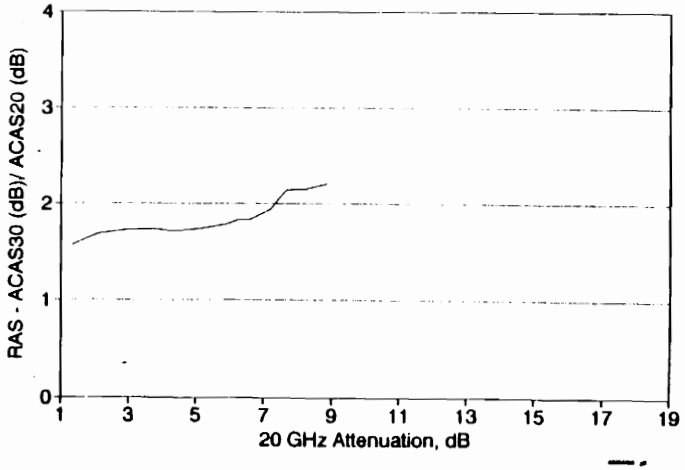

30/20 STATISTICAL ATTENUATION RATIO
April 1991 (ACAS20 > 1 dB)

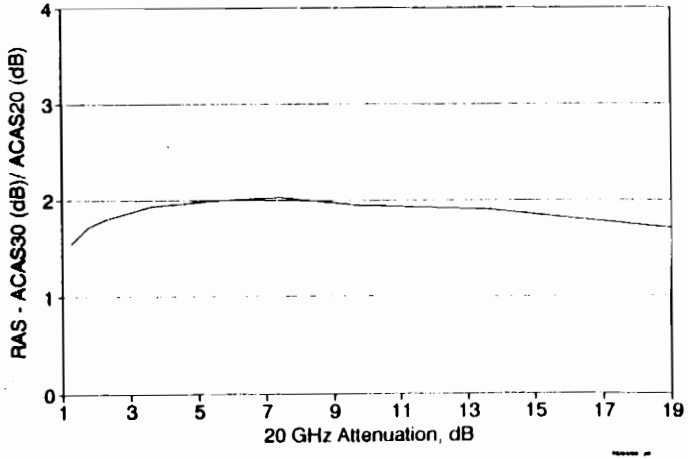

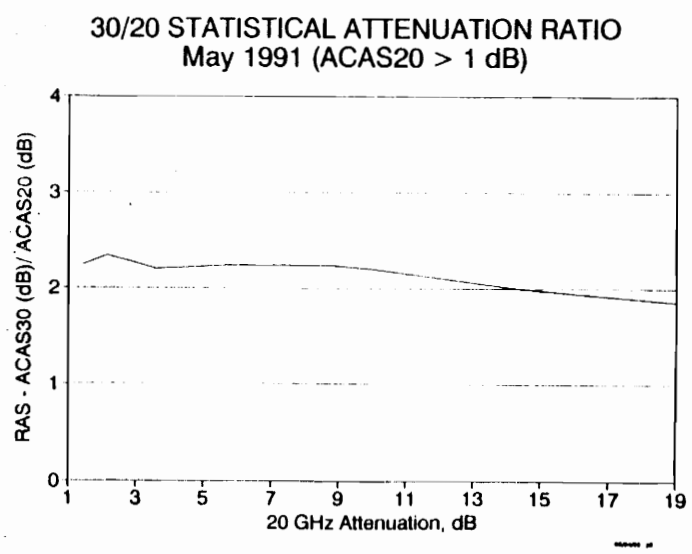
30/20 STATISTICAL ATTENUATION RATIO
May 1991 (ACAS20 > 1 dB)
RAS - ACAS30 (dB)/ ACAS20 (dB)
0
1
2
3
4
1
3
5
7
9
11
13
15
17
19
20 GHz Attenuation, dB

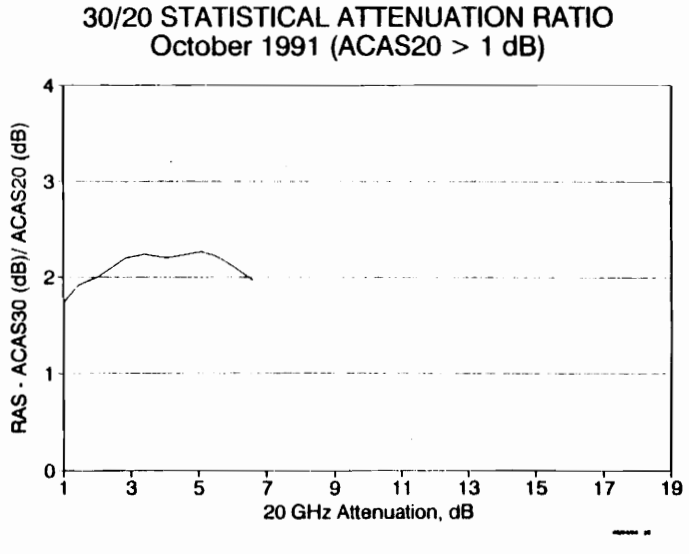
30/20 STATISTICAL ATTENUATION RATIO
October 1991 (ACAS20 > 1 dB)
RAS - ACAS30 (dB)/ ACAS20 (dB)
0
1
2
3
4
1
3
5
7
9
11
13
15
17
19
20 GHz Attenuation, dB

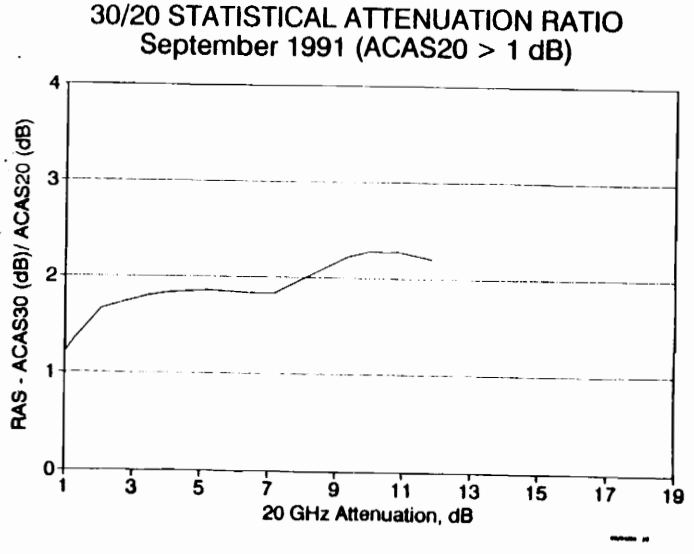
30/20 STATISTICAL ATTENUATION RATIO
September 1991 (ACAS20 > 1 dB)
RAS - ACAS30 (dB)/ ACAS20 (dB)
0
1
2
3
4
1
3
5
7
9
11
13
15
17
19
20 GHz Attenuation, dB

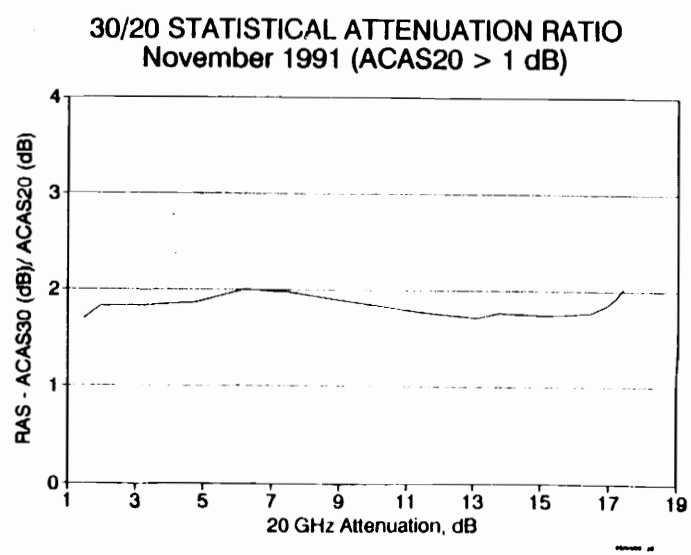
30/20 STATISTICAL ATTENUATION RATIO
November 1991 (ACAS20 > 1 dB)
RAS - ACAS30 (dB)/ ACAS20 (dB)
0
1
2
3
4
1
3
5
7
9
11
13
15
17
19
20 GHz Attenuation, dB

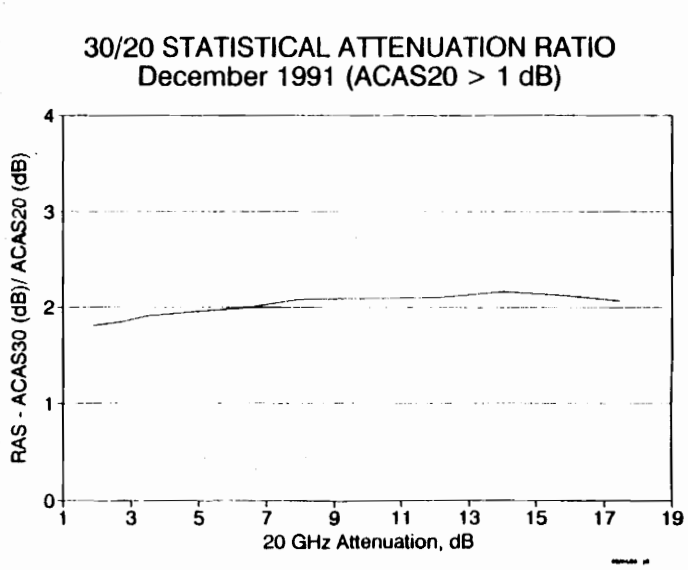
30/20 STATISTICAL ATTENUATION RATIO
December 1991 (ACAS20 > 1 dB)
RAS - ACAS30 (dB)/ ACAS20 (dB)
0
1
2
3
4
1
3
5
7
9
11
13
15
17
19
20 GHz Attenuation, dB

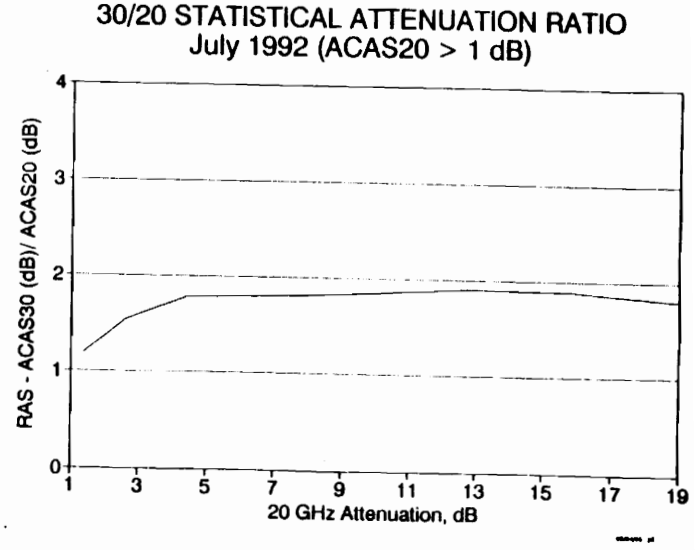
30/20 STATISTICAL ATTENUATION RATIO
July 1992 (ACAS20 > 1 dB)
RAS - ACAS30 (dB)/ ACAS20 (dB)
0
1
2
3
4
1
3
5
7
9
11
13
15
17
19
20 GHz Attenuation, dB

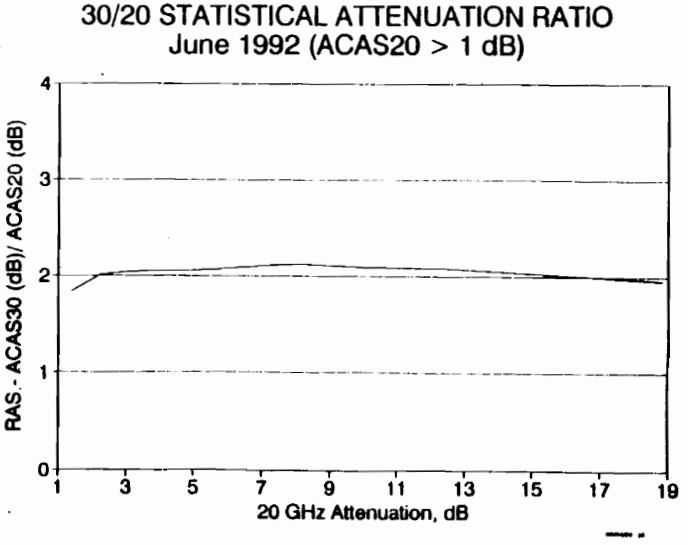
30/20 STATISTICAL ATTENUATION RATIO
June 1992 (ACAS20 > 1 dB)
RAS - ACAS30 (dB)/ ACAS20 (dB)
0
1
2
3
4
1
3
5
7
9
11
13
15
17
19
20 GHz Attenuation, dB

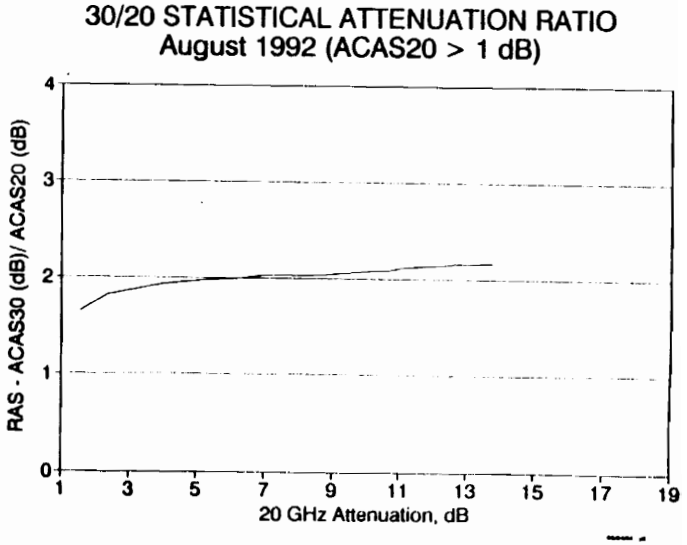
30/20 STATISTICAL ATTENUATION RATIO
August 1992 (ACAS20 > 1 dB)
RAS - ACAS30 (dB)/ ACAS20 (dB)
0
1
2
3
4
1
3
5
7
9
11
13
15
17
19
20 GHz Attenuation, dB

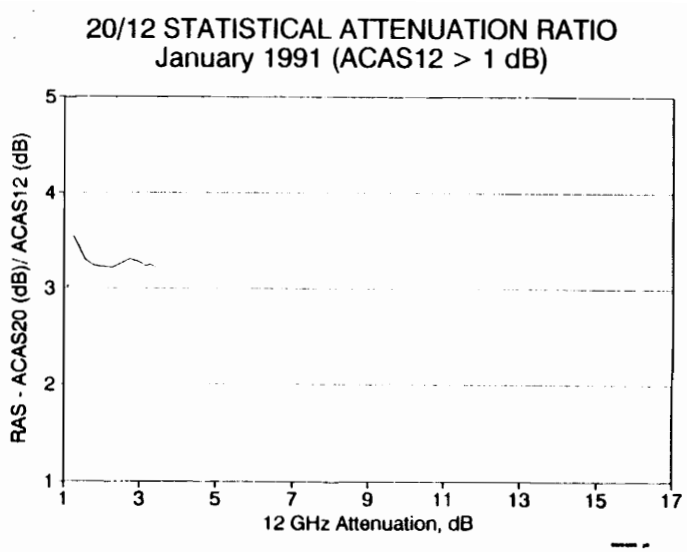
20/12 STATISTICAL ATTENUATION RATIO
January 1991 (ACAS12 > 1 dB)
RAS - ACAS20 (dB)/ ACAS12 (dB)
12 GHz Attenuation, dB

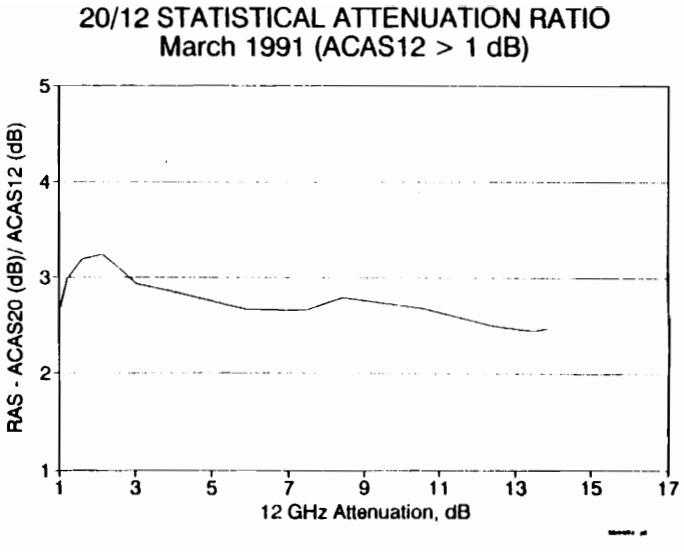
20/12 STATISTICAL ATTENUATION RATIO
March 1991 (ACAS12 > 1 dB)
RAS - ACAS20 (dB)/ ACAS12 (dB)
12 GHz Attenuation, dB

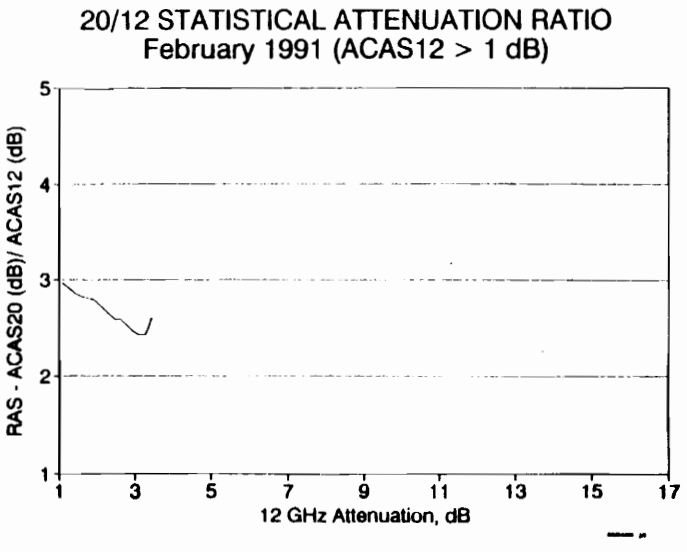
20/12 STATISTICAL ATTENUATION RATIO
February 1991 (ACAS12 > 1 dB)
RAS - ACAS20 (dB)/ ACAS12 (dB)
12 GHz Attenuation, dB

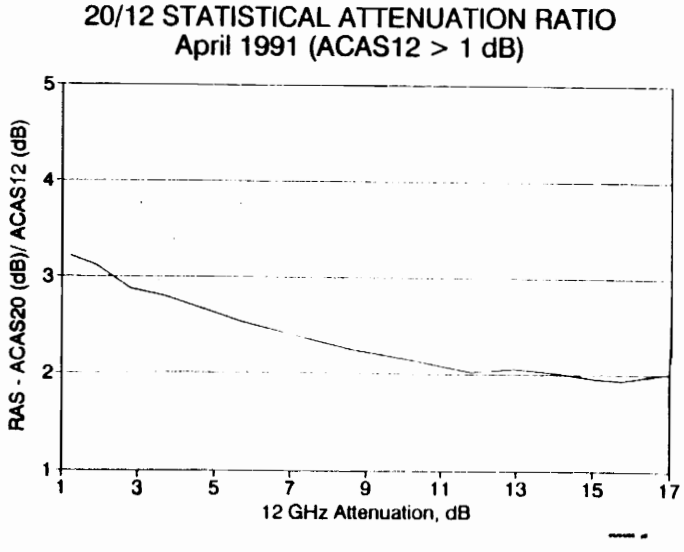
20/12 STATISTICAL ATTENUATION RATIO
April 1991 (ACAS12 > 1 dB)
RAS - ACAS20 (dB)/ ACAS12 (dB)
12 GHz Attenuation, dB

20/12 STATISTICAL ATTENUATION RATIO
May 1991 (ACAS12 > 1 dB)

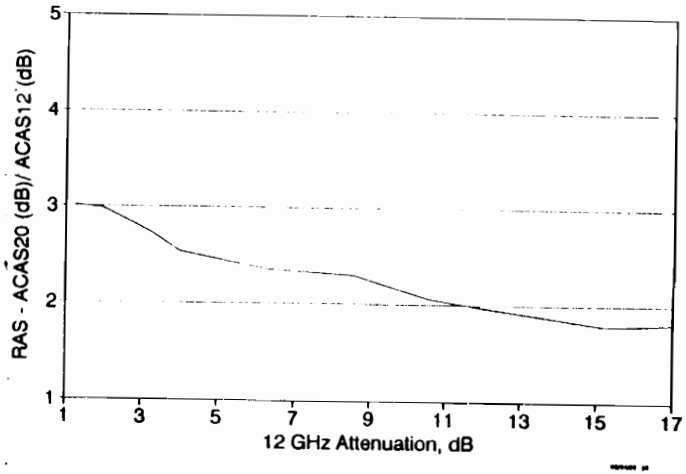

20/12 STATISTICAL ATTENUATION RATIO
October 1991 (ACAS12 > 1 dB)

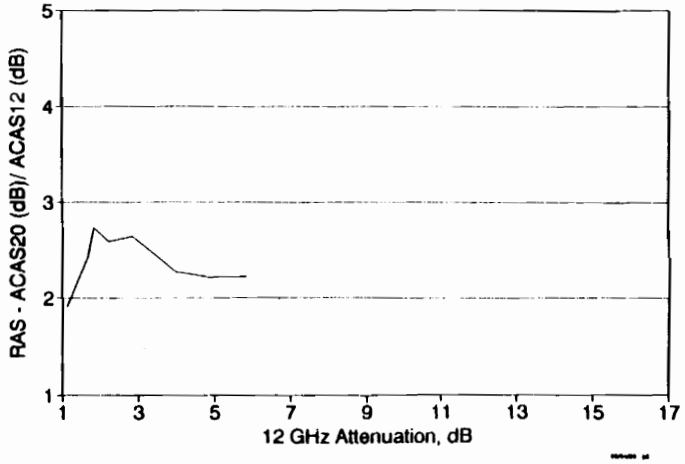

20/12 STATISTICAL ATTENUATION RATIO
September 1991 (ACAS12 > 1 dB)

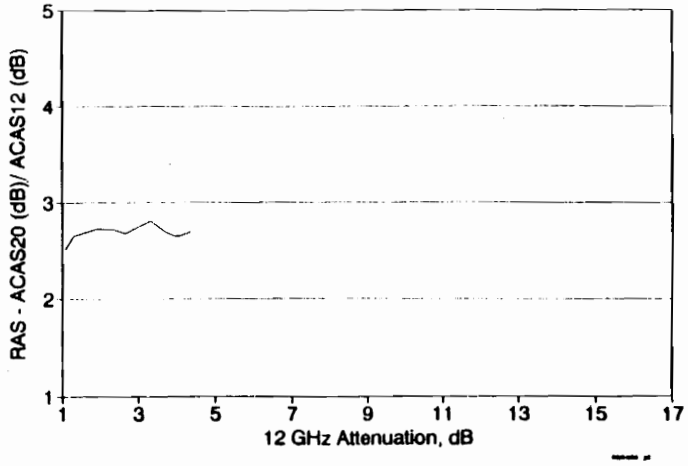

20/12 STATISTICAL ATTENUATION RATIO
November 1991 (ACAS12 > 1 dB)

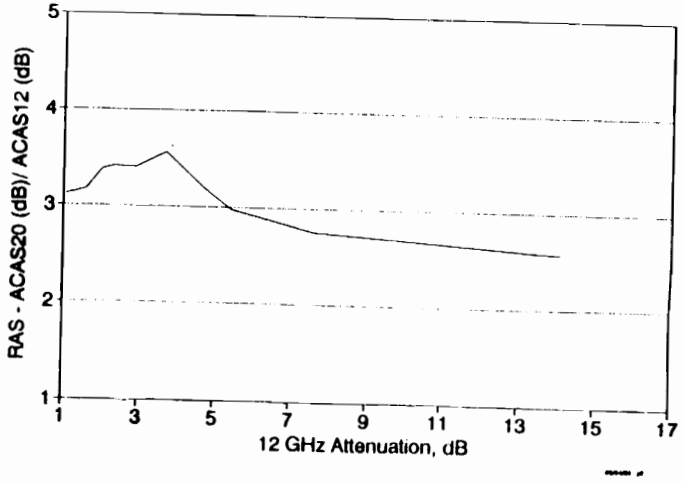

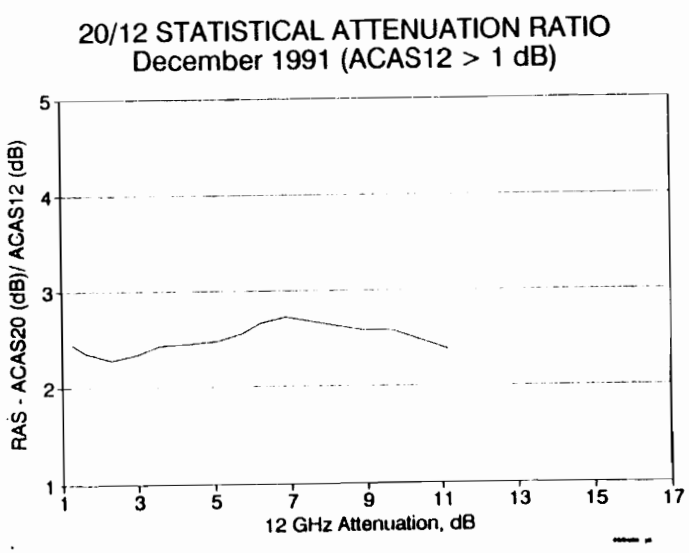
20/12 STATISTICAL ATTENUATION RATIO
December 1991 (ACAS12 > 1 dB)
RAS - ACAS20 (dB)/ ACAS12 (dB)
12 GHz Attenuation, dB

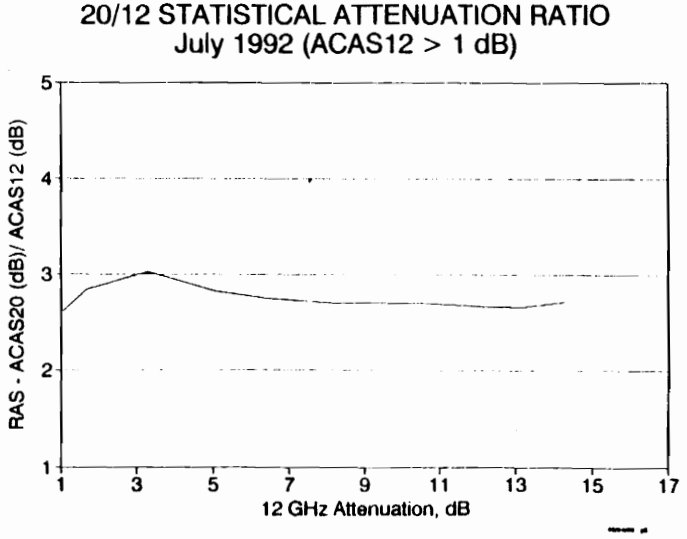
20/12 STATISTICAL ATTENUATION RATIO
July 1992 (ACAS12 > 1 dB)
RAS - ACAS20 (dB)/ ACAS12 (dB)
12 GHz Attenuation, dB

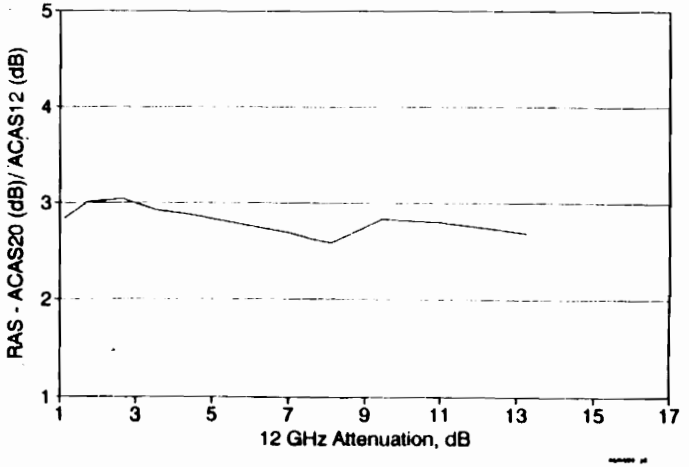
20/12 STATISTICAL ATTENUATION RATIO
June 1992 (ACAS12 > 1 dB)
RAS - ACAS20 (dB)/ ACAS12 (dB)
12 GHz Attenuation, dB

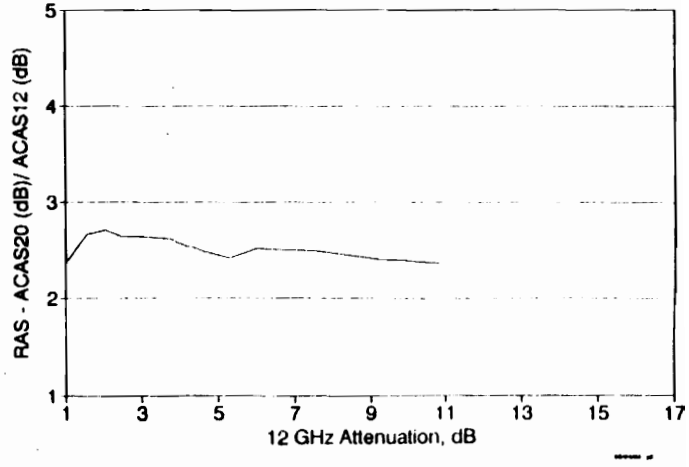
20/12 STATISTICAL ATTENUATION RATIO
August 1992 (ACAS12 > 1 dB)
RAS - ACAS20 (dB)/ ACAS12 (dB)
12 GHz Attenuation, dB

30/12 STATISTICAL ATTENUATION RATIO
January 1991 (ACAS12 > 1 dB)

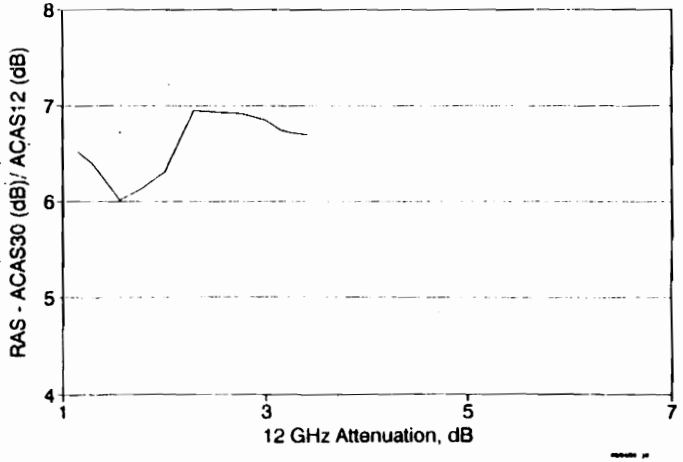

30/12 STATISTICAL ATTENUATION RATIO
March 1991 (ACAS12 > 1 dB)

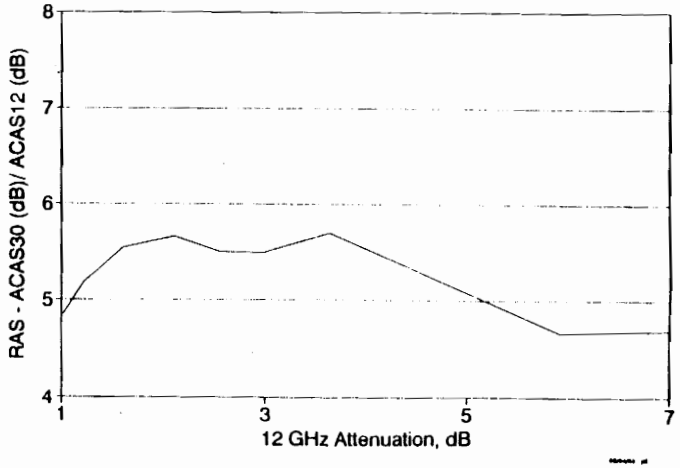

30/12 STATISTICAL ATTENUATION RATIO
February 1991 (ACAS12 > 1 dB)

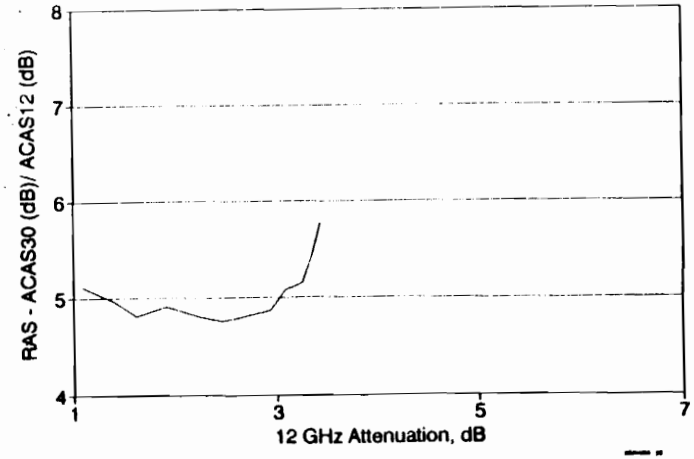

30/12 STATISTICAL ATTENUATION RATIO
April 1991 (ACAS12 > 1 dB)

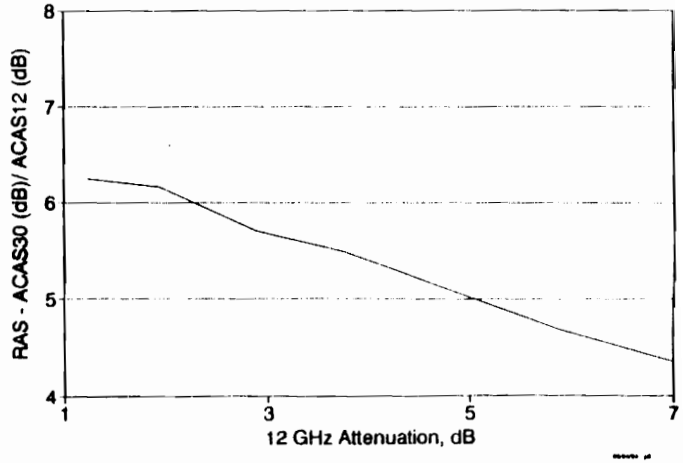

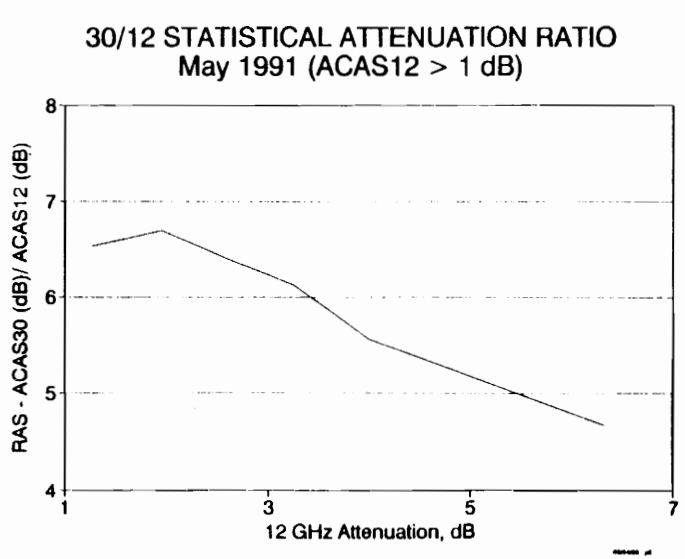
30/12 STATISTICAL ATTENUATION RATIO
May 1991 (ACAS12 > 1 dB)
RAS - ACAS30 (dB)/ ACAS12 (dB)
8
7
6
5
4
1
3
5
7
12 GHz Attenuation, dB

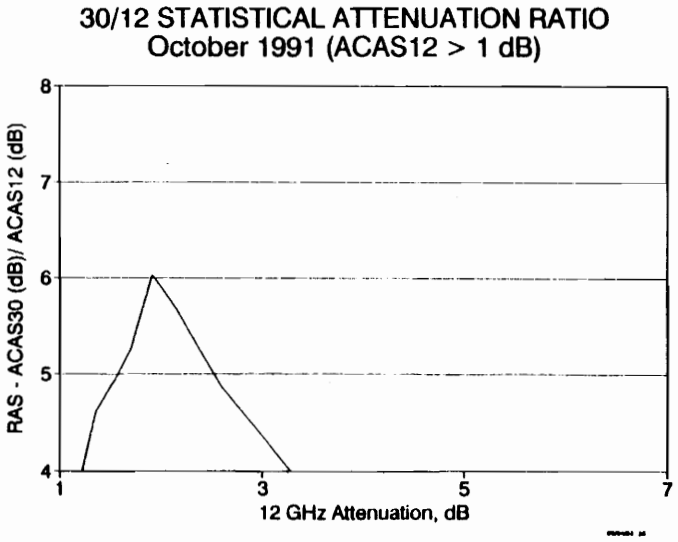
30/12 STATISTICAL ATTENUATION RATIO
October 1991 (ACAS12 > 1 dB)
RAS - ACAS30 (dB)/ ACAS12 (dB)
8
7
6
5
4
1
3
5
7
12 GHz Attenuation, dB

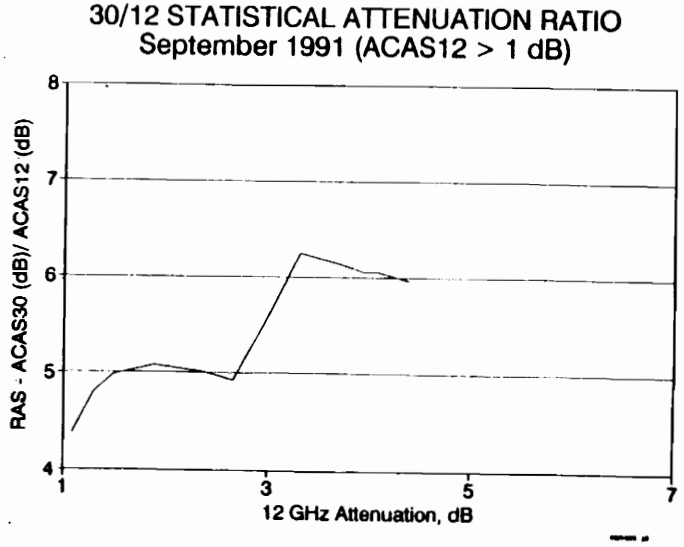
30/12 STATISTICAL ATTENUATION RATIO
September 1991 (ACAS12 > 1 dB)
RAS - ACAS30 (dB)/ ACAS12 (dB)
8
7
6
5
4
1
3
5
7
12 GHz Attenuation, dB

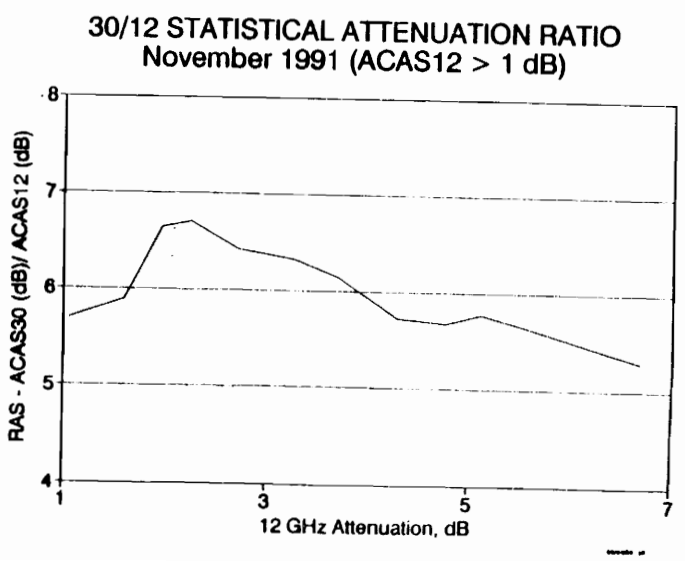
30/12 STATISTICAL ATTENUATION RATIO
November 1991 (ACAS12 > 1 dB)
RAS - ACAS30 (dB)/ ACAS12 (dB)
8
7
6
5
4
1
3
5
7
12 GHz Attenuation, dB

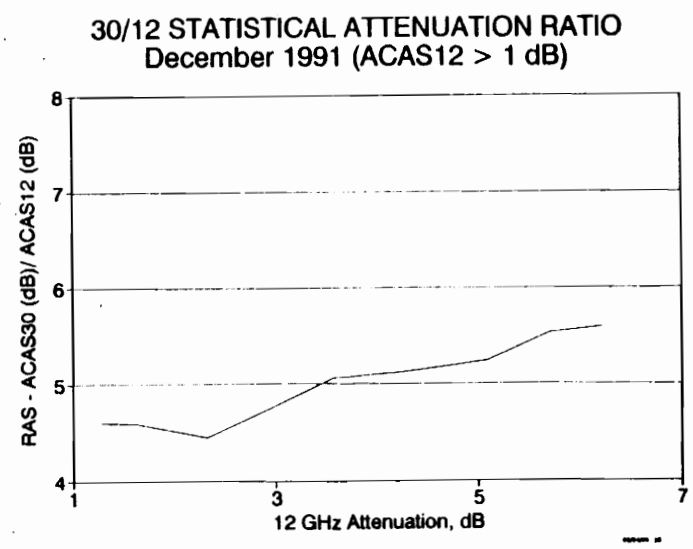
30/12 STATISTICAL ATTENUATION RATIO
December 1991 (ACAS12 > 1 dB)
RAS - ACAS30 (dB)/ ACAS12 (dB)
8
7
6
5
4
1
3
5
7
12 GHz Attenuation, dB

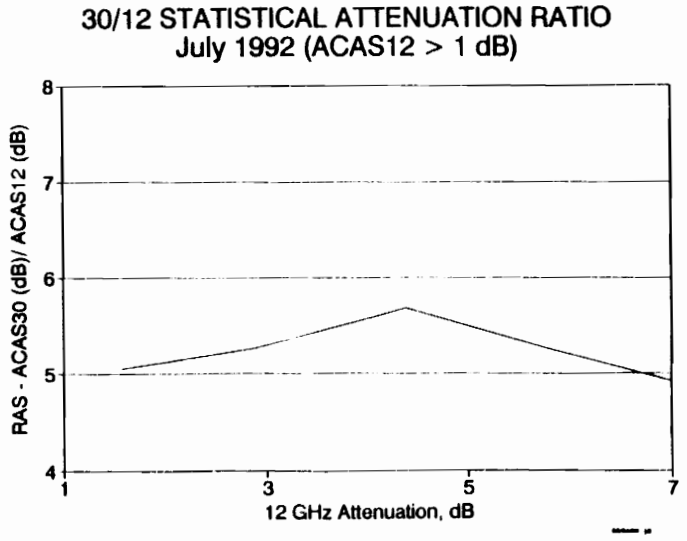
30/12 STATISTICAL ATTENUATION RATIO
July 1992 (ACAS12 > 1 dB)
RAS - ACAS30 (dB)/ ACAS12 (dB)
8
7
6
5
4
1
3
5
7
12 GHz Attenuation, dB

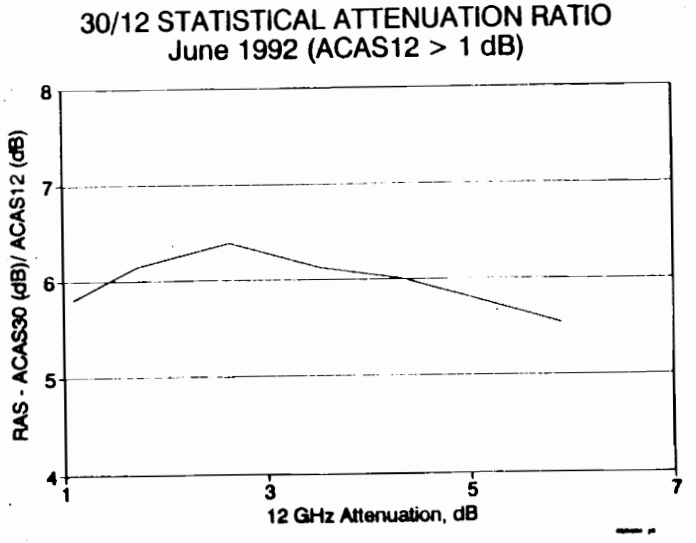
30/12 STATISTICAL ATTENUATION RATIO
June 1992 (ACAS12 > 1 dB)
RAS - ACAS30 (dB)/ ACAS12 (dB)
8
7
6
5
4
1
3
5
7
12 GHz Attenuation, dB

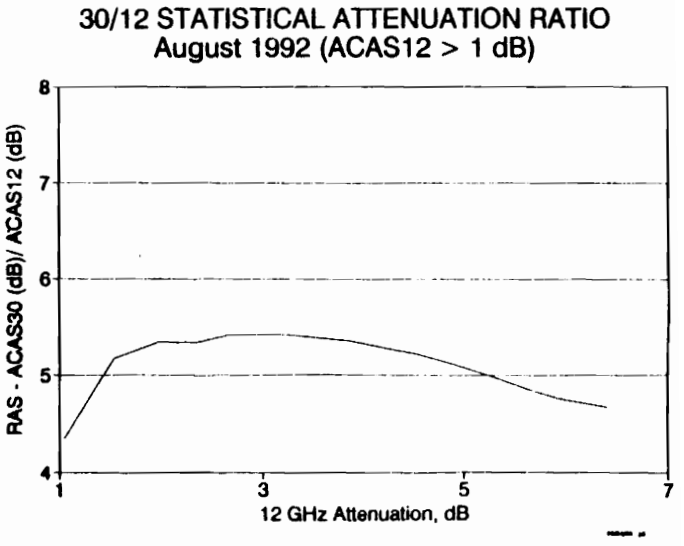
30/12 STATISTICAL ATTENUATION RATIO
August 1992 (ACAS12 > 1 dB)
RAS - ACAS30 (dB)/ ACAS12 (dB)
8
7
6
5
4
1
3
5
7
12 GHz Attenuation, dB

Vita

Jeff Laster was born on June 7, 1962 in Fitzgerald, Georgia. Upon graduation from Stratford Academy in Macon, Georgia in June 1980, he spent two years studying engineering at Georgia Tech, where he was employed as a co-op at the Georgia Tech Research Institute. He then transferred to obtain a Bachelor of Arts in the Humanities from Bob Jones University in May 1984. In 1989, he enrolled in Virginia Tech and obtained with a Bachelor of Science in Electrical Engineering in May 1991. He pursued graduate studies at Virginia Tech on a Bradley Fellowship and a DuPont Fellowship and earned a Master of Science in Electrical Engineering in November 1993. He is presently pursuing a doctorate in electrical engineering at Virginia Tech.